



UNIVERSIDADE DE BRASÍLIA
INSTITUTO DE GEOCIÊNCIAS
PROGRAMA DE PÓS-GRADUAÇÃO EM GEOLOGIA
GEOQUÍMICA

**REFERTILIZATION OF THE LITHOSPHERIC MANTLE
BENEATH THE SOUTHWESTERN PART OF THE SÃO
FRANCISCO CRATON, BRAZIL**

*“REFERTILIZAÇÃO DO MANTO LITOSFÉRICO ABAIXO DA PARTE
SUDOESTE DO CRÁTON SÃO FRANCISCO, BRASIL”*

Master Dissertation N° 498

Dissertação de mestrado N° 498

Rodrigo Antonio de Freitas Rodrigues

This study was financed in part by the Coordenação de Aperfeiçoamento de Pessoal de Nível Superior – Brasil (CAPES) – Finance Code 001

O presente trabalho foi realizado com apoio da Coordenação de Aperfeiçoamento de Pessoal de Nível Superior – Brasil (CAPES) – Código de Financiamento 001

Brasília-DF, Brazil



UNIVERSIDADE DE BRASÍLIA
INSTITUTO DE GEOCIÊNCIAS
PROGRAMA DE PÓS-GRADUAÇÃO EM GEOLOGIA
GEOQUÍMICA

**REFERTILIZATION OF THE LITHOSPHERIC MANTLE
BENEATH THE SOUTHWESTERN PART OF THE SÃO
FRANCISCO CRATON, BRAZIL**

*“REFERTILIZAÇÃO DO MANTO LITOSFÉRICO ABAIXO DA PARTE
SUDOESTE DO CRÁTON SÃO FRANCISCO, BRASIL”*

Rodrigo Antonio de Freitas Rodrigues

A Dissertation submitted in partial fulfillment of the requirements for the degree of Master of Science in Geology at the Geoscience Institute of the University of Brasília.

Area of research: Geochemistry

Advisor: Tiago Luis Reis Jalowitzki

Co-advisor: Fernanda Gervasoni

Examination Board: Dr. Reinhardt Adolfo Fuck – UnB

Dr. Rommulo Vieira Conceição – UFRGS

Dr. Catarina Labouré Bemfica Toledo – UnB (Substitute)

Brasília-DF, Brazil

October, 2022

Ficha catalográfica elaborada automaticamente,
com os dados fornecidos pelo(a) autor(a)

RR696r Rodrigues, Rodrigo Antonio de Freitas
REFERTILIZATION OF THE LITHOSPHERIC MANTLE BENEATH THE
SOUTHWESTERN PART OF THE SÃO FRANCISCO CRATON, BRAZIL
"REFERTILIZAÇÃO DO MANTO LITOSFÉRICO ABAIXO DA PARTE SUDOESTE
DO CRÁTON SÃO FRANCISCO, BRASIL" / Rodrigo Antonio de
Freitas Rodrigues; orientador Tiago Jalowitzki; co
orientador Fernanda Gervasoni. -- Brasília, 2022.
226 p.

Dissertação (Mestrado em Geologia) -- Universidade de
Brasília, 2022.

1. Mantle xenoliths. 2. Mineral chemistry. 3. Metasomatism. 4. Refertilization. 5. São Francisco Craton. I. Jalowitzki, Tiago, orient. II. Gervasoni, Fernanda, co orient. III. Título.

AKNOWLEDGEMENT

During my time as a master's student, I was extremely fortunate to work with and benefit from some inspiring people. First and foremost I would like to thank my supervisors, Tiago Jalowitzki and Fernanda Gervasoni, whose level of advice, guidance, and patience has been incredible. Thank you both for the constant support and encouragement throughout this long journey. No matter how busy you were you always had the time.

I extend my sincere thanks to Juliana Pertille, who was instrumental in introducing me to the scientific world and has encouraged me and provided support and assistance whenever needed.

To all of my friends, thank you for the encouragement to keep going. A special mention is made to Caroline Silveira.

To my sister Thaliny – thank you for the immense emotional support you have given me throughout the years.

Finally, I thank my parents, Ângela and João Antônio, for their endless love and support. I can never thank them enough!

This study was financed in part by the Coordenação de Aperfeiçoamento de Pessoal de Nível Superior – Brasil (CAPES) – Finance Code 001

O presente trabalho foi realizado com apoio da Coordenação de Aperfeiçoamento de Pessoal de Nível Superior – Brasil (CAPES) – Código de Financiamento 001

TABLE OF CONTENTS

LIST OF FIGURES	vii
TABLE LIST	x
Article.....	x
Supplementary material.....	x
RESUMO EXPANDIDO	11
1. Introdução	11
2. Métodos.....	12
3. Resultados e discussões.....	13
4. Conclusões	14
CHAPTER 1 – INTRODUCTION.....	16
CHAPTER 2 – GEOLOGICAL SETTING	18
2.1 Brasília Belt.....	18
2.2 Alto Paranaíba Igneous Province.....	20
CHAPTER 3 – LITERATURE REVIEW.....	24
3.2 Mantle xenoliths.....	24
3.3 Mantle metasomatism.....	25
3.5 Generation of carbonatite melt in the mantle	27
3.7 Wehlitzitization: a process caused by carbonatite metasomatism	34
3.4.4 Geochemical signatures of clinopyroxenes metasomatized by carbonatite melts	36
3.10 Metasomatism caused by kimberlite melts	38
3.11 Silicate melt metasomatism	41
3.13 Refertilization of the cratonic lithosphere.....	43
CHAPTER 4 – METHODOLOGY.....	46
4.1 Petrography	46
4.2 Electron microprobe analysis	46
4.3 LA-ICP-MS.....	47
4.4 Spectroscopy analysis.....	48
CHAPTER 5 – SCIENTIFIC ARTICLE	49
5.1 Introduction.....	51
5.2 Geological setting	53
5.3 Analytical methods.....	56
5.3.1 Electron microprobe analysis	56
5.3.2 Laser ablation inductively coupled plasma mass spectrometry	57
5.3.3 Raman spectroscopy	58

5.4. Petrography	58
5.4.1 Garnet-phlogopite wehrellites	58
5.4.2 Harzburgite.....	59
5.4.3 Spinel lherzolites	60
5.5 Mineral Chemistry.....	64
5.6 Results of Raman spectroscopy	79
5.7 Geothermobarometry.....	80
5.8 Geochemical modeling of partial melting.....	80
5.9 Discussion	81
5.9.1 The lithosphere beneath the southwestern edge of the SFC	81
5.9.2.1 Primary metasomatism in the deep lithospheric mantle beneath Catalão caused by K-rich hydrous fluids/melts forming low-Ti-Cr phlogopite (Phl1).....	83
5.9.2.2 Carbonate-rich melt metasomatism in the deep cratonic lithosphere recorded by clinopyroxenes from wehrellites and harzburgite	85
5.9.2.3 Proto-kimberlite melt as a metasomatic agent forming high-Ti-Cr phlogopite (Phl2) in the deep lithospheric mantle	89
5.9.3 Lithosphere stratification with multiple metasomatic overprints beneath the southwestern border of the São Francisco Craton: indication for cratonic rejuvenation?	93
5.10 Conclusions	98
5.11 Acknowledgments	100
5.12 References	100
CHAPTER 6 – FINAL CONSIDERATIONS	111
CHAPTER 7 – DISSERTATION REFERENCES	113
CHAPTER 8 – SUPPLEMENTARY MATERIAL	129

LIST OF FIGURES

Dissertation

Figure 1. Cratons and Brasiliano/Pan-African orogenic systems of West Gondwana. Brasília Belt represented by the terrains in the western border of the São Francisco Craton (SFC). K = Kalahari, WA = West Africa, A = Amazonian, P = Paranapanema, DP = Rio de La Plata) (after Alkmin and Martins-Neto, 2012).....	18
Figure 2. Geology of the Brasília fold belt (after Bogossian et al., 2021).....	20
Figure 3. Geological setting of the Alto Paranaíba region (after Oliveira, 2015).....	23
Figure 4. Stability fields of mantle mineral assemblages in pressure-temperature space (from Condie, 2021).....	25
Figure 5. Effect of interfacial energy (θ) on fluid geometry in granular aggregates (after Watson et al., 1990).....	27
Figure 6. Melting of CO_2 -saturated peridotite at moderate pressures in the CMS- CO_2 , CMAS- CO_2 , and in a complex natural system (Hawaiian Pyrolite) (after Hammouda and Keshav, 2015).....	30
Figure 7. Solidus curve for model carbonated lherzolite in the CMAS- CO_2 system (after Dalton and Presnall, 1998).....	31
Figure 8. Weakening and erosion of the cratonic lithosphere. (a) Plume at the base of the cratonic lithosphere generating low degree melts that react with the depleted peridotite. Major magmatism is confined to craton margins – 1. (b) Later episodes of reactivation increase the impregnation points forming linear incisions due to melting of the metasomatic minerals – 2. (c) These linear incisions cause the delamination of large blocks – 3, and lateral erosion by small mantle convection – 4. (d) Melting of amphibole-bearing assemblage forming nephelinites at 80-90 km – 5, and ultramafic lamprophyre at deep mantle – 6 (after Foley, 2008)	45

Article

Figure 1. Simplified geological map from the Alto Paranaíba volcanic rocks in the context of the Mata da Corda Formation (after Barbosa et al., 2012).....	56
Figure 2. Photomicrographs of Catalão mantle xenoliths showing the main mineral assemblages and main textures. (a) Porphyroclastic texture with garnet porphyroclasts rimmed by Cr-spinel and phlogopite (plane-polarized light, sample 1B-139B). (b) Phl2 with kink band and in contact with Cr-Spinel around garnet (plane-polarized light, sample 1B-139A). (c) Zoned phlogopite crystal with Phl1 in the inner and Phl2 in the outer zones (plane-polarized light, sample 1B-139B). (d) Phl2 fills the interstices of the matrix (plane-polarized light, sample 1B-139A). (e) Clinopyroxene with thick spongy rims (plane-polarized light, sample 1A-81). (f) Spinel-orthopyroxene symplectite (plane-polarized light, sample 1A-81). (g) Olivine displaying kink band (crossed-polarized light, sample 1A-81A) (h) Spinel bleb in an equilibrated mantle assemblage (crossed-polarized light, sample 1A-76A). (i) Recrystallization of clinopyroxene (crossed-polarized light, sample 1A-76C). Mineral abbreviations: Ol – olivine, Opx – orthopyroxene, Cpx – clinopyroxene, Grt – garnet, Phl – phlogopite, sp – spinel.....	61

- Figure 3. BSE photomicrographs of garnet-phlogopite wehrlite xenoliths (1B-139A and 1B-139B). (a) Relics of garnet porphyroblast surrounded by Cr-spinel and zoned phlogopite grains (1B-139B). (b) Total consumption of garnet by spinel-pyroxene symplectites and zoned phlogopite grains (1B-139B). (b) Total consumption of garnet formation of Cr-spinel and large Phl2 (1B-139A). (c) Relics of garnet porphyroblast embedded in a large mass of Cr-spinel. Zoned phlogopite at the top shows irregular Phl1 rimmed by Phl2, indicating resorption of Phl1 during the formation of Phl2 (1B-139A). (d) Large garnet porphyroblast rimmed by Cr-spinel lamellae and zoned and homogenous phlogopite crystals (1B-139B). Mineral abbreviations: Grt – garnet, Phl – phlogopite 62
- Figure 4. Trace and rare earth elements diagrams normalized to the primitive mantle (PM, Sun and McDonough, 1989) for orthopyroxenes of harzburgite (a-b) and lherzolites (c-d)..... 65
- Figure 5. Bivariate plots of major and minor elements (wt.%) as a function of Mg# in clinopyroxenes of Catalão xenoliths (circles, squares, and triangles). Experimental (Yaxley and Green, 1998; Rapp et al., 1999; Yaxley, 2000; Wang et al., 2010; Mallik and Dasgupta, 2012; Wang et al., 2013; Gervasoni et al., 2017), and natural studies (Kilian et al., 2002; Schilling et al., 2005) of clinopyroxenes products of silicate melt metasomatism (light blue field). Experimental (Brey et al., 2008; Sokol et al., 2016) and natural studies (Yaxley et al., 1998; Coltorti et al., 1999; Su et al., 2010; Deng et al., 2017; Ionov et al., 2018; Kopylova et al., 2021) of clinopyroxenes products of carbonatite melt metasomatism (light brown field). Natural studies (Kargin et al., 2016; Fitzpayne et al., 2020) of clinopyroxenes products of kimberlite melt metasomatism (purple field). 67
- Figure 6. Trace element (LA-ICP-MS) compositions of clinopyroxenes from garnet-phlogopite wehrlites (a, b) from harzburgite (c, d) and from spinel lherzolites (e, f). Primitive mantle values for normalization are from Sun and McDonough (1989). Each dashed line indicates the percentage of partial melting (F) from 2 to 20 % following the increment of 2 %. See text for details about the parameters employed in the modeling. 68
- Figure 7. Bivariate plots for major and minor elements of the phlogopite types of the studied xenoliths. Fields of phlogopite from metasomatized xenoliths worldwide (pink field “M”), H-Ti phlogopite from mantle xenoliths including polymict breccia (brown field, “H-Ti”), phlogopites from kimberlite groundmass (green field, “K”) are from Giuliani et al. (2016). High-Ti-Cr phlogopite around garnet from metasomatized xenoliths (grey field “H-Ti-Cr”), Low-Ti-Cr phlogopite around garnet from metasomatized xenoliths (light purple field “L-Ti-Cr”) are from Kargin et al. (2019). The arrows show compositional trends towards more evolved compositions of groundmass phlogopite. 70
- Figure 8. Trace elements of phlogopite of the grt-phl wehrlites xenoliths normalized to the primitive mantle (Sun and McDonough, 1989). 71
- Figure 9. Raman spectra between 120 and 1300 cm⁻¹ of analyzed olivine (a, b), dolomite (a), and magnesite (b) (all indicated in black). The overlapped spectrum in blue is relative to olivine (ID R040052; RUFFTM) while red ones represent the carbonates (dolomite ID R050357.2 and magnesite ID 040114; RUFF™)..... 79
- Figure 10. (a) Plots of Ca/Al (atomic ratios) vs. Mg# of clinopyroxenes. Experimental and natural studies of clinopyroxenes metasomatized by carbonatite melts (light brown field) are from Yaxley et al. (1998), Coltorti et al. (1999), Brey et al., (2008), Su et al. (2010), Su et al. (2016), Sokol et al. (2016), Deng et al. (2017), Ionov et al. (2018), and Kopylova et al. (2021). Clinopyroxenes metasomatized by silicate-carbonate melts are from Neumann et al. (2002). Experimental and natural studies of clinopyroxenes metasomatized by silicate melts (light blue field) are from Yaxley and Green (1998), Rapp et al. (1999), Yaxley (2000), Kilian et al. (2002), Schilling et al. (2005), Wang et al. (2010), Mallik and Dasgupta (2012), Wang et al. (2013), and Gervasoni et al. (2017). (b) Plots of La/Yb_N vs. Ti/Eu ratios of clinopyroxenes and garnet (stars). The Grey area represents carbonatite

metasomatism from Coltorti et al. (1999). (c-d) Plots of Sr vs. Ti/Eu and Ti/Nb vs. Zr/Hf of clinopyroxenes. The field of clinopyroxenes metasomatized by carbonate melts (light brown field) is from Coltorti et al. (1999), Zheng et al. (2005), McCoy-West et al. (2015), Su et al. (2016), Deng et al. (2017), Ionov et al. (2018) and Pattnaik et al. (2020). Clinopyroxenes metasomatized by silicate-carbonate melts (pink field) are from Neumann et al. (2002). Clinopyroxenes metasomatized by silicate melts (light blue field) are from Zhang et al. (2011) and Potkó et al. (2020). Arrows show metasomatic trends for carbonatite and silicate metasomatisms. Stars represent garnet compositions.	88
Figure 11. Selected trace elements vs. Ti of clinopyroxenes of spinel lherzolites from Catalão show a strong positive correlation.	93
Figure 12. (a) Metasomatic events in the SW border of the SFC. (b) Reaction between volatile-rich fluid and garnet forming Phl1, Cr-Spinel, and carbonate. (c) Wehrlitization caused by carbonatite melt. During this process, carbonate inclusions in olivine were formed. (d) At this stage proto-kimberlite melt reacts forming Phl2 and consuming Phl1. (e) Cryptic metasomatism caused by silicate melt. Some clinopyroxenes display enrichment in incompatible elements.	97

TABLE LIST

Article

Table 1. Sample list with a summary of modal data and temperature and pressure estimates.	63
Table 2. Major element compositions of the mineral phases from Catalão, SFC.	72
Table 3. Trace element compositions of the mineral phases from Catalão, SFC.....	75

Supplementary material

Table S1. LA-ICP-MS trace element data of calibration reference materials (NIST612, 355OL, BHVO-2G and BR-1G).....	133
Table S2. Major elements of each analyzed olivines from the Catalão xenoliths.	135
Table S3. Major elements of each analyzed orthopyroxenes from the Catalão xenoliths.	149
Table S4. Major elements of each analyzed clinopyroxenes from the Catalão xenoliths.	162
Table S5. Major elements of each analyzed spinel from the Catalão xenoliths.	180
Table S6. Major elements of each analyzed garnet from the Catalão xenoliths.....	190
Table S7. Major elements of each analyzed phlogopite from the Catalão xenoliths.....	193
Table S8. Trace elements of each analyzed olivine from the Catalão xenoliths	203
Table S9. Trace elements of each analyzed orthopyroxene from the Catalão xenoliths.	210
Table S10. Trace elements of each analyzed clinopyroxene from the Catalão xenoliths.....	216
Table S11. Trace elements of each analyzed garnet from the Catalão xenoliths.	223
Table S12. Trace elements for each analyzed phlogopite from the Catalão xenoliths.	225

RESUMO EXPANDIDO

1. Introdução

Xenólitos mantélicos são fragmentos do manto litosférico trazidos a superfície por vulcanismo geralmente de natureza alcalina (ex., kimberlito). Essas amostras fornecem informações diretas sobre os processos ocorridos em diversas profundidades da coluna litosférica, como fusão parcial e metassomatismo. Esses dois processos são responsáveis pelas heterogeneidades no manto, uma vez que os processos de fusão parcial causam depleção da litosfera mantélica e o metassomatismo gera re-enriquecimento (i.e., refertilização) ([Tang et al., 2013](#); [Aulbach et al., 2013](#)).

Quando essas reações metassomáticas ocorrem na base da litosfera mantélicas abaixo de cráttons, os peridotitos depletados que tipicamente constituem essas regiões tem sua química e mineralogia modificadas ([Foley, 2008](#)). Dessa forma, esses peridotitos depletados são substituídos por peridotitos que representam um manto fértil, como lherzolitos e wehrlitos ([Kelemen et al., 1998](#); [Ionov et al., 2005, 2018](#); [Gervasoni et al., 2017](#)). Além disso, essas reações podem gerar fases minerais hidratadas como flogopitas e anfibólios ([Giuliani et al., 2014, 2016](#); [Tappe et al., 2018](#); [Kargin et al., 2019](#); [Gervasoni et al., 2022](#)).

Essas reações metassomáticas na base da litosfera cratônica podem causar diversas modificações como, o aumento da densidade devido aos processos de refertilização, modificação do estado de oxidação e redução da temperatura de fusão dessa porção da litosfera, uma vez que essas assembleias hidratadas fundirão em temperaturas bem mais baixas em eventos posteriores quando comparadas com as fases minerais anteriormente presentes nos peridotitos depletados (olivina e ortopiroxênio) ([Foley, 2008](#); [Tang et al., 2013](#)). Assim, esses eventos de refertilização podem acarretar

uma desestabilização dessas porções do manto litosférico e posterior afinamento (Foley, 2008).

A partir disso, este estudo visa compreender a evolução do manto litosférico abaixo do cráton do São Francisco, especificamente abaixo da região de Catalão, GO. Para isso foram estudadas amostras de xenólitos peridotíticos representativos de diversas profundidades do manto (fácies espinélio e granada). As análises petrográficas, de química mineral (elementos maiores e traços) e espectroscopia Raman associadas a cálculos de pressão e temperatura e modelagens de fusão parcial indicaram que o manto abaixo da região de Catalão é estratificado. O manto profundo (~170 km) interagiu com líquidos de diversas naturezas enquanto o manto mais raso (~50 km) registra principalmente eventos de fusão parcial.

2. Métodos

Inicialmente foram realizadas descrições sistemáticas das texturas, estruturas de deformação e contagens das fases minerais para classificação dos peridotitos. Foram contados 3.000 pontos por lâminas com o uso do software JMicroVision e posteriormente foi utilizado o microscópio de luz transmitida da Universidade Federal de Goiás para maior detalhamento. Para a obtenção dos elementos maiores nas fases minerais primárias e metassomáticas (olivina, ortopiroxênio, clinopiroxênio, espinélio, granada e flogopita) foi utilizada a EPMA (Electron Probe Micro Analyzer) do Instituto de Brasília, Universidade de Brasília. Para a obtenção dos elementos traços nas mesmas fases minerais foi utilizado o LA-ICP-MS (Laser Ablation Inductively Coupled Plasma Mass Spectrometry) da Universidade de Münster, Alemanha. A caracterização das inclusões minerais dentro dos cristais de olivina foi realizada com o uso do espectrômetro Raman, Instituto de Física, Universidade de Brasília.

3. Resultados e discussões

Os peridotitos estudados variam de espinélio lherzolitos (876-915 °C; 1,5 GPa) e harzburgito contendo clinopiroxênio (914 °C; 5,28 GPa) a granada-flogopita wehrlitos (1066-1101 °C; 5,03-5,23 GPa). A composição química desses peridotitos revelam um manto litosférico subcontinental estratificado sob o Cráton do São Francisco. O manto mais profundo (~170 km) passou por vários eventos metassomáticos, enquanto o manto mais raso é caracterizado por fusão parcial com poucas evidências de metassomatismo. O manto profundo sofreu ~10 % de fusão parcial e registra episódios metassomáticos causados por fluidos ricos em álcalis, líquidos carbonatíticos e proto-kimberlíticos.

Os granada-flogopita wehrlitos e harzburgitos que representam o manto profundo sofreu ~10 % de fusão parcial e posterior metassomatismo. Apresentam fases minerais metassomáticas como clinopiroxênios e flogopitas. A geração da flogopita de baixo Ti-Cr (Ph11) que ocorre associada a Cr-espinélio ao redor da granada em granada-flogopita wehrlitos é devido as reações metassomáticas, envolvendo fluidos ricos em álcalis (K_2O , H_2O , CO_2 , F, ± Cl). Essa flogopita possui composição semelhante a flogopita de xenólitos metassomatizados ao redor do mundo e xenocristais de flogopita presente em kimberlitos. A reação entre fluidos ricos em álcalis e peridotitos geraram os cristais de flogopita com baixo teor de Ti e Cr, Cr-espinélio e carbonato às custas de granada.

Os cristais de clinopiroxênio com alto teor de Cr e baixo teor de Al presentes em granada-flogopita wehrlitos e harzburgito apresentam altas razões de Mg#, Ca/Al, La/Yb_N, Zr/Hf e altos teores de Sr, além de razões baixas a intermediárias de Ti/Eu e Ti/Nb, sugerindo que foram gerados por reações envolvendo líquidos de composição carbonatítica. As olivinas presentes em granada-flogopita wehrlitos e harzburgito contêm inclusões de carbonato identificadas por espectroscopia Raman como magnesita

(picos em 213, 330, 738 e 1095 cm⁻¹) e dolomita (picos em 175, 300, 723 e 1097 cm⁻¹), reforçando a hipótese de metassomatismo por líquido rico em carbonato.

A flogopita que apresenta alto Ti-Cr (Phl2) ocorrem como bordas ao redor de Phl1 e como cristais ao redor de granada e na matriz. A composição desta flogopita é semelhante a flogopita de brechas polimíticas do manto. Além disso, essa Phl2 presente nas amostras de wehrlitos são também semelhantes a outras flogopitas alto Ti-Cr observadas nos crátons Kaapvaal e Leste Europeu. Flogopitas alto Ti-Cr são interpretadas como produtos de metassomatismo de afinidade proto-kimberlítica no manto profundo. Essas flogopitas não apresentam afinidade geoquímica com flogopitas cristalizadas a partir de líquidos kimberlíticos em níveis crustais, como as flogopitas presentes na matriz de kimberlitos. Dessa forma, a Phl2 presente nos wehrlitos são classificadas como flogopitas primárias, i.e., flogopitas geradas no manto profundo.

Por outro lado, o manto mais raso (~50 km), representado por espinélio lherzolitos, registram essencialmente processos de fusão parcial (2-4 %) e leve enriquecimento em elementos incompatíveis. Os cristais de clinopiroxênio dessas amostras apresentam alto teor de Al e baixo teor de Cr e alguns mostram leve enriquecimento em LILE, LREE e Ti. Também apresentam baixas razões Ca/Al, alto Mg#, baixas razões La/Yb_N, Zr/Hf e baixos conteúdos de Sr. Além disso, apresentam altas razões de Ti/Eu e Ti/Nb e fortes correlações positivas entre Ti e HFSE e LREE, sugerindo interação com líquido silicático subalcalino empobrecido em elementos incompatíveis.

4. Conclusões

Os xenólitos mantélicos da região de Catalão, porção sudoeste do Cráton do São Francisco, centro-oeste do Brasil, forneceram informações valiosas sobre a natureza e a

evolução da litosfera continental. As composições químicas dos minerais, juntamente com dados geotermobarométricos e estimativas de fusão parcial, indicam que o manto litosférico subcontinental sob a região de Catalão é estratificado. A refertilização nas partes mais profundas do Cráton do São Francisco é atribuída a fluidos e líquidos gerados por baixas taxas de fusão, ambos enriquecidos em elementos incompatíveis que reagiram com os peridotitos empobrecidos tipicamente presentes na raiz de litosfera cratônica de idade Arqueana. Esse processo modifica química e mineralogicamente a litosfera, podendo gerar grandes impactos na estabilidade tectônica do cráton.

CHAPTER 1 – INTRODUCTION

The stability of a craton owes much to its thick, cold, and chemically depleted mantle lithosphere (Foley, 2008). However, the advance in geophysical methods and the continuum studies of mantle xenoliths as well as inclusions in diamonds have demonstrated that the ancient and depleted lithosphere mantle beneath the crust of cratons has been chemically modified at some locations by interactions with deep-seated fluids and melts. These reactions re-enrich the depleted peridotites in incompatible elements that had been lost during the extensive episodes of partial melting processes along the geological time.

The introduction of incompatible elements occurs through the chemical modification of pre-existing minerals (cryptic metasomatism) and also by the addition of exotic minerals (modal metasomatism). Geochemical studies of cratonic magmatism coupled with xenolith studies have shown that rejuvenation and erosion of cratonic lithosphere are very common processes (Foley, 2008; Tang et al., 2013). These processes have a great impact on the stability of cratonic regions. Therefore, the conventional view that cratons act as inert objects onto which continental crust is accreted and is not affected by the opening and closing of oceanic basins has been reviewed.

Metasomatic reactions in distinct depths of the São Francisco cratonic lithosphere have been revealed by geophysical and mantle xenoliths data (Costa, 2008; Almeida et al., 2014; Pinto et al., 2010). Magnetotelluric deep soundings, gravity, and geoid modeling indicated rejuvenation of the southern part of the São Francisco cratonic lithosphere caused by interactions with carbonatite and melts enriched in Fe and H₂O, leading to the oxidation of the deep lithosphere, and also adding metasomatic minerals in depths beyond 120 km (Pinto et al., 2010). Oxidation of the lithosphere coupled with

the addition of hydrated minerals plays an important role in the partial melting process (Foley, 2008). Oxidizing conditions and the presence of CO₂ and H₂O seems to be prerequisite for the formation of carbonatite and kimberlite during partial melting (Foley, 1989). In addition, mantle xenoliths of spinel and garnet facies from the São Francisco Craton (hereafter SFC) containing hydrated and exotic minerals (e.g., pargasite, phlogopite, mathiasite-loveringite, and priderite) were already reported (Costa, 2008; Almeida et al., 2014; Nannini, 2016). Therefore, the São Francisco Craton lithosphere shows evidence of widespread metasomatism.

In the context described above, this study provides the first mineral chemistry data (major and traces elements) of mantle xenoliths from the Catalão region, southwestern border of the São Francisco Craton, which are equilibrated at spinel and garnet facies. Based on these results, this research aims to provide evidence and contribute to a better understanding of the partial melting and distinct metasomatic events recorded by silicate minerals from the peridotite xenoliths of the Catalão region.

CHAPTER 2 – GEOLOGICAL SETTING

2.1 Brasília Belt

The Brasília, Araguaia, and Paraguay belts constitute the Tocantins Province. They were formed during the amalgamation of West Gondwana. The Brasília Belt extends for approximately 1100 km in the N-S direction and surrounds the west and southwest border of the SFC (Fig. 1). The Rio Preto, Riacho do Pontal and Sergipano belts define the northern boundary, while the Araçuaí and Ribeira belts border the southern tip of the SFC (Fuck et al., 2017). The Brasília Belt is the result of the Neoproterozoic Gondwana assembly, developed during the collision between Amazonian and São Francisco paleoplates and Paranapanema micro-continent at 670-610 Ma (Valeriano et al., 2008, Valeriano, 2017) (Fig. 1).

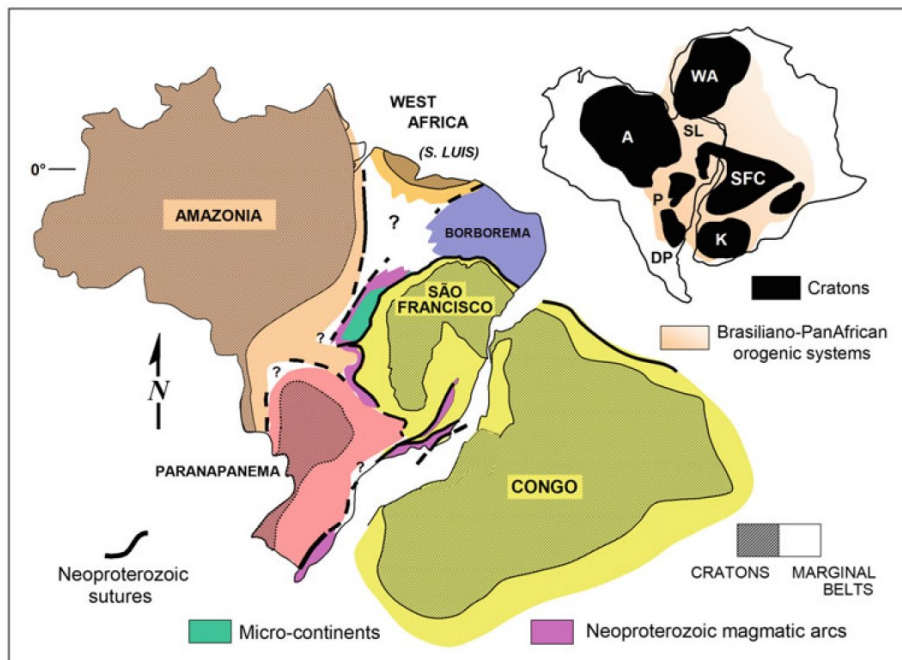


Figure 1. Cratons and Brasiliano/Pan-African orogenic systems of West Gondwana. Brasília Belt represented by the terrains in the western border of the São Francisco Craton (SFC). K = Kalahari, WA = West Africa, A = Amazonian, P = Paranapanema, DP = Rio de La Plata) (after Alkmin and Martins-Neto, 2012).

The Brasília Belt (Fig. 2) is composed of a thick package of passive margin sedimentary deposits, younger deep-sea sediments associated with volcanic arc rocks, as well as an ophiolite mélange, arc type rocks, and calc-alkaline volcanics and intrusives, and S-type collisional granites ([Fuck et al., 2017](#)). The metamorphic conditions increase to the west and vary from greenschist to amphibolite and granulite facies ([Valeriano et al., 2008](#)), with the metamorphic peak constrained at 790 and 630-610 Ma ([Pimentel et al., 1997](#)).

The tectonic framework of the southern Brasília Belt, where the studied area is located, can be defined as follows, from the base to the top (or from east to west): (1) the cratonic zone composed of basement assemblages older than 1.8 Ga unconformably overlain by the Neoproterozoic Vazante (composed of metapelite and metadolomites) and Bambuí (composed of calcilutites, stromatolitic dolomites, calcarenites, metapelites, and limestones) groups ([Alkmim and Martins-Neto, 2012](#)). The cratonic basement is comprised of Archean granite-greenstone complexes.

(2) the external metamorphic fold-thrust belt is formed of the Paranoá, Canastra, and Ibiá groups, with maximum ages of sedimentation of 1.04 Ga, 1.0 Ga, and 0.9 Ga, respectively ([Rodrigues et al., 2010; Matteini et al., 2012](#)).

(3) the upper nappe complex intensely metamorphosed, reaching granulite facies, is mainly represented by the rocks of the Araxá Group (composed of metapelitic schists and paragneisses, fewer quartzites). The youngest detrital zircon age is constrained at 0.6 Ga ([Valeriano et al., 2017](#)). The Anápolis-Itauçu complex is a high-grade terrane characterized by metamorphic rocks of granulite facies. This high-grade metamorphism was dated at 633 ± 28 Ma ([Fischel et al., 1998](#)) (Fig. 2).

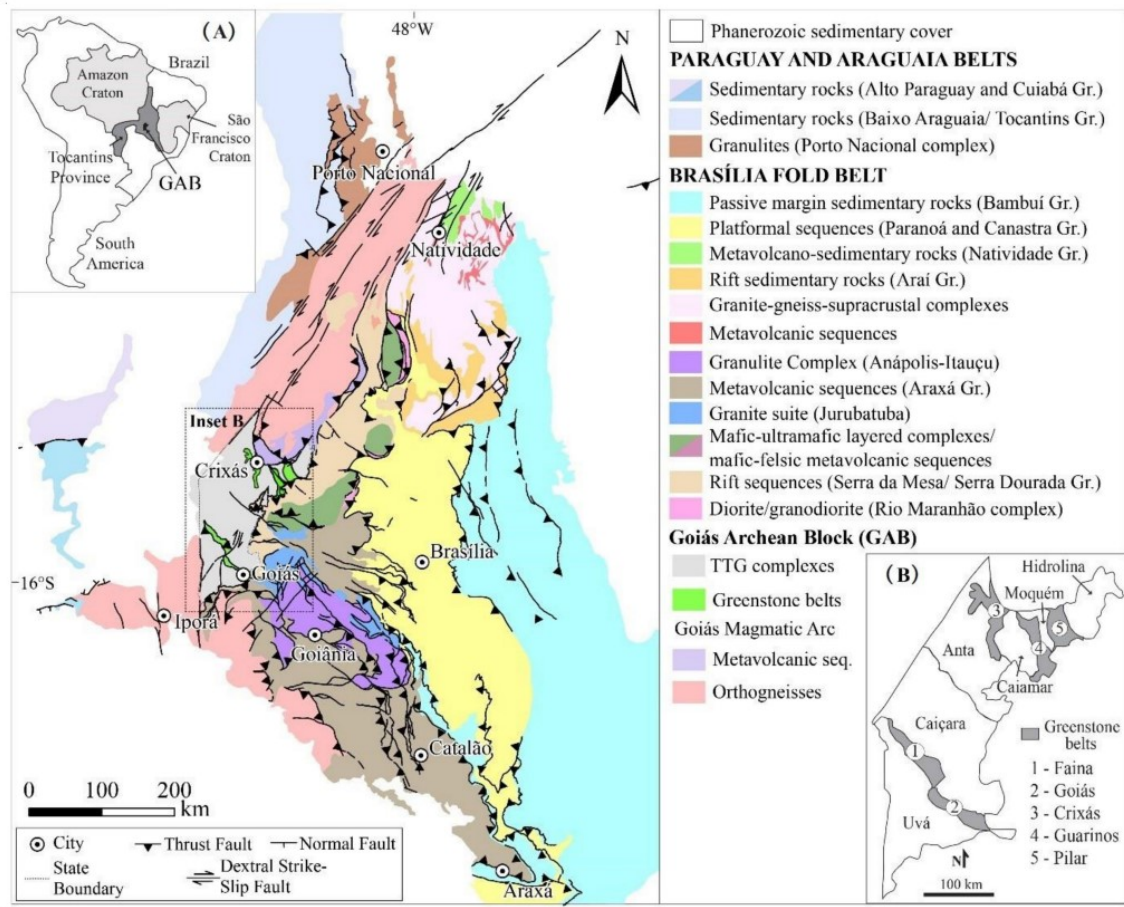


Figure 2. Geology of the Brasília fold belt (after Bogossian et al., 2021).

2.2 Alto Paranaíba Igneous Province

The Alto Paranaíba Igneous Province (hereafter APIP) is located in southeast Minas Gerais and southwest Goiás states and is one of the numerous provinces that occur around the margin of the Paraná Basin (see a review of other alkaline provinces in the South American Platform in Ferreira et al. (2022)). The APIP represents one of the most voluminous potassic provinces in the world, covering an area of approximately 20,000 km² (Araújo et al., 2001; Comin-Chiaromonti and Gomes, 2005; Guarino et al., 2013) (Fig. 3). The APIP together with other alkaline provinces forms the large NW-SE-trending zone (Azimuth 125°) of Late Cretaceous that extends for 2,000 km (Gibson et al. 1995). This NW-SE lineament is theorized by some authors as the record of a

plume track (Gibson et al., 1995; Thompson et al., 1998). On the surface, the APIP rocks are emplaced at the SE end of the metamorphosed and deformed Proterozoic supracrustal sequences of the Brasília Belt.

The definition of the western cratonic boundary of the SFC has been a matter of continuous debate. However, geophysical (e.g., Bouguer anomaly) and seismic tomographic data have evidenced a larger extent for the western border of the São Francisco Craton than that observed on the surface (Assumpção et al., 2004, 2017; Pereira and Fuck, 2005; Rocha et al., 2011, 2019). These studies, integrated with geochemical data of xenoliths and xenocrysts hosted by kimberlites from APIP, confer the status of cratonic domain rather than the mobile belt for this complex tectonic setting (Gibson et al., 1995; Carlson et al., 2007; Carvalho et al., 2022; Fernandes et al., 2021). In this context, the APIP would be underlain by an ancient cratonic lithosphere overlain by deformed rocks units of the easternmost portion of the Brasília Belt.

The APIP is composed of mafic potassic to ultrapotasssic alkaline magmatism that was emplaced as plugs, dykes, diatremes, lava flows, pyroclastic deposits, and plutonic intrusions (Brod et al., 2000; Araújo et al., 2001). The rock types identified in this province include kimberlite, lamproite, lamprophyre, kamafugite, and small carbonatite intrusions. Bebedourite, dunite, perovskitite, tinguaita, trachyte, phoscorite, glimmerite, melilitite, and basanite-ankararitite occur in subordinate amounts (Gibson et al., 1995; Brod et al., 2000, Gomes and Comin-Chiaromonti, 2005; Carlson et al., 2007; Barbosa et al., 2012). Spinel and garnet peridotite xenoliths are also reported hosted by the alkaline volcanic rocks (Danni and Gaspar, 1994; Almeida et al., 2014; Fernandes et al., 2021).

One of the most important magmatic events in the APIP is represented by the lava flows and tuff beds of the Mata da Corda Formation, which cover an area of ~8,000

km^2 , with a thickness of ~100-120 m (Sgarbi et al., 2000; Read et al., 2004; Guarino et al., 2013). This formation is chiefly composed of kamafugites and alkaline-carbonatite complexes, with fewer amounts of alkaline intrusions (Read et al., 2004; Comin-Chiaromonti and Gomes, 2005; Guarino et al., 2013). Most of the alkaline rocks of APIP were formed in a wide time span, ranging from 91 to 71 Ma (Bazzi, 1995; Gibson et al., 1995; Read et al., 2004; Guarino et al., 2013, 2017; Felgate, 2014). However, older rocks are present, like the diamond-bearing Canastra-1 kimberlite, with ages around 120 Ma (Pereira and Fuck, 2005). The youngest magmatic event is represented by kamafugites with radiometric ages obtained by U-Pb dating of perovskite from Mata da Corda kamafugites ranging from 81 to 61 Ma (Sgarbi et al., 2000; Read et al., 2004).

The source of the APIP magmatism remains a matter of debate. The two main models include mantle plume influence (e.g., Gibson et al., 1995; Thompson et al., 1998) and melting of a heterogeneous and enriched lithospheric mantle (Araújo et al., 2001; Carlson et al., 1997). However, the geochemical and isotopic data of kimberlites and kamafugites of the APIP indicate the melting of an enriched mantle source, without any sign of a mantle plume. The high concentrations of incompatible elements in the kamafugites ($\text{La/Yb}_N = 50\text{-}136$; where N = chondritic normalized values) and kimberlites ($\text{La/Yb}_N = 91\text{-}155$) of the APIP indicate a veined mantle source rather than depleted lherzolites and harzburgite peridotites (Comin-Chiaromonti and Gomes, 2005).

This enrichment in the lithospheric mantle was probably caused by (1) fluids or melts derived from subducted slabs (Maury et al., 1992) or (2) volatile-bearing small volume melts derived from the asthenosphere that have veined the overlying lithospheric mantle at distinct depths and times (Foley et al., 1992, 2008). The constant behavior of the $^{147}\text{Sm}/^{144}\text{Nd}$ ratios (0.085 ± 0.009) in the APIP allowed Comin-Chiaromonti and Gomes (2005) to consider that the Nd model ages are indicative of the

main metasomatic event, which was constrained at 0.99 ± 0.10 Ga. The Sr-Nd-Pb initial ratios indicate that the APIP magmatism is derived from a mixture between dominant enriched mantle (EMI) and subordinate HIMU components (Bazzi et al., 1993, 1995; Danni and Gaspar, 1994; Toyoda et al., 1994; Meyer et al., 1994; Gibson et al., 1995; Araújo et al., 2001). $^{187}\text{Os}/^{188}\text{Os}$ isotopic data coupled with Sm-Nd model ages indicate that kimberlites from APIP are derived from lithospheric mantle sources that were variously Re-depleted, probably at the late Archean to mid-Proterozoic times (Araújo et al., 2001; Carlson et al., 2007). At approximately 1 Ga these lithospheric sources were enriched in LILE by fluid/melt metasomatism, possibly during the mobile belt formation along the western border of the São Francisco Craton (Araújo et al., 2001; Comin-Chiaromonti and Gomes, 2005).

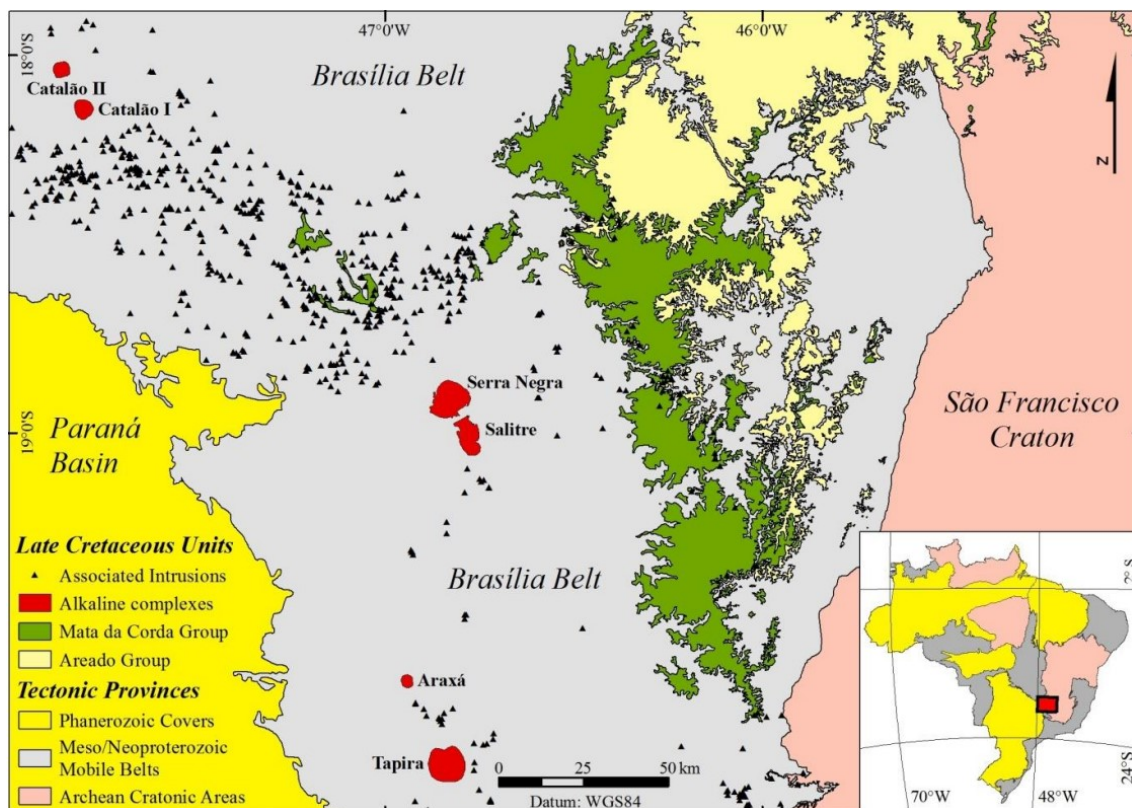


Figure 3. Geological setting of the Alto Paranaíba region (after Oliveira, 2015).

CHAPTER 3 – LITERATURE REVIEW

3.2 Mantle xenoliths

A critical advance in the understanding of Earth's geodynamics emerged with the increasing studies of peridotite massifs and mantle xenoliths together with studies of physical properties recorded by geophysical data (Downes, 2001; O'Reilley and Griffin, 2013). In contrast to massifs that provide field relations and proportions of the mantle lithologies, mantle xenoliths provide snapshots of a larger vertical mantle section beneath a single locality in cratonic and noncratonic regions. In addition, differently from massifs peridotites, which are tectonically emplaced, mantle xenoliths are rapidly transported to the surface, precluding a re-equilibration during its ascent. Therefore, the study of mantle xenoliths provides direct insights into the mantle processes even right before their host magma generation. They can record the removal and/or addition of melt, including reactions with fluids derived from the subducted slab or asthenospheric upwelling (Downes, 2001). Since xenoliths are equilibrated at mantle depths the use of geothermobarometric equations applied to equilibrated mineral pairs assists the definition of geotherms through the lithosphere, which has a crucial role in the understanding of the mantle geodynamic.

Xenoliths from any tectonic setting are commonly found in volcanic rocks of alkaline nature such as (i) alkali basalts sensu lato (alkali basalt-basanite and more evolved derivatives), nephelinites, and melilitites; (ii) lamprophyres and related magmas (e.g., minettes, monchiquites, and alnoites) and lamproites; and (iii) kimberlites series (groups I, II and transitional) (Pearson et al., 2003).

The lithological variability of mantle xenoliths is normally ascribed to the host volcanic rock type and the tectonic settings. Magmatism in cratonic regions (e.g.,

kimberlites) sample suites of xenoliths from crustal levels to more than 200 km depth, which are frequently depleted in composition, whereas in off-craton regions the xenoliths are less depleted and come from depths less than 100 km (Boyd, 1989; Griffin et al., 1998, 1999, 2003, 2009; O'Reilly et al., 2001; Pearson et al., 2003). Therefore, volcanism of kimberlitic-affinity frequently samples peridotites belonging to spinel and garnet-facies, whereas, alkaline basalts, nephelinites, melilitites, and lamprophyres in off-craton regions tend to sample peridotites belonging predominantly to spinel-facies. The shallower mantle is represented by peridotites equilibrated at the plagioclase stability field (e.g., plagioclase lherzolite), which are more commonly observed in ophiolites (Fig. 4).

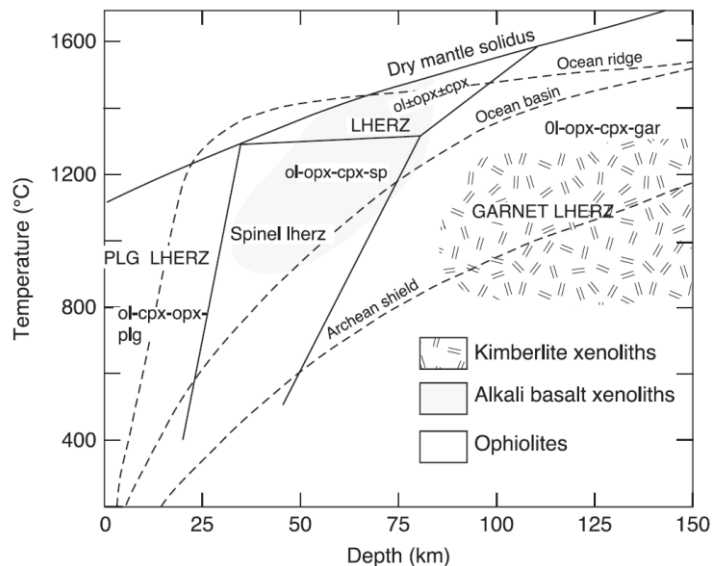


Figure 4. Stability fields of mantle mineral assemblages in pressure-temperature space (from Condie, 2021).

3.3 Mantle metasomatism

Studies of mantle xenoliths, xenocrysts, and peridotite massifs were crucial to the introduction of the concept of mantle metasomatism in the early 1970s (O'Reilly

and Griffin, 2013). In early studies, a considerable discussion took place concerning the chemical modification of xenoliths, which can occur during their ascent or even in their residence in the mantle. The infiltration of melts and exsolved fluid from the host magma into the xenoliths along cracks and grain boundaries is frequently observed in mantle xenoliths worldwide (O'Reilly and Griffin, 2013). This interaction can form veins into the xenoliths constituted by mineral assemblage typical of the host magma composition or secondary minerals at expense of the peridotitic assemblage.

Metasomatic processes that cause chemical and mineralogical heterogeneities in the upper mantle involve an enormous variety of types, such as silicate melts (mafic to ultramafic); carbonatite melts; C-O-H fluids ranging from water to CH₄ and CO₂; dense brines; and hydrocarbon-bearing fluids (O'Reilly and Griffin, 2013; Gervasoni et al., 2017). These fluids can migrate through the mantle in two main ways: grain-boundary migration and crack propagation. The infiltration of fluids along grain boundaries is an effective mechanism of cryptic metasomatism and also stealth metasomatism by reactions with pre-existing minerals (O'Reilly and Griffin, 2013). However, the infiltration of fluids by grain boundary migration is controlled by interfacial energy, turning this mechanism into a slow process compared to fluid infiltration by crack propagation (O'Reilly and Griffin, 2013). The composition of the fluid dictates the rate of grain-boundary infiltration. Some fluid composition forms low wetting angles with olivine grain boundaries forming a continuous 3-dimensional network and making this fluid an important mechanism for pervasive metasomatism (e.g., Bodinier et al., 1990; Le Roux et al., 2007) (Fig. 5). This explains the effectiveness of carbonatite as metasomatic agents since they form a low wetting angle with olivine grain boundaries. In contrast, silicate melts, and H₂O-CO₂ fluids have high wetting angles with olivine

grain boundaries and tend to form disconnected pores at grain boundaries (Watson et al., 1990) (Fig. 5).

Otherwise, crack propagation produces instantaneous movement of significant volumes of fluid. This is the way that magmas ascent through the mantle. The crack formation is due to fluid overpressure. Evidence of this process is recorded in mantle xenoliths and peridotite massifs. Straight-sided dikes cross-cutting other structures in peridotite massifs, as well as metasomatized xenoliths containing veins filled with secondary phases such as amphibole and mica, are strong evidence of crack propagation by fluid overpressure (O'Reilly and Griffin, 2010).

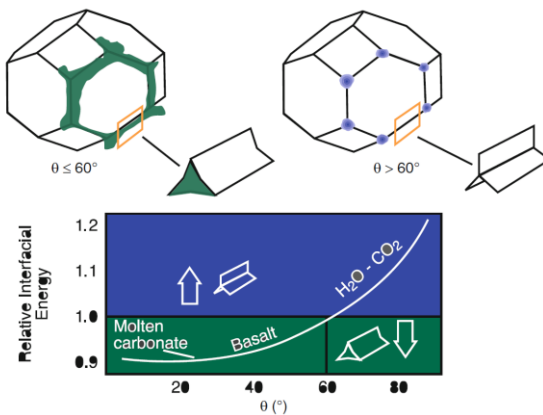


Figure 5. Effect of interfacial energy (θ) on fluid geometry in granular aggregates (after Watson et al., 1990).

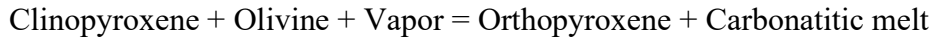
3.5 Generation of carbonatite melt in the mantle

The generation of melts with carbonatite affinity in mantle depths is complex and has an important role in the global geodynamics and geochemical cycles (Dasgupta and Hirschmann, 2007, 2010; Ghosh et al., 2007). The generation of these melts can occur in the mantle beneath continental regions as well as in oceanic basins (Dasgupta and Hirschmann, 2006). However, the occurrence of this magmatism on the surface (e.g., carbonatite and kimberlites) is rare and usually restrict to cratonic regions. Studies

involving thermal modeling of subducting plates show that significant amounts of carbonates can be recycled to great mantle depths without undergoing dissociation, which is the main process responsible for C replenishment in the mantle (Kerrick and Cannolly, 2001). The form in which C will be stored will depend on the depth and oxygen fugacity, occurring in its reduced form as diamond, graphite, carbonates, and CO₂ in the oxidized form (Luth, 1993, 1999; Dasgupta and Hirschmann, 2006). Despite advances in the understanding of the generation of these magmas through seismic, experimental, mantle xenoliths, and diamonds studies, different origins have been proposed for the generation of these melts in the mantle (Dalton and Presnall, 1998; Pilbeam et al., 2013; Kamenetsky and Yaxley, 2015), which include a low degree of partial melting of peridotites in the presence of CO₂, and the separation from a silicarbonated melt by liquid immiscibility (Lee and Wyllie, 1997). The wide variation of the major components of carbonate melts, including variable degrees of enrichment in alkali and trace elements, associated with different isotopic signatures identified in carbonatites, makes it difficult to understand the generation of these melts through experimental and natural studies.

The possibility of carbonatitic melts being generated in the upper mantle has spurred experimental studies involving the melting of synthetic carbonated peridotites (Wyllie and Huang, 1976a; Eggler, 1978). These studies showed that carbonatitic melts can be generated at pressures greater than 2-3 GPa, which would be CO₂ enriched (>40 wt.%) and compositionally similar to carbonatitic lavas, while melts generated at pressures lower than 2 GPa would have silicate compositions with low amounts of dissolved CO₂ (Luth, 1999; Gudfinnsson and Presnall, 2005). Figure 6 shows the equilibrium ranges for CO₂, carbonates, and carbonatitic melt. The negative slope on the solidus in CMS-CO₂ (CaO-MgO-SiO₂-CO₂) and CMAS-CO₂ (CaO-MgO-Al₂O₃-SiO₂-

CO_2) systems, shown in Figures 6 and 7 (curved region) was observed in several experimental studies and called **carbonate ledge** ([Eggle, 1987a](#)), where the reaction below occurs:



According to [Dalton and Presnall \(1998\)](#), the ledge is caused by the intersection of two curves in the P-T diagram, generating an invariant point where the mineral assemblage, vapor phase, carbonate, and melt coexist. The melt generated along the ledge (in equilibrium with olivine, orthopyroxene, clinopyroxene, and vapor) in the CMS- CO_2 system between 2.5 and 2.8 GPa was determined by [Willie and Huang \(1975\)](#) to be of carbonatitic composition.

According to [Eggle \(1987\)](#), the vapor solubility gradually increases in the melt phase from ~2 to 3 GPa, which could be the cause for the appearance of the ledge. This increase in solubility with increasing pressure along the ledge would be responsible for modifying the composition of an unsaturated basaltic melt (5 wt.% CO_2), up to carbonatitic compositions, when maximum solubility is reached. More recent studies conducted by [Keshav and Gudfinnsson \(2013\)](#) and [Novella et al. \(2014\)](#) confirmed this hypothesis. According to these authors, the range in which the increase in solubility is significant is between 1.9 and 2.1 GPa, generating melts with carbonatitic compositions (40 wt.% CO_2) at 2.1 GPa, while silicate melts (7 wt.% CO_2) would be generated at 1.9 GPa.

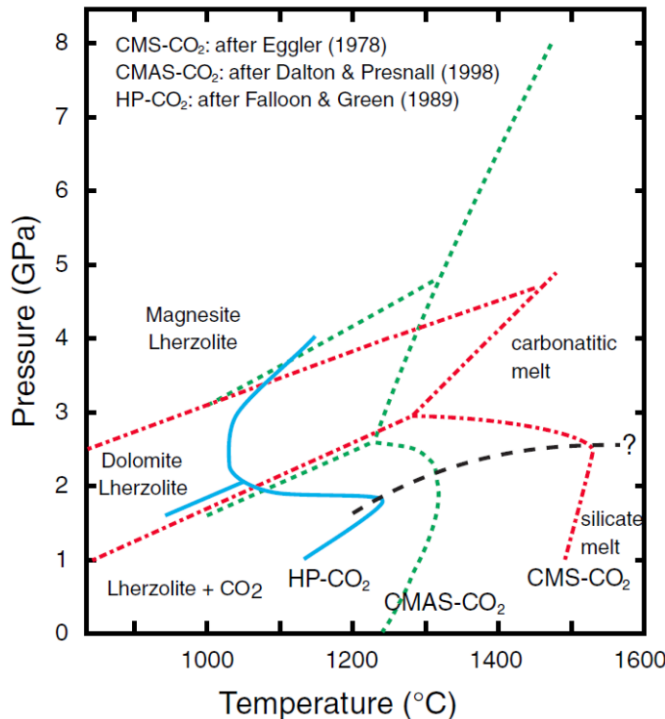
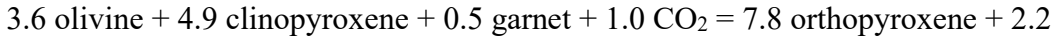


Figure 6. Melting of CO₂-saturated peridotite at moderate pressures in the CMS-CO₂, CMAS-CO₂, and in a complex natural system (Hawaiian Pyrolite) (after Hammouda and Keshav, 2015).

Therefore, the ledge represents the barrier beyond which CO₂ is not stable. Above the ledge (>2.5 GPa), the vapor phase reacts with silicate minerals to form carbonates or carbonatitic melts, while below the ledge the carbonates undergo decarbonation and release CO₂. Experimental studies determined the solidus position of a lherzolite containing CO₂ in the CMAS-CO₂ system, with pressures varying from 3 to 7 GPa, through the location of two invariant points (I₁ and I₂) in P-T diagrams, where a liquid phase of carbonatitic composition coexisted with olivine, orthopyroxene, clinopyroxene, garnet and carbonate (Dalton and Presnall, 1998) (Fig. 7). I₁ represents the transition from CO₂ to dolomite (2.6 GPa; 1230 °C) and I₂ marks the transition from dolomite to magnesite (4.8 GPa; 1320 °C) (Dalton and Presnall, 1998) according to the reactions below:



dolomite (I₁)

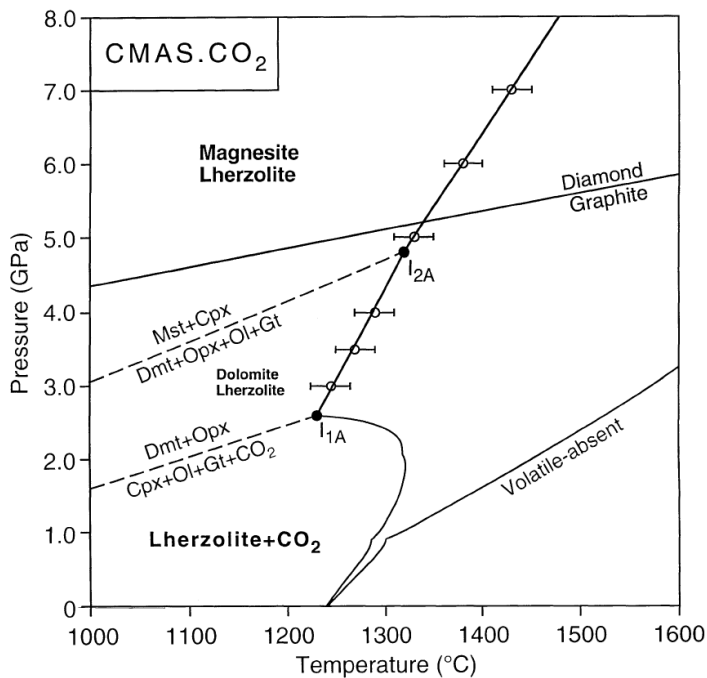
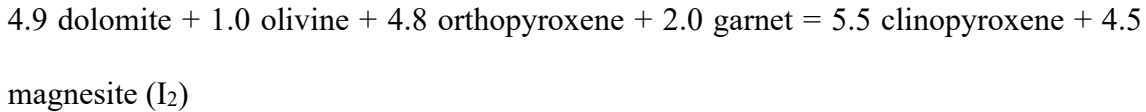
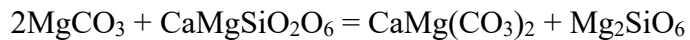


Figure 7. Solidus curve for model carbonated lherzolite in the CMAS-CO₂ system (after Dalton and Presnall, 1998).

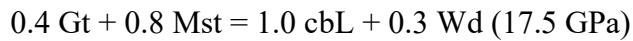
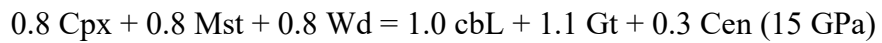
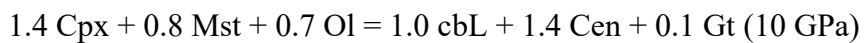
Dalton and Presnall (1998) observed that the carbonatitic melt generated in the stability field of magnesite has a dolomitic composition, with Ca/(Ca + Mg) ratio of 0.45, 0.49, and 0.51 for pressures of 7, 6, and 5 GPa, respectively. Similarly, at higher pressures, magnesite has a lower amount of Ca. With the pressure reduction from I₂ to 3 GPa, the carbonatitic melt migrates towards compositions richer in Ca, with a Ca/(Ca + Mg) ratio of 0.51, 0.56, and 0.59 for pressures of 4, 3.5, and 3 GPa, respectively. The carbonate phase in equilibrium between 3.5 and 3 GPa has a magnesium calcitic composition. This tendency of the carbonatitic melt to migrate to more magnesian compositions with increasing pressure has also been observed in other studies (Dalton

and Wood, 1993; Sweeney, 1994; Dasgupta and Hirschmann, 2006; Dasgupta and Hirschmann, 2007). Despite the significant compositional variations of the melts generated in the solidus curve in the pressure range from 3 to 7 GPa, all of them presented carbonatitic compositions ($\text{CO}_2 > 40$ wt.% and $\text{SiO}_2 < 6$ wt.%).

Dasgupta and Hirschmann (2007) generated typical mineral assemblages of magnesite lherzolites at pressures of 6.6 GPa and temperature of 1125-1250 °C, using CO_2 concentrations of 1.02-5.01 wt.%. The authors defined that the main melting reaction for the generation of carbonatitic melts under these conditions involves the consumption of magnesite and clinopyroxene, and can be described as:



Ghosh et al. (2009) demonstrated that carbonatitic melts can also be generated at great depths in the mantle (1300-1630 °C; 10-20 GPa) by partial melting of lherzolites with significant amounts of CO_2 (5 wt.%). These authors produced quenched melts with magnesium-carbonatitic compositions, showing low contents of SiO_2 (1.1-5.9 wt.%), Al_2O_3 (<0.5 wt.%), and TiO_2 (<0.4 wt.%), associated with a notable reduction of $\text{Ca}^{\#}$ ($\text{Ca}/(\text{Ca} + \text{Mg})$) with the increase of temperature and pressure, as observed in the previously mentioned experiments. The composition of the melts produced is very similar to lavas with magnesium-carbonatitic compositions (Bailey, 1989). The following melting reactions were observed by the authors close to the “apparent” solidus (Cpx = clinopyroxene, Ol = olivine, Gt = garnet, Mst = magnesite, cbL = carbonatitic liquid, Wd = wadsleyite, Rw = ringwoodite, Cen = clinoenstatite):

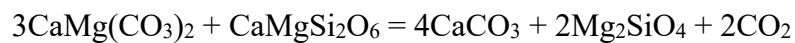


$$0.3 + 1.0 \text{ Mst} = 1.0 \text{ cbL} + 0.3 \text{ Rw (20 GPa)}$$

Although several experimental studies show that carbonatitic melts can be generated at medium to high pressures in the mantle, the compositions of these melts are rich in magnesium. Magnesium-carbonatitic lavas represent only a fraction of the compositional spectrum of carbonatitic lavas found at the surface, with calcium-carbonatitic lavas being the most common in crustal complexes. However, experimental studies and studies on mantle xenoliths also showed that carbonatitic melts with calcitic compositions can be equilibrated at lower pressures under specific conditions. At lower pressures (below the ledge) carbonatitic melts can remain stable only through reaction with a harzburgitic mantle ([Hammouda et al., 2014](#)). Mantle xenoliths of harzburgitic composition, equilibrated at pressures of 1.5 GPa, containing calcium-carbonatitic melts were reported by [Kogarko et al. \(1995\)](#). The occurrence of these melts was restricted to regions with a predominance of clinopyroxene and olivine. The carbonate composition showed Ca# ranging from 0.85 to 0.95. These authors state that the parental carbonatitic melt would have dolomitic composition and formed at greater depths in the mantle and that the result of metasomatic interactions between this liquid and the harzburgite would have produced wehrlitic assemblages, stabilizing Ca-enriched liquids as follows.



During the metasomatic reaction of primary dolomitic melt with clinopyroxene, the Ca/Mg ratio would increase, generating Ca-enriched melt, according to the following reaction:



Experiments carried out in the presence of water showed that carbonatitic melts coexisting with depleted lherzolites and harzburgites would have more magnesian

compositions ($\text{Ca}\# < 72$), while carbonatitic melts in equilibrium with wehrlitic assemblages (without orthopyroxene) would have calcitic compositions ($\text{Ca}\# > 72$) at pressures of 1.5 GPa (Dalton and Wood, 1993). The Ca enrichment would occur through the reaction with clinopyroxene through the above reactions.

As stated above, the stability of the carbonate phases, as well as the carbonatitic melts generated in the mantle, seems to be controlled by numerous variables. Decarbonation reactions are the main factors why carbonates are rare on the surface since the ledge makes it difficult for carbonatitic magma to reach the surface. As mentioned, carbonatitic melts can escape the ledge through a reaction with depleted peridotites, enriching Ca during ascent. The rarity of surface carbonatitic magmas does not seem to be associated with the difficulty of generating them in the mantle, but the conditions present in the lithosphere make it difficult for these magmas to remain stable during their ascent to the surface. Although carbonatite magma derived directly from the mantle is not a common phenomenon, mantle xenoliths displaying features of carbonatite metasomatism at great depths are often reported in the literature.

3.7 Wehrlitization: a process caused by carbonatite metasomatism

The percolation of carbonatitic melts through the lithospheric column plays an important role in the modification of the mantle rheology, the alteration of oxygen fugacity, and the generation of wehrlitic assemblages (clinopyroxene and olivine). The formation of wehrlites is commonly associated with reactions involving carbonatitic melts and depleted peridotites, releasing CO_2 as a by-product (Yaxley et al., 1998; Gervasoni et al., 2017; Aulbach et al., 2020). The wehrlitization process consists of the modal increase of clinopyroxene to orthopyroxene compared to other peridotites in the

same suite. Transitional phases between wehrlites and harzburgites may also occur, such as clinopyroxene-rich lherzolites, with clinopyroxene/orthopyroxene ratios >1 , and orthopyroxene-poor harzburgites (Lin et al., 2020). Pure carbonatitic melts are not the only metasomatic agents capable of generating wehrlites, and silicate-carbonate ultramafic melts and CO₂-rich silicate melts can be also included.

According to Wallace and Green (1988), decarbonation reactions responsible for the generation of wehrlitic assemblages can occur at low depths (1.5-2.0 GPa) due to the presence of the ledge in the solidus curve of carbonated peridotites in the P-T diagram, where clinopyroxene is generated. The formation of wehrlites in deeper regions, at pressures similar to those of the garnet and diamond stability field, is also possible. Experimental studies have simulated metasomatic processes based on reactions between peridotites and SiO₂-unsaturated and CO₂-enriched melts (e.g., Gervasoni et al., 2017), which resulted in wehrlitization under deep lithosphere conditions (1200 °C, 6 GPa). In addition, the presence of garnet wehrlites xenoliths in kimberlites is very common (Aulbach et al., 2017; Zong and Liu, 2018), indicating that carbonatitic melts may not only react with peridotites at low depths but also in the deep regions of the mantle.

Carbonatitic melts easily react with mantle-depleted peridotites, mainly due to their low viscosity and density (Kamenetsky and Yaxley, 2015), modifying the structure and composition of the lithospheric mantle. Reactions involving silica-rich melts and peridotites commonly form orthopyroxene and amphibole as metasomatic products ($\text{ol} + \text{cpx} + \text{opx}(1) + \text{sp} + \text{melt} = \text{amp} + \text{opx}_{(2)}$). Conversely, carbonatitic melts interacting with peridotites consume orthopyroxene generating clinopyroxene and olivine ($2\text{Mg}_2\text{Si}_2\text{O}_6(\text{opx}) + \text{CaMg}(\text{CO}_3)_2(\text{melt}) = \text{Mg}_2\text{SiO}_4(\text{ol}) + \text{CaMgSi}_2\text{O}_6(\text{cpx}) + \text{CO}_2(\text{fluid})$) (Dalton and Wood, 1993; Yaxley and Green, 1996; Gervasoni et al., 2017). The substitution of orthopyroxene for clinopyroxene occurs due to the low amount of silica

in the metasomatic agent. The interaction between carbonatitic melts and peridotites forms not only clinopyroxene and olivine but can also form apatite, amphiboles, and carbonates (Yaxley et al., 1998). Through wehrlitization, the tendency is for the released CO₂ fluid to continue to percolate through the lithosphere and react with other minerals or to become trapped in minerals as fluid inclusions.

3.4.4 Geochemical signatures of clinopyroxenes metasomatized by carbonatite melts

Studies in xenoliths metasomatized by carbonatitic melts showed that clinopyroxenes formed through the reaction $2\text{Mg}_2\text{Si}_2\text{O}_{6(\text{opx})} + \text{CaMg}(\text{CO}_3)_{2(\text{melt})} = \text{Mg}_2\text{SiO}_{4(\text{ol})} + \text{CaMgSi}_2\text{O}_{6(\text{cpx})} + \text{CO}_{2(\text{fluid})}$ have a high Ca/Al ratio and low Ti contents (Yaxley et al., 1991). In addition, experiments involving reactions between carbonatitic melts and lherzolites confirmed the enrichment in Ca and the depletion in Al and Ti in the clinopyroxenes generated, associated with the consumption of orthopyroxene and consequently the formation of wehrellites (Gervasoni et al., 2017).

Carbonatitic melts have a high Ca/Al ratio, both being stoichiometric elements in clinopyroxenes. Thus, the Ca/Al ratio can be considered as a tracer of carbonatitic metasomatism in both clinopyroxene and whole-rock, since wehrlitization will also leave the rock proportionately richer in Ca. In addition, clinopyroxenes generated as products of the above reaction show high #Mg (Mg/Mg+Fe, atomic ratio), suggesting low Fe contents in carbonatitic melts. Opposite to this type of metasomatism, there are clinopyroxenes generated through the reaction of peridotites with silicate melts, which are enriched in Fe, Ti, Al, and Ca (Rudnick et al., 1993). Due to the concomitant enrichment in Ca and Al, the Ca/Al ratio in these clinopyroxenes formed by silicate

melts will be low, showing the difference between the two types of metasomatism. Furthermore, experimental studies have confirmed that clinopyroxenes generated experimentally by the interaction between peridotites and eclogite-derived silica-rich melts have a low Ca/Al ratio (Yaxley and Green, 1998; Wang et al., 2010). Clinopyroxenes generated by silicate metasomatism show Ca/Al values lower than 5 and #Mg lower than 92. However, Ca/Al ratios greater than 5 are observed in clinopyroxenes that reacted with carbonatitic melts. Values greater than 500 are also commonly reported.

Trace elements of metasomatic clinopyroxenes can provide geochemical signatures that also allow the identification of the metasomatic agent. Just as the Ca/Al ratio associated with low Ti contents is used to identify carbonatitic metasomatism, other geochemical signatures using trace element concentrations are also applied as proxies for carbonatite metasomatism. Since carbonatitic melts are extremely enriched in incompatible elements, high levels of light rare earth elements (LREE) are expected in these melts.

Coltorti et al. (1999) suggest that clinopyroxenes generated from carbonatitic metasomatism have La/Yb_N ratio > 3-4. However, several studies of clinopyroxenes in xenoliths metasomatized by carbonatitic melts commonly show that these ratios can be much higher (La/Yb_N = 5-100) (Su et al., 2016; Xu et al. al., 2008; Zong and Liu, 2018). The Ti/Eu ratio in clinopyroxenes is also used as a tracer of carbonatitic metasomatism since these melts tend to have low levels of Ti. Additionally, when the valence of Eu changes from +3 to +2, it performs substitutions with Ca and Sr under reducing conditions. Note that Ca and Sr are elements enriched in carbonatitic melts. Therefore, clinopyroxenes metasomatized by these melts have low Ti/Eu ratios. This ratio should generally be less than 1500, however, clinopyroxenes metasomatized by carbonatitic

melts can reach values up to 2000 ([Zong and Liu, 2018](#)). Higher Ti/Eu values (>2500-3000) are generally obtained in clinopyroxenes metasomatized by silicate melts or that have been affected by partial melting ([Yaxley et al., 1991, 1998; Coltorti et al., 1999; Zong and Liu, 2018](#)).

3.10 Metasomatism caused by kimberlite melts

Metasomatism induced by kimberlite melts has been reported worldwide in many cratonic regions. In the Slave Craton, Canada, [Bussweiller et al. \(2018\)](#) observed compositional similarities between Cr-rich megacrysts and lherzolite phases, which lead the authors to suggest that kimberlite melts had interacted with lherzolites in the cratonic lithosphere. In addition, trace elements and Re-Os isotopes obtained for clinopyroxenes present in cratonic lherzolites from Lesotho kimberlites, Kaapvaal Craton, Africa, indicate that they crystallized from melts precursory to the host kimberlites ([Simon et al., 2003](#)). Furthermore, [Grégoire et al. \(2003\)](#), based on major and trace elements of lherzolites from several localities of the South African part of the Kaapvaal Craton, achieved a similar conclusion. These authors compared clinopyroxene of garnet lherzolite xenoliths with those of PIC (phlogopite-ilmenite-clinopyroxene) and MARID (mica-amphibole-rutile-ilmenite-diopside) suite observing strong similarities. The formation of PIC and MARID xenoliths are commonly ascribed to the group I and group II kimberlite, respectively ([Grégoire et al. 2002, 2003; Fitzpayne et al., 2018, 2018, 2019](#)).

In the Kaapvaal Craton, clinopyroxenes of wehrlites and lherzolites metasomatized by kimberlite melts have high Mg# (90.6-92.3) and low Ca# (0.44-0.46) and high jadeite contents (4.6-18.5 mol%). In terms of trace elements, they have high Zr

and Hf contents (~60-75 ppm Zr; 3.0-4.9 ppm Hf), and low concentrations of Sr (~100-200 ppm) and LREE (<2.3 ppm La, <10 ppm Ce), leading to low La/Zr ratios (<0.04). The chondrite-normalized Ce/Yb ratios of these clinopyroxenes vary between 13 and 23 (Fitzpayne et al., 2020). Similarly, clinopyroxenes of PIC samples from the same region have Mg# of 89.0-91.0, Ca# of 0.45-0.48, and jadeite of 3.7-10.0 mol%. They have Sr of 120-150 ppm, La/Zr ratios <0.03, and (Ce/Yb)_N between 11 and 21 (Fitzpayne et al., 2018).

In addition to clinopyroxene compositions, major and trace elements of phlogopites are also useful to constrain kimberlite metasomatism. Phlogopites are found in many modally metasomatized xenoliths, including polymict breccias, peridotites, and also as xenocrysts in kimberlites. Polymict breccias (also known as polymict peridotites) are complex rocks formed of rocks fragments and mineral clasts of distinct parageneses (harzburgitic, lherzolitic, eclogitic, pyroxenitic, megacrystic), cemented together by a fine-grained matrix composed of variable quantities of olivine, orthopyroxene, phlogopite, ilmenite, rutile, and minor sulfides (Höfer et al., 2009; Giuliani et al., 2013, 2014). These rocks are derived from primitive or precursor kimberlite magmas, representing failed kimberlite intrusions, which metasomatized the magmatic conduit. Polymict breccias comprise porphyroclasts of phlogopite which are often rimmed by an overgrowth of the same mineral but with a different composition (Zhang et al., 2001). These phlogopites display high Mg# (88.1-92.5), high TiO₂ concentrations (3.0-4.0 wt.%) and Cr₂O₃ contents (~0.5-2.0 wt.%) (Giuliani et al., 2014, 2016).

Phlogopite macrocrysts in kimberlites comprise complex zoning patterns formed by rims of distinct compositions, mainly in terms of TiO₂ and Cr₂O₃ contents (Giuliani et al., 2016). The cores of these macrocrysts are depleted in TiO₂ and Cr₂O₃ and often

resorbed with rounded or embayed outlines and are overgrown by one or more zones. The zones that are in contact with the low-Ti-Cr core are enriched in TiO_2 and Cr_2O_3 contents. Some macrocrysts have also cores enriched in TiO_2 and Cr_2O_3 with no preserved low-Ti-Cr regions. These high-Ti-Cr phlogopites have a large range of Cr_2O_3 (1.7 ± 0.5 wt.%) values and narrow range of TiO_2 (3.6 ± 0.3 wt.%), Al_2O_3 (14.0 ± 0.5 wt.%) and Mg# (90.2 ± 0.5) and most minor element concentrations (Nb = 19 ± 2 , Sr = 32 ± 5 , V = 198 ± 29 ppm) ([Giuliani et al., 2016](#)). High-Ti-Cr rims on macrocrysts of similar composition were observed by [Shee \(1985\)](#) and [Kargin et al. \(2019\)](#) in the Wesselton kimberlite, Kaapvaal Craton, and in the Grib kimberlite, East European Craton, respectively. Furthermore, metasomatized mantle xenoliths from Bultfontein kimberlite, Kaapvaal Craton, containing phlogopite with low-Ti-Cr cores and high-Ti-Cr rims were observed by [Giuliani et al. \(2016\)](#). The composition of these high-Ti-Cr rims in metasomatized xenoliths overlaps the field of phlogopite from polymict breccias and high-Ti-Cr rims of kimberlite macrocrysts (see [Giuliani et al., 2016](#)).

The composition similarities between the high Ti-Cr zones of kimberlite phlogopite macrocrysts, phlogopite from polymict breccias, and the rims of phlogopite in mantle xenoliths suggest a common genesis ([Giuliani et al., 2016](#)). Several authors considered that phlogopites with high Ti-Cr zones were formed by crystallization of kimberlite-related melts in the mantle immediately before entrainment by the kimberlite magma (<5,000 years for T ~1000 °C) ([Farmer and Boettcher, 1981](#); [Giuliani et al., 2014, 2016](#)). The proposition of a primary origin for these high Ti-Cr phlogopites is supported by the deformation features observed in most of these phlogopites.

In some cases, an outer zone occurs in these phlogopites. This zone overgrows the high Ti-Cr zone and is characterized by high TiO_2 (up to 4 wt.%) contents, low Cr_2O_3 (up to 0.5 wt.%), and Mg# (86-92). This zone also has high values of Al_2O_3

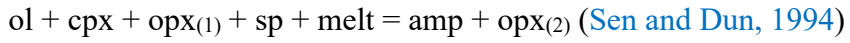
(11.9-17.5 wt.%) Ba (4,000-22,000 ppm), Zr (~50-500 ppm), and Nb (~30-80 ppm) relative to high-Ti-Cr phlogopites ([Giuliani et al., 2016](#)). These high-Ti low-Cr phlogopites are representative of phlogopites from kimberlite groundmass ([Giuliani et al., 2016; Kargin et al., 2019](#)). These authors state that the higher values of Mg, Ni, and Cr of high-Ti-Cr phlogopites compared to those of high-Ti phlogopite suggest the former crystallized from less fractionated kimberlite melts, extensively modified by interaction with refractory peridotite wall rocks. Therefore, although high-Ti-Cr phlogopite crystallized from earlier pulses of kimberlite melt they cannot be in equilibrium with the erupted/entraining kimberlite magma.

3.11 Silicate melt metasomatism

The origin and compositions of silicate melts vary widely. Experimental results indicate that the partial melting of eclogite can produce melts rich in Si and Al, similar to dacite and andesites ([Gervasoni et al., 2017](#)). Silicate-rich melts can also be formed by the evolution of a carbonate-silicate melt during its ascent to the surface. In addition, a high degree of partial melting of peridotites can also generate silica-rich melts, similar in composition to basaltic magmas ([Hirose and Kawamoto, 1995; Kogiso et al., 1998](#)). Therefore, metasomatic reactions involving peridotites and silicate melts are considered a widespread phenomenon in the mantle lithosphere.

Experiments reacting silicate melts derived from the partial melting of hydrous eclogite with peridotites at 2.2 and 2.5 GPa showed the occurrence of modal metasomatic reactions with consumption of the primary mineral phases ([Gervasoni et al., 2017](#)). These experiments simulate the reactions between the melts derived from the partial melting of the subducted slab with the mantle wedge in the subduction zone

setting. The metasomatic assemblage formed is constituted of Mg-rich amphibole and Al-rich orthopyroxene, in which orthopyroxene is the dominant phase ([Gervasoni et al., 2017](#)).



Melts derived from the partial melting of the subducted slab are called adakites. [Kilian and Stern \(2002\)](#) studied natural xenolith samples and demonstrated that these siliceous slab melts can react with the mantle wedge causing preferential dissolution of clinopyroxene and spinel relative to olivine and orthopyroxene as proposed by [Gervasoni et al. \(2017\)](#). The adakitic melts present high SiO₂ content and high Sr/Y and La/Nb ratios, and lower TiO₂, K₂O, Y, and HREE concentrations. Clinopyroxenes equilibrated with this melt decreased their Cr and Mg# and increased their Na₂O concentrations. They also show enrichment in LREE and display positive Sr and negative Nb and Ta anomalies. Orthopyroxene and olivine also have their Mg# decreased ([Kilian and Stern, 2002](#)).

On the other hand, peridotites metasomatized by basaltic melts display enrichment in basaltic components (CaO, Al₂O₃, FeO, TiO₂, MnO) that correlate positively with each other, and also have low Mg# (e.g., <90 Mg#). Clinopyroxenes equilibrated with basaltic melts usually present low concentrations of highly incompatible elements (Th, U, Nb, Ta, Pb). In general, clinopyroxenes metasomatized by silicate melts have low Ca/Al and low La/Yb_N ratios while Ti/Eu ratios are high. Although clinopyroxene commonly demonstrates depletion in Zr, Hf, Nb, and Ta in a multi-element diagram normalized to primitive mantle, positive correlations between HFSE (Zr, Hf, Ta, and Nb and Ti) are frequently observed in clinopyroxene metasomatized by basaltic melts (e.g., [Patkó et al., 2020](#)).

3.13 Refertilization of the cratonic lithosphere

Cratonic lithospheres of Archean age are mostly composed of refractory peridotites (e.g., harzburgite and dunites). These lithologies are the products of episodic high-degree extraction of mafic and ultramafic melts, which make the SCLM refractory and buoyant and then tectonically stable for billions of years (Pearson, 1999). Conversely, many studies have shown that the stability of some Archean to Proterozoic SCLM has been compromised due to clear evidence for the loss of portions of its root (Tang et al., 2013). The thinning and consequently destabilization of the cratonic lithosphere have been related to several mechanisms, such as the delamination model (Chu et al., 2009), the thermo-mechanical erosion model (Huang et al., 2012), the replacement model (Zheng, 2009), and the progressive melt modification model (Tang et al., 2008).

The delamination, thermo-mechanical erosion, and replacement models have been contradicted by isotopic studies. According to delamination, thermo-mechanical erosion, and replacement models only an old and a young lithosphere could coexist. For instance, Re-Os data should indicate two peaks of Archean and Mesozoic ages due to the widespread thinning during the Mesozoic (Griffin et al., 1998; Zhang et al., 2009). Conversely, Re-Os isotopic data for Cenozoic basalt-hosted xenoliths demonstrated large variation of ages varying from Archean to Cenozoic, which contradict these three models (Tang et al., 2013).

On the other hand, the progressive melt modification model indicated that the old and refractory SCLM interacted with melts changing its chemical and isotopic compositions. According to Tang et al. (2013), the SCLM beneath the continents experienced a multi-stage history of melt depletion followed by episodic refertilization processes which will result in a large variety of ages.

These melts would be derived from the upwelling of fertile asthenospheric material (O'Reilly et al., 2001) and, therefore, the refertilization of cratonic and circum-cratonic lithosphere can be considered a widespread phenomenon. After the melt-rock reaction, the old and refractory lithosphere is substituted by a young and fertile one (Zhang et al., 2002; Xu et al., 2008). Although the refertilization processes can be observed in several cratonic regions worldwide (e.g., Wyoming and North China cratons) the degree of refertilization varies among cratons.

Experimental studies showed that the presence of even small amounts of melt in olivine-rich rocks can result in a decrease in its strength (Soustelle et al., 2010). As a consequence the melt/fluid infiltration in the ancient SCLM can change its geophysical properties by reducing the viscosity and increasing the density and heat flow, leading to destabilization (Hu et al., 2000; O'Reilly et al., 2001; Peslier, 2010).

According to Foley (2008), the model for the destabilization of SCLM integrates alteration by metasomatic melts and delamination processes. Melts and fluids derived from the asthenosphere would react with the cratonic roots at some zones forming hydrated ultramafic metasomatic assemblages (Fig. 8a). At further stages, these hydrated assemblages would be melted forming linear incisions at the base of the lithosphere (Fig. 8b). These magmatic incisions would assist the delamination of large blocks (Fig. 8c), which cause the upwards migration of the lithosphere-asthenosphere boundary. In later stages, nepheline magmas would be produced from the melting of amphibole-bearing assemblage (Fig. 8d) while lamprophyric magmas would be produced in the deeper mantle (Fig. 8d). The generation of carbonatitic magmas is also common during this stage.

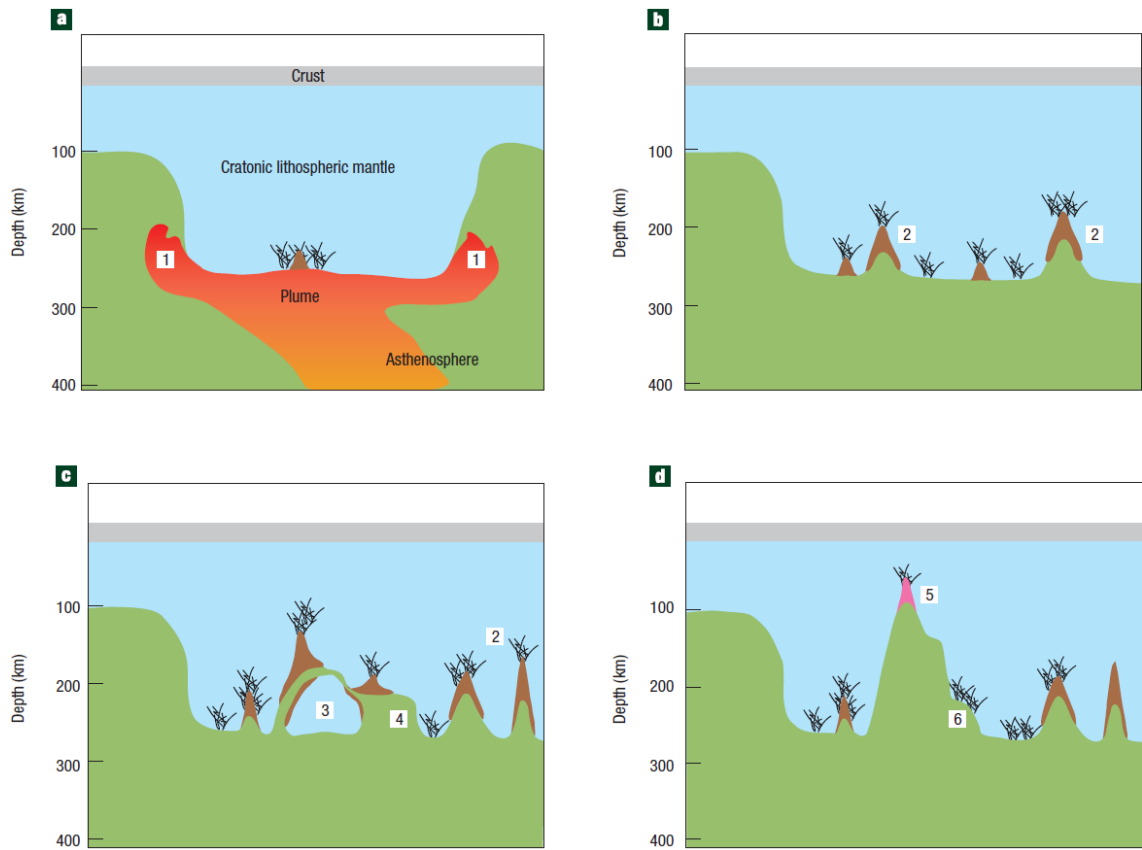


Figure 8. Weakening and erosion of the cratonic lithosphere. (a) Plume at the base of the cratonic lithosphere generating low degree melts that react with the depleted peridotite. Major magmatism is confined to craton margins – 1. (b) Later episodes of reactivation increase the impregnation points forming linear incisions due to melting of the metasomatic minerals – 2. (c) These linear incisions cause the delamination of large blocks – 3, and lateral erosion by small mantle convection – 4. (d) Melting of amphibole-bearing assemblage forming nephelinites at 80-90 km – 5, and ultramafic lamprophyre at deep mantle – 6 (after [Foley, 2008](#)).

CHAPTER 4 – METHODOLOGY

4.1 Petrography

The aims of the petrographic description were the identification of the mineral parageneses and the main textures using the optical petrographic microscope. The petrographic analyses allowed to determine (1) primary minerals and those added by metasomatic processes, (2) deformational features, such as undulatory extinction and kink bands, and (3) mineral zonation and reaction rims. The zonation in phlogopites was observed by an optical microscope due to the difference in the pleochroism. The petrographic description was conducted at the Laboratório de Microscopia at the Universidade Federal de Goiás (UFG). The quantification of the minerals phases for rock classification was determined using scanned images and the software JMicro Vision ([Roduit, 2007](#)) counting 3,000 points for each thin section.

4.2 Electron microprobe analysis

The major element compositions were determined for olivine, orthopyroxene, clinopyroxene, spinel, garnet, and phlogopite of the nine thin sections from the Catalão xenoliths. To observe compositional zonation, the core and rim of minerals were analyzed. These analyses were conducted at the Laboratório de Microssonda Eletrônica, Instituto de Geociências, Universidade de Brasília (UnB), Brazil, using a JEOL JXA 8900 Electron Microprobe Micro Analyzer (EPMA). The analytical conditions were acceleration voltage of 15 kV, beam current of 10 nA, and a beam diameter of 1 μm in the spot mode. The counting time for each element during the analysis was 10 s on the peak and 5 s on the background. Standards used for the quantitative measurements were

andradite (CaO and FeO), albite (Na₂O), forsterite (MgO), topaz (F), microcline (K₂O, Al₂O₃, and SiO₂), vanadinite (Cl and V₂O₃), pyrophanite (TiO₂ and MnO), chromite (Cr₂O₃) and nickel oxide (NiO). To a better understanding of the compositional zoning of phlogopite, a JEOL JXA-8230 Electron Micro Analyzer (EPMA) was used at the Laboratório de Microscopia e Microanálises (LMIC), Departamento de Geologia, Universidade Federal de Ouro Preto (UFOP). The same analytical conditions were maintained, except for a beam current of 20 nA and a spot size of 1 µm. Standards used for the quantitative measurements were fluorapatite (CaO), magnetite (FeO), anorthoclase (Na₂O), forsterite (MgO), fluorite (F), microcline (K₂O), corundum (Al₂O₃), quartz (SiO₂), meionite (Cl), rhyolitic Corning glass IR-W (V₂O₃), rutile (TiO₂), Mn (MnO), chromite (Cr₂O₃) and nickel oxide (NiO).

4.3 LA-ICP-MS

Trace element compositions of olivine, orthopyroxene, clinopyroxene, garnet, and phlogopite were obtained by Laser Ablation (LA) Inductively Coupled Plasma Mass Spectrometry (ICP-MS) at the Institute of Mineralogy, University of Münster Germany, using a Thermo Scientific Element XR single collector ICP-MS. The laser spot size was 85 µm, with a repetition rate of 5 Hz, and a fluence of 4 J/cm². The ablation time was 40 s, the background (gas blank) was counted for 30 s before each ablation, and the washout time was 20 s. The standards used were NIST SRM 612, silicate glasses BIR-1G, BHVO-2G, and natural olivine 355OL. The software Iolite was used for data reduction.

4.4 Spectroscopy analysis

In the search for fluid inclusions in olivines, carbonate inclusions were found. To characterize these inclusions a confocal LabRAM HR (high resolution) Evolution multichannel spectrometer of the Horiba Jobin-Yvon Instruments at the Laboratório de Espectroscopia Óptica, Instituto de Física, UnB was used. The red laser (532 nm) with a spot size of 1-2 μm and emission power of 50 mW was used during the measurements.

CHAPTER 5 – SCIENTIFIC ARTICLE

Multiple metasomatic events recorded by a stratified lithosphere beneath the SW margin of the São Francisco Craton, SE Brazil

Rodrigo Antonio de Freitas Rodrigues¹, Fernanda Gervasoni^{2,3}, Tiago Jalowitzki¹, Yannick Bussweiler⁴, Jasper Berndt⁵, Nilson Francisquini Botelho¹, Gláucia Queiroga⁶, Marcos Paulo de Castro⁶, Sebastião William da Silva⁷, Brunno Abilio Ciriaco¹, Ítalo Lopes de Oliveira¹, Stephan Klemme⁵

¹Programa de Pós-graduação em Geologia, Instituto de Geociências, Universidade de Brasília (UnB), Brasília, Brazil.

²Centro de Engenharias, Universidade Federal de Pelotas, Pelotas, Brazil.

³Programa de Pós-Graduação em Geociências, Universidade Federal do Rio Grande do Sul, Porto Alegre, Brazil

⁴Institut für Geologie und Mineralogie, Universität zu Köln, Germany.

⁵Institut für Mineralogie, Universität Münster, Germany.

⁶Departamento de Geologia, Universidade Federal de Ouro Preto (UFOP).

⁷Instituto de Física, Universidade de Brasília (UnB), Brasília, Brazil

Highlights

- Mantle xenoliths from the SW margin of the SFC record a stratified lithosphere.
- Low-Ti-Cr phlogopite records alkaline-rich fluids metasomatism.
- Clinopyroxene from grt-phl wehrlites was formed by carbonatite metasomatism.
- High-Ti-Cr phlogopite indicates metasomatic reaction involving proto-kimberlite melts.
- Clinopyroxene from sp lherzolites essentially records partial melting events.

Abstract

A suite of kimberlite-hosted mantle xenoliths from the Catalão region, southwestern border of the São Francisco Craton (SFC), Brazil, consists of spinel lherzolites, harzburgite, and garnet-phlogopite wehrlites. The chemical composition of these xenoliths provides evidence for a stratified subcontinental lithospheric mantle (SCLM) where the deeper mantle xenoliths have experienced partial melting followed by multiple metasomatic events, but the shallower mantle rocks are products of partial melting process slightly overprinted by metasomatic melts. Samples derived from the deeper mantle (~170 km) underwent ~ 10 % of partial melting and are represented by garnet-phlogopite wehrlites (1066-1101 °C; 5.03-5.23 GPa) and one harzburgite (950 °C; 5.28 GPa). These xenoliths record multiple metasomatic events that were caused by alkaline-rich fluids (K_2O , H_2O , CO_2 , F, $\pm \text{Cl}$), carbonatite and proto-kimberlite melts. Low-Ti-Cr phlogopite (Ph11) found in garnet wehrlites was formed by metasomatic reactions of alkaline-rich fluids with peridotites. High-Cr and low-Al clinopyroxene present in garnet-phlogopite wehrlites and harzburgite have high Mg#, high Ca/Al, $\text{La}_{\text{N}}/\text{Yb}_{\text{N}}$, Zr/Hf ratios, and high Sr contents, coupled with low to intermediate Ti/Eu and Ti/Nb ratios, suggesting that they were formed by carbonatite melt metasomatism. These geochemical signatures together with the presence of magnesite and dolomite inclusions trapped in the olivine of garnet-phlogopite wehrlites and harzburgite confirm carbonate-rich melt as a metasomatic agent. Metasomatic reactions involving garnet-phlogopite wehrlites and a proto-kimberlite melt formed high-Ti-Cr phlogopite (Ph12), which occurs as rims around Ph11, as isolated flakes around garnet, and in the matrix of wehrlites. Conversely, the shallower mantle (~50 km), represented by spinel lherzolites (876-915 °C; 1.5 GPa), underwent a lower degree of partial melting (2-4 %) and records little evidence of metasomatic processes. These samples contain low-Cr high-Al

clinopyroxene depleted in incompatible trace elements, with geochemical trace element patterns typical of partial melting processes. Some clinopyroxene crystals, however, show slight enrichment in light rare earth elements (LREE), large ion lithophile elements (LILE), and Ti. Their low Ca/Al, La_N/Yb_N, and Zr/Hf ratios, high Sr contents, high Ti/Eu, Ti/Nb ratios, and strong positive correlation between Ti with the other high field strength elements (HFSE) and LREE, indicate that these clinopyroxene crystals were metasomatized by a subalkaline silicate melt depleted in incompatible elements. The stratification of the SCLM beneath the southwestern border of the SFC shown by different degrees of partial melting and metasomatic processes occurring within the cratonic lithosphere may suggest refertilization and possible rejuvenation that might weaken and modify the lithosphere, with a substantial impact on its long-lasting tectonic stability.

Key-words: Mantle xenoliths, Mineral Chemistry, Metasomatism, Refertilization, São Francisco Craton

5.1 Introduction

Mantle xenoliths representing the Archean subcontinental lithospheric mantle (SCLM) may be strongly depleted in incompatible elements due to several episodes of partial melting throughout geological time. For instance, the extraction of basaltic melts results in the depletion of basaltic components (Al₂O₃, TiO₂, MnO, CaO, and Na₂O) in the solid residue, resulting in a refractory, buoyant, and tectonically stable SCLM (Foley, 2008; Tang et al., 2013). Conversely, the enrichment, i.e., refertilization, of the SCLM occurs during metasomatic interactions of melt and/or fluids with depleted mantle rocks. Xenoliths from the cratonic lithospheric mantle brought to the surface by

kimberlites or similar volcanic rocks may sample the SCLM at different depths, allowing the investigation of mantle metasomatism throughout a vertical mantle section. The heterogeneities found in these cratonic mantle samples may reflect the distinct metasomatic agents that act in different depths (e.g., [Aulbach et al., 2013](#) and references therein).

It is generally assumed that the percolation of melts or fluids is responsible for the metasomatic enrichment of peridotites, but the nature and composition of such metasomatic agents remain a matter of debate. In particular, the origin of pyroxene-rich peridotites has commonly been ascribed to alkaline-rich, volatile-bearing melts ([Kelemen et al., 1998](#); [Ionov et al., 2005](#)). For instance, it is widely accepted that wehrlites are formed by the reaction between carbonatite melts and peridotites (e.g., [Klemme et al. 1995](#); [Ionov et al., 2018](#); [Gervasoni et al., 2017](#)). Moreover, the presence of phlogopite with different compositions in mantle xenoliths from the cratonic lithosphere suggests that the SCLM reacted with K₂O- and C-O-H-rich fluids ([Kargin et al., 2019](#)), as well as alkaline and hydrous silicate carbonate melts, i.e., so-called proto-kimberlite melts ([Giuliani et al., 2014, 2016](#); [Tappe et al., 2018](#); [Kargin et al., 2019](#); [Gervasoni et al., 2022](#)).

Due to successive episodes of refertilization, the SCLM is susceptible to rejuvenation processes, which consist of either partial modification or even complete overprint of the original Archean cratonic mantle. This chemical rejuvenation induces mechanical modifications in the SCLM that are capable of leading to further weakening of the lithosphere, making it gravitationally unstable and thinner (e.g., [Foley, 2008](#); [Tang et al., 2013](#)). In particular, the cratonic margins (mobile belts) provide the invaluable opportunity of revealing the complex history recorded by the SCLM due to the several stages and types of metasomatism along the cratonic mantle.

In recently drilled kimberlite pipes in the Catalão region (hereafter Catalão kimberlites), Alto Paranaíba Igneous Province (hereafter APIP), a suite of metasomatized mantle xenoliths from the southwestern border of the São Francisco Craton (SFC) were recovered. In this study, we present the first mineral chemistry data (major and trace elements) of these xenoliths and the first Raman spectroscopy data of mineral inclusions found in olivine crystals. The samples consist of spinel lherzolites, harzburgite and garnet-phlogopite wehrlites. We also use geothermobarometry, together with melting model to constrain the composition and evolution of the cratonic mantle beneath the southwestern border of the SFC. Our mantle xenoliths show different metasomatic processes at distinct depths, which is evidence of a stratified cratonic lithosphere with possible refertilization/rejuvenation promoted by a range of metasomatic agents, including alkaline fluids, carbonatite, proto-kimberlite, and silicate melts.

5.2 Geological setting

The kimberlite (*sensu lato*) pipes in the Catalão region are part of the huge Coromandel – Três Ranchos kimberlite field, which contains ca. 580 small alkaline intrusions ([Cabral Neto et al., 2017](#)). The largest part of these bodies is not kimberlite *sensu stricto*, but mainly kamafugites (e.g. [Gibson et al., 1995](#); [Araújo et al., 2001](#); [Guarino et al., 2013](#)). This kimberlite field is part of the APIP, in SE Brazil, which is one of several Late Cretaceous alkaline provinces that occur along an NW-SE structural zone so-called Azimuth 125° lineament ([Gibson et al., 1995](#)).

It covers an intense and widespread, mafic, potassic to ultrapotassic magmatism that took place during the Late Cretaceous, mostly between ca. 90 and 80 Ma (e.g.,

Gibson et al., 1995; Guarino et al., 2013). This province comprises mostly kamafugite lavas and pyroclastic deposits (i.e., the Mata da Corda Formation; Fig. 1), but it also contains a large number of small intrusive bodies (dykes, pipes, plugs, and diatremes) with both kamafugite and kimberlite affinities, as well as few major alkaline-carbonatite plutonic complexes (e.g. Gibson et al., 1995; Araújo et al., 2001; Guarino et al., 2013; Oliveira et al., 2017).

Most of these alkaline rocks occur emplaced into a narrow strip of low-grade Neoproterozoic metasedimentary rocks of the Brasília Mobile Belt (Valeriano et al., 2017), between the NE margin of the Paraná Basin and the SW border of the SFC (e.g., Gibson et al., 1995; Araújo et al., 2001). Although the rocks from the APIP outcrop on the surface within the Brasília Mobile Belt (Fig. 1), this province is mostly underlying by ancient lithosphere. The definition of the western cratonic boundary of the SFC has been a matter of continuous debate (see Heilbron et al., 2017). However, Bouguer anomaly and seismic tomographic data have shown that a larger extent of the western border of the SFC occurs beneath the Brasília Belt, beyond the current limits observed on the surface (Rocha et al., 2019 and references therein). The geophysical studies, integrated with geochemical data from xenoliths and xenocrysts hosted by volcanic rocks from APIP (e.g., Fernandes et al., 2021; Carvalho et al., 2022a, b), as well as radiogenic isotopes of lavas (Gibson et al., 1995; Carlson et al., 2007; Araújo et al., 2001), renders the status of the cratonic domain (or at least, marginal to the craton) rather than “off-craton” tectonic setting for the Catalão kimberlites (see also Leonardos et al. 1993).

Previous works on mantle xenoliths from APIP also record strong evidence of partial melting process followed by metasomatism in the SCLM. The Três Ranchos, Canastra, Limeira, Indaiá, and Sucesso (Abel Régis) kimberlite clusters brought to the

surface several types of mantle xenoliths, including peridotites (dunites, lherzolites, and harzburgites) and pyroxenites (websterites and clinopyroxenites) from spinel and garnet facies, and also eclogites, all containing hydrous minerals such as mica and amphibole (e.g., [Leonardos et al. 1993](#); [Costa, 2008](#); [Nannini, 2016](#); [Almeida et al., 2014](#); [Fernandes et al., 2021](#)). In addition, glimmerites and peridotites containing some rare alkali-bearing Ti oxides, carbonates, and phosphates also have been reported for this province xenoliths ([Almeida et al., 2014](#)).

The Catalão kimberlite pipes, the host of the xenoliths investigated in this study, were recently sampled by the Five Star Diamonds company. The intrusions are located ca. 30 km southeast of Catalão (Fig. 1), close to the Três Ranchos-04 kimberlite, a well-known body source of the first garnet lherzolites found in the APIP ([Leonardos et al., 1993](#)). The freshest rock samples from drill cores CAT-01A (76.23 and 81.40 m) and CAT-01B (139.35 m) contain a total of nine mantle xenoliths (see Table 1).

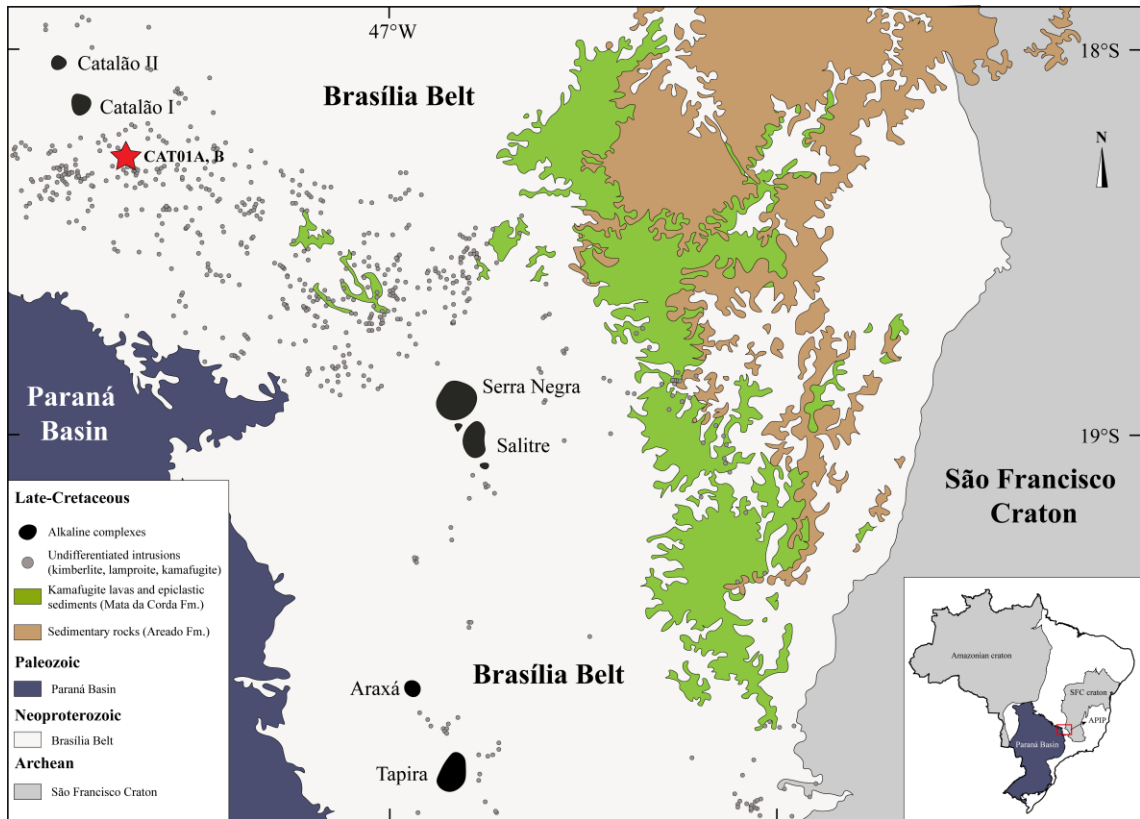


Figure 1. Simplified geological map from the Alto Paranaíba volcanic rocks in the context of the Mata da Corda Formation (after [Barbosa et al., 2012](#)).

5.3 Analytical methods

5.3.1 Electron microprobe analysis

Major element compositions of olivine, orthopyroxene, clinopyroxene, spinel, garnet, and phlogopite of nine thin sections from Catalão xenoliths were determined by a JEOL JXA-8900 Electron Probe Micro Analyzer (EPMA), equipped with five wavelength-dispersive spectrometers (WDS) at the Laboratório de Microssonda Eletrônica, Instituto de Geociências, Universidade de Brasília (UnB), Brazil. The analytical conditions were acceleration voltage of 15 kV, beam current of 10 nA, and a beam diameter of 1 μm in the spot mode. The counting time for each element during the analysis was 10 s on the peak and 5 s on the background. Standards used for the quantitative measurements were andradite (CaO and FeO), albite (Na₂O), forsterite

(MgO), topaz (F), microcline (K₂O, Al₂O₃, and SiO₂), vanadinite (Cl and V₂O₃), pyrophanite (TiO₂ and MnO), chromite (Cr₂O₃) and nickel oxide (NiO). Matrix effects were controlled using an in-house ZAF correction program. Additional analyses of phlogopite in two samples (1B-139A and 1B-139B) were obtained using a JEOL JXA-8230 EPMA at the Laboratório de Microscopia e Microanálises (LMIC), Departamento de Geologia, Universidade Federal de Ouro Preto (UFOP) for a better spatial resolution. Similar analytical conditions were used, except for a beam current of 20 nA and a spot size of 1 μm. Standards used for the quantitative measurements were fluorapatite (CaO), magnetite (FeO), anorthoclase (Na₂O), forsterite (MgO), fluorite (F), microcline (K₂O), corundum (Al₂O₃), quartz (SiO₂), meionite (Cl), rhyolitic Corning glass IR-W (V₂O₃), rutile (TiO₂), Mn (MnO), chromite (Cr₂O₃), and nickel oxide (NiO).

5.3.2 Laser ablation inductively coupled plasma mass spectrometry

Trace element compositions of silicate minerals in the same thin sections were determined by laser ablation (LA) inductively coupled plasma mass spectrometry (ICP-MS) at the Institute of Mineralogy, University of Münster, Germany. They were analyzed using a Thermo Scientific Element XR single collector ICP-MS coupled to a 193 nm ArF excimer LA system (Teledyne Photon Machines Analyte G2). Sample ablation was conducted in an Ar gas-filled sampling cell. The ablated material was transported from the ablation cell to the ICP-MS by a He carrier gas. The laser was operated at a spot size of 85 μm, a repetition rate of 5 Hz, and a fluence of 4 J/cm². The ablation time was 40 s, the background (gas blank) was counted for 30 s before each ablation, and the washout time was 20 s. For external standardization, NIST reference glass standard SRM 612 was used, with ²⁹Si as the internal standard. For the samples, the Si content measurement by EPMA was used. To monitor precision and accuracy, other reference materials were analyzed including silicate glasses BIR-1G and BHVO-

2G, as well as a natural olivine 355OL ([Bussweiler et al., 2019](#)). Data reduction and evaluation were carried out using the Iolite software ([Paton et al., 2011](#)).

5.3.3 Raman spectroscopy

Raman spectroscopy was performed using a confocal micro-spectrometer (LabRAM HR Evolution, Horiba Scientific, France) with a spectral resolution of $\sim 1.0 \text{ cm}^{-1}$ and spatial resolution of $\sim 1 \mu\text{m}$. A video image of the sample was used for accurate positioning of the laser spot on the sample. The excitation laser beam (532 nm) with 10 mW power was focused on the sample using a long-working distance microscope objective MPLANFL N 50X (0.50 NA, Olympus). These measurements were performed at the Laboratório de Espectroscopia Óptica, Instituto de Física (IF) of the UnB.

5.4. Petrography

Nine peridotite xenoliths between 5 and 9 cm in diameter were investigated. This suite comprises two garnet-phlogopite wehrlites (1B-139A, 1B-139B), one harzburgite (1A-81) and six spinel lherzolites (1A-76A, 1A-76B, 1A-76C, 1A-81A, 1A-81B, 1A-81C). Mineral modes and petrographic observations are provided in Table 1. All the peridotite xenoliths have coarse-grained protogranular to porphyroclastic textures ([Mercier and Nicolas, 1975](#)).

5.4.1 Garnet-phlogopite wehrlites

The garnet-rich phlogopite wehrlites are porphyroclastic and contain coarse garnet crystals (6-8 mm) together with olivine, clinopyroxene, and phlogopite. Olivine is commonly 2-4 mm in size, anhedral to subhedral, strongly fractured, and contains kink bands. Clinopyroxene displays irregular shapes and variable sizes (2-6 mm). In both samples, garnet has rims composed of Cr-spinel and phlogopite (Fig. 2a, b). The

fine-grained Cr-spinel (0.03-0.1 mm) predominates on the outermost side of the garnet crystals and advances inwards, until the total consumption of the garnet. Large phlogopite crystals (0.5-1.2 mm) occur associated with Cr-spinel and garnet (Fig. 2a, b, c).

Based on petrographic and chemical composition (see details below) two types of phlogopite can be distinguished. Type 1 phlogopite (Phl1) is rarely preserved and occurs as cores in phlogopite type 2 (Phl2) (Figs. 2c, 3a, c, d). Phl2 is the most common type and occurs as large euhedral lamellar crystals around garnet porphyroclasts and also as discrete crystals in the matrix (Figs. 2b, c, d, 3a, b, c, d). The rounded/irregular contacts observed between inner (Phl1) and outer (Phl2) zones indicate the resorption of Phl1 prior to the formation of Phl2 (Figs. 2c, 3c). Some Phl2 crystals display deformational features such as kink banding, undulatory extinction, and arched cleavage.

5.4.2 Harzburgite

The only harzburgite xenolith has a coarse-grained protogranular texture with large crystals of olivine and orthopyroxene (up to 5 mm), as well as small grains of clinopyroxene (0.7 mm), with curvilinear grain boundaries. Orthopyroxene shows exsolution lamellae of clinopyroxene and kink bands. Clinopyroxene is typically interstitial, found between olivine and orthopyroxene. It commonly displays a turbid appearance and thick spongy rims, which predominate in up to 60 % of the mineral volume (Fig. 2e). Spinel occurs in localized areas, forming symplectite textures with orthopyroxene, being interpreted as a product of garnet destabilization (Fig. 2f).

5.4.3 Spinel lherzolites

The spinel lherzolites have textures varying from protogranular (1A-81A, 1A-81B, 1A-81C) to medium-porphyroclastic (1A-76A, 1A-76B, 1A-76C). Crystals show well-developed triple-point grain boundaries and lobate contacts, typical of equilibrated mantle assemblages (Fig. 2h). In samples with porphyroclastic texture, large porphyroclasts of orthopyroxene (12 mm) occur together with recrystallized olivine and clinopyroxene. Clinopyroxene size varies from 0.8 to 1.2 mm, and they often show exsolution lamellae of orthopyroxene. Olivine varies in size from 1 to 1.5 mm, and they contain kink bands (Fig. 2g). Spinel is abundant and generally occurs as ameboid grains or blebs ranging from small discrete grains (0.4 mm) to large grains (8 mm) (Fig. 2h). Two samples (1A-76A, 1A-76B) show strong evidence of partial melting, with larger spinel grains having recrystallized rims, and orthopyroxene and clinopyroxene grains showing recrystallization and consumption (Fig. 2i).

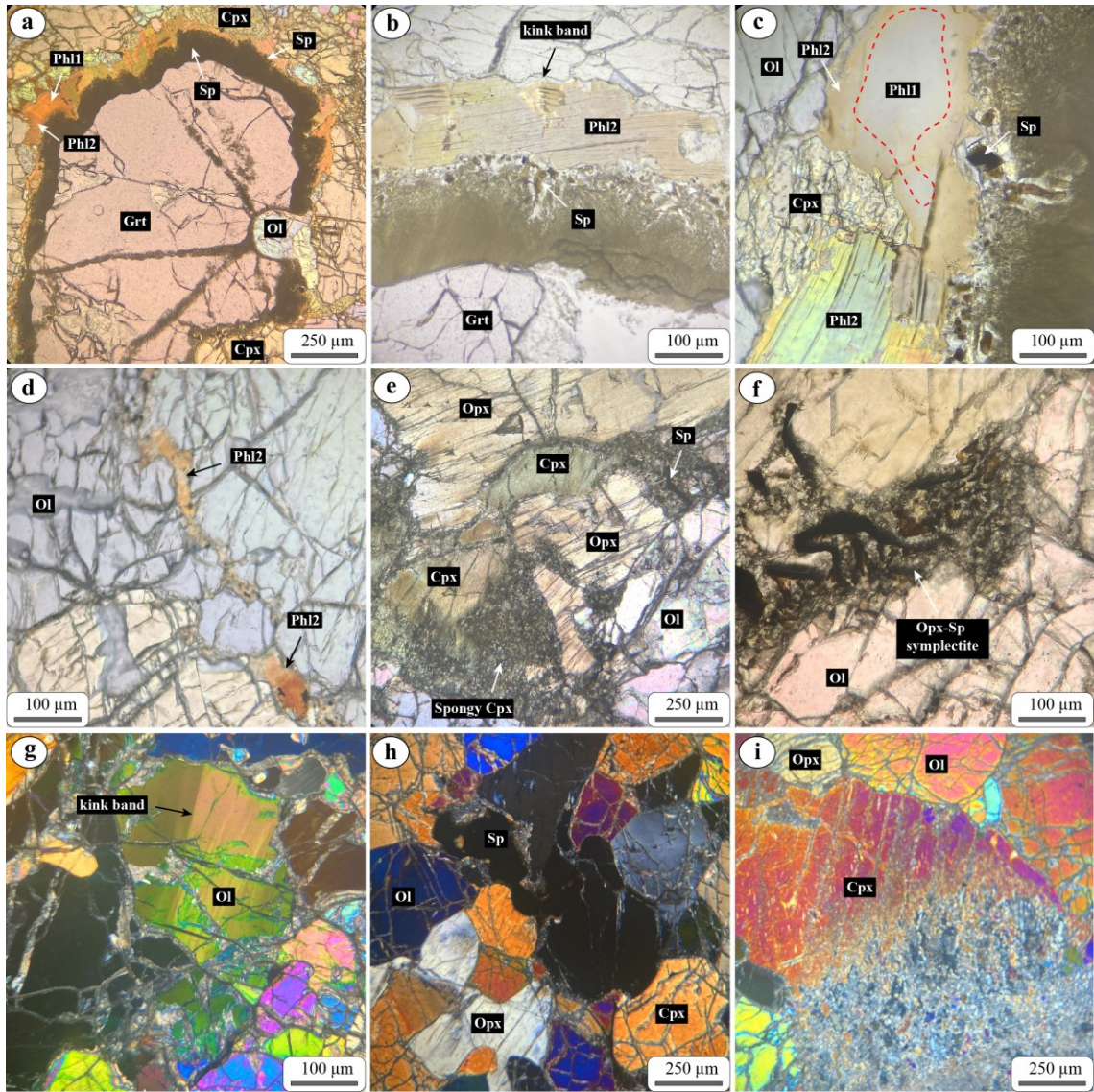


Figure 2. Photomicrographs of Catalão mantle xenoliths showing the main mineral assemblages and main textures. (a) Porphyroclastic texture with garnet porphyroclasts rimmed by Cr-spinel and phlogopite (plane-polarized light, sample 1B-139B). (b) Phl2 with kink band and in contact with Cr-Spinel around garnet (plane-polarized light, sample 1B-139A). (c) Zoned phlogopite crystal with Phl1 in the inner and Phl2 in the outer zones (plane-polarized light, sample 1B-139B). (d) Phl2 fills the interstices of the matrix (plane-polarized light, sample 1B-139A). (e) Clinopyroxene with thick spongy rims (plane-polarized light, sample 1A-81). (f) Spinel-orthopyroxene symplectite (plane-polarized light, sample 1A-81). (g) Olivine displaying kink band (crossed-polarized light, sample 1A-81A). (h) Spinel bleb in an equilibrated mantle assemblage (crossed-polarized light, sample 1A-76A). (i) Recrystallization of clinopyroxene (crossed-polarized light, sample 1A-76C). Mineral abbreviations: Ol – olivine, Opx – orthopyroxene, Cpx – clinopyroxene, Grt – garnet, Phl – phlogopite, sp – spinel.

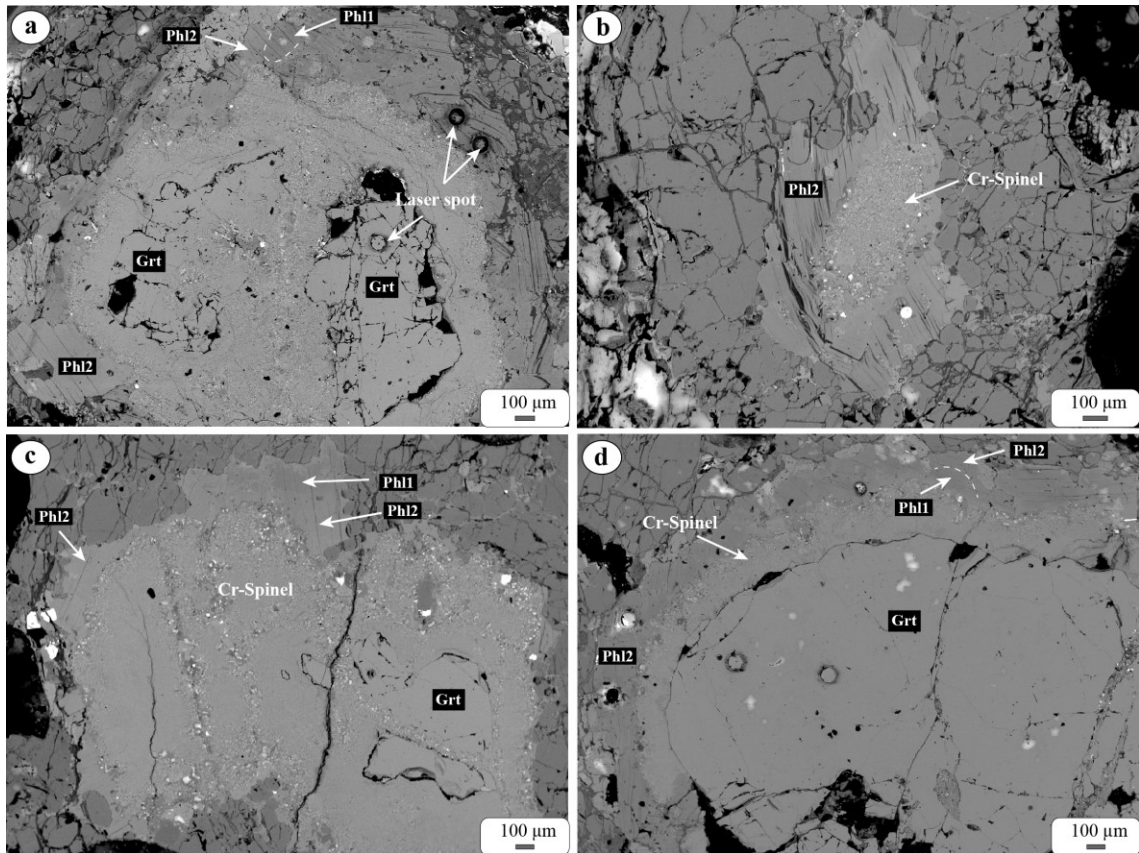


Figure 3. BSE photomicrographs of garnet-phlogopite wehrlite xenoliths (1B-139A and 1B-139B). (a) Relics of garnet porphyroblast surrounded by Cr-spinel and zoned phlogopite grains (1B-139B). (b) Total consumption of garnet by spinel-pyroxene symplectites and zoned phlogopite grains (1B-139B). (b) Total consumption of garnet formation of Cr-spinel and large Phl2 (1B-139A). (c) Relics of garnet porphyroblast embedded in a large mass of Cr-spinel. Zoned phlogopite at the top shows irregular Phl1 rimmed by Phl2, indicating resorption of Phl1 during the formation of Phl2 (1B-139A). (d) Large garnet porphyroblast rimmed by Cr-spinel lamellae and zoned and homogenous phlogopite crystals (1B-139B). Mineral abbreviations: Grt – garnet, Phl – phlogopite.

Table 1. Sample list with a summary of modal data and temperature and pressure estimates.

Sample	Lithology	Texture	Modal composition (%)						Equilibrium temperature and pressure						
			ol	opx	cpx	sp	grt	phl	T _{Cpx} (M ₈₀)	T _{REE} (L ₁₃)	T _{Ca-in-Opx} (BK ₉₀)	T _{Cr-in-Cpx} (NT ₀₀)	P (NT ₀₀)		
1A-76A	lherzolite	porphyroclastic	42.0	23.5	30.0	4.5			955	933	834			907	
1A-76B	lherzolite	porphyroclastic	44.3	19.0	33.3	3.4			909	930	832			890	
1A-76C	lherzolite	porphyroclastic	41.0	25.1	27.2	6.7			901	989	854			915	
1A-81	harzburgite	protogranular	61.2	26.0	10.2	2.6			975	886	990		5.28	950	
1A-81A	lherzolite	protogranular	51.0	19.4	25.6	4.0			941	834	852			876	
1A-81B	lherzolite	protogranular	49.0	13.8	33.2	4.0			893	888	892			891	
1A-81C	lherzolite	protogranular	60.8	8.7	25.5	5.0			892	930	832			885	
1B-139A	wehrlite	porphyroclastic	62.0		30.0		5.0	3.0	1164				1039	5.23	1101
1B-139B	wehrlite	porphyroclastic	60.0		24.8		6.2	8.3	1099				1034	5.03	1066

5.5 Mineral Chemistry

Minerals in the peridotite xenoliths are homogeneous in major elements based on core and rim analyses, except for the zoned phlogopites. Average compositions of mineral phases are given in Tables 1 and 2. The complete data set is given in the supplementary material.

Olivine crystals are forsterite-rich with high Mg# (0.89-0.92) [Mg/(Mg+Fe) atomic ratio] and NiO (0.26-0.51 wt.%) content, coupled with low CaO (<0.11 wt.%). In the multielement diagram, the olivine of harzburgite display positive anomalies of U, Th, Pb, Li, Nb, and La, with high La_N/Lu_N (2.35-4.08, where N = primitive mantle (PM) normalized values of Sun and McDonough, 1989), whereas olivine from wehrlites is enriched in Li, Nb, Ta, Zr, and Hf (La/Lu_N ratio was not calculated because Lu is below detection limits). Olivine from lherzolites is depleted in incompatible trace elements, with samples 1A-76A and 1A-76C showing positive anomalies of Pb and Li, and La_N/Lu_N of 0.04-0.63 (Fig. S1).

Orthopyroxene crystals in the harzburgite (En_{90.12-91.65}, Fs_{7.64-8.65}, Wo_{0.28-1.77}) and lherzolites (En_{88.37-90.17}, Fs_{9.11-10.59}, Wo_{0.18-1.82}) are enstatite-rich characterized by high Mg# (harzburgite = 0.92; lherzolite = 0.89-0.91), with Al₂O₃ varying from 2.95 to 4.97 wt.%. There is no well-defined correlation between major elements and Mg#. Orthopyroxene is absent in the wehrlite samples. The orthopyroxene trace element compositions vary drastically depending on the rock type (Fig. 4, Table S9). The trace element concentrations are mostly below the primitive mantle composition (Fig. 4). Harzburgite orthopyroxenes have a U-shaped pattern characterized by the enrichment of rare earth elements (REE) (La/Sm_N = 8.59-16.28; Gd/Yb_N = 0.11-0.26) (Fig. 4a). Conversely, lherzolites orthopyroxenes are strongly depleted in light REEs (LREE) compared to heavy REEs (HREE) (La/Yb_N = 0.001-0.060) (Fig. 4c). In the PM-

normalized multielement diagram, harzburgites orthopyroxenes display positive anomalies of Th, U, La, Pb, Sr, Zr, Hf, Ti, and Li, whereas lherzolites are characterized by positive anomalies of Cs, Pb, Hf, Ti, and Li (Fig. 4b, d).

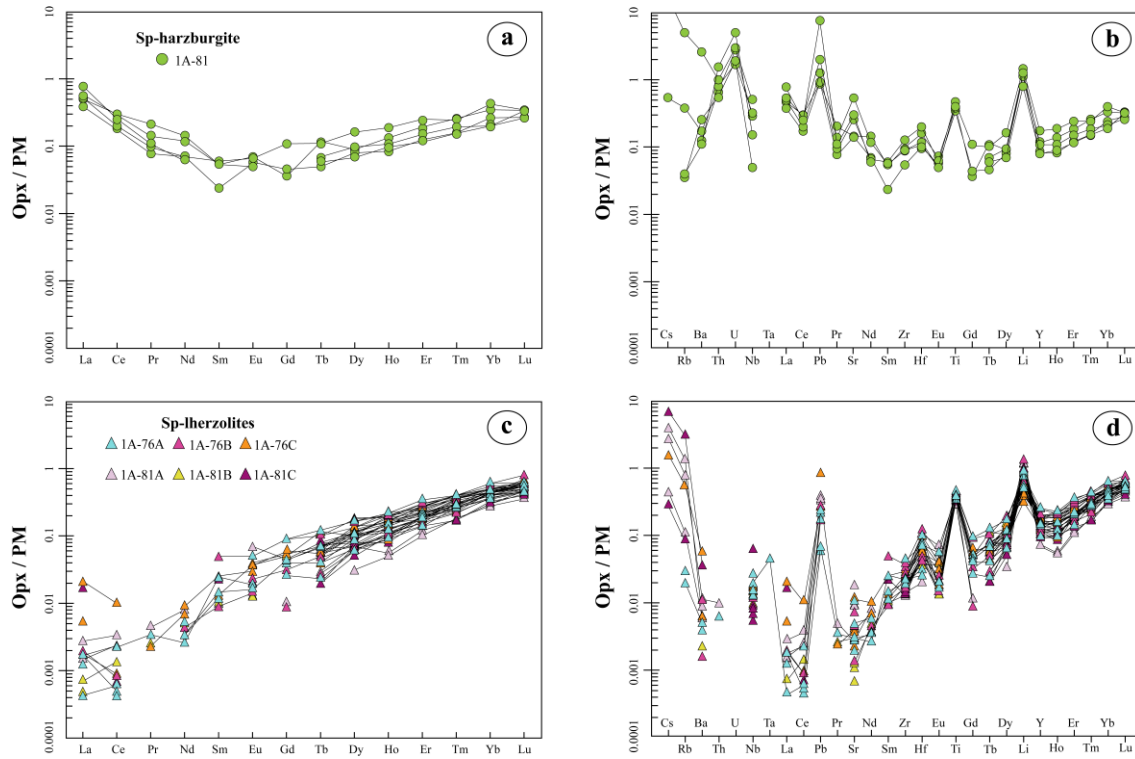


Figure 4. Trace and rare earth elements diagrams normalized to the primitive mantle (PM, Sun and McDonough, 1989) for orthopyroxenes of harzburgite (a-b) and lherzolites (c-d).

Clinopyroxene crystals are diopside (En_{45-54} , Fs_{2-5} , Wo_{41-51}). In general, they present high Mg# values (0.90-0.95), with lherzolitic clinopyroxenes containing a variable range (0.90-0.94), whereas wehrlitic (0.91-0.93) and harzburgitic (0.93-0.95) are more restricted. They share similar CaO (19.16-22.82 wt.%) and Na₂O (1.01-2.05 wt.%) contents. Clinopyroxene in spinel lherzolites contains lower Cr₂O₃ (0.49-0.99 wt.%) and Ca/Al ratios (3.91-5.52), coupled with higher Al₂O₃ (5.39-6.95 wt.%) and TiO₂ (0.10-0.72 wt.%, with 66 measurements >0.36 wt.%) when compared to clinopyroxene on wehrlites (CaO = 19.16-20.93 wt.%; Na₂O = 1.04-1.74 wt.%; Cr₂O₃ = 1.38-2.18 wt.%; Ca/Al = 18.02-27.28; Al₂O₃ = 1.02-1.48 wt.%; TiO₂ <0.37 wt.%) and

clinopyroxene on harzburgite ($\text{CaO} = 21.77\text{-}22.82 \text{ wt.\%}$; $\text{Na}_2\text{O} = 1.01\text{-}1.88 \text{ wt.\%}$; $\text{Cr}_2\text{O}_3 = 1.15\text{-}1.87 \text{ wt.\%}$; $\text{Ca}/\text{Al} = 16.95\text{-}25.27$; $\text{Al}_2\text{O}_3 = 1.19\text{-}1.82 \text{ wt.\%}$; $\text{TiO}_2 < 0.36 \text{ wt.\%}$) (Fig. 5).

Clinopyroxene trace element concentrations show a large variation (Fig. 6, Table S10). The REE-normalized diagram demonstrates three distinct patterns (Fig. 6). Clinopyroxene crystals of wehrlites and harzburgite are defined as high-Cr low-Al, but the former is characterized by a strongly LREE-enriched pattern ($\text{La}/\text{Yb}_N = 56.79\text{-}117.88$) while the latter is less enriched ($\text{La}/\text{Yb}_N = 7.59\text{-}10.52$) (Fig. 6a, b). The REE pattern of harzburgite clinopyroxenes also shows La/Sm_N between 4.81 and 7.77 coupled with a flat pattern from middle REE (MREE) to HREE ($\text{Sm}/\text{Yb}_N = 1.24\text{-}1.86$). As observed in the orthopyroxene, the low-Cr high-Al clinopyroxene of spinel lherzolites has an LREE-depleted pattern ($\text{La}/\text{Yb}_N = 0.001\text{-}0.073$), although they record some degree of re-enrichment, especially for samples 1A-76A and 1A-81B (Fig. 6e).

In the PM-normalized multielement diagram (Fig. 6), clinopyroxenes of wehrlites show positive anomalies of LREE (e.g., La and Ce) coupled with negative anomalies of Pb, Ti, and Li (Fig. 6b). Clinopyroxenes of the harzburgite are characterized by positive anomalies of La, Pb, and Sr while Nb, and especially Ta, Zr, Ti, and Li define negative anomalies (Fig. 6d). Concerning the clinopyroxene crystals of spinel lherzolites, they present negative anomalies of Zr, Hf, Ti, and Li (Fig. 6f). Especially regarding the results of wehrlites and lherzolites, the highly incompatible elements (i.e., Cs to U) are strongly scattered (Fig. 6b, f). Comparatively, wehrlites have the lowest Ti/Eu ratios (481-1069), followed by harzburgite (2583-3252) and by lherzolites (4410-6904), which contain the highest values.

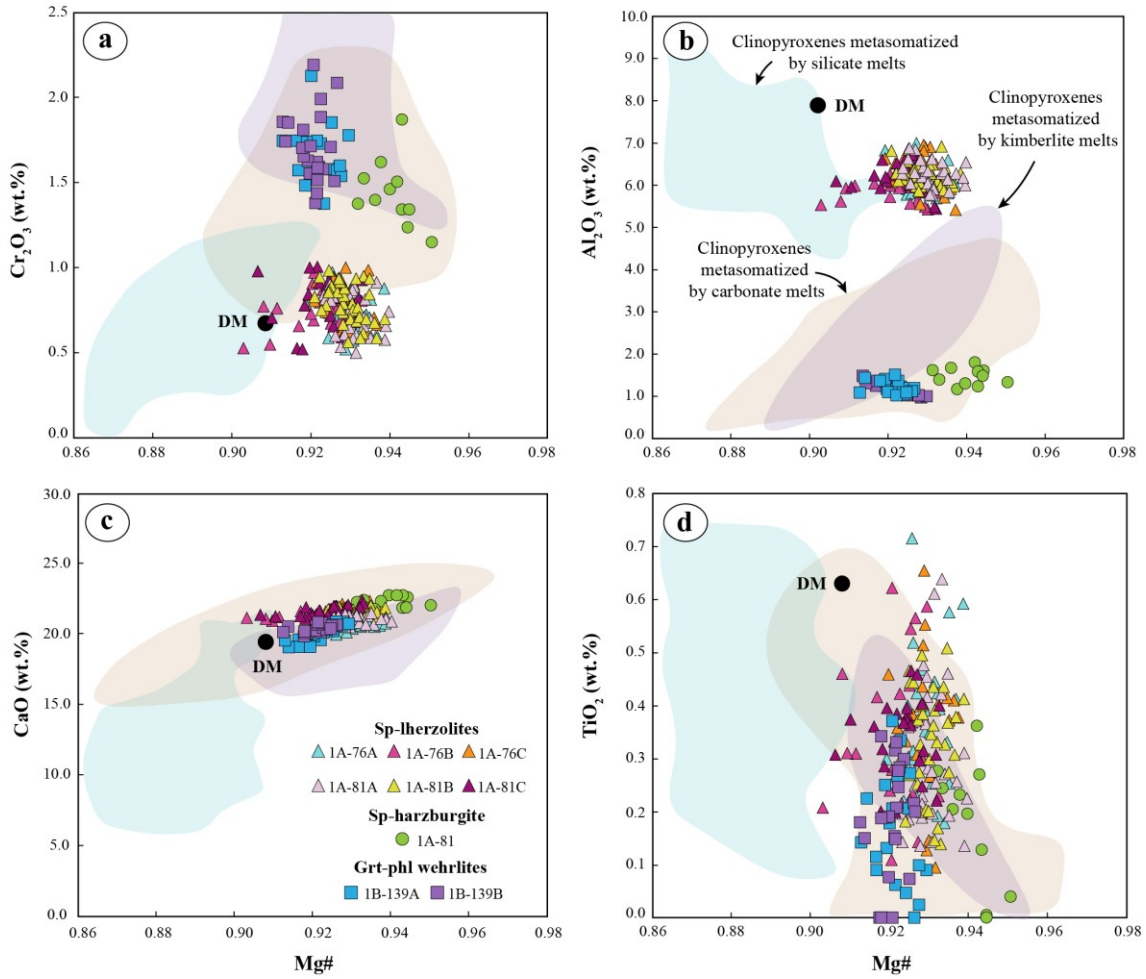


Figure 9. Bivariate plots of major and minor elements (wt.%) as a function of Mg# in clinopyroxenes of Catalão xenoliths (circles, squares, and triangles). Experimental (Yaxley and Green, 1998; Rapp et al., 1999; Yaxley, 2000; Wang et al., 2010; Mallik and Dasgupta, 2012; Wang et al., 2013; Gervasoni et al., 2017), and natural studies (Kilian et al., 2002; Schilling et al., 2005) of clinopyroxenes products of silicate melt metasomatism (light blue field). Experimental (Brey et al., 2008; Sokol et al., 2016) and natural studies (Yaxley et al., 1998; Coltorti et al., 1999; Su et al., 2010; Deng et al., 2017; Ionov et al., 2018; Kopylova et al., 2021) of clinopyroxenes products of carbonatite melt metasomatism (light brown field). Natural studies (Kargin et al., 2016; Fitzpayne et al., 2020) of clinopyroxenes products of kimberlite melt metasomatism (purple field).

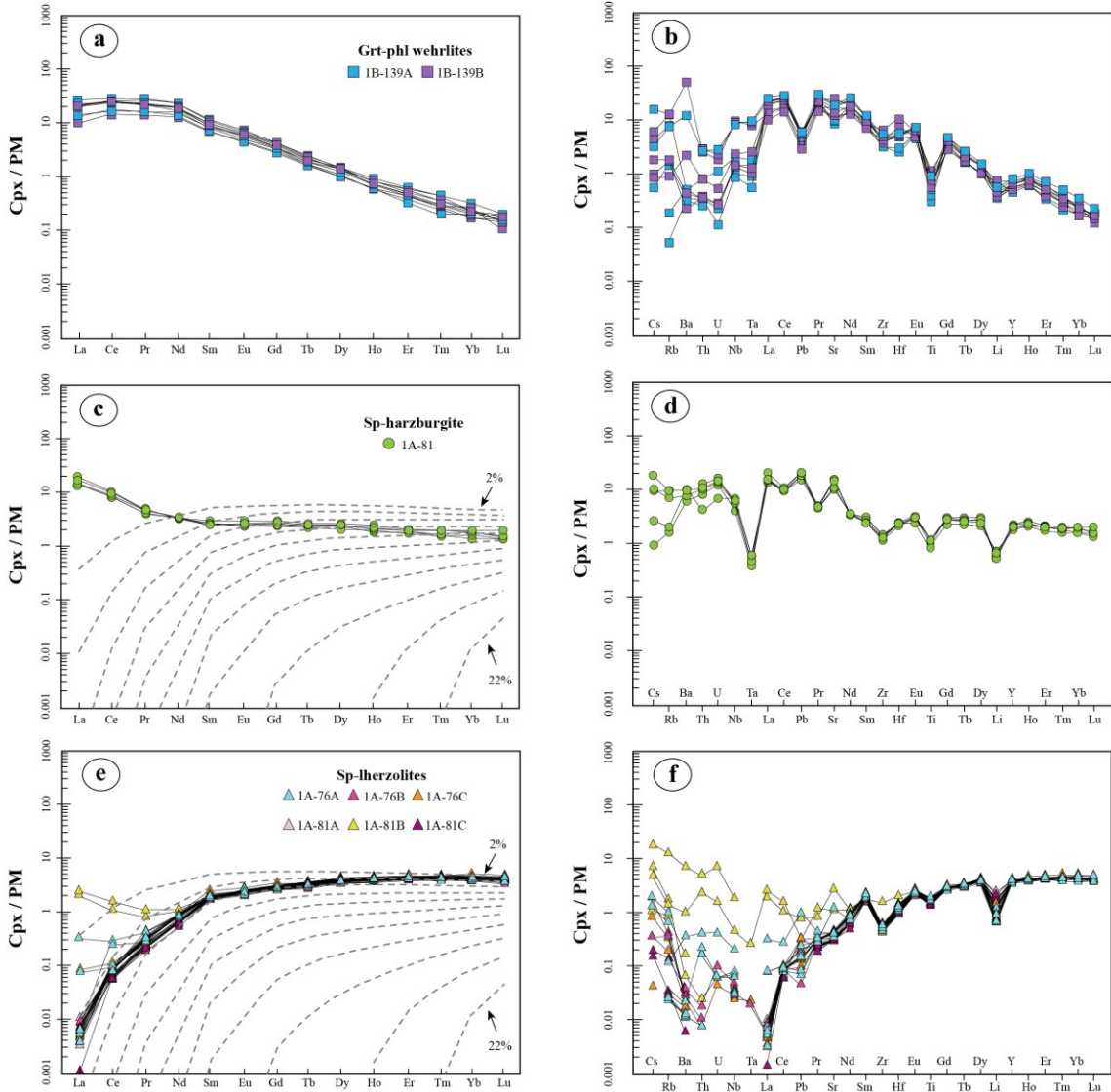


Figure 6. Trace element (LA-ICP-MS) compositions of clinopyroxenes from garnet-phlogopite wehrlites (a, b) from harzburgite (c, d) and from spinel lherzolites (e, f). Primitive mantle values for normalization are from Sun and McDonough (1989). Each dashed line indicates the percentage of partial melting (F) from 2 to 20 % following the increment of 2 %. See text for details about the parameters employed in the modeling.

Garnet is chromium pyrope ($\text{Py}_{67.96-69.31} \text{Alm}_{16.24-17.31} \text{Gr}_{13.21-14.34} \text{Sp}_{0.47-1.18}$) and its occurrence is restricted to the wehrlite xenoliths (Tables S5 and S11). The Mg# of the studied garnet crystals varies from 80 to 84 (0.81 on average) and their Cr_2O_3 contents vary between 4.88 and 5.82 wt.%. CaO contents range from 5.08 to 5.56 wt.%, Al_2O_3 from 18.72 to 19.79 wt.%, and Na_2O from 0.01 to 0.20 wt.%. TiO_2 concentrations are very low and when the values are above the detection limit, they vary

between 0.02 and 0.33 wt.% TiO₂. In the PM-normalized REE diagram (Fig. S2a), garnet shows depleted LREE compared to HREE (La/Yb_N = 0.003-0.014), and a slightly sinusoidal pattern defined by the positive peak at Sm_N (Sm/Sm* = 1.16 and 1.06) considering the average values (where Sm/Sm* = Sm_N/Nd_N×Eu_N^{1/2}). In the PM-normalized multielement diagram (Fig. S2b), the garnet data show positive anomalies of U, Nb, and Pb, whereas Th, La, Sr, and Li define negative anomalies. In the diagrams of Griffin and Ryan (1995) and Griffin et al. (1999) garnets plot in the depleted fields (Fig. S3).

Spinel occurs as three different types in mantle xenoliths from the Catalão region. In spinel lherzolites, they are low-Ti (<0.20 wt.%) with Cr# [Cr/(Cr + Al)] of 9.12-10.67, Mg# of 70.96-74.81, and NiO content in the range of 0.25-0.50 wt.%. Spinel crystals found as symplectites in the harzburgite (CAT-1A-81) are also low in TiO₂ (<0.21 wt.%) with intermediate values of Cr# (27.53-29.15), Mg# (61.79-64.95), and NiO contents (0.13-0.26 wt.%). Spinel crystals from the garnet-phlogopite wehrlites are restricted to the dark rims around garnet, containing high TiO₂ (4.79-5.09 wt.%) with the highest Cr# (73.18-74.50) coupled with the lowest Mg# (45.31-46.25) and NiO content (<0.23 wt.%).

Phlogopites (Phl1 and Phl2) from Catalão mantle xenoliths display a wide variation in terms of major element concentrations (Fig. 7). Phl1 displays lower TiO₂ (0.86-1.32 wt.%, 1.12 wt.% on average) and Cr₂O₃ contents (0.45-0.98 wt.%, 0.72 wt.% on average), coupled with similar Al₂O₃ contents (12.01-14.48 wt.%) compared to Phl2 (TiO₂ = 2.58-4.88 wt.%, Cr₂O₃ = 1.85-4.09 wt.%, Al₂O₃ = 12.97-15.12 wt.%). Usually, Phl1 is characterized by higher MgO (23.46-25.93 wt.%) and lower FeO (3.01-4.06 wt.%) than Phl2 (MgO = 18.69-23.02 wt.%, FeO = 3.51-5.51 wt.%), implying higher Mg# for the former (0.92-0.93) compared to the latter (0.87-0.92). Considering the PM-

normalized REE diagram, both phlogopite types display similar and variable HREE concentrations ($\text{Yb}_N = 0.01\text{-}2.69$). However, Phl2 has higher LREE concentrations ($\text{La/Lu}_N = 4.20\text{-}39.35$) than Phl2 ($\text{La/Lu}_N = 0.35\text{-}4.71$) (Fig. 8a). In the PM-normalized multielement diagram (Fig. 8b), both phlogopite types are enriched in Rb, Nb, Ta, Pb (less pronounced in Phl2), Sr, Zr, Hf, Ti, and Li.

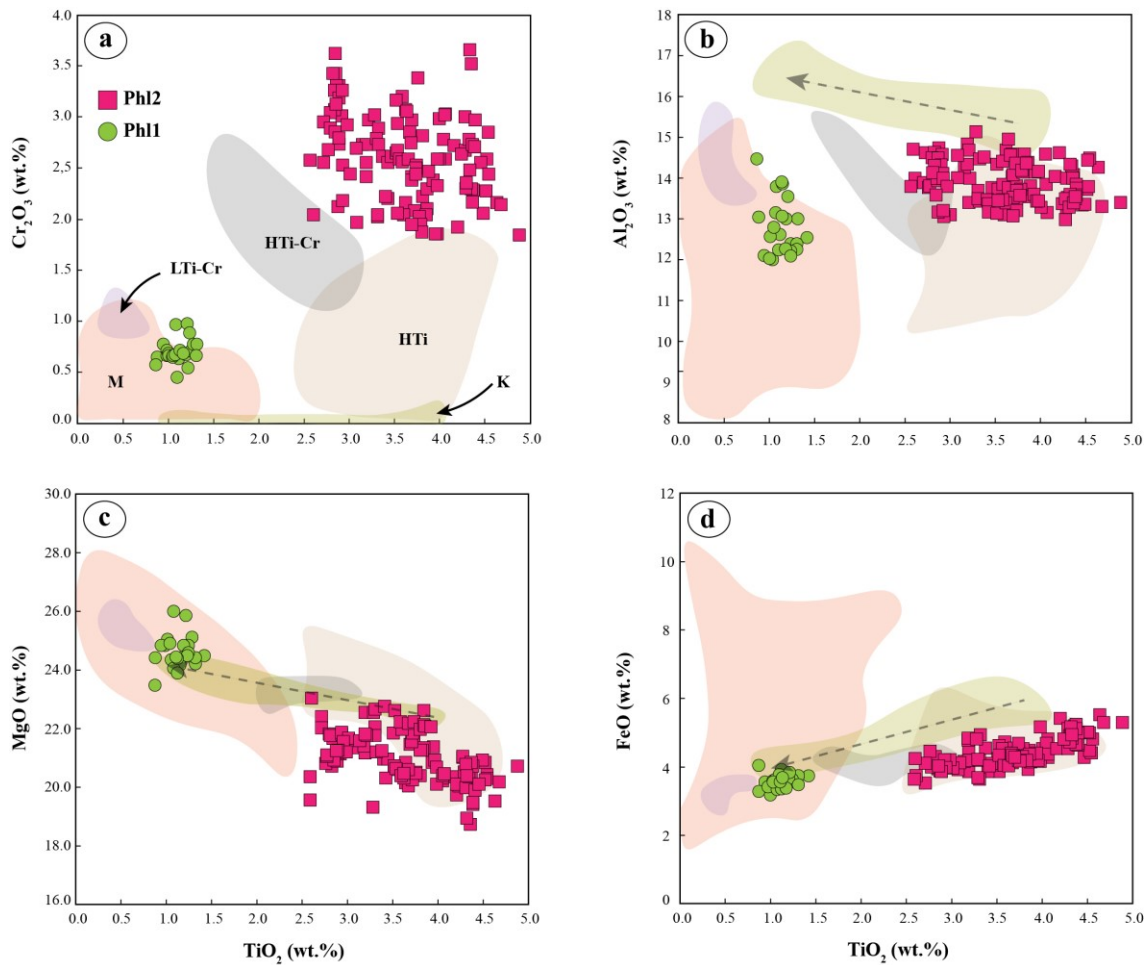


Figure 7. Bivariate plots for major and minor elements of the phlogopite types of the studied xenoliths. Fields of phlogopite from metasomatized xenoliths worldwide (pink field “M”), H-Ti phlogopite from mantle xenoliths including polymict breccia (brown field, “H-Ti”), phlogopites from kimberlite groundmass (green field, “K”) are from [Giuliani et al. \(2016\)](#). High-Ti-Cr phlogopite around garnet from metasomatized xenoliths (grey field “H-Ti-Cr”), Low-Ti-Cr phlogopite around garnet from metasomatized xenoliths (light purple field “L-Ti-Cr”) are from [Kargin et al. \(2019\)](#). The arrows show compositional trends towards more evolved compositions of groundmass phlogopite.

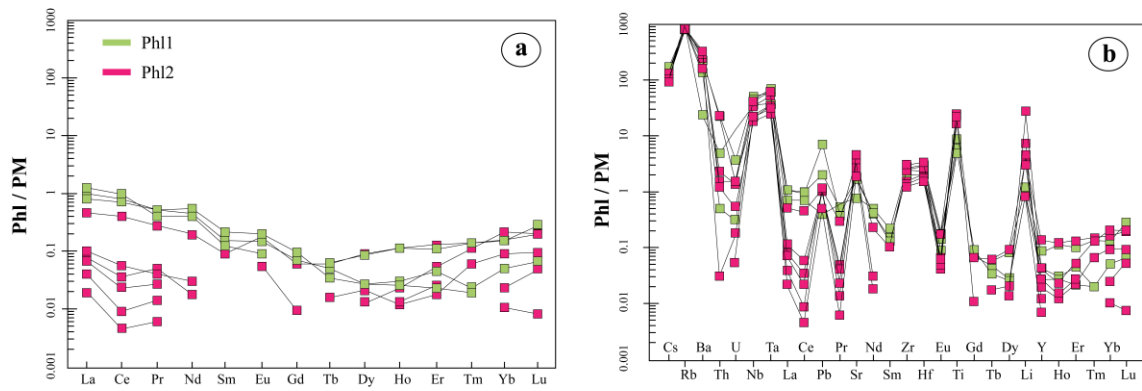


Figure 8. Trace elements of phlogopite of the grt-phl wehrlites xenoliths normalized to the primitive mantle ([Sun and McDonough, 1989](#)).

Table 2. Major element compositions of the mineral phases from Catalão, SFC.

Sample		CAT-1A-76A				CAT-1A-76B				CAT-1A-76C			
Lithology	Sp-lherz	Sp-lherz	Sp-lherz	Sp-lherz	Sp-lherz	Sp-lherz	Sp-lherz	Sp-lherz	Sp-lherz	Sp-lherz	Sp-lherz	Sp-lherz	n
Mineral	O1	Opx	Cpx	Sp	O1	Opx	Cpx	Sp	O1	Opx	Cpx	Sp	n
SiO₂	40.54	55.38	53.02	0.00	39.65	55.02	53.44	0.00	40.54	54.87	52.65	0.00	
TiO₂	0.03	0.07	0.35	0.05	0.02	0.09	0.34	0.04	0.03	0.10	0.36	0.05	
Al₂O₃	0.00	4.32	6.18	57.68	0.00	3.54	5.88	57.40	0.01	4.45	6.38	57.43	
Cr₂O₃	0.02	0.36	0.75	9.31	0.00	0.28	0.76	9.24	0.03	0.38	0.81	9.96	
FeOt	9.69	6.48	1.99	12.21	9.90	6.70	2.17	12.60	10.07	6.59	2.01	13.06	
MnO	0.13	0.12	0.08	0.15	0.15	0.13	0.09	0.11	0.12	0.14	0.08	0.15	
MgO	49.10	33.05	14.54	19.40	49.46	33.32	14.47	19.57	48.96	32.87	14.61	18.81	
NiO	0.36	0.07	0.04	0.33	0.36	0.08	0.03	0.33	0.38	0.08	0.04	0.35	
CaO	0.01	0.36	20.54	0.00	0.01	0.36	21.38	0.01	0.01	0.40	21.58	0.01	
BaO	0.02	0.03	0.03	0.04	0.03	0.03	0.02	0.03	n.a.	n.a.	n.a.	n.a.	
Na₂O	0.03	0.04	1.47	0.01	0.03	0.06	1.62	0.02	0.01	0.06	1.86	0.01	
K₂O	0.01	0.01	0.02	0.00	0.01	0.01	0.01	0.01	0.01	0.01	0.02	0.01	
Cl	0.03	0.01	0.01	0.01	0.02	0.01	0.02	0.01	0.00	0.00	0.00	0.00	
F	n.a.	n.a.	n.a.	n.a.	n.a.	n.a.	n.a.	n.a.	n.a.	n.a.	n.a.	n.a.	
V	0.01	0.02	0.05	0.08	0.01	0.02	0.06	0.07	0.01	0.03	0.05	0.08	
Total	99.98	100.34	99.08	99.28	99.67	100.02	100.31	99.43	100.16	100.01	100.44	99.92	
Mg#	90.03	90.10	92.87	73.91	89.90	89.86	92.25	73.46	89.65	89.89	92.85	71.98	
Cr#			9.76				9.74				10.42		

Note: Mg# = Mg/(Mg + Fe) x 100; Cr# = Cr/(Cr + Al) x 100.

(*) spinel symplectite

Table 2. Continued.

Sample		CAT-1A-81				CAT-1A-81A				CAT-1A-81B			
Lithology	Harz	Harz	Harz	Harz	Sp-lherz	Sp-lherz	Sp-lherz	Sp-lherz	Sp-lherz	Sp-lherz	Sp-lherz	Sp-lherz	Sp-lherz
Mineral	Ol	Opx	Cpx	Sp*	Ol	Opx	Cpx	Sp	Ol	Opx	Cpx	Sp	Sp
n	20	22	11	10	17	24	32	26	22	24	35	20	
SiO₂	41.13	55.80	53.86	0.01	40.42	55.45	53.78	0.00	40.22	54.92	52.50	0.00	
TiO₂	0.04	0.06	0.18	0.10	0.05	0.08	0.30	0.03	0.03	0.09	0.32	0.02	
Al₂O₃	0.01	3.56	1.49	40.83	0.00	4.11	6.23	57.93	0.01	3.91	6.20	58.30	
Cr₂O₃	0.03	0.60	1.44	24.15	0.02	0.31	0.73	9.48	0.02	0.34	0.77	9.17	
FeOt	8.16	5.42	1.93	17.16	9.80	6.50	1.94	11.88	9.81	6.49	1.97	12.05	
MnO	0.10	0.15	0.07	0.18	0.14	0.17	0.07	0.11	0.14	0.16	0.08	0.10	
MgO	50.53	33.99	17.08	16.72	49.17	33.37	14.63	19.18	49.52	33.46	14.59	19.13	
NiO	0.39	0.08	0.03	0.21	0.37	0.07	0.03	0.35	0.37	0.08	0.05	0.33	
CaO	0.01	0.46	22.34	0.01	0.01	0.40	20.87	0.01	0.01	0.49	21.45	0.01	
BaO	n.a.	n.a.	n.a.	n.a.	0.02	0.03	0.02	0.03	0.02	0.02	0.02	0.03	
Na₂O	0.01	0.05	1.51	0.02	0.02	0.05	1.54	0.01	0.02	0.06	1.71	0.01	
K₂O	0.01	0.01	0.03	0.01	0.01	0.01	0.01	0.00	0.01	0.01	0.01	0.01	
Cl	0.01	0.00	0.01	0.00	0.01	0.01	0.01	0.01	0.01	0.01	0.01	0.01	
F	n.a.	n.a.	n.a.	n.a.	n.a.	n.a.	n.a.	n.a.	n.a.	n.a.	n.a.	n.a.	
V	0.01	0.02	0.04	0.11	0.01	0.02	0.05	0.06	0.01	0.04	0.05	0.06	
Total	100.44	100.22	100.02	99.53	100.06	100.59	100.24	99.09	100.21	100.07	99.77	99.26	
Mg#	91.69	91.80	94.06	63.48	89.94	90.16	93.05	74.22	89.99	90.18	92.97	73.88	
Cr#				28.40				9.89				9.55	

Table 2. Continued.

Sample	CAT-1A-81C				CAT-1B-139A					CAT-1B-139B				
Lithology	Sp-lherz	Sp-lherz	Sp-lherz	Sp-lherz	Grt-wehr	Grt-wehr	Grt-wehr	Grt-wehr	Grt-wehr	Grt-wehr	Grt-wehr	Grt-wehr	Grt-wehr	Grt-wehr
Mineral	Ol	Opx	Cpx	Sp	Ol	Cpx	Grt	Phl1	Phl2	Ol	Cpx	Grt	Phl1	Phl2
n	16	23	23	14	26	20	17	1	83	20	21	15	21	36
SiO₂	40.60	55.33	52.55	0.00	40.57	54.32	41.58	39.60	39.17	40.81	54.71	41.44	41.50	39.51
TiO₂	0.03	0.07	0.34	0.06	0.06	0.16	0.08	0.87	3.58	0.04	0.18	0.05	1.12	3.69
Al₂O₃	0.00	4.05	6.16	57.98	0.02	1.20	19.35	14.48	14.03	0.01	1.24	19.29	12.72	13.54
Cr₂O₃	0.04	0.27	0.79	9.65	0.04	1.66	5.37	0.59	2.60	0.02	1.70	5.29	0.71	2.72
FeOt	9.87	6.58	2.14	12.19	8.70	2.69	8.43	4.07	4.38	8.69	2.71	8.36	3.58	4.39
MnO	0.11	0.15	0.08	0.12	0.11	0.09	0.47	0.00	0.01	0.11	0.09	0.40	0.02	0.02
MgO	48.89	32.86	14.52	19.16	49.98	17.70	19.20	23.46	21.24	49.81	17.70	19.02	24.67	20.55
NiO	0.37	0.07	0.03	0.35	0.38	0.07	0.01	0.15	0.12	0.35	0.06	0.01	0.18	0.12
CaO	0.01	0.36	21.56	0.00	0.05	20.07	5.29	0.00	0.02	0.05	20.28	5.34	0.03	0.02
BaO	n.a.	n.a.	n.a.	n.a.	n.a.	n.a.	n.a.	0.12	0.00	n.a.	n.a.	n.a.	0.03	0.00
Na₂O	0.02	0.05	1.82	0.01	0.03	1.38	0.03	0.17	0.17	0.03	1.38	0.04	0.20	0.18
K₂O	0.01	0.01	0.01	0.00	0.02	0.10	0.05	10.31	10.15	0.01	0.09	0.01	10.37	10.24
Cl	0.01	0.01	0.01	0.00	0.01	0.01	0.01	0.02	0.02	0.00	0.00	0.00	0.02	0.02
F	n.a.	n.a.	n.a.	n.a.	n.a.	n.a.	n.a.	0.63	0.50	n.a.	n.a.	n.a.	0.73	0.44
V	0.02	0.03	0.06	0.07	0.01	0.05	0.06	0.00	0.06	0.02	0.05	0.06	0.03	0.07
Total	99.96	99.82	100.06	99.61	99.98	99.48	99.94	94.47	96.07	99.96	100.19	99.31	95.92	95.50
Mg#	89.82	89.90	92.37	73.70	91.10	92.16	80.24	91.13	89.61	91.08	92.08	80.22	92.46	89.24
Cr#				10.04										

Table 3. Trace element compositions of the mineral phases from Catalão, SFC.

Sample	CAT-1A-76A			CAT-1A-76B			CAT-1A-76C			CAT-1A-81			CAT-1A-81A		
Lithology	Lherz	Lherz	Lherz	Lherz	Lherz	Lherz	Lherz	Lherz	Lherz	Harz	Harz	Harz	Lherz	Lherz	Lherz
Mineral	Ol	Opx	Cpx	Ol	Opx	Cpx	Ol	Opx	Cpx	Ol	Opx	Cpx	Ol	Opx	Cpx
ppm															
Li	1.623	1.116	1.301	1.700	1.371	1.121	1.660	0.794	1.528	1.324	1.900	0.959	1.712	1.648	2.779
B	0.407	0.579	0.505	0.370	0.425	0.398	0.426	0.520	0.412	0.614	0.972	2.204	0.456	0.914	0.547
Ti	5.498	514.817	2217	6.987	519.667	2191	4.810	540.167	2369	27.373	530.4	1346.4	4.044	420.18	1910
Rb	–	0.015	0.198	–	–	0.128	–	0.357	0.122	–	0.899	3.728	–	0.457	0.026
Sr	0.022	0.090	11.143	–	0.082	8.125	0.014	0.105	8.080	0.030	5.990	269.4	–	0.199	6.367
Y	–	0.691	16.643	0.002	0.731	15.917	0.003	0.713	17.405	0.004	0.526	8.696	–	0.514	17.995
Zr	–	0.273	5.940	–	0.272	5.717	–	0.285	6.295	–	1.038	14.226	–	0.186	5.238
Nb	0.002	0.013	0.056	–	0.009	0.027	0.011	0.011	0.023	0.190	0.189	3.640	0.002	0.011	0.027
Cs	–	0.051	–	–	0.035	–	0.051	0.014	–	0.278	0.267	–	0.077	–	–
Ba	–	0.031	0.579	0.009	0.042	0.159	0.011	0.158	0.132	0.008	4.800	57.675	0.009	0.055	0.071
La	0.001	0.001	0.049	0.002	0.001	0.005	0.003	0.006	0.003	0.018	0.376	11.266	–	0.001	0.004
Ce	0.002	0.002	0.210	0.008	0.002	0.149	0.006	0.010	0.149	0.014	0.436	17.104	0.001	0.005	0.111
Pr	0.001	0.001	0.092	0.001	–	0.083	–	0.001	0.081	0.002	0.035	1.304	–	0.001	0.063
Nd	–	0.005	1.084	–	0.006	1.083	–	0.011	1.098	–	0.127	4.816	–	0.011	0.858
Sm	–	0.008	0.859	–	0.013	0.859	–	0.009	0.882	–	0.022	1.225	–	0.004	0.787
Eu	0.001	0.005	0.386	–	0.005	0.378	–	0.005	0.407	–	0.010	0.464	–	0.007	0.398
Gd	0.003	0.030	1.617	–	0.027	1.617	0.005	0.035	1.695	–	0.038	1.653	0.005	0.017	1.787
Tb	–	0.007	0.333	–	0.007	0.321	–	0.006	0.344	–	0.009	0.280	–	0.006	0.369
Dy	0.006	0.077	2.788	0.004	0.094	2.597	0.003	0.078	2.828	0.007	0.073	1.888	0.005	0.057	2.988
Ho	–	0.025	0.650	–	0.026	0.619	–	0.026	0.666	0.001	0.020	0.361	–	0.018	0.684
Er	–	0.108	2.050	–	0.118	1.922	–	0.114	2.091	0.003	0.080	0.959	–	0.083	2.042
Tm	–	0.023	0.309	0.001	0.025	0.302	0.001	0.026	0.329	0.001	0.015	0.133	–	0.019	0.316
Yb	0.004	0.228	2.117	0.005	0.239	1.998	0.004	0.230	2.196	0.003	0.141	0.891	0.005	0.184	2.133

Table 3. Continued.

Sample	CAT-1A-76A			CAT-1A-76B			CAT-1A-76C			CAT-1A-81			CAT-1A-81A		
Lithology	Lherz	Lherz	Lherz	Lherz	Lherz	Lherz	Lherz	Lherz	Lherz	Harz	Harz	Harz	Lherz	Lherz	Lherz
Mineral	Ol	Opx	Cpx	Ol	Opx	Cpx	Ol	Opx	Cpx	Ol	Opx	Cpx	Ol	Opx	Cpx
ppm															
Lu	0.001	0.040	0.303	0.001	0.044	0.280	0.001	0.045	0.313	0.001	0.023	0.120	0.001	0.035	0.306
Hf	–	0.019	0.357	–	0.020	0.355	–	0.021	0.389	0.003	0.043	0.675	0.004	0.017	0.294
Ta	0.001	0.002	–	–	–	0.001	–	–	0.001	0.001	–	0.021	–	–	0.124
Pb	0.021	0.028	0.051	0.009	0.041	0.021	0.030	0.083	0.029	0.032	0.475	3.420	–	0.057	–
Th	–	0.001	0.018	–	–	0.001	0.001	–	0.001	0.011	0.079	0.752	–	0.001	–
U	–	–	0.004	–	–	0.002	0.001	–	0.001	0.009	0.062	0.259	–	–	–
REE	0.005	0.544	12.845	0.008	0.571	12.210	0.011	0.551	13.081	0.035	1.384	42.465	0.004	0.418	12.844
(La/Yb)N	0.274	0.001	0.016	0.148	0.001	0.002	0.228	0.010	0.001	4.356	2.172	9.088	–	0.004	0.001
Ti/Eu	5772			5801			5830			2914			4814		

Table 3. Continued.

Sample	CAT-1A-81B			CAT-1A-81C			CAT-1B-139A				CAT-1B-139B				
Lithology	Lherz	Lherz	Lherz	Lherz	Lherz	Lherz	Wehr	Wehr	Wehr	Wehr	Wehr	Wehr	Wehr	Wehr	Wehr
Mineral	Ol	Opx	Cpx	Ol	Opx	Cpx	Ol	Cpx	Grt	Phl2	Ol	Cpx	Grt	Phl1	Phl2
ppm															
Li	1.794	1.240	2.039	1.668	1.290	2.736	1.903	0.741	0.100	7.068	2.028	0.832	0.101	1.555	1.313
B	0.507	0.558	1.274	0.397	0.661	0.600	0.502	0.884	0.614	1.673	0.570	1.086	0.643	7.863	0.960
Ti	12.114	467.4	1983.4	7.507	450.16	2033.2	94.767	712.4	332.450	26265	108.100	944.800	338.250	7906	27215
Rb	–	–	2.130	–	0.982	0.056	0.018	2.660	0.035	539.250	–	3.120	0.051	552	593.5
Sr	–	0.036	20.372	0.014	0.129	6.334	–	277.340	0.071	65.800	0.025	359.120	0.057	29.700	62.850
Y	0.005	0.731	17.632	–	0.525	17.914	0.007	2.829	3.074	0.219	0.006	2.878	3.190	0.231	0.117
Zr	–	0.248	7.700	–	0.167	5.378	1.113	44.120	1.285	21.908	1.157	53.060	1.283	25.967	13.765
Nb	0.002	0.010	0.361	–	0.013	0.020	0.305	1.968	0.201	19.725	0.339	3.301	0.203	30.760	13.360
Cs	–	–	0.257	–	0.112	0.006	–	0.208	–	3.690	–	0.088	–	4.570	3.170
Ba	–	0.015	15.013	–	0.248	0.120	0.035	19.324	–	1879.25	–	87.478	–	903.333	1826.5
La	0.000	0.000	0.795	–	0.011	0.002	0.002	14.198	0.011	0.118	0.002	11.768	0.011	0.673	0.031
Ce	–	0.003	1.050	–	0.001	0.104	0.004	42.300	0.070	0.221	0.005	37.604	0.073	1.503	0.024
Pr	–	0.001	0.148	–	–	0.056	–	6.320	0.028	0.027	0.001	5.296	0.022	0.132	0.005
Nd	–	0.007	1.070	–	–	0.759	–	26.446	0.209	0.120	0.006	24.004	0.197	0.609	–
Sm	–	0.005	0.770	–	0.010	0.797	–	4.118	0.091	0.041	–	4.074	0.075	0.073	–
Eu	–	0.005	0.396	–	0.003	0.393	–	1.001	0.030	0.015	–	1.044	0.032	0.025	0.010
Gd	–	0.030	1.723	–	–	1.730	–	2.202	0.129	0.039	–	2.268	0.144	0.050	0.006
Tb	–	0.008	0.362	–	0.006	0.364	–	0.220	0.034	0.004	–	0.227	0.033	0.005	–
Dy	–	0.086	2.918	–	0.052	2.960	0.004	0.915	0.354	0.039	–	1.021	0.361	0.033	0.009
Ho	–	0.029	0.675	–	0.018	0.678	0.001	0.122	0.112	0.008	–	0.127	0.117	0.009	0.004
Er	–	0.111	2.100	–	0.085	2.150	0.002	0.235	0.469	0.027	–	0.244	0.487	0.026	0.023
Tm	0.001	0.026	0.320	–	0.019	0.311	–	0.025	0.092	0.007	0.001	0.024	0.097	0.004	0.008
Yb	0.003	0.228	2.164	–	0.184	2.090	–	0.112	0.853	0.034	0.007	0.118	0.882	0.044	0.097

Table 3. Continued.

Sample	CAT-1A-81B			CAT-1A-81C			CAT-1B-139A				CAT-1B-139B				
Lithology	Lherz	Lherz	Lherz	Lherz	Lherz	Lherz	Wehr	Wehr	Wehr	Wehr	Wehr	Wehr	Wehr	Wehr	Wehr
Mineral	Ol	Opx	Cpx	Ol	Opx	Cpx	Ol	Cpx	Grt	Phl2	Ol	Cpx	Grt	Phl1	Phl2
ppm															
Lu	0.004	0.041	0.303	0.002	0.036	0.302	–	0.013	0.153	0.006	–	0.011	0.154	0.009	0.015
Hf	–	0.017	0.397	–	0.014	0.306	0.024	1.259	0.030	0.765	0.029	2.119	0.036	0.740	0.493
Ta	–	–	0.011	0.001	–	–	0.020	0.115	0.006	1.734	0.019	0.176	–	2.265	1.069
Pb	–	–	0.209	–	–	–	–	0.967	0.027	0.179	0.000	0.874	–	0.575	0.144
Th	–	–	0.058	–	–	–	–	0.074	0.006	0.574	–	0.121	0.007	0.795	0.100
U	–	–	–	–	–	–	–	0.022	0.007	0.025	–	0.022	0.009	0.117	0.005
REE	0.002	0.540	14.633	0.001	0.396	12.695	0.004	98.227	2.604	0.582	0.008	87.831	2.623	3.164	0.150
(La/Yb)N	–	0.001	0.208	–	0.007	0.000	–	93.332	0.005	2.986	–	70.812	0.005	14.968	0.352
Ti/Eu	5018			5186			713				926				

5.6 Results of Raman spectroscopy

Olivine crystals in the harzburgite (sample 1A-81) and wehrlite (sample 1B-139B) samples contain highly birefringent crystals that were identified by Raman spectroscopy as carbonates. In the harzburgite, olivine contains inclusions of dolomite identified by Raman shifts at 175, 300, 723, and 1098 cm⁻¹ (Fig. 9a). On the other hand, the carbonate inclusions identified in olivine crystals of wehrlite are magnesite with characteristic peaks at 213, 738, and 1095 cm⁻¹ (Fig. 9b). Note that the olivine spectra in both cases are well-defined through their doublets at 823 and 855 cm⁻¹, as well as by less intense peaks at 882 cm⁻¹, 917-918 cm⁻¹, and 961-962 cm⁻¹.

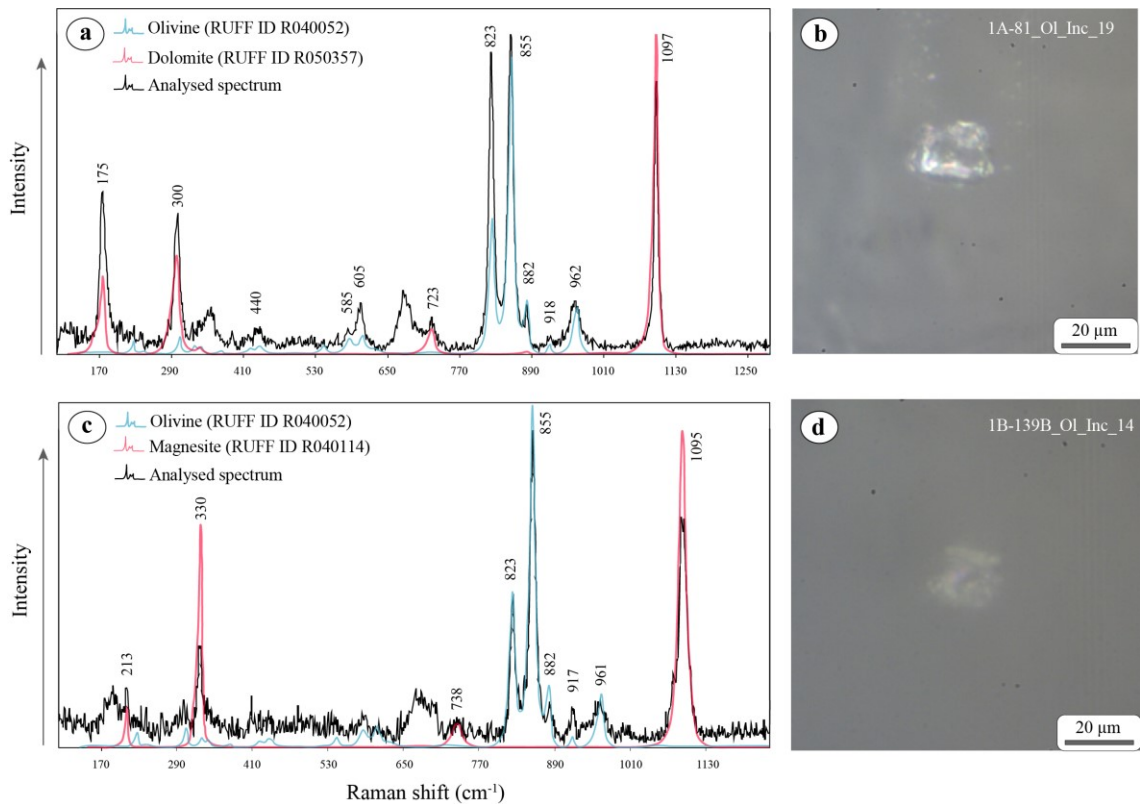


Figure 9. Raman spectra between 120 and 1300 cm⁻¹ of analyzed olivine (a, b), dolomite (a), and magnesite (b) (all indicated in black). The overlapped spectrum in blue is relative to olivine (ID R040052; RUFFTM) while red ones represent the carbonates (dolomite ID R050357.2 and magnesite ID 040114; RUFFTM).

5.7 Geothermobarometry

The equilibrium temperatures and pressures (Table 1) of Catalão mantle xenoliths investigated in this work were obtained for average compositions (i.e., core and rim measurements). This was justified due to the negligible compositional variations observed for major elements (< 1 wt.%). The temperatures for spinel lherzolites were calculated with the Mg-Fe two-pyroxene thermometer ($T_{\text{Mg-Fe}}$; [Brey and Köhler, 1990](#)), REEs, and Y two-pyroxene thermometer (T_{REE} ; [Liang et al., 2013](#)), and the single-pyroxene thermometer (T_{Cpx} ; [Mercier, 1980](#)). The average temperatures obtained for these peridotites vary from 876 to 915 °C, whereas garnet-phlogopite wehrlites were equilibrated at higher temperatures (1066-1101 °C; [Mercier, 1980](#); [Nimis and Taylor, 2000](#)) (Table 1). The temperatures for harzburgite were calculated using Ca-in-Opx thermometer ($T_{\text{Ca-in-Opx}}$; [Brey and Köhler, 1990](#)) and single-pyroxene thermometer (T_{Cpx} ; [Mercier, 1980](#)) varying from 975 to 990 °C. Temperature calculated using T_{REE} thermometer displays a lower temperature of 886 °C (Table 1.) Reliable pressure estimates were obtained only for garnet wehrlites using the geobarometer proposed by [Nimis and Taylor \(2000\)](#) (P_{NT00}), yielding between 5.03 and 5.23 GPa. Testing the [Nimis and Taylor \(2000\)](#) geobarometer in the harzburgite, a similar pressure was obtained (5.28 GPa)

5.8 Geochemical modeling of partial melting

To determine partial melting degrees (F), the HREEs (i.e., Yb and Lu) of clinopyroxenes were selected because they have similar partition coefficients and, consequently, similar geochemical behavior. The extent of partial melting was reconstructed using the non-modal batch melting equation of [Johnson et al. \(1990\)](#):

$$\frac{C_i^{cpx}}{C_i^{o,cpx}} = \left[1 - \frac{PF}{D_i^o}\right]^{\left(\frac{1}{P} - 1\right)}$$

Where C is the concentration of the element in the solid, D_i is the partition coefficient of the element between solid and liquid, P is the bulk distribution coefficient of the element for the assemblage in equilibrium with the liquid, and F is the fraction of the liquid (melt) (Shaw, 2006). As source, we used the primitive mantle REE values (Sun and McDonough, 1989) and a modal spinel peridotite composition (Ol = 0.62, Opx = 0.24, Cpx = 0.12, Sp = 0.02) (McDonough, 1990). The melt modes for spinel facies (Ol = -0.06, Opx = 0.28, Cpx = 0.60, Sp = 0.11) are from Johnson (1998) while the mineral/melt partition coefficients were taken from Ionov et al. (2002). Spinel lherzolites record between 2 and 4 % of melt extraction, whereas harzburgite records around 10 %. A reliable F estimate for wehrlites was not achieved applying the same parameters described above but observing the change from spinel to garnet facies (Ol = 0.03, Opx = -0.16, Cpx = 0.88, Grt = 0.09) (Johnson, 1998) and the modal average composition of our wehrlites (Ol = 0.65, Opx = 0.00, Cpx = 0.29, Grt = 0.06). However, considering that wehrlites are the most depleted samples of Catalão, and comparing their HREE normalized concentrations with the harzburgite that has 10 % of partial melting, certainly, they represent the solid residue after higher degrees of melting extraction (Fig. 6c).

5.9 Discussion

5.9.1 The lithosphere beneath the southwestern edge of the SFC

Based on previous geophysical investigations, the SFC domain extends beyond that constrained by its surface boundaries (Rocha et al., 2011, 2019; Carvalho et al.,

2022). Tomographic data revealed that the SFC belongs to a larger block – the São Francisco Paleocontinent (Rocha et al., 2011) – that was amalgamated during the consolidation of the Columbia (or Nuna) supercontinent at around 2.0 Ga. This conclusion is based on the existence of a high-velocity anomaly, typical of cratonic regions, that extends beneath the Neoproterozoic Brasília mobile belt domain westward of the current SFC outcropping limits (Rocha et al., 2011, 2019). These results are supported by temperature and pressure estimates of mantle xenoliths and xenocrysts (garnet and clinopyroxene) hosted by alkaline volcanic rocks from the APIP, which display typical cratonic geotherms (~ 35 mW/m²; Leonardos et al., 1993; Costa, 2008; Fernandes et al., 2021; Carvalho et al., 2022a, b). In addition, magnetotelluric investigations, gravimetric, and geoid anomaly modeling of the southern part of the SFC demonstrated that the lithosphere underneath has been modified by episodic percolation of fluids and/or melts possibly rich in Fe, H₂O, and CO₃ components derived from depths higher than 180-200 km (Pinto et al., 2010). These authors also observed an increase in density of the APIP lithosphere from 120 km (40 kg/m³) up to 200 km (50 kg/m³), which has been attributed to the presence of progressively denser metasomatic assemblages.

The APIP xenoliths and xenocrysts from kimberlites display strong evidence of both modal and cryptic metasomatism. The modal metasomatism is evidenced by the crystallization of secondary clinopyroxene, phlogopite, ilmenite, amphibole, and exotic accessory mineral phases (e.g., mathiasite-loveringite and priderite) (Costa, 2008; Almeida et al., 2014; Nannini, 2016). The cryptic nature of metasomatism was established by the enrichment of incompatible elements in primary minerals (Nannini, 2016). According to Fernandes et al. (2021), spinel peridotites from Indaiá-1 and Limeira-1 kimberlites have a more depleted composition than garnet peridotites from

the Canastra-1 kimberlite. Similarly, pyrope xenocrysts from the Osvaldo França 1 kimberlite revealed a stratified SCLM, with the deeper mantle (3.6-4.3 GPa) being enriched in incompatible elements represented by sinusoidal and spoon-like trace element patterns, whereas the shallower mantle (2.0-3.2 GPa) contains a more depleted character (Carvalho et al. 2022a, b).

The garnet and spinel peridotites of the Catalão mantle xenoliths evidenced the metasomatism beneath the SFC and also the stratified nature of the SCLM beneath the APIP. This corroborates the early observations made by radiogenic isotope studies on the mafic potassic/ultrapotassic volcanic rocks (e.g., Gibson et al., 1995; Carlson et al., 2007). As observed in other samples from the APIP (Fernandes et al., 2021; Carvalho et al., 2022), garnet wehrlites beneath Catalão represent a deep and strongly metasomatized cratonic lithosphere (from a depth of ~170 km) that reacted with deep-seated melts or fluids (see details below), whereas the spinel lherzolites represent a shallower (from a depth of ~50 km) and depleted mantle, which is only slightly metasomatized.

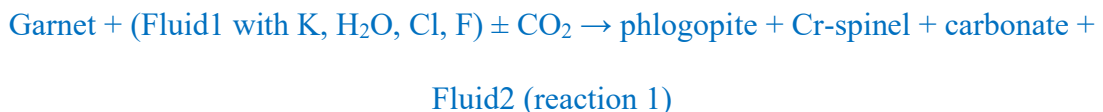
5.9.2. *Nature of metasomatism in the southwestern SFC lithosphere*

5.9.2.1 *Primary metasomatism in the deep lithospheric mantle beneath Catalão caused by K-rich hydrous fluids/melts forming low-Ti-Cr phlogopite (Phl1)*

In the Catalão xenoliths, the occurrence of phlogopite is restricted to garnet wehrlites. These can be divided into two groups: Phl1 contain low TiO₂ (1.12 wt.%, on average) and Cr₂O₃ (0.71 wt.%, on average) coupled with high Mg# (~0.92) compared to Phl2 (TiO₂ = 3.6 wt.%, Cr₂O₃ = 2.58 wt.%, and Mg# = 0.90). Regarding fluorine contents, phlogopites display wide and similar variation from 0.12 to 0.21 wt.% (Phl1: average of 0.16 wt.%) and from 0.05 to 0.24 wt.% (Phl2: average of 0.11 wt.%). In

general, phlogopite with low TiO_2 (<1.5 wt.%) and Cr_2O_3 (<1 wt.%) are similar to minerals in equilibrium with a metasomatized garnet peridotite assemblage in the upper mantle (Carswell, 1975; Giuliani et al., 2016; Kargin et al., 2019). Note that Ph11 is classified as low-Ti-Cr, being compositionally similar to large phlogopite crystals from the metasomatized lithospheric mantle formed before the generation of the host kimberlite (Ph11 from Kargin et al., 2019), as well as with phlogopite from metasomatized mantle xenoliths worldwide (Giuliani et al., 2016) (Fig. 7). Trace element contents (Ti vs. Cr, Ba, V, Sr, Zr, and Nb) of Ph11 from the studied wehrlites also overlap the field defined for phlogopite of metasomatized xenoliths (Giuliani et al., 2016) (Fig. S4).

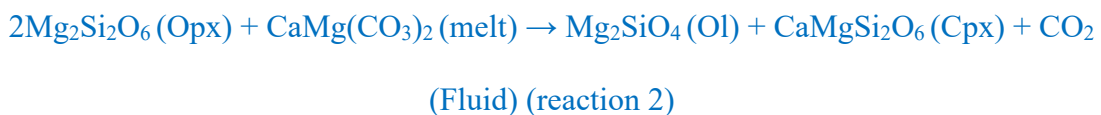
Kopylova et al. (2010) studied different types of phlogopites present in kimberlites and concluded that low-Ti-Cr phlogopite is not related to the kimberlite crystallization but is probably related to inherited xenocrysts from metasomatized mantle xenoliths. Furthermore, phlogopite with low TiO_2 is not in equilibrium with kimberlite melts because equilibrated mica should contain high TiO_2 (>2 wt.%), as typically observed in phlogopite from polymict breccias, high-Ti-Cr phlogopite macrocrysts from kimberlite, and phlogopite from the kimberlite groundmass (e.g., Carswell, 1975; Giuliani et al., 2016; Kargin et al., 2019). According to Kargin et al. (2019), the low-Ti-Cr phlogopite is formed by the interaction of K, $\text{H}_2\text{O} \pm \text{F}$, and CO_2 -rich fluids with peridotite as described in the reaction (1):



Therefore, Ph11 of wehrlites is a primary mineral with low Ti-Cr contents, which belongs to a metasomatized deep cratonic lithosphere that formed before the generation of the host kimberlite (i.e., has a primary metasomatic origin).

5.9.2.2 Carbonate-rich melt metasomatism in the deep cratonic lithosphere recorded by clinopyroxenes from wehrlites and harzburgite

Among the studied xenoliths, two garnet wehrlites were stable at the deep mantle (~170 km) beneath the Catalão region. The conversion of lherzolite or harzburgite to wehrlite or orthopyroxene-poor mantle rock requires the interaction with a CO₂-rich melt (e.g., Yaxley et al., 1998; Aulbach et al., 2020). Experimental investigations focused on the reactions between carbonatite and/or ultramafic silicate-carbonate melts with mantle peridotite confirmed the formation of wehrlites (Gervasoni et al., 2017). Secondary clinopyroxene and olivine crystallized at the expense of orthopyroxene by reaction (2) (Klemme et al., 1995; Gervasoni et al., 2017) may explain the studied wehrlites and indicate the presence of carbonate-rich melt as a metasomatic agent that affected the deeper lithospheric mantle of the SFC beneath Catalão.



Moreover, in terms of chemical composition, the interaction of carbonatite melts with peridotites favors the enrichment of CaO, Cr₂O₃, Na₂O, CO₂, H₂O, and Mg#, coupled with the depletion of TiO₂ and Al₂O₃ contents. In addition, carbonatite melt metasomatism is characterized by high Ca/Al and Zr/Hf ratios, low Ti/Eu ratio, extremely fractionated LREE over HREE (i.e., high La/Yb_N), and relative depletion in HFSE (Zr, Hf, Nb, Ta) compared to LREE (Yaxley et al., 1998; Klemme et al., 1995; Coltorti et al., 1999).

Very similar features are observed in both wehrlites studied here, where clinopyroxenes are strongly fractionated in LREE over HREE (La/Yb_N = 56.79-117.88)

(Fig. 6a). In contrast, clinopyroxenes of the harzburgite are characterized by flat REE pattern from Nd to Lu, with steep positive slopes in the LREE ($\text{La/Yb}_N = 7.59\text{-}10.52$) (Fig. 6c). Orthopyroxene usually records partial melting in peridotites being characterized by strong depletion of LREE compared to HREE. In the studied harzburgite the orthopyroxene retains the depleted REE pattern from Lu to Sm ($\text{Sm/Lu}_N = 0.08\text{-}0.21$) but displays selective enrichment from Sm to La ($\text{La/Sm}_N = 8.59\text{-}16.28$) (Fig. 4a). It also displays the highest average content of Sr (5.99 ppm) and Zr/Hf ratio (24.62), and the lowest average of Ti/Nb (5480) and Ti/Eu (53767) ratios compared to orthopyroxenes from spinel lherzolites ($\text{Sr} = 0.10 \text{ ppm}$, $\text{Zr/Hf} = 14.60$, $\text{Ti/Nb} = 43827$, $\text{Ti/Eu} = 110883$).

Furthermore, the high-Cr low-Al clinopyroxene crystals from garnet-phlogopite wehrlites and the harzburgite present a positive correlation between CaO vs. $\text{Mg}^{\#}$ (Fig. 5c) and Ca/Al vs. $\text{Mg}^{\#}$ (Fig. 10a). These clinopyroxenes have Ca/Al ratios between 18.02 and 27.28, which are significantly higher compared to typical metasomatism promoted by carbonatite melts (usually >5) (Klemme et al., 1995; Yaxley and Green, 1998; Neumann et al., 2002; Brey et al., 2008; Gervasoni et al., 2017). The high $\text{Mg}^{\#}$ of these samples corroborates this assumption. Figure 10b correlates La/Yb_N vs. Ti/Eu since these element ratios are key for distinguishing carbonatite from silicate melt metasomatism (e.g., Klemme et al., 1995; Coltorti et al., 1999). Clinopyroxene crystals from harzburgite and garnet-phlogopite wehrlites are the result of a carbonatite melt metasomatism in the deep cratonic lithosphere from the SFC beneath the Catalão region.

The trace element ratios depicted in Figure 10c-d, displaying Sr vs. Ti/Eu and Zr/Hf vs. Ti/Nb , also support the affinity of these clinopyroxenes with carbonatite melt metasomatism, although it is less evident for the harzburgite sample (Coltorti et al.,

1999; Neumann et al., 2002; McCoy-West et al., 2015; Su et al., 2016; Deng et al., 2017; Ionov et al., 2018). Therefore, we can conclude that both pyroxenes of the Catalão harzburgite and wehrlites are products of variable extents of carbonatite melt metasomatism, considering the significant difference in their partition coefficients and, consequently, of the trace element concentrations. Additional evidence of carbonatite metasomatism in the Catalão mantle xenoliths is the presence of abundant inclusions of dolomite (in harzburgite) and magnesite (in wehrlite) in olivine crystals (Fig. 9).

However, the distinction between carbonatite and kimberlite metasomatism is often obstructed due to the similarities between major and trace elements, as observed in Figures 5 and 10. Several authors argue that reactions between peridotite and kimberlite melt are capable of generating clinopyroxene, such as type I clinopyroxenes of Grégoire et al. (2002), which would be very similar to those of PIC (Phlogopite-Ilmenite-Clinopyroxene) mantle suite (Grégoire et al., 2002; Fitzpayne et al., 2018, 2020) or so-called megacrysts (Bussweiler et al., 2018 and references therein). According to trace element modeling, clinopyroxene of PIC assemblage is related to metasomatism caused by failed kimberlite intrusions in the deepest regions of the lithospheric mantle (Fitzpayne et al., 2018, 2020). These clinopyroxenes are characterized by lower Mg# (89-91), Sr (120-150 ppm), La/Zr (<0.03), and Ce/Yb_N (11-21) (Fitzpayne et al., 2018, 2020) when compared to wehrlites and harzburgite clinopyroxenes from Catalão (Mg# = 0.91-0.94; Sr = 187-531 ppm; La/Zr = 0.13-1.09; Ce/Yb_N = 82.20-132.63). Note that the low Ce/Yb_N ratio (4.61-5.82) is a characteristic of harzburgite due to its near-flat REE pattern. Therefore, we conclude that the compositional features discussed above are conspicuous evidence of carbonatite melt metasomatism recorded by clinopyroxenes of wehrlites and harzburgite.

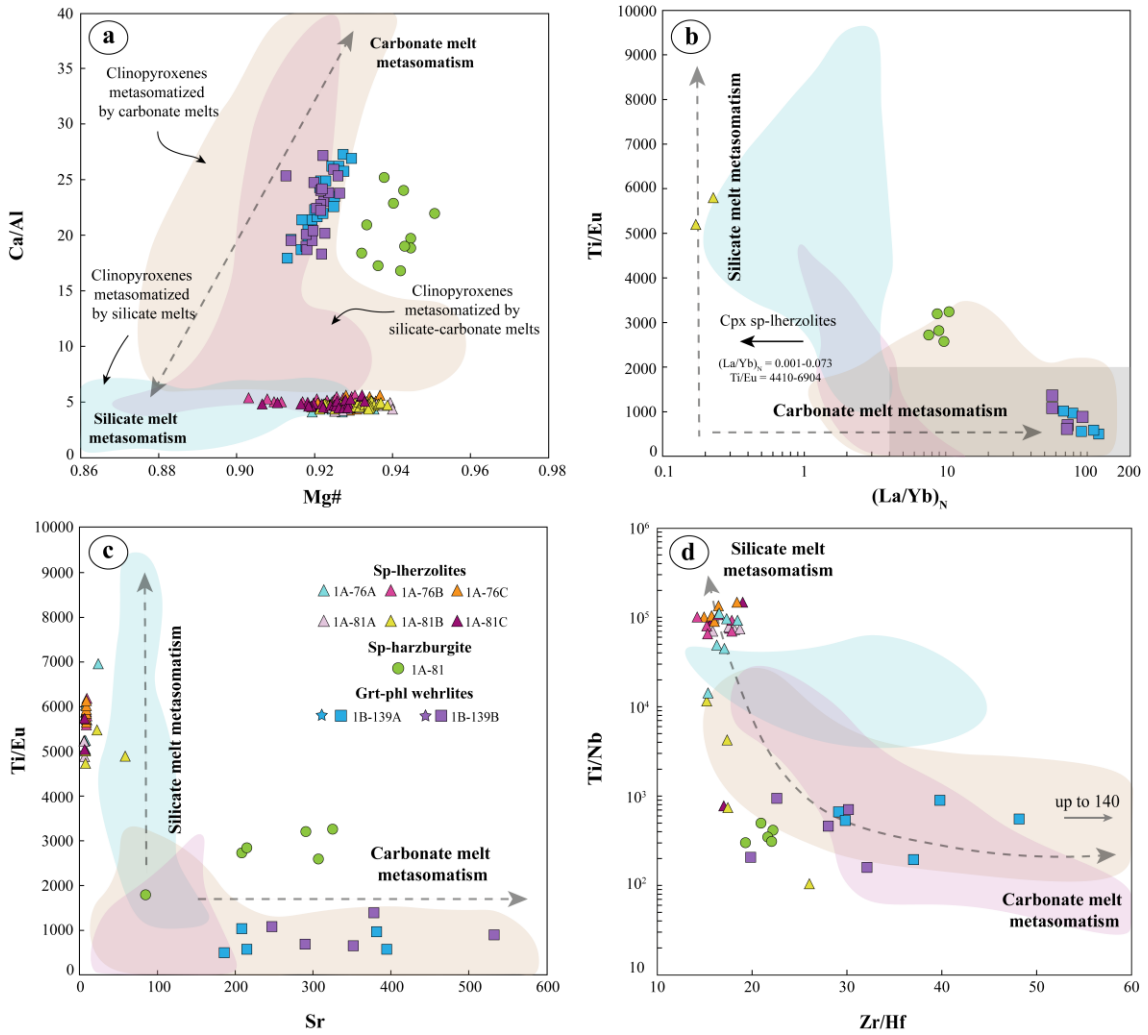


Figure 10. (a) Plots of Ca/Al (atomic ratios) vs. Mg# of clinopyroxenes. Experimental and natural studies of clinopyroxenes metasomatized by carbonatite melts (light brown field) are from [Yaxley et al. \(1998\)](#), [Coltorti et al. \(1999\)](#), [Brey et al., \(2008\)](#), [Su et al. \(2010\)](#), [Su et al. \(2016\)](#), [Sokol et al. \(2016\)](#), [Deng et al. \(2017\)](#), [Ionov et al. \(2018\)](#), and [Kopylova et al. \(2021\)](#). Clinopyroxenes metasomatized by silicate-carbonate melts are from [Neumann et al. \(2002\)](#). Experimental and natural studies of clinopyroxenes metasomatized by silicate melts (light blue field) are from [Yaxley and Green \(1998\)](#), [Rapp et al. \(1999\)](#), [Yaxley \(2000\)](#), [Kilian et al. \(2002\)](#), [Schilling et al. \(2005\)](#), [Wang et al. \(2010\)](#), [Mallik and Dasgupta \(2012\)](#), [Wang et al. \(2013\)](#), and [Gervasoni et al. \(2017\)](#). (b) Plots of La/Yb_N vs. Ti/Eu ratios of clinopyroxenes and garnet (stars). The Grey area represents carbonatite metasomatism from [Coltorti et al. \(1999\)](#). (c-d) Plots of Sr vs. Ti/Eu and Ti/Nb vs. Zr/Hf of clinopyroxenes. The field of clinopyroxenes metasomatized by carbonatite melts (light brown field) is from [Coltorti et al. \(1999\)](#), [Zheng et al. \(2005\)](#), [McCoy-West et al. \(2015\)](#), [Su et al. \(2016\)](#), [Deng et al. \(2017\)](#), [Ionov et al. \(2018\)](#) and [Pattnaik et al. \(2020\)](#). Clinopyroxenes metasomatized by silicate-carbonate melts (pink field) are from [Neumann et al. \(2002\)](#). Clinopyroxenes metasomatized by silicate melts (light blue field) are from [Zhang et al. \(2011\)](#) and [Patkó et al. \(2020\)](#). Arrows show metasomatic trends for carbonatite and silicate metasomatisms. Stars represent garnet compositions.

5.9.2.3 Proto-kimberlite melt as a metasomatic agent forming high-Ti-Cr phlogopite (*Phl2*) in the deep lithospheric mantle

Peridotite xenoliths from the cratonic lithosphere may record modal metasomatic events with the formation of mineral phases caused by interactions with kimberlite melts. High-Ti phlogopites (>2 wt.% TiO₂) that are usually present as xenocrysts in kimberlite groundmass and high-Ti rims of phlogopites in cratonic mantle xenoliths are typical micas formed during reaction with kimberlite melts (e.g., [Carswell, 1975](#); [Giuliani et al., 2014, 2016](#); [Kargin et al., 2019](#); [Gervasoni et al., 2022](#)). The interaction between kimberlite melts and peridotites with a concomitant phlogopite generation can occur either during the magma ascent to the surface (i.e., secondary phlogopite) or within the lithosphere by melts that froze at mantle depths (i.e., primary phlogopite). Nevertheless, the major question about these reactions is whether the metasomatic agent is the proper kimberlite magma that carries the mantle xenoliths, or another precursory melt or fluid similar in composition.

According to [Giuliani et al. \(2016\)](#), successive episodes of magma pulses at the base of the cratonic lithosphere can interact with the mantle wall rocks, preventing its ascending to the surface probably due to the highly reactive nature of these melts and their small volumes. [Tappe et al. \(2018\)](#) also suggest that kimberlites represent magma drainage of incipient melts that are continuously present at the lithosphere-asthenosphere boundary, and not a single mantle melting event. A rare type of xenolith, the so-called polymict mantle breccias are often assumed to be crystallized from failed kimberlite melts, and phlogopite in these breccias displays high TiO₂ and Cr₂O₃ contents ([Giuliani et al., 2014](#)).

High-Ti phlogopite is common in mica-rich clinopyroxenite xenoliths from the Carolina kimberlite beneath the Amazonian Craton ([Gervasoni et al., 2022](#)), and is also

reported in garnet peridotite and clinopyroxene-phlogopite xenoliths as rims around low-Ti-Cr phlogopite and as small flakes around garnet porphyroblasts, both present in the Bultfontein kimberlite, Kaapvaal Craton ([Giuliani et al., 2016](#)) and Grib kimberlite, East European Craton ([Kargin et al., 2019, 2022](#)). Such high Ti-Cr rims are characterized as products of proto-kimberlite melt metasomatism in the deep cratonic mantle.

In garnet-phlogopite wehrlite xenoliths from the Catalão region, Phl2 occurs as an overgrowth rim around Phl1 (Figs. 2c, 3c), as large and equilibrated flakes around garnet porphyroblasts (Figs. 2b, 3), as well as in the wehrlite matrix (Fig. 2d). Major and trace element compositions of Phl2 overlap those of phlogopite from polymict breccias ([Giuliani et al., 2016](#)), high-Ti-Cr phlogopites from garnet peridotites, and high-Ti-Cr macrocrysts from kimberlites ([Giuliani et al., 2016; Kargin et al., 2019, 2021](#)) (Figs. 7, S4). Moreover, Phl2 also shows major and trace element compositions very distinct from those of mica typical in the kimberlite groundmass (Figs. 7, S4).

Phlogopite in kimberlite groundmass crystallized at crustal levels is characterized by enrichment of Al_2O_3 (11.90-17.50 wt.%), Zr (76-438 ppm), Nb (39-78 ppm), and Ba (4000-22000 ppm), coupled with lower values of Mg# (86-92), Ni (74-353 ppm), and Cr_2O_3 (up to 0.5 wt.%) than phlogopites formed at mantle depths ([Giuliani et al., 2016; Kargin et al., 2019](#)). In general, Phl2 of the Catalão xenoliths contains a contrasting chemical composition compared with shallower phlogopites, characterized by similar Al_2O_3 (12.20-15.12 wt.%), lower Zr (13.18-30.30 ppm), Nb (13.11-26.97 ppm), and Ba (1227-2426 ppm), coupled with higher Mg# (0.92-0.93), Ni (1018-1460 ppm), and Cr_2O_3 (1.85-4.09 wt.%). Consequently, Phl2 was likely crystallized by less fractionated kimberlite melts that extensively interacted with refractory wall rock peridotite as opposed to phlogopite from the kimberlite

groundmass. Therefore, Phl2 cannot be in equilibrium with the erupted/entraining kimberlite magma, following the interpretation of Giuliani et al. (2016) for high-Ti-Cr phlogopites from Bultfontein kimberlite, Kimberley, South Africa.

When Phl2 overgrows Phl1, the contacts are rounded (Fig. 2c), often irregular (Fig. 3c), forming embayed textures. This indicates the resorption of the former phlogopite (Phl1) during the formation of the latter (Phl2). In addition, based on the composition of both phlogopites, it is possible to assume that the kimberlite melt, responsible for producing the Phl2, was not in equilibrium with Phl1. The restricted preservation of Phl1 as cores of Phl2 indicates that the metasomatism caused by the kimberlite occurs immediately prior to xenoliths entrainment in the kimberlite host magma. Therefore, we assume that the formation of Phl2 is a consequence of proto-kimberlite melt metasomatism in the deep cratonic lithosphere beneath Catalão, prior to the eruption of the host kimberlite magma.

9.2.4 Silicate melt metasomatism in the shallower mantle

Compared with garnet wehrlites and harzburgite ($F \geq 10\%$), the spinel lherzolites ($F = 2-4\%$) hosted by the Catalão 01 pipe represent the shallower and less depleted SCLM beneath the SW margin of the SFC. Differently from garnet-phlogopite wehrlite and harzburgite xenoliths that record carbonatite and proto-kimberlite metasomatism, spinel lherzolites show less pronounced enrichment related to the percolation of a silicate melt. This process is evidenced by the REE patterns of pyroxenes that are essentially depleted ($\text{Cpx La/Yb}_N = 0.001-0.073$ and $\text{Opx La/Yb}_N = 0.001-0.060$), except for La and Ce slopes (Fig. 6e). Conversely, pyroxenes of garnet-phlogopite wehrlites ($\text{Cpx La/Yb}_N = 56.79-117.88$) and harzburgite ($\text{Cpx La/Yb}_N = 7.59-10.52$ and $\text{Opx La/Sm}_N = 8.59-16.28$) are notably enriched (Fig. 6a, c). Regarding $\text{Mg}^{\#}$ vs. Cr_2O_3 and Al_2O_3 (Fig. 5a, b), clinopyroxene signatures of spinel lherzolites plot

close to the depleted mantle average ([Workman and Hart, 2005](#)), demonstrating a strong compositional affinity with the fields defined for clinopyroxene metasomatized by basaltic melts. Additional evidence for the role of a silicate melt in the metasomatism of Catalão lherzolites is exemplified by clinopyroxenes with low Ca/Al (usually <5) at high Mg# (0.90-0.94), low La/Yb_N (0.001-0.073), and Sr (6.18-59.2 ppm, 9.87 ppm on average) at high Ti/Eu (4410-6904) and Ti/Nb (756-143233, average of 74751) ratios, as well as by low Zr/Hf ratios (14.30-26.01) (Fig. 10). The metasomatism recorded by lherzolites is corroborated by the well-defined positive correlation of Ti vs. HFSE (i.e., Zr and Hf) and LREE (i.e., Ce) (Fig. 11). Ti enrichment in pyroxenes was also observed in other xenoliths of spinel facies from APIP ([Almeida et al., 2014](#); [Fernandes et al., 2021](#)). Thus, we suggest that a silicate melt, similar in composition to basaltic melts slightly enriched in incompatible elements (probably subalkaline) metasomatized the shallower mantle column beneath the SFC.

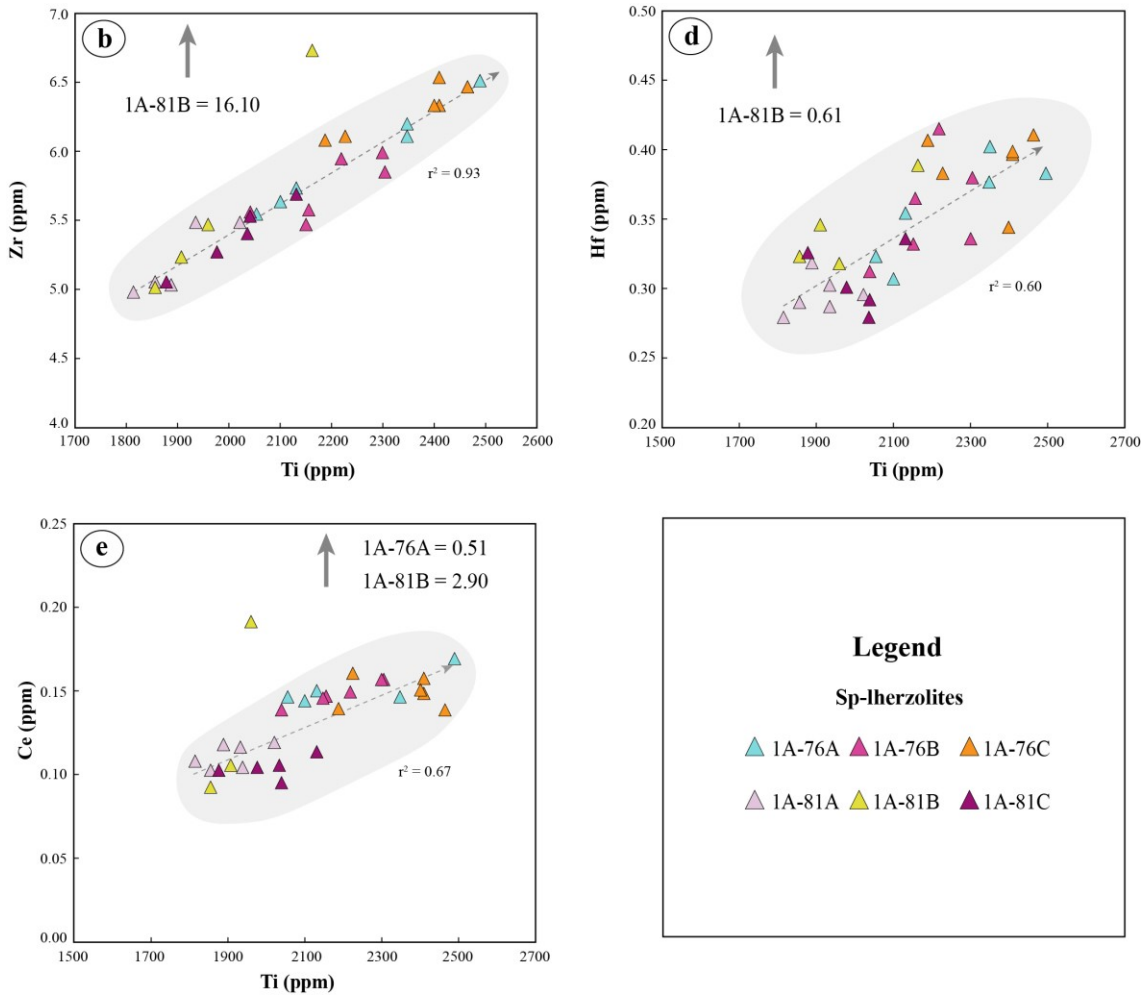


Figure 11. Selected trace elements vs. Ti of clinopyroxenes of spinel lherzolites from Catalão show a strong positive correlation.

5.9.3 Lithosphere stratification with multiple metasomatic overprints beneath the southwestern border of the São Francisco Craton: indication for cratonic rejuvenation?

One of the probable causes for mantle stratification observed in several cratonic lithospheres is that the shallower mantle is mostly subjected to partial melting events whereas the deeper mantle is continuously metasomatized by deep-seated fluids and melts derived from the asthenosphere. The metasomatic reactions that take place at the bottom of the lithospheric mantle can convert depleted harzburgite to enriched lherzolite and wehrlites. In the Catalão region, SW border of the SFC, xenoliths equilibrated at the deep mantle (~170 km) provide strong evidence for interactions with volatile-rich

fluids, carbonatitic and alkaline silicate-carbonate melts, the latter analogous to protokimberlite melts (Fig. 12a). The origin of these melts in the SFC SCLM, however, remains unknown. Although our results cannot constrain the mechanism of formation of these melts, we can bring up several hypotheses for discussion.

The carbonatite melt that reacted in depth with depleted mantle rocks to form wehrlites and minor amounts of clinopyroxene into the harzburgite at ~170 km beneath the Catalão region, could be explained by incipient low-degree partial melting of a metasomatized carbonated peridotite. We propose that the deep cratonic lithosphere beneath the SW border of the SFC was first metasomatized by K₂O- and C-, O-, H-rich fluids that reacted with the mantle wall rock to form hydrous- and carbonate-rich peridotites, marking this event with the formation of Phl1 present in the wehrlites (reaction 1) (Fig 12b). We assume that we did not find carbonate crystals equilibrated with the peridotitic assemblage in our samples because they were all consumed during low-degree of partial melting of a later event to form incipient carbonatite melts. We presume that, due to a thermal anomaly, carbonates that were present in the carbonated peridotites, were melted, reacting with orthopyroxenes to form the wehrlites, which leads to the formation of CO₂ according to reaction 2 (Fig 12c). After the metasomatic reactions between these melts and the depleted peridotites, the remaining CO₂ percolated through the mantle and was incorporated as fluid inclusions in the new metasomatic minerals or it may have even reacted with the mantle minerals to form carbonate minerals, such as the magnesite and dolomite found in olivines from wehrlites and harzburgite (Fig. 9 and 12c). In addition, in case carbonatite melts were not exhausted in the deep cratonic lithosphere, they may have migrated to shallower levels due to their high mobility (e.g., [Minarik and Watson, 1995](#)), low density (e.g., [Ritter et al., 2020](#)), and high reactivity ([Gervasoni et al., 2017](#)). This percolation would generate

reactions with the wall rock, dissolving orthopyroxenes, and getting richer in SiO₂, thereby decreasing the CO₂ solubility ([Russel et al., 2012](#)).

Moreover, we propose that the proto-kimberlite melt metasomatism recorded in Catalão wehrlites occurred at a later stage, after the carbonatite metasomatism (Fig. 12d). Due to the homogenous composition of the minerals formed by carbonatite melt metasomatism and the incomplete equilibration of Ph12 formed by proto-kimberlite melt with Ph11, we suggest that carbonatite and proto-kimberlite metasomatism represent two distinct events. We surmise that the proto-kimberlite metasomatism occurred shortly prior to the kimberlite host magma eruption.

Furthermore, in the shallower portions of the cratonic lithosphere (1.5 GPa, ~50 km) our studied spinel lherzolite xenoliths show similar chemical composition compared to rocks affected by silicate melt metasomatism. We propose that clinopyroxene crystals from the Catalão spinel lherzolite xenoliths were metasomatized by the passage of a subalkaline silicate melt, similar in composition to basaltic melts. The origin and composition of such melt remain unknown. Based on the chemical composition of clinopyroxenes, the metasomatic agent may be a silicate melt depleted in incompatible elements (e.g., LILE and REE).

Metasomatic processes ([Costa, 2008](#); [Almeida et al., 2014](#); [Nannini, 2016](#)) and a stratified cratonic mantle ([Carvalho et al., 2022a, b](#)) were also observed in other parts of the lithosphere beneath the SW border of the SFC, in the Oswaldo França 1, Canastra, Indaiá-I, and Limeira-I kimberlites, for instance. Overall, these observations may indicate that pervasive fluids and melts had acted from the base (~170km) to shallower parts (~50km) of the continental lithosphere in the APIP region. According to the petrophysical analysis of spinel and garnet peridotite of the APIP, the cratonic root of the SFC was modified by melt percolation, with minor associated deformation

(Fernandes et al., 2021). The percolation of these fluids and melts in different cratonic sections may indicate a lithosphere rejuvenation (Aulbach et al., 2017) that might be occurring on the border of the SFC.

According to the progressive melt modification model, the old and refractory SCLM is chemically modified through melt-rock reactions (Xu et al., 2008; Tang et al., 2013). These episodic refertilization events caused by low-degree melts have a great impact on the long-lasting tectonic stability of the cratons (Tang et al., 2013). According to Foley (2008), the impregnation of melts at a few locations can weaken and modify the lithosphere. The metasomatic assemblage formed would be denser than the surrounding depleted peridotites leading to local density anomalies (Foley, 2008). In addition, metasomatism of the Archean SCLM may reduce its buoyancy enough to produce localized delamination.

As a consequence, some portions of the ancient and depleted cratonic lithosphere are replaced by a young and fertile one (Tang et al., 2013). Seismological and mantle xenolith data have shown that the keels of many cratonic lithospheres have been either removed or are in the early stages of disruption (Foley, 2008). These disruptions are thought to be melt-related (Aulbach et al., 2017). For instance, the Wyoming Craton and the North China Craton are good examples of lithosphere destabilization by mechanical destruction (lithospheric thinning and rifting) and episodic events of refertilization (chemical re-enrichment) (Tang et al., 2013). Considering these examples, the melt-related disruption may lead eventually to the lithosphere rejuvenation accompanied by Fe-enrichment, which may explain, for instance, the low resistivity of the deep lithosphere along with observed positive geoid and Bouguer gravity anomalies, as observed in the south region of the SFC (Pinto et al., 2010; Aulbach et al., 2017). We suggest that the refertilization recognized in our

samples was caused by different metasomatic agents in distinct depths, which may lead to future rejuvenation of the cratonic lithosphere beneath the SW border of the SFC and may eventually lead to delamination of the lower SCLM.

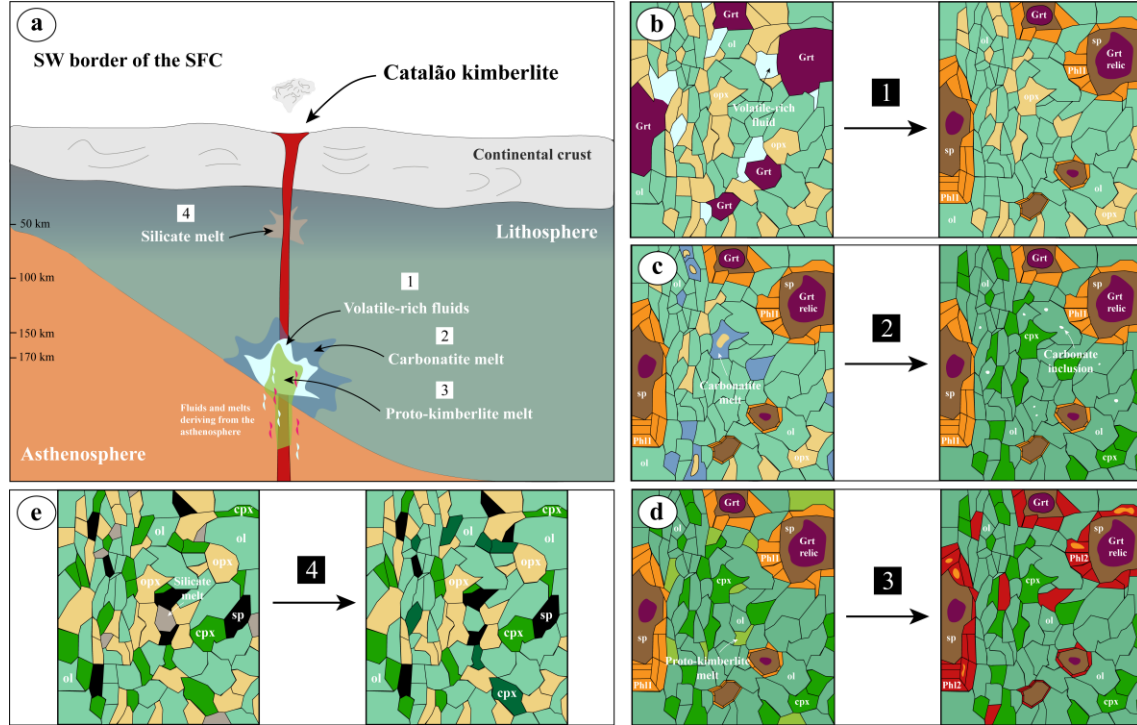


Figure 12. (a) Metasomatic events in the SW border of the SFC. (b) Reaction between volatile-rich fluid and garnet forming Phl1, Cr-Spinel, and carbonate. (c) Wehrlitization caused by carbonatite melt. During this process, carbonate inclusions in olivine were formed. (d) At this stage proto-kimberlite melt reacts forming Phl2 and consuming Phl1. (e) Cryptic metasomatism caused by silicate melt. Some clinopyroxenes display enrichment in incompatible elements.

5.10 Conclusions

The Catalão 01 kimberlite intrusions were recently discovered in the APIP, SE Brazil. Although this province is located within the Brasília mobile belt, previous investigations support that mantle xenoliths and xenocrysts are related to the context of the SFC, representing cratonic samples. Based on new mineral chemistry data, we conclude:

- Major and trace elements together with geothermometry data of spinel lherzolites, harzburgite, and garnet wehrlites indicate a stratified SCLM beneath the Catalão region. The shallow mantle (~50 km) represented by the spinel lherzolite xenoliths that record geochemical patterns typical of partial melting events, while the deep mantle (~170 km), represented by of garnet wehrlites and harzburgite that have been affected by multiple metasomatic events.
- Low-Ti-Cr phlogopite found in the garnet wehrlites is compositionally similar to phlogopite from metasomatized xenoliths globally and with macrocrysts of kimberlites interpreted as xenocrysts. This phlogopite was formed through metasomatic reactions promoted by alkaline-rich fluids with high K, H₂O ± F, and CO₂ at the base of the cratonic lithosphere. These reactions caused the consumption of garnet and orthopyroxene and the formation of phlogopite, Cr-spinel, and carbonate.
- Clinopyroxene crystals of the garnet wehrlites and harzburgite were formed by carbonatite melt metasomatism. This melt may have formed from low-degree partial melting of carbonated peridotite that generated incipient melts responsible for the metasomatic reaction to generate clinopyroxene and olivine at the expense of orthopyroxene. This reaction formed the clinopyroxene-

bearing harzburgite and wehrellites, which preserved garnet relics inside Cr-spinel rims. The entrapment of carbonate (dolomite and magnesite) inclusions in olivine of these samples occurred at this stage.

- High-Ti-Cr phlogopite widespread in garnet wehrellites has a similar composition to phlogopite from polymict breccias, high-Ti-Cr phlogopites from garnet peridotites, and high-Ti-Cr macrocrysts from kimberlites. This type of phlogopite is defined as a product of proto-kimberlite melt metasomatism in the deep cratonic mantle.
- Shallower mantle represented by spinel lherzolites mostly records partial melting processes, with some clinopyroxenes showing slight enrichment in incompatible elements and geochemical features that resemble clinopyroxenes metasomatized by a depleted subalkaline silicate melt.
- The stratification of the SCLM beneath the APIP is shown by different degrees of partial melting, followed by multiple metasomatic agents that acted from the base (~170km) to the shallower mantle column (~50km) of the lithospheric mantle, suggesting the percolation of pervasive fluids and melts. These partial melting and refertilization processes might have a great impact on the stability of the cratonic lithosphere and may indicate the rejuvenation that might be occurring on the border of the SFC.

5.11 Acknowledgments

We are thankful to Mr. Paulo Ilidio de Brito and Five Star Diamonds for providing the drill samples of the Catalão kimberlite. Thanks to Beate Schmitte for her help during the LA-ICP-MS analyses in Münster, and to Prof. Dr. Marcelo Peres Rocha for constructive and clarifying comments about tomography beneath the southwestern margin of the São Francisco Craton. We also thank the financial support given by the Instituto Serrapilheira [grant numbers Serra-1709-18152 and Serra-1912-31377], and by the Coordenação de Aperfeiçoamento de Pessoal de Nível Superior – Brasil (CAPES) [Finance Code 001]. The first author also thanks CAPES for a master's degree scholarship.

5.12 References

- Almeida, V.V., Janasi, V.A., Svisero, D.P., Nannini, F. 2014. Mathiasite-loveringite and priderite in mantle xenoliths from the Alto Paranaíba Igneous Province, Brazil: genesis and constraints on mantle metasomatism. Central European Journal of Geosciences. 6, 614-632. <https://doi.org/10.2478/s13533-012-0197-5>.
- Araújo, A.L.N., Carlson, R.W., Gaspar, J.C., Bizzi, L.A. 2001. Petrology of kamafugites and kimberlites from the Alto Paranaíba Alkaline Province, Minas Gerais, Brazil. Contributions to Mineralogy and Petrology. 142, 163-177. <https://doi.org/10.1007/s004100100280>.
- Aulbach, S., Griffin, W.L., Pearson, N.J., O'Reilly, S.Y. 2013. Nature and timing of the metasomatism in the stratified mantle lithosphere beneath the central Slave craton (Canada). Chemical Geology. 352, 153-169. doi.org/10.1016/j.chemgeo.2013.05.037.
- Aulbach, S., Massuyeau, M., Gaillard, F. 2017. Origins of cratonic mantle discontinuities: A view from petrology, geochemistry and thermodynamic models. Lithos. 268-271, 364-382. <https://doi.org/10.1016/j.lithos.2016.11.004>.

- Aulbach, S., Lin, A.-B., Weiss, Y., Yaxley, G.M. 2020. Wehrlites from continental mantle monitor the passage and degassing of carbonated melts. *Geochemical Perspectives Letters*. 15, 30-34. 10.7185/geochemlet.2031.
- Barbosa, E.S.R., Brod, J.A., Junqueira-Brod, T.C., Dantas, E.L., Cordeiro, P.F.O., Gomide, C.S. 2012. Bebedourite from its type area (Salitre I complex): A key petrogenetic series in the Late-Cretaceous Alto Paranaíba kamafugite-carbonatite-phoscorite association, Central Brazil. *Lithos*. 144-145, 56-72. <https://doi.org/10.1016/j.lithos.2012.04.013>.
- Brey, G.P., Köhler, T. 1990. Geothermobarometry in Four-phase Iherzolites II. New Thermobarometers, and Practical Assessment of Existing Thermobarometers. *Journal of Petrology*. 31, 1353-1378. <https://doi.org/10.1093/petrology/31.6.1353>.
- Brey, G.P., Bulatov, V.K., Girnis, A.V., Lahaye, Y. 2008. Experimental Melting of Carbonated Peridotite at 6-10 GPa. *Journal of Petrology*. 49, 797-821. <https://doi.org/10.1093/petrology/egn002>.
- Bussweiler, Y., Pearson, D.G., Stachel, T., Kjarsgaard, B.A. 2018. Cr-rich megacrysts of clinopyroxene and garnet from Lac de Gras kimberlites, Slave Craton, Canada – implications for the origin of clinopyroxene and garnet in cratonic Iherzolites. *Mineralogy and Petrology*. 112, 583-596. <https://doi.org/10.1007/s00710-018-0599-2>.
- Bussweiler, Y., Giuliani, A., Greig, A., Kjarsgaard, B.A., Petts, D., Jackson, S.E., Barret, N., Luo, Y., Pearson, D.G. 2019. Trace element analysis of high-Mg olivine by LA-ICP-MS – Characterization of natural olivine standards for matrix-matched calibration and application to mantle peridotites. *Chemical Geology*. 524, 136-157. <https://doi.org/10.1016/j.chemgeo.2019.06.019>.
- Cabral Neto, I., Nannini, F., Valdir Silveira, F., Matos Cunha, L. 2017. Áreas kimberlíticas e diamantíferas do estado de Minas Gerais: Programa Geologia do Brasil, Série Pedras Preciosas nº 10, Projeto Diamante. Serviço Geológico do Brasil – CPRM.
- Carlson, R.W., Araujo, A.L.N., Junqueira-Brod, T.C., Gaspar, J.C., Brod, J.A., Petrinovic, I.A., Hollanda, M.H.B.M., Pimentel, M.M., Sichel, S. 2007. Chemical and isotopic relationships between peridotite xenoliths and mafic-

ultrapotassic rocks from Southern Brazil. Chemical Geology. 242, 415-434.
<https://doi.org/10.1016/j.chemgeo.2007.04.009>.

Carswell, D.A. 1975. Primary and secondary phlogopites and clinopyroxenes in garnet lherzolite xenoliths. Physics and Chemistry of the Earth. 9, 417-429.
[https://doi.org/10.1016/0079-1946\(75\)90031-2](https://doi.org/10.1016/0079-1946(75)90031-2).

Carvalho, L.D.V., Jalowitzki, T., Sholz, R., Gonçalves, G.O., Rocha, M.P., Pereira, R.S., Lana, C., Castro, M.P., Queiroga, G., Fuck, R.A. 2022a. An exotic Cretaceous kimberlite linked to metasomatized lithospheric mantle beneath the southwestern margin of the São Francisco Craton, Brazil. Geoscience Frontiers. 13, 1011281. <https://doi.org/10.1016/j.gsf.2021.101281>.

Carvalho, L.D.V., Stachel, T., Pearson, D.G., Fuck, R.A., Jalowitzki, T., Timmerman, S., Steele-MacInnis, M., Gonçalves, G.O., Pereira, R.S., Sholz, R. 2022b. Diamond formation beneath the Coromandel area, southwestern São Francisco Craton – The role of re-fertilization and subduction. 430-431, 106856.
<https://doi.org/10.1016/j.lithos.2022.106856>.

Coltorti, M., Bonadiman, C., Hinton, R. W., Siena, F., Upton, B. G. J., 1999. Carbonatite metasomatism of the oceanic upper mantle: evidence from clinopyroxenes and glasses in ultramafic xenoliths of Grande Comore, Indian Ocean. Journal of Petrology. 40, 133-165.
<https://doi.org/10.1093/petroj/40.1.133>.

Costa, G.V., 2008. Química mineral e geotermobarometria de xenólitos mantélicos do kimberlito Canastra-01. M.Sc. thesis, University of Brasília, 137 p. (in Portuguese).

Deng, L., Liu, Y., Zong, K., Zhu, L., Xu, R., Hu, Z., Gao, S., 2017. Trace element and Sr isotope records of multi-episode carbonatite metasomatism on the eastern margin of the North China Craton. Geochemistry, Geophysics, Geosystems. 18, 220-237. <https://doi.org/10.1002/2016GC006618>.

Fernandes, P.R., Tommasi, A., Vauchez, A., Neves, S.P., Nannini, F. 2021. The São Francisco cratonic root beneath the Neoproterozoic Brasilia belt (Brazil): Petrophysical data from kimberlite xenoliths. Tectonophysics. 816, 229011.
<https://doi.org/10.1016/j.tecto.2021.229011>.

- Fitzpayne, A., Giuliani, A., Hergt, J., Phillips, D., Janney, P. 2018. New geochemical constraints on the origins of MARID and PIC rocks: Implications for mantle metasomatism and mantle-derived potassic magmatism. *Lithos*. 318-319, 478-493. <https://doi.org/10.1016/j.lithos.2018.08.036>.
- Fitzpayne, A., Giuliani, A., Hergt, J., Woodhead, J.D., Mass, R. 2020. Isotopic analyses of clinopyroxenes demonstrate the effects of kimberlite melt metasomatism upon the lithospheric mantle. *Lithos*. 370-371, 105595. <https://doi.org/10.1016/j.lithos.2020.105595>.
- Foley, S. 2008. Rejuvenation and erosion of the cratonic lithosphere. *Nature Geoscience*. 1, 503-510. <https://doi.org/10.1038/ngeo261>.
- Gervasoni, F., Klemme, S., Rohrbach, A., Grützner, T., Berndt, J. 2017. Experimental constraints on mantle metasomatism caused by silicate and carbonate melts. *Lithos*. 282-283, 173-186. <https://doi.org/10.1016/j.lithos.2017.03.004>.
- Gervasoni, F., Jalowitzki, T., Rocha, M.P., Weska, R.K., Novais-Rodrigues, E., Rodrigues, R.A.F., Bussweiler, Y., Barbosa, E.S.R., Berndt, J., Dantas, E.L., Souza, V.S., Klemme, S. 2022. Recycling process and proto-kimberlite melt metasomatism in the lithosphere-asthenosphere boundary beneath the Amazonian Craton recorded by garnet xenocrysts and mantle xenoliths from the Carolina kimberlite. *Geoscience Frontiers*. 13, 101429. <https://doi.org/10.1016/j.gsf.2022.101429>.
- Giuliani, A., Phillips, D., Kamenetsky, V.S., Goemann, K. 2016. Constraints on kimberlite ascent mechanisms revealed by phlogopite compositions in kimberlites and mantle xenoliths. *Lithos*. 240-243, 189-201. <https://doi.org/10.1016/j.lithos.2015.11.013>.
- Giuliani, A., Phillips, D., Kamenetsky, V.S., Kendrick, M.A., Wyatt, B.A., Goemann, K., Hutchinson, G. 2014. Petrogenesis of mantle polymict breccias: insights into mantle processes coeval with kimberlite magmatism. *Journal of Petrology*. 55, 831-858. <https://doi.org/10.1093/petrology/egu008>.
- Gibson, S.A., Thompson, R.N., Leonardos, O.H., Dickin, A.P., Mitchell, J.G. 1995. The Late Cretaceous Impact of the Trindade Mantle Plume: Evidence from Large-volume, Mafic, Potassic Magmatism in SE Brazil. *Journal of Petrology*. 36, 189-229. <https://doi.org/10.1093/petrology/36.1.189>.

- Grégoire, M., Bell, D.R., le Roex, A.P. 2002. Trace element geochemistry of phlogopite-rich mafic mantle xenoliths: their classification and their relationship to phlogopite-bearing peridotites and kimberlites revisited. Contributions to Mineralogy and Petrology. 142, 603-625. <https://doi.org/10.1007/s00410-001-0315-8>.
- Griffin, W.L., Ryan, C.G. 1995. Trace elements in indicator minerals: Area selection and target evaluation in diamond exploration. Journal of Geochemical Exploration. 53, 311-337. [https://doi.org/10.1016/0375-6742\(94\)00015-4](https://doi.org/10.1016/0375-6742(94)00015-4).
- Griffin, W.L., Shee, S.R., Ryan, C.G., Win, T.T., Wyatt, B.A. 1999. Harzburgite to lherzolite and back again: Metasomatic processes in ultramafic xenoliths from the Wesselton kimberlite, Kimberly, South Africa. Contributions to Mineralogy and Petrology. 134, 232-250. <https://doi.org/10.1007/s004100050481>.
- Guarino, V., Wu, F.Y., Lustrino, M., Melluso, L., Brotzu, P., Gomes, C.B., Ruberti, E., Tassinari, C.C.G., Svisero, D.P. 2013. U-Pb ages, Sr-Nd isotope geochemistry, and petrogenesis of kimberlites, kamafugites and phlogopite-picrites of the Alto Paranaíba Igneous Province, Brazil. Chemical Geology. 353, 65-82. <https://doi.org/10.1016/j.chemgeo.2012.06.016>.
- Heilbron, M., Cordani, U.G., Alkmin, F.F. 2017. The São Francisco Craton and its Margins. In: Heilbron, M., Cordani, U., Alkmim, F. (eds) São Francisco Craton, Eastern Brazil. Regional Geology Reviews. Springer, Cham. https://doi.org/10.1007/978-3-319-01715-0_1.
- Ionov, D.A., Chanefo, I., Bodinier, J.L. 2005. Origin of Fe-rich lherzolites and wehrlites from Tok, SE Siberia by reactive melt percolation in refractory mantle peridotites. Contributions to Mineralogy and Petrology. 150, 335-353. <https://doi.org/10.1007/s00410-005-0026-7>.
- Ionov, D.A. 2002. Mechanisms and Sources of Mantle Metasomatism: Major and Trace Element Compositions of Peridotite Xenoliths from Spitsbergen in the Context of Numerical Modelling. Journal of Petrology. 43, 2219-2259. <https://doi.org/10.1093/petrology/43.12.2219>.
- Ionov, D.A., Doucet, L. S., Xu, Y., Golovin, A. V., Oleinikov, O. B. 2018. Reworking of Archean mantle in the NE Siberian craton by carbonatite and silicate melt metasomatism: evidence from a carbonate-bearing, dunite-to-websterite

xenoliths suite from the Obnazhennaya kimberlite. *Geochimica et Cosmochimica Acta*. 224, 132-153. <https://doi.org/10.1016/j.gca.2017.12.028>.

Johnson, K.T.M. 1998. Experimental determination of partition coefficients for rare earth and high-field-strength elements between clinopyroxene, garnet, and basaltic melt at high pressures. *Contributions to Mineralogy and Petrology*. 133, 60-68. <https://doi.org/10.1007/s004100050437>.

Johnson, K.T.M., Dick, H.J.B., Shimizu, N. 1990. Melting in the oceanic upper mantle: An ion microprobe study of diopsides in abyssal peridotites. *Journal of Geophysical Research*. 95, 2661. <https://doi.org/10.1029/JB095iB03p02661>.

Kargin, A.V., Sazonova, L.V., Nosova, A.A., Tretyachenko, V.V. 2016. Composition of garnet and clinopyroxene in peridotite xenoliths from the Grib kimberlite pipe, Arkhangelsk diamond province, Russia: Evidence for mantle metasomatism associated with kimberlite melts. *Lithos*. 262, 442-455. <https://doi.org/10.1016/j.lithos.2016.07.015>.

Kargin, A.V., Sazonova, L.V., Nosova, A.A., Lebedeva, N.M., Kostitsyn, Yu.A., Kovalchuk, E.V., Tretyachenko, V.V., Tikhomirova, Ya.S. 2019. Phlogopite in mantle xenoliths and kimberlite from the Grib pipe, Arkhangelsk province, Russia: Evidence for multi-stage mantle metasomatism and origin of phlogopite in kimberlite. *Geoscience Frontiers*. 10, 1941-1959. <https://doi.org/10.1016/j.gsf.2018.12.006>.

Kargin A, Bussweiler Y, Nosova A, Sazonova L, Berndt J, Klemme S. 2021. Titanium-rich metasomatism in the lithospheric mantle beneath the Arkhangelsk Diamond Province, Russia – Insights from ilmenite-bearing xenoliths and HP-HT reaction experiments. *Contributions to Mineralogy and Petrology* 176,12, 101. <https://doi.org/10.1007/s00410-021-01863-9>.

Kelemen, P.B., Hart, S.R., Bernstein, S. 1998. Silica enrichment in the continental upper mantle via melt/rock reaction. *Earth and Planetary Science Letters*. 164, 387-406. [https://doi.org/10.1016/S0012-821X\(98\)00233-7](https://doi.org/10.1016/S0012-821X(98)00233-7).

Kilian, R., Stern, C.R. 2002. Constraints on the interaction between slab melts and the mantle wedge from adakitic glass in peridotite xenoliths. *European Journal of Mineralogy*. 14, 25-36. <https://doi.org/10.1127/0935-1221/2002/0014-0025>.

Klemme, S., van der Laan, S.R., Foley, S.F., Günther, D. 1995. Experimentally determined trace and minor element partitioning between clinopyroxene and carbonatite melt under upper mantle conditions. *Earth and Planetary Science Letters*. 133, 439-448. [https://doi.org/10.1016/0012-821X\(95\)00098-W](https://doi.org/10.1016/0012-821X(95)00098-W).

Kopylova, M.G., Mogg, T., Smith, B.S. 2010. Mineralogy of the Snap Lake kimberlite, northwest territories, Canada, and compositions of phlogopites as records of its crystallization. *The Canadian Mineralogist*. 48, 549-570. <https://doi.org/10.3749/canmin.48.3.549>.

Kopylova, M.G., Ma, F., Tso, E. 2021. Constraining carbonation freezing and petrography of the carbonated cratonic mantle with natural samples. *Lithos*. 388-389, 106045. <https://doi.org/10.1016/j.lithos.2021.106045>.

Leonardos, O.H., Carvalho, J.B., Tallarico, F.H.B., Gibson, S.A., Thompson, R.N., Meyer, H.O.A., Dickin, A.P. 1993. O xenólito de Granada Iherzolito de 3 Ranchos 4: Uma rocha matriz do diamante na Província Magmática Cretácea do Alto Paranaíba, Goiás. *Anais I Simpósio Brasileiro de Geologia do Diamante*. 3-16.

Liang, Y., Sun, C., Yao, L., 2013. A REE-in-two-pyroxene thermometer for mafic and ultramafic rocks. *Geochimica et Cosmochimica Acta*. 102, 246-260. <https://doi.org/10.1016/j.gca.2012.10.035>.

Mallik, A., Dasgupta, R. 2012. Reaction between MORB-eclogite derived melts and fertile peridotite and generation of ocean island basalts. *Earth and Planetary Science Letters*. 329-330, 97-108. <https://doi.org/10.1016/j.epsl.2012.02.007>.

Mercier, J.C.C., Nicolas, A. 1975. Textures and Fabrics of Upper-Mantle Peridotites as Illustrated by Xenoliths from Basalts. *Journal of Petrology*. 16, 454-487. <https://doi.org/10.1093/petrology/16.1.454>.

McCoy-West, A. J., Bennett, V. C., O'Neill, H. St. C., Hermann, J., Puchtel, I.S. 2015. The interplay between melting, refertilization, and carbonatite metasomatism in off-cratonic lithospheric mantle under Zealandia: an integrated major, trace and platinum group element study. *Journal of Petrology*. 56, 563-604. <https://doi.org/10.1093/petrology/egv011>.

- McDonough, W.F. 1990. Constraints on the composition of the continental lithospheric mantle. *Earth and Planetary Science Letters*. 101, 1-18. [https://doi.org/10.1016/0012-821X\(90\)90119-I](https://doi.org/10.1016/0012-821X(90)90119-I).
- Mercier, J.C.C. 1980. Single-pyroxene thermobarometry. *Tectonophysics*. 70, 1-37. [https://doi.org/10.1016/0040-1951\(80\)90019-0](https://doi.org/10.1016/0040-1951(80)90019-0).
- Minarik, W. G., and E. B. Watson. 1995. Interconnectivity of carbonate melt at low melt fraction. *Earth and Planetary Science Letters*. 133, 423–437. [https://doi.org/10.1016/0012-821X\(95\)00085-Q](https://doi.org/10.1016/0012-821X(95)00085-Q).
- Nannini, F. 2016. Geologia e petrologia de xenólitos mantélicos da Província Ígnea do Alto Paranaíba. PhD. thesis, Universidade de São Paulo, 298 p. (in Portuguese).
- Neumann, E.-R., Wulff-Pedersen, E., Pearson, N. J., Spencer, E. A. 2002. Mantle xenoliths from Tenerife (Canary Islands): evidence for reactions between mantle peridotites and silicic carbonatite melts inducing Ca metasomatism. *Journal of Petrology*. 43, 825-857. <https://doi.org/10.1093/petrology/43.5.825>.
- Nimis, P., Taylor, W.R. 2000. Single clinopyroxene thermobarometry for garnet peridotites. Part I. Calibration and testing of a Cr-in-Cpx barometer and an enstatite-in-Cpx Thermometer. *Contributions to Mineralogy and Petrology*. 139, 541-554. <https://doi.org/10.1007/s004100000156>.
- Oliveira, I.L., Brod, J.A., Cordeiro, P.F.O., Dantas, E.L., Mancini, L.H. 2017. Insights into the late-stage differentiation processes of the Catalão I carbonatite complex in Brazil: New Sr-Nd and C-O isotopic data in minerals from niobium ores. *Lithos*. 274-275, 214-224. <https://doi.org/10.1016/j.lithos.2016.12.034>.
- Paton, C., Hellstrom, J., Paul, B., Woodhead, J., Hergt, J. 2011. Iolite: Freeware for the visualization and processing of mass spectrometric data. *Journal of Analytical Atomic Spectrometry*. 26, 2508-2508. <https://doi.org/10.1039/C1JA10172B>.
- Patkó, L., Liptai, N., Aradi, L. E., Klébesz, R., Sendula, E., Bodnar, R. J., Kovács, I. J., Hidas, K., Cesare, B., Novák, A., Trásy, B., Szabó, C. 2020. Metasomatism-induced wehrlite formation in the upper mantle beneath the Nógrád-Gömör Volcanic Field (Northern Pannonian Basin): evidence from xenoliths. *Geoscience Frontiers*. 11, 943-964. <https://doi.org/10.1016/j.gsf.2019.09.012>.

- Pinto, L.G.R., Pádua, M.B., Ussami, N., Vitorello, I., Padilha, A.L., Braitenberg, C. 2010. Magnetotelluric deep soundings, gravity and geoid in the south São Francisco craton: Geophysical indicators of cratonic lithosphere rejuvenation and crustal underplating. *Earth and Planetary Science Letters*. 297, 423-434. <https://doi.org/10.1016/j.epsl.2010.06.044>.
- Rapp, R.P., Shimizu, N., Norman, M.D., Applegate, G.S. 1999. Reaction between slab-derived melts and peridotite in the mantle wedge: experimental constraints at 3.8 GPa. *Chemical Geology*. 160, 335-356. [https://doi.org/10.1016/S0009-2541\(99\)00106-0](https://doi.org/10.1016/S0009-2541(99)00106-0).
- Ritter, X., Sanchez-Valle, C., Sator, N., Desmaele, E., Guignot, N., King, A., Kupenko, I., Berndt, J., Guillot, B. 2020. Density of hydrous carbonate melts under pressure, compressibility of volatiles and implications for carbonate melt mobility in the upper mantle. *Earth and Planetary Science Letters*. 533, 116043. <https://doi.org/10.1016/j.epsl.2019.116043>.
- Rocha, M.P., Schimmel, M., Assumpção, M. 2011. Upper-mantle seismic structure beneath SE and Central Brazil from P- and S-wave regional travelttime tomography. *Geophysical Journal International*. 184, 268-286. <https://doi.org/10.1111/j.1365-246X.2010.04831.x>.
- Rocha, M.P., Azevedo, P.A., Assumpção, M., Pedrosa-Soares, A.C., Fuck, R., Von Huelsen, M.G., 2019. Delimiting the Neoproterozoic São Francisco Paleocontinental Block with P-wave travelttime tomography. *Geophysical Journal International*. 219, 633-644. <https://doi.org/10.1093/gji/ggz323>.
- Russel, J.K., Porritt, L.A., Lavallée, Y., Dingwell, D.B. 2012. Kimberlite ascent by assimilation-fuelled buoyancy. *Nature*. 481, 352-356. <https://doi.org/10.1038/nature10740>.
- Schilling, M., Conceição, R.V., Mallmann, G., Koester, E., Kawashita, K., Hervé, F., Morata, D., Motoki, A. 2005. Spinel-facies mantle xenoliths from Cerro Redondo, Argentine Patagonia: Petrographic, geochemical, and isotopic evidence of interaction between xenoliths and host basalt. *Lithos*. 82, 485-502. <https://doi.org/10.1016/j.lithos.2004.09.028>.
- Shaw, D.M. 2006. Trace Elements in Magmas: A Theoretical Treatment. Cambridge University Press. (256 pp.).

- Sokol, A.G., Kruk, A.N., Chebotarev, D.A., Palyanov, Y.N. 2016. Carbonatite melt-peridotite interaction at 5.5-7.0 GPa: Implications for metasomatism in lithospheric mantle. *Lithos*. 248-251, 66-79. <https://doi.org/10.1016/j.lithos.2016.01.013>.
- Su, B.X., Zhang, H.F., Sakyi, P.A., Ying, J.F., Tang, Y.J., Yang, Y.H., Zhao, X.M. 2010. Compositionally stratified lithosphere and carbonatite metasomatism recorded in mantle xenoliths from the Western Qinling (Central China). *Lithos*. 116, 111-128. <https://doi.org/10.1016/j.lithos.2010.01.004>.
- Su, B., Chen, Y., Guo, S., Chu, Z. Y., Liu, J. B., Gao, Y. J., 2016. Carbonatitic metasomatism in orogenic dunites from Lijiatun in the Sulu UHP terrane, eastern China. *Lithos*. 262, 266-284. <https://doi.org/10.1016/j.lithos.2016.07.007>.
- Sun, S.-s., McDonough, W.F. 1989. Chemical and isotopic systematics of oceanic basalts: implications for mantle composition and processes. Geological Society, London, Special Publications. 42, 313-345. <http://dx.doi.10.1144/GSL.SP.1989.042.01.19>.
- Tang, Y.J., Zhang, H.F., Ying, J.F., Su, B.X. 2013. Widespread refertilization of cratonic and circum-cratonic lithospheric mantle. *Earth-Science Reviews*. 118, 45-68. <https://doi.org/10.1016/j.earscirev.2013.01.004>.
- Tappe, S., Smart, K., Torsvik, T., Massuyseau, M., de Wit, M. 2018. Geodynamics of kimberlites on a cooling Earth: Clues to plate tectonic evolution and deep volatile cycles. *Earth and Planetary Science Letters*. 484, 1-14. <https://doi.org/10.1016/j.epsl.2017.12.013>.
- Valeriano, C.M. 2017. The Southern Brasília Belt. In: Heilbron, M., Cordani, U., Alkmim, F. (eds) São Francisco Craton, Eastern Brazil. Regional Geology
- Wang, C., ZhenMin, J., Shan, G., JunFeng, Z., Shu, Z. 2010. Eclogite-melt/peridotite reaction: Experimental constraints on the destruction mechanism of the North China Craton. *Science China Earth Sciences*. 53, 797-809. <https://doi.org/10.1007/s11430-010-3084-2>.
- Wang, C., Liang, Y., Xu, W., Dygert, N. 2013. Effect of melt composition on basalt and peridotite interaction: laboratory dissolution experiments with applications to

mineral compositional variations in mantle xenoliths from the North China Craton. Contribution to Mineralogy and Petrology. 166, 1469-1488.
<https://doi.org/10.1007/s00410-013-0938-6>.

Workman, R.K., Hart, S.R. 2005. Major and trace element composition of the depleted MORB mantle (DMM). Earth and Planetary Science Letters. 231, 53-72.
<https://doi.org/10.1016/j.epsl.2004.12.005>.

Xu, X.S., Griffin, W.L., O'Reilly, S.Y., Pearson, N.J., Geng, H.Y., Zheng, J.P. 2008. Re-Os isotopes of sulfides in mantle xenoliths from eastern China: progressive modification of lithospheric mantle. Lithos. 102, 43-64.
<https://doi.org/10.1016/j.lithos.2007.06.010>.

Yaxley, G.M., Green, D.H. 1998. Reactions between eclogite and peridotite: mantle refertilisation by subduction of oceanic crust. Schweizerische Mineralogische und Petrographische Mitteilungen. 78, 243-255.

Yaxley, G.M., Green, D.H., Kamenetsky, V. 1998. Carbonatite Metasomatism in the Southeastern Australian Lithosphere. Journal of Petrology. 39, 1917-1930.
<https://doi.org/10.1093/petroj/39.11-12.1917>.

Yaxley, G.M. 2000. Experimental study of the phase and melting relations of homogeneous basalt + peridotite mixtures and implications for the petrogenesis of flood basalts. Contributions to Mineralogy and Petrology. 139, 326-338.
<https://doi.org/10.1007/s004100000134>.

Zhang, Y. L., Liu, C. Z., Ge, W. C., Wu, F. Y., Chu, Z. Y., 2011. Ancient sub-continental lithospheric mantle (SCLM) beneath the eastern part of the Central Asian Orogenic Belt (CAOB): implications for crust-mantle decoupling. Lithos. 126, 233-247. <https://doi.org/10.1016/j.lithos.2011.07.022>.

Ziberna L, Klemme S. 2016. Application of thermodynamic modelling to natural mantle xenoliths: Examples of density variations and pressure-temperature evolution of the lithospheric mantle. Contributions to Mineralogy and Petrology. 171, 1-14.
<https://doi.org/10.1007/s00410-016-1229-9>.

CHAPTER 6 – FINAL CONSIDERATIONS

Geophysical and mineral chemistry data of peridotites and xenocrysts hosted by kimberlite already reported in the literature indicate that the APIP is underlain by a cratonic lithosphere. The studied suite of kimberlite-hosted mantle xenoliths from the Catalão region, APIP, southwestern border of the SFC, Brazil, also confirms this hypothesis. Based on the mineral chemistry of the primary and metasomatic minerals, together with geothermobarometric and partial melting estimates the subcontinental lithospheric mantle beneath Catalão is chemically stratified.

The deep mantle beneath the APIP is represented by the garnet-phlogopite wehrlites (1066-1101 °C and 5.03-5.23 GPa) and harzburgite (914 °C and 5.28 GPa) equilibrated at depths ~170 km. These peridotites underwent ~10% of partial melting and record multiple metasomatic events characterized by the formation of two types of phlogopites and the addition of clinopyroxenes. The first type of phlogopite (Phl1) has low-Ti-Cr contents and occurs associated with garnet and Cr-spinel. The composition of this phlogopite is similar to phlogopite from metasomatized xenoliths worldwide and xenocrysts present in kimberlites, interpreted as derived from the disaggregation of mantle xenoliths during the kimberlite ascent. The formation of low-Ti-Cr phlogopite is attributed to reactions between garnet peridotite and alkaline-rich fluids (K_2O , H_2O , CO_2 , F, ± Cl). The reaction involves the consumption of garnet and the formation of phlogopite, Cr-spinel, and carbonate.

The high-Cr low-Al clinopyroxenes, present in the garnet-phlogopite wehrlites and harzburgite have high Mg#, high Ca/Al, La_N/Yb_N , Zr/Hf ratios, and high Sr contents, coupled with low to intermediate Ti/Eu and Ti/Nb ratios, suggesting that they were formed by carbonatite melt metasomatism. These geochemical signatures together

with the presence of magnesite and dolomite inclusions within olivine in wehrlites and harzburgite confirm a carbonate-rich melt as a metasomatic agent.

The second type of phlogopite (Phl2) has high-Ti-Cr contents and occurs as rims around Phl1, as isolated flakes around garnets, and in the matrix of wehrlites. This type of phlogopite has compositions similar to phlogopite from polymict mantle breccias, interpreted as crystallized from failed kimberlite melts in the deep mantle, and different from phlogopite compositions present in kimberlite groundmass crystallized at crustal levels. Therefore, the formation of Phl2 in the wehrlites is attributed to reactions with proto-kimberlite melt in the deep mantle.

Conversely, the shallow mantle represented by the spinel lherzolites (876-915 °C; 1.5 GPa) equilibrated at ~50 km underwent ~2-4% of partial melting and record cryptic metasomatism evidenced by the clinopyroxenes compositions. Most of the clinopyroxenes in these samples display a geochemical pattern typical of partial melting processes with some crystals showing slight enrichment in LREE, LILE, and Ti. Their low Ca/Al, La_N/Yb_N, Zr/Hf ratios and Sr contents, associated with high Ti/Eu, Ti/Nb ratios and a strong positive correlation between Ti and HFSE and LREE indicate that they were metasomatized by subalkaline silicate melt depleted in incompatible elements.

The studied mantle xenoliths indicate that pervasive fluids and melts percolated the subcontinental lithospheric mantle beneath Catalão. However, the chemical and mineralogical modifications were more intense in the deeper mantle regions due to interactions with reactive deep-seated fluid and melt extremely enriched in incompatible elements. These refertilization events with the addition of metasomatic phases into the depleted peridotites may have great impacts on the tectonic stability of the SFC.

CHAPTER 7 – DISSERTATION REFERENCES

- Alkmim, F.F., Martins-Neto, M.A. 2012. Proterozoic first-order sedimentary sequences of the São Francisco craton, eastern Brazil. *Marine and Petroleum Geology*. 33, 127-139. <https://doi.org/10.1016/j.marpetgeo.2011.08.011>.
- Almeida, V.V., Janasi, V.A., Svisero, D.P., Nannini, F. 2014. Mathiasite-loveringite and priderite in mantle xenoliths from the Alto Paranaíba Igneous Province, Brazil: genesis and constraints on mantle metasomatism. *Central European Journal of Geosciences*. 6, 614-632. <https://doi.org/10.2478/s13533-012-0197-5>.
- Araújo, A.L.N., Carlson, R.W., Gaspar, J.C., Bizzi, L.A. 2001. Petrology of kamafugites and kimberlites from the Alto Paranaíba Alkaline Province, Minas Gerais, Brazil. *Contributions to Mineralogy and Petrology*. 142, 163-177. <https://doi.org/10.1007/s004100100280>.
- Assumpção, M., An, M., Bianchi, M., França, G.S.L., Rocha, M., Barbosa, J.R., Berrocal, J. 2004. Seismic studies of the Brasília fold belt at the western border of the São Francisco Craton, Central Brazil, using receiver function, surface-wave dispersion and teleseismic tomography. *Tectonophysics*. 388, 173-185. <https://doi.org/10.1016/j.tecto.2004.04.029>.
- Assumpção, M., Azevedo, P.A., Rocha, M.P., Bianchi, M.B. 2017. Lithospheric Features of the São Francisco Craton. In: Heilbron, M., Cordani, U., Alkmim, F. (Eds.), São Francisco Craton, Eastern Brazil. *Regional Geology Review*. Springer, Cham. https://doi.org/10.1007/978-3-319-01715-0_2.
- Aulbach, S., Massuyneau, M., Gaillard, F. 2017. Origins of cratonic mantle discontinuities: A view from petrology, geochemistry and thermodynamic models. *Lithos*. 268-271, 364-382. <https://doi.org/10.1016/j.lithos.2016.11.004>.
- Aulbach, S., Lin, A.-B., Weiss, Y., Yaxley, G.M. 2020. Wehrellites from continental mantle monitor the passage and degassing of carbonated melts. *Geochemical Perspectives Letters*. 15, 30-34. [10.7185/geochemlet.2031](https://doi.org/10.7185/geochemlet.2031).
- Bailey, D.K., 1989. Carbonate melt from the mantle in the volcanoes of south-east Zambia, *Nature*. 388, 415-455. <https://doi.org/10.1038/338415a0>.
- Barbosa, E.S.R., Brod, J.A., Junqueira-Brod, T.C., Dantas, E.L., Cordeiro, P.F.O., Gomide, C.S. 2012. Bebedourite from its type area (Salitre I complex): A key

petrogenetic series in the Late-Cretaceous Alto Paranaíba kamafugite-carbonatite-phoscorite association, Central Brazil. *Lithos*. 144-145, 56-72.
<https://doi.org/10.1016/j.lithos.2012.04.013>.

Bizzi, L.A., Smith, C.B., de Wit, M.J., Armstrong, R.A., Meyer, H.O. 1993. Mesozoic kimberlites and related alkalic rocks in south western São Francisco craton: a case for local mantle reservoirs and their interaction. *Proceedings 5th International Kimberlite Conference*. 156-171.

Bizzi, L.A., Wit, M.J., Smith, B., McDonald, I., Armstrong, R.A. 1995. Heterogeneous enriched mantle materials and dupal-type magmatism along the SW margin of the São Francisco Craton, Brazil. *Journal of Geodynamics*. 20, 469-491.
[https://doi.org/10.1016/0264-3707\(95\)00028-8](https://doi.org/10.1016/0264-3707(95)00028-8).

Brod, J.A., Gibson, S.A., Thompson, R.N., Junqueira-Brod, T.C., Seer, H.J., Moraes, L.C., Boaventura, G.R. 2000. The kamafugite-carbonatite association in the Alto Paranaíba Igneous Province (APIP) southeastern Brazil. *Revista Brasileira de Geociências*. 30, 408-412.

Bodinier, J.L., Vassuer, G., Vernieres, J., Dupuy, C., Fabries, J. 1990. Mechanisms of Mantle Metasomatism: Geochemical Evidence from the Lherz Orogenic Peridotite. *Journal of Petrology*. 31, 597-628.
<https://doi.org/10.1093/petrology/31.3.597>.

Bogossian, J., Kemp, A.I.S., Hagemann, S.G. 2021. Linking Gold Systems to the Crust-Mantle Evolution of Archean Crust in Central Brazil. *Minerals*. 11, 944.
<https://doi.org/10.3390/min11090944>.

Bussweiler, Y., Pearson, D.G., Stachel, T., Kjarsgaard, B.A. 2018. Cr-rich Megacrysts of Clinopyroxenes and Garnet from Lac de Gras Kimberlites, Slave Craton, Canada, Canada – implications for the Origin of Clinopyroxenes and Garnet in Cratonic Peridotites. *Mineralogy and Petrology*. 112, 583-596.
<https://doi.org/10.1007/s00710-018-0599-2>.

Carlson, R.W., Araujo, A.L.N., Junqueira-Brod, T.C., Gaspar, J.C., Brod, J.A., Petrinovic, I.A., Hollanda, M.H.B.M., Pimentel, M.M., Sichel, S. 2007. Chemical and isotopic relationships between peridotite xenoliths and mafic-ultrapotassic rocks from Southern Brazil.
<https://doi.org/10.1016/j.chemgeo.2007.04.009>.

- Carvalho, L.D.V., Jalowitzki, T., Sholz, R., Gonçalves, G.O., Rocha, M.P., Pereira, R.S., Lana, C., Castro, M.P., Queiroga, G., Fuck, R.A. 2022. An exotic Cretaceous kimberlite linked to metasomatized lithospheric mantle beneath the southwestern margin of the São Francisco Craton, Brazil. *Geoscience Frontiers*. 13, 1011281. <https://doi.org/10.1016/j.gsf.2021.101281>.
- Coltorti, M., Bonadiman, C., Hinton, R. W., Siena, F., Upton, B. G. J., 1999. Carbonatite metasomatism of the oceanic upper mantle: evidence from clinopyroxenes and glasses in ultramafic xenoliths of Grande Comore, Indian Ocean. *Journal of Petrology*. 40, 133-165. <https://doi.org/10.1093/petroj/40.1.133>.
- Comin-Chiaromonti, P., Gomes, C.B. 2005. Some notes on the Alto Paranaíba Igneous Province. In: Comin-Chiaromonti, P., Gomes, C.B. (Eds), Mesozoic to Cenozoic Alkaline Magmatism in the Brazilian Platform. Fapesp, São Paulo, Brazil, pp. 317-340.
- Condie, K.C. 2021. Earth as an evolving planetary system. (fourth edition). Elsevier.
- Costa, G.V., 2008. Química mineral e geotermobarometria de xenólitos mantélicos do kimberlito Canastra-01. M.S. thesis, University of Brasília, 137 p. (in Portuguese).
- Dalton, J.A., Wood, B.J. 1993. The compositions of primary carbonate melts and their evolution through wallrock reaction in the mantle. *Earth and Planetary Science Letters*. 119, 511-525. [https://doi.org/10.1016/0012-821X\(93\)90059-I](https://doi.org/10.1016/0012-821X(93)90059-I).
- Dalton, J.A., Presnall, D.C. 1998. Carbonatitic melts along the solidus of model lherzolite in the system CaO-MgO-Al₂O₃-SiO₂-CO₂ from 3 to 7 GPa. *Contributions to Mineralogy and Petrology*. 131, 123-135. <https://doi.org/10.1007/s004100050383>.
- Danni, J.C.M., Gaspar, J.C. 1994. Química do katungito de amorinópolis – Goiás: contribuição ao estudo do magmatismo kamafugítico. *Geochimica Brasiliensis*. 8, 119-134.
- Dasgupta, R., Hirschmann, M.M. 2006. Melting in the Earth's deep upper mantle caused by carbon dioxide. *Nature*. 440, 659-662. <https://doi.org/10.1038/nature04612>.

Dasgupta, R., Hirschmann, M.M. 2007. Effect of variable carbonate concentration on the solidus of mantle peridotite. *American Mineralogist*. 92, 370-379.
<https://doi.org/10.2138/am.2007.2201>.

Dasgupta, R., Hirschmann, M.M. 2010. The deep carbon and melting in Earth's interior. *Earth and Planetary Science Letters*. 298, 1-13.
<https://doi.org/10.1016/j.epsl.2010.06.039>.

Downes, H. 2001. Formation and Modification of the Shallow Sub-continental Lithospheric Mantle: a Review of Geochemical Evidence from Ultramafic Xenolith Suites and Tectonically Emplaced Ultramafic Massifs of Western and Central Europe. *Journal of Petrology*. 42, 233-250.
<https://doi.org/10.1093/petrology/42.1.233>.

Eggler, D.H. 1978. The effect of CO₂ upon partial melting of peridotite in the system Na₂O-CaO-Al₂O₃-MgO-SiO₂-CO₂ to 35 kb, with an analysis of melting in a peridotite-H₂O-CO₂ system. *American Journal of Science*. 278, 305-434.
<https://doi.org/10.2475/ajs.278.3.305>.

Eggler, D.H. 1987. Discussion of recent papers on carbonated peridotite, bearing on metasomatism and magmatism: an alternative. *Earth and Planetary Science Letters*. 82. 398-400. [https://doi.org/10.1016/0012-821X\(87\)90214-7](https://doi.org/10.1016/0012-821X(87)90214-7).

Farmer, G.L., Boettcher, A.L. 1981. Petrologic and crystal-chemical significance of some deep-seated phlogopites. *American Mineralogist*. 66, 1154-1163.

Fernandes, P.R., Tommasi, A., Vauchez, A., Neves, S.P., Nannini, F. 2021. The São Francisco cratonic root beneath the Neoproterozoic Brasilia belt (Brazil): Petrophysical data from kimberlite xenoliths. *Tectonophysics*. 816, 229011.
<https://doi.org/10.1016/j.tecto.2021.229011>.

Felgate, M.R. 2014. The petrogenesis of Brazilian kimberlites and kamafugites intruded along the 125° lineament: improved geochemical and geochronological constraints on magmatism in Rondonia and the Alto Paranaíba Igneous Province. Ph.D. Thesis, University of Melbourne, p. 275.

Ferreira, A.C.D., Conceição, R.V., Mizusaki, A.M.P. 2022. Mesozoic to Cenozoic alkaline and tholeiitic magmatism related to West Gondwana break-up and

dispersal. Gondwana Research. 106, 15-33.
<https://doi.org/10.1016/j.gr.2022.01.005>.

Fischel, D.P., Pimentel, M.M., Fuck, R.A. 1998. Idade do metamorfismo de alto grau no complexo Anápolis-Itauçu, Goiás, determinada pelo método Sm-Nd. Revista Brasileira de Geociências. 28, 543-544.

Fitzpayne, A., Giuliani, A., Hergt, J., Phillips, D., Janney, P. 2018a. New geochemical constraints on the origins of MARID and PIC rocks: Implications for mantle metasomatism and mantle-derived potassic magmatism. Lithos. 318-319, 478-493. <https://doi.org/10.1016/j.lithos.2018.08.036>.

Fitzpayne, A., Giuliani, A., Phillips, D., Hergt, J., Woodhead, J.D., Farquhar, J., Fiorentini, M.L., Drysdale, R.N., Wu, N. 2018b. Kimberlite-related metasomatism recorded in MARID and PIC mantle xenoliths. Mineralogy and Petrology. 112, 71-84. <https://doi.org/10.1007/s00710-018-0573-z>.

Fitzpayne, A., Giuliani, A., Maas, R., Hergt, J., Janney, P., Phillips, D. 2019. Progressive metasomatism of the mantle by kimberlites melts: Sr-Nd-Hf-Pb isotope compositions of MARID and PIC minerals. Earth and Planetary Science Letters. 509, 15-26. <https://doi.org/10.1016/j.epsl.2018.12.013>.

Fitzpayne, A., Giuliani, A., Hergt, J., Woodhead, J.D., Maas, R. 2020. Isotopic analyses of clinopyroxenes demonstrate the effects of kimberlite melt metasomatism upon the lithospheric mantle. Lithos. 370-371, 105595. <https://doi.org/10.1016/j.lithos.2020.105595>.

Foley, S.F. 1989. Experimental constraints on phlogopite chemistry in lamproites: 1. The effect of water activity and oxygen fugacity. European Journal of Mineralogy. 1, 411-426.

Foley, S. 1992. Petrological characterization of the source components of potassic magmas: geochemical and experimental constraints. Lithos. 28, 187-204. [https://doi.org/10.1016/0024-4937\(92\)90006-K](https://doi.org/10.1016/0024-4937(92)90006-K).

Foley, S. 2008. Rejuvenation and erosion of the cratonic lithosphere. Nature Geoscience. 1, 503-510. <https://doi.org/10.1038/ngeo261>.

Fuck, R.A., Pimentel, M.M., Alvarenga, C.J.S., Dantas, E.L. 2017. The Northern Brasília Belt. In: Heilbron, M., Cordani, U., Alkmim, F. (eds) São Francisco

Craton, Eastern Brazil. Regional Geology Reviews. Springer, Cham.
https://doi.org/10.1007/978-3-319-01715-0_11.

Gervasoni, F., Klemme, S., Rohrbach, A., Grützner, T., Berndt, J. 2017. Experimental constraints on mantle metasomatism caused by silicate and carbonate melts. *Lithos*. 282-283, 173-186. <https://doi.org/10.1016/j.lithos.2017.03.004>.

Ghosh, S., Ohtani, E., Litasov, K., Suzuki, A., Sakamaki, T. 2007. Stability of carbonated magmas at the base of the Earth's upper mantle. *Geophysical Research Letters*. 34, L22312. <https://doi.org/10.1029/2007GL031349>.

Ghosh, S., Ohtani, E., Litasov, K.D., Terasaki, H. 2009. Solidus of carbonated peridotite from 10 to 20 GPa and origin of magnesiocarbonatite melt in the Earth's deep mantle. *Chemical Geology*. 262, 17-28.
<https://doi.org/10.1016/j.chemgeo.2008.12.030>.

Giuliani, A., Phillips, D., Kamenetsky, V.S., Kendrick, M.A., Wyatt, B.A., Goemann, K., Hutchinson, G. 2014. Petrogenesis of mantle polymict breccias: insights into mantle processes coeval with kimberlite magmatism. *Journal of Petrology*. 55, 831-858. <https://doi.org/10.1093/petrology/egu008>.

Giuliani, A., Kamenetsky, V.S., Kendrick, M.A., Phillips, D., Goemann, K. 2013. Nickel-rich metasomatism of the lithospheric mantle by pre-kimberlitic alkalic-S-Cl-rich C-O-H fluids. *Contributions to Mineralogy and Petrology*. 165, 155-171. <https://doi.org/10.1007/s00410-012-0801-1>.

Giuliani, A., Phillips, D., Kamenetsky, V.S., Goemann, K. 2016. Constraints on kimberlite ascent mechanisms revealed by phlogopite compositions in kimberlites and mantle xenoliths. *Lithos*. 240-243, 189-201.
<https://doi.org/10.1016/j.lithos.2015.11.013>.

Grégoire, M., Bell, D.R., le Roex, A.P. 2002. Trace element geochemistry of phlogopite-rich mafic mantle xenoliths: their classification and their relationship to phlogopite-bearing peridotites and kimberlites revisited. *Contributions to Mineralogy and Petrology*. 142, 603-625. <https://doi.org/10.1007/s00410-001-0315-8>.

- Grégoire, M., Bell, D.R., le Roex, A.P. 2003. Garnet Lherzolites from the Kaapvaal Craton (South Africa): Trace Element Evidence for a Metasomatic History. *Journal of Petrology*. 44, 629-657. <https://doi.org/10.1093/petrology/44.4.629>.
- Griffin, W.L., O'Reilly, S.L., Ryan, C.G., Gaul, O., Ionov, D. 1998. Secular variation in the composition of the subcontinental lithospheric mantle. In: Braun, J., Dooley, J.C., Goleby, B.R., van der Hilst, R.D., Klootwijk, C.T. (Eds.), *Structure & Evolution of the Australian Continent, Geodynamics*. Volume 26, AGU, Washington D.C. pp. 1-26.
- Griffin, W.L., Fisher, N.I., Friedman, J.H., Ryan, C.G., O'Reilly, S.Y. 1999. Cr-pyrope garnets in the lithospheric mantle I. Compositional systematics and relations to tectonic setting. *Journal of Petrology*. 40, 679-705. <https://doi.org/10.1093/petroj/40.5.679>.
- Griffin, W.L., O'Reilly, S.Y., Abe, N., Aulbach, S., Davies, R.M., Pearson, N.J., Doyle, B.J., Kivi, K. 2003. The origin and evolution of Archean lithospheric mantle. *Precambrian Research*. 127, 19-41. [https://doi.org/10.1016/S0301-9268\(03\)00180-3](https://doi.org/10.1016/S0301-9268(03)00180-3).
- Guarino, V., Wu, F.Y., Lustrino, M., Melluso, L., Brotzu, P., Gomes, C.B., Ruberti, E., Tassinari, C.C.G., Svisero, D.P. 2013. U-Pb ages, Sr-Nd isotope geochemistry, and petrogenesis of kimberlites, kamafugites and phlogopite-picrites of the Alto Paranaíba Igneous Province, Brazil. *Chemical Geology*. 353, 65-82. <https://doi.org/10.1016/j.chemgeo.2012.06.016>.
- Gibson, S.A., Thompson, R.N., Leonardos, O.H., Dickin, A.P., Mitchell, J.G. 1995. The Late Cretaceous Impact of the Trindade Mantle Plume: Evidence from Large-volume, Mafic, Potassic Magmatism in SE Brazil. *Journal of Petrology*. 36, 189-229. <https://doi.org/10.1093/petrology/36.1.189>.
- Guarino, V., Wu, F.Y., Melluso, L., Gomes, C.B., Tassinari, C.C.G., Ruberti, E., Brilli, M. 2017. U-Pb ages, geochemistry, C-O-Nd-Sr-Hf isotopes and petrogenesis of the Catalão II carbonatitic complex (Alto Paranaíba Igneous Province, Brazil): implications for regional-scale heterogeneities in the Brazilian carbonatite associations. *International Journal of Earth Science*. 106, 1963-1989. <https://doi.org/10.1007/s00531-016-1402-4>.

Gudfinnsson, G.H., Presnall, D.C. 2005. Continuous Gradations among Primary Carbonatitic, Kimberlitic, Melilititic, Basaltic, Picritic, and Komatiitic Melts in Equilibrium with Garnet Lherzolite at 3-8 GPa. *Journal of Petrology*. 46, 1645-1659. <https://doi.org/10.1093/petrology/egi029>.

Hammouda, T., Chantel, J., Manthilake, G., Guignard, J., Crichton, W. Hot mantle geotherms stabilize calcic carbonatite magmas up to the surface. *Geology*. 42, 911-914. <https://doi.org/10.1130/G35778.1>.

Hammouda, T., Keshav, S. 2015. Melting in the mantle in the presence of carbon: Review of experiments and discussion on the origin of carbonatites. *Chemical Geology*. 418, 171-188. <https://doi.org/10.1016/j.chemgeo.2015.05.018>.

Hirose, K., Kawamoto, T. 1995. Hydrous partial melting of lherzolite at 1 GPa: The effect of H₂O on the genesis of basaltic magmas. *Earth and Planetary Science Letters*. 133, 463-473. [https://doi.org/10.1016/0012-821X\(95\)00096-U](https://doi.org/10.1016/0012-821X(95)00096-U).

Höfer, H.E., Lazarov, M., Brey, G.P., Woodland, A.B. 2009. Oxygen fugacity of the metasomatizing melt in polymict peridotite from Kimberley. *Lithos*. 112, 1150-1154. <https://doi.org/10.1016/j.lithos.2009.05.037>.

Hu, S., He, L., Wang, J. 2000. Heat flow in the continental area of China: a new data set. *Earth and Planetary Science Letters*. 179, 407-419. [https://doi.org/10.1016/S0012-821X\(00\)00126-6](https://doi.org/10.1016/S0012-821X(00)00126-6).

Huang, X.L., Zhong, J.W., Xu, Y.G. 2012. Two tales of the continental lithospheric mantle prior to the destruction of the North China Craton: Insights from Early Cretaceous mafic intrusions in western Shandong, East China. *Geochimica et Cosmochimica Acta*. 96, 193-214. <https://doi.org/10.1016/j.gca.2012.08.014>.

Kamenetsky, V.S., Yaxley, G.M. 2015. Carbonate-silicate liquid immiscibility in the mantle propels kimberlite magma ascent. *Geochimica et Cosmochimica Acta*. 158, 48-56. <https://doi.org/10.1016/j.gca.2015.03.004>.

Kargin, A.V., Sazonova, L.V., Nosova, A.A., Lebedeva, N.M., Kostitsyn, Yu.A., Kovalchuk, E.V., Tretyachenko, V.V., Tikhomirova, Ya.S. 2019. Phlogopite in mantle xenoliths and kimberlite from the Grib pipe, Arkhangelsk, province, Russia: Evidence for multi-stage mantle metasomatism and origin of phlogopite

in kimberlite. Geoscience Frontiers. 10, 1941-1959.
<https://doi.org/10.1016/j.gsf.2018.12.006>.

Kerrick, D.M., Connolly, J.A.D. 2001. Metamorphic devolatilization of subducted marine sediments and the transport of volatiles into the Earth's mantle. Nature. 411, 293-296. <https://doi.org/10.1038/35077056>.

Keshav, S., Gudfinnsson, G.H. 2013. Silicate liquid-carbonatite liquid transition along the melting curve of model, vapor-saturated peridotite in the system CaO-MgO-Al₂O₃-SiO₂-CO₂ from 1.1 to 2 GPa. <https://doi.org/10.1002/jgrb.50249>.

Kilian, R., Stern, C.R. 2002. Constraints on the interaction between slab melts and the mantle wedge from adakitic glass in peridotite xenoliths. European Journal of Mineralogy. 14, 25-36. <https://doi.org/10.1127/0935-1221/2002/0014-0025>.

Kogarko, L.N., Henderson, C.M.B., Pacheco, H. 1995. Primary Ca-rich carbonatite magma and carbonate-silicate-sulphide liquid immiscibility in the upper mantle. Contributions to Mineralogy and Petrology. 121, 267-274. <https://doi.org/10.1007/BF02688242>.

Kogiso, T., Hirose, K., Takahashi, E. 1998. Melting experiments on homogeneous mixtures of peridotite and basalt: application to the genesis of ocean island basalts. Earth and Planetary Science Letters. 162, 45-61. [https://doi.org/10.1016/S0012-821X\(98\)00156-3](https://doi.org/10.1016/S0012-821X(98)00156-3).

Lee, W.J., Wyllie, P.J. 1997. Liquid immiscibility between nepheline and carbonatite from 1.0 to 2.5 GPa compared with mantle melt compositions. Contributions to Mineralogy and Petrology. 127, 1-16. <https://doi.org/10.1007/s004100050261>.

Lin, A-B., Zheng, J-P., Aulbach, S., Xiong, Q., Pan, S-K. 2020. Causes and consequences of wehrlitization beneath Trans-Lithospheric Fault: evidence from Mesozoic basalt-borne wehrlite xenoliths from the Tan-Lu Fault Belt, North China Craton. Journal of Geophysical Research. 124, 1-23. <https://doi.org/10.1029/2019JB019084>.

Luth, R.W. 1993. Diamonds, eclogites, and oxidation state of the Earth's mantle. Science. 261, 66-88. <https://www.science.org/doi/abs/10.1126/science.261.5117.66>.

Luth, R.W. 1999. Carbon and carbonates in the mantle. In: Y. Fei, C.M. Bertka, and B.O. Mysen, Ed., Mantle Petrology: Field observation and High Pressure Experimentation: A Tribute to Francis R. (Joe) Boyd, 6, p. 297-316. The Geochemical Society, Houston, Texas.

Matteini, M., Dantas, E.L., Pimentel, M.M., Alvarenga, C.J.S., Dardenne, M.A. 2012. U-Pb and Hf isotope study on detrital zircons from the Paranoá Group, Brasília Belt Brazil: Constraints on depositional age at Mesoproterozoic – Neoproterozoic transition and tectono-magmatic events in the São Francisco Craton. *Precambrian Research.* 206-207, 168-181.
<https://doi.org/10.1016/j.precamres.2012.03.007>.

Maury, R.C., Defant, M.J., Joron, J.L. 1992. Metasomatism of the sub-arc mantle inferred from trace elements in Philippine xenoliths. *Nature.* 360, 661-663.

Meyer, H.O.A., Zhang, A., Milledge, H.J., Mendelssohn, M.J. 1994. Diamonds and inclusions in diamonds from Chinese Kimberlite. CPRM Special Publication 1/A. 1, 98-115.

Nannini, F. 2016. Geologia e petrologia de xenólitos mantélicos da Província Ígnea do Alto Paranaíba. PhD. thesis, Universidade de São Paulo, 298 p. (in Portuguese).

Novella, D., Keshav, S., Gudfinnsson, G.H., Ghosh, S. 2014. Melting phase relations of model carbonated peridotite from 2 to 3 GPa in the system CaO-MgO-Al₂O₃-SiO₂-CO₂ and further indication of possible unmixing between carbonatite and silicate liquids. *Journal of Geophysical Research.* 119, 2780-2800.
<https://doi.org/10.1002/2013JB010913>.

Oliveira, I.L. 2015. Isótopos de Nd e Sr em minerais de diferentes séries petrogenéticas nos complexos alcalino-carbonatíticos de Salitre e Catalão I. Master Dissertation. Universidade de Brasília. 245 p.

O'Reilly, S.Y., Griffin, W.L., Djomani, Y.H.P., Morgan, P. 2001. Are lithospheres forever? Tracking changes in subcontinental lithospheric mantle through time. *GSA Today.* 11, 4-10.

O'Reilly, S.Y., Griffin, W.L. 2010. The continental lithosphere-asthenosphere boundary: Can we sample it? *Lithos.* 120, 1-13.
<https://doi.org/10.1016/j.lithos.2010.03.016>.

- O'Reilly, S.Y., Griffin, W.L. 2013. Mantle Metasomatism. In: Metasomatism and the Chemical Transformation of Rock. Lecture Notes in Earth Sciences. Springer, Berlin, Heidelberg. https://doi.org/10.1007/978-3-642-28394-9_12.
- Patkó, L., Liptai, N., Aradi, L. E., Klébesz, R., Sendula, E., Bodnar, R. J., Kovács, I. J., Hidas, K., Cesare, B., Novák, A., Trásy, B., Szabó, C. 2020. Metasomatism-induced wehrlite formation in the upper mantle beneath the Nograd-Gömör Volcanic Field (Northern Pannonian Basin): evidence from xenoliths. *Geoscience Frontiers.* 11, 943-964. <https://doi.org/10.1016/j.gsf.2019.09.012>.
- Pearson, D.G. 1999. Evolution of Cratonic Lithospheric Mantle: An Isotopic Perspective. In: Fei, Y., Berka, C.M., Mysen, B.O. (Eds). *Mantle Petrology: Field Observations and High-Pressure Experimentation: A Tribute to Francis R. (Joe) Boyd*: The Geochemical Society Special Publication. pp. 57-78.
- Pearson, D.G., Canil, D., Shirey, S.B. 2003. 2.05 – Mantle Samples Included in Volcanic Rocks: Xenoliths and Diamonds. In: Holland, H.D., Turekian, K.K. (Eds.), 2003. *Treatise on Geochemistry*. Pergamon. pp. 171-275. <https://doi.org/10.1016/B0-08-043751-6/02005-3>.
- Pereira, R.S., Fuck, R.A. 2005. Archean nuclei and the distribution of kimberlite and related rocks in the São Francisco Craton, Brazil. *Revista Brasileira de Geociências.* 35, 93-104.
- Peslier, A.H. 2010. A review of water contents of nominally anhydrous natural minerals in the mantles of Earth, Mars and the Moon. *Journal of Volcanology and Geothermal Research.* 197, 239-258. <https://doi.org/10.1016/j.jvolgeores.2009.10.006>.
- Pimentel, M.M., Fuck, R.A. 1992. Neoproterozoic crustal accretion in central Brazil. *Geology.* 20, 375-379. [https://doi.org/10.1130/0091-7613\(1992\)020%3C0375:NCAICB%3E2.3.CO;2](https://doi.org/10.1130/0091-7613(1992)020%3C0375:NCAICB%3E2.3.CO;2).
- Pimentel, M.M., Whitehouse, M.J., Viana, M.G., Fuck, R.A., Machado, N. 1997. The Mara Rosa arc in the Tocantins Province: further evidence for Neoproterozoic crustal accretion in central Brazil. *Precambrian Research.* 81, 299-310. [https://doi.org/10.1016/S0301-9268\(96\)00039-3](https://doi.org/10.1016/S0301-9268(96)00039-3).

- Pinto, L.G.R., Pádua, M.B., Ussami, N., Vitorello, I., Padilha, A.L., Braitenberg, C. 2010. Magnetotelluric deep soundings, gravity and geoid in the south São Francisco craton: Geophysical indicators of cratonic lithosphere rejuvenation and crustal underplating. *Earth and Planetary Science Letters*. 297, 423-434. <https://doi.org/10.1016/j.epsl.2010.06.044>.
- Pilbeam, L.H., Nielson, T.F.D., Waught, T.E. 2013. Digestion Fractional Crystallization (DFC): an Important Process in the Genesis of Kimberlites. Evidence from Olivine in the Majuagaa kimberlite, Southern West Greenland. *Journal of Petrology*. 54, 1399-1425. <https://doi.org/10.1093/petrology/egt016>.
- Read, G., Grütter, H., Winter, S., Luckman, N., Gaunt, F. 2004. Stratigraphic relations, kimberlite emplacement and lithospheric thermal evolution, Quirico Basin, Minas Gerais State, Brazil. *Lithos*. 77, 803-818. <https://doi.org/10.1016/j.lithos.2004.04.011>.
- Rocha, M.P., Schimmel, M., Assumpção, M. 2011. Upper-mantle seismic structure beneath SE and Central Brazil from P- and S-wave regional travelttime tomography. *Geophysical Journal International*. 184, 268-286. <https://doi.org/10.1111/j.1365-246X.2010.04831.x>.
- Rocha, M.P., Azevedo, P.A., Assumpção, M., Pedrosa-Soares, A.C., Fuck, R., Von Huelsen, M.G., 2019. Delimiting the Neoproterozoic São Francisco Paleocontinental Block with P-wave travelttime tomography. *Geophysical Journal International*. 219, 633-644. <https://doi.org/10.1093/gji/ggz323>.
- Rodrigues, J.B., Pimentel, M.M., Dardenne, M.A., Armstrong, R.A. 2010. Age, provenance and tectonic setting of the Canastra and Ibiá Groups (Brasília Belt, Brazil): Implications for the age of a Neoproterozoic glacial event in central Brazil. 29, 512-521. <https://doi.org/10.1016/j.jsames.2009.08.008>.
- Roduit, N. 2007. JMicrоВision: un logiciel d'analyse d'images pétrographiques polyvalent. *Terre Environ*. <https://doi.org/10.13097/archive-ouverte/unige:468>.
- Rudnick, R.L., McDonough, W.F., Chappell, B.W. 1993. Carbonatite metasomatism in the northern Tanzanian mantle: petrography and geochemical characteristics. *Earth and Planetary Science Letters*. 114, 463-475. [https://doi.org/10.1016/0012-821X\(93\)90076-L](https://doi.org/10.1016/0012-821X(93)90076-L).

- Sen, C., Dunn, T. 1994. Experimental modal metasomatism of a spinel lherzolite and the production of amphibole-bearing peridotite. Contribution to Mineralogy and Petrology. 119, 422-432. <https://doi.org/10.1007/BF00286939>.
- Shee, S. 1985. The petrogenesis of the Wesselton Mine kimberlites, Kimberley, Cape Province, R.S.A. Unpublished Ph.D. Thesis, University of Cape Town, p. 220.
- Sgarbi, P.B.A., Gaspar, J.C., Valen  a, J.G., 2000. Clinopyroxene from Brazilian kamafugites. Lithos. 53, 165-171. [https://doi.org/10.1016/S0024-4937\(00\)00011-6](https://doi.org/10.1016/S0024-4937(00)00011-6).
- Simon, N.S.C., Irvine, G.J., Davies, G.R., Pearson, D.G., Carlson, R.W. 2003. The origin of garnet and clinopyroxene in “depleted” Kaapvaal peridotites. Lithos. 71, 289-322. [https://doi.org/10.1016/S0024-4937\(03\)00118-X](https://doi.org/10.1016/S0024-4937(03)00118-X).
- Soustelle, V., Tommasi, A., Demouchy, S., Ionov, D.A. 2010. Deformation and fluid-rock interaction in the supra-subduction mantle: microstructures and water contents in peridotite xenoliths from the Avacha volcano, Kamchatka. Journal of Petrology. 51, 363-394. <https://doi.org/10.1093/petrology/egp085>.
- Su, B., Chen, Y., Guo, S., Chu, Z. Y., Liu, J. B., Gao, Y. J., 2016. Carbonatitic metasomatism in orogenic dunites from Lijiatun in the Sulu UHP terrane, eastern China. Lithos. 262, 266-284. <https://doi.org/10.1016/j.lithos.2016.07.007>.
- Sweeney, R.J. 1994. Carbonatite melt compositions in the Earth's mantle. Earth and Planetary Science Letters. 128, 259-270. [https://doi.org/10.1016/0012-821X\(94\)90149-X](https://doi.org/10.1016/0012-821X(94)90149-X).
- Tang, Y.J., Zhang, H.F., Ying, J.F., Zhang, J., Liu, X.M. 2008. Refertilization of ancient lithospheric mantle beneath the central North China Craton: evidence from petrology and geochemistry of peridotite xenoliths. Lithos. 101, 435-452. <https://doi.org/10.1016/j.lithos.2007.09.006>.
- Tang, Y.J., Zhang, H.F., Ying, J.F., Su, B.X. 2013. Widespread refertilization of cratonic and circum-cratonic lithospheric mantle. Earth-Science Reviews. 118, 45-68. <https://doi.org/10.1016/j.earscirev.2013.01.004>.
- Thompson, R.N., Gibson, S.A., Mitchell, J.G., Dickin, A.P., Leonardos, O.H., Brod, J.A., Greenwood, J.C. 1998. Migrating Cretaceous-Eocene magmatism in the

- Serra do Mar Alkaline Province, SE Brazil: melts from the deflected Trindade mantle plume? Journal of Petrology. 39, 1493-1526.
<https://doi.org/10.1093/petroj/39.8.1493>.
- Toyoda, K., Horiuchi, H., Takonami, M. 1994. Dupal anomaly of Brazilian carbonatites: Geochemical correlations with hotspots in the South Atlantic and implications for the mantle source. Earth and Planetary Science Letters. 126, 315-331. [https://doi.org/10.1016/0012-821X\(94\)90115-5](https://doi.org/10.1016/0012-821X(94)90115-5).
- Valeriano, C.M., Pimentel, M.M., Heilbron, M., Almeida, J.C.H., Trouw, R.A.J. 2008. Tectonic evolution of the Brasília Belt, Central Brazil, and early assembly of Gondwana. Geological Society, London, Special Publications. 294, 197-210. <https://doi.org/10.1144/SP294.11>.
- Valeriano, C.M. 2017. The Southern Brasília Belt. In: Heilbron, M., Cordani, U., Alkmim, F. (eds) São Francisco Craton, Eastern Brazil. Regional Geology Reviews. Springer, Cham. https://doi.org/10.1007/978-3-319-01715-0_10.
- Wallace, M.E., Green, D.H. 1988. An experimental determination of primary carbonatite magma composition. Nature. 335, 343-346. <https://doi.org/10.1038/335343a0>.
- Wang, C., ZhenMin, J., Shan, G., JunFeng, Z., Shu, Z. 2010. Eclogite-melt/peridotite reaction: Experimental constraints on the destruction mechanism of the North China Craton. Science China Earth Sciences. 53, 797-809. <https://doi.org/10.1007/s11430-010-3084-2>.
- Watson, E.B., Brenan, J.M., Baker, D.R. 1990. Distribution of fluids in the mantle. In: Menzies, M.A. (Eds.), Continental mantle. Clarendon, Oxford, UK.
- Wyllie, P.J., Huang, W.L., 1975. Influence of mantle CO₂ in the generation of carbonatites and kimberlites. Nature. 257, 297-299. <https://doi.org/10.1038/257297a0>.
- Wyllie, P.J., Huang, W.L. 1976. Carbonation and melting reactions in the system CaO-MgO-SiO₂-CO₂ at mantle pressures with geophysical and petrological applications. Contributions to Mineralogy and Petrology. 54, 79-107. <https://doi.org/10.1007/BF00372117>.
- Xu, W., Hergt, J.M., Gao, S., Pei, F., Wang, W., Yang, D., 2008. Interaction of adakitic melt-peridotite: implications for the high-Mg# signature of Mesozoic adakitic rocks in the

eastern North China Craton. *Earth Planet. Sci. Lett.* 265(1-2), 123-137.
<https://doi.org/10.1016/j.epsl.2007.09.041>.

Yaxley, G.M., Crawford, A.J., Green, D.H. 1991. Evidence of carbonatite metasomatism in spinel peridotite xenoliths from western Victoria, Australia. *Earth and Planetary Science Letters*. 107, 305-317. [https://doi.org/10.1016/0012-821X\(91\)90078-V](https://doi.org/10.1016/0012-821X(91)90078-V).

Yaxley, G.M., Green, D.H., 1996. Experimental reconstruction of sodic dolomitic carbonatite melts from metasomatised lithosphere. *Contrib. Mineral Petrol.* 124, 359-364. <https://doi.org/10.1007/s004100050196>.

Yaxley, G.M., Green, D.H. 1998. Reactions between eclogite and peridotite: mantle refertilisation by subduction of oceanic crust. *Schweizerische Mineralogische und Petrographische Mitteilungen*. 78, 243-255.

Yaxley, G.M., Green, D.H., Kamenetsky, V. 1998. Carbonatite Metasomatism in the Southeastern Australian Lithosphere. *Journal of Petrology*. 39, 1917-1930. <https://doi.org/10.1093/petroj/39.11-12.1917>.

Zhang, H.F., Menzies, M.A., Mattey, D.P., Richard, W.H., Gurney, J.J. 2001. Petrology, mineralogy and geochemistry of oxide minerals in polymict xenoliths from the Bultfontein kimberlites, South Africa: implication for low bulk-rock oxygen isotopic ratios. *Contribution to Mineralogy and Petrology*. 141, 367-379. <https://doi.org/10.1007/s004100100254>.

Zhang, H.F., Sun, M., Zhou, X.H., Fan, W.M., Zhai, M.G., Ying, J.F. 2002. Mesozoic lithosphere destruction beneath the North China Craton: evidence from major-trace-element and Sr-Nd-Pb isotope studies of Fangcheng basalts. *Contributions to Mineralogy and Petrology*. 144, 241-253.

Zhang, H.F. 2009. Peridotite-melt interaction: key point for the destruction of cratonic lithospheric mantle. *Chinese Science Bulletin*. 54, 3417-3437. <https://doi.org/10.1007/s11434-009-0307-z>.

Zheng, J.P. 2009. Comparison of mantle-derived materials from different spatiotemporal settings: implications for destructive and accretional processes of the North China Craton. *Chinese Science Bulletin*. 54, 3397-3416. <https://doi.org/10.1007/s11434-009-0308-y>.

Zhong, K., Liu, Y. 2018. Carbonate metasomatism in the lithospheric mantle: Implications for cratonic destruction in North China. *Science China Earth Sciences*. 61, 711-729. <https://doi.org/10.1007/s11430-017-9185-2>.

CHAPTER 8 – SUPPLEMENTARY MATERIAL

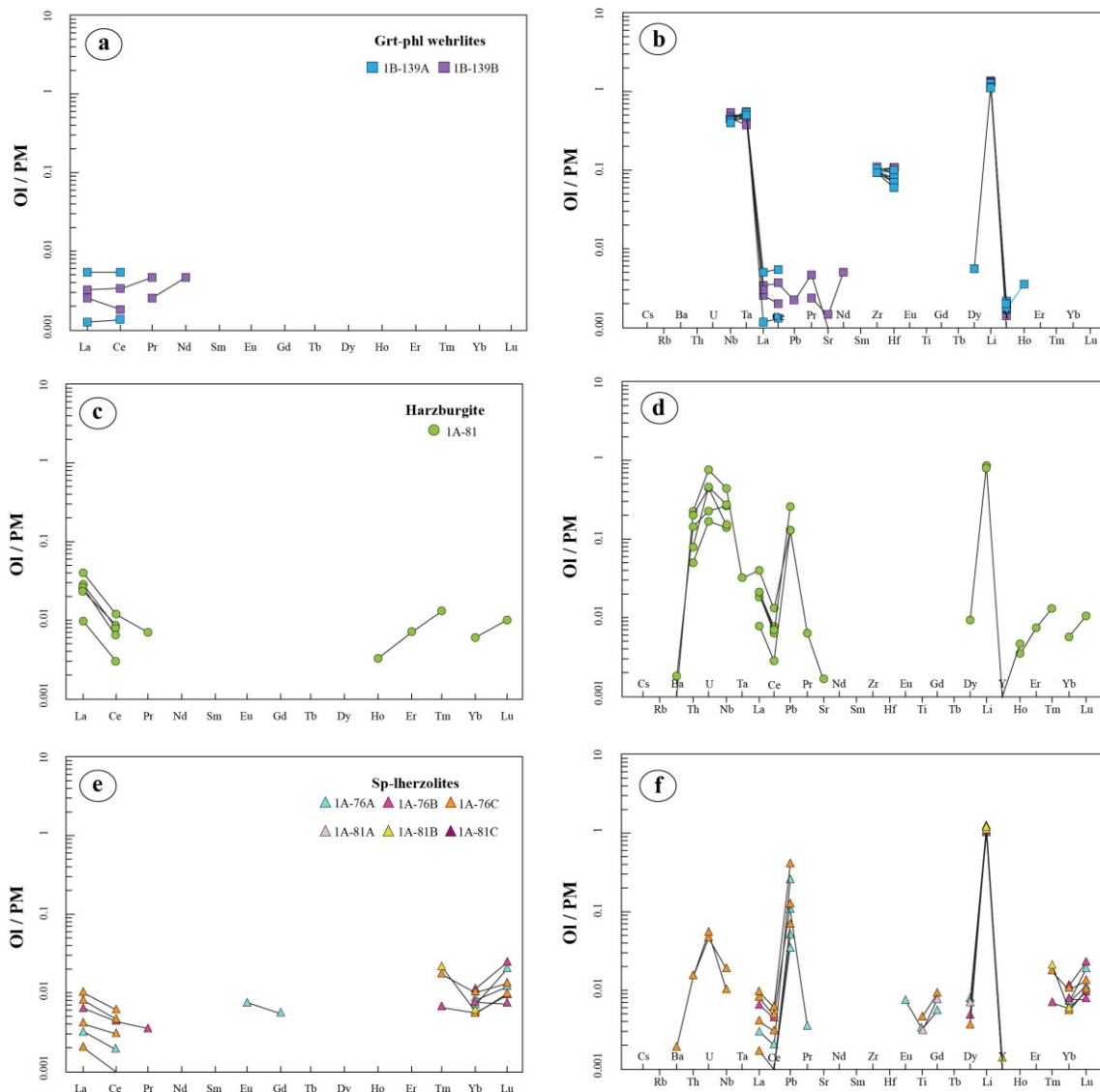


Figure S1. Trace elements of olivines of the grt-phl wehrellites, harzburgite and sp-lherzolites xenoliths normalized to the primitive mantle ([Sun and McDonough, 1989](#)).

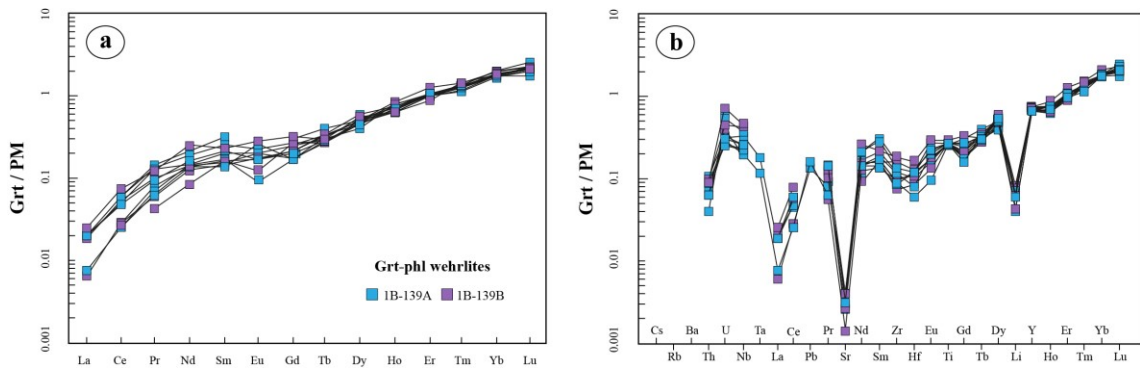


Figure S2. Trace elements of garnet of the grt-phl wehrellites xenoliths normalized to the primitive mantle ([Sun and McDonough, 1989](#)).

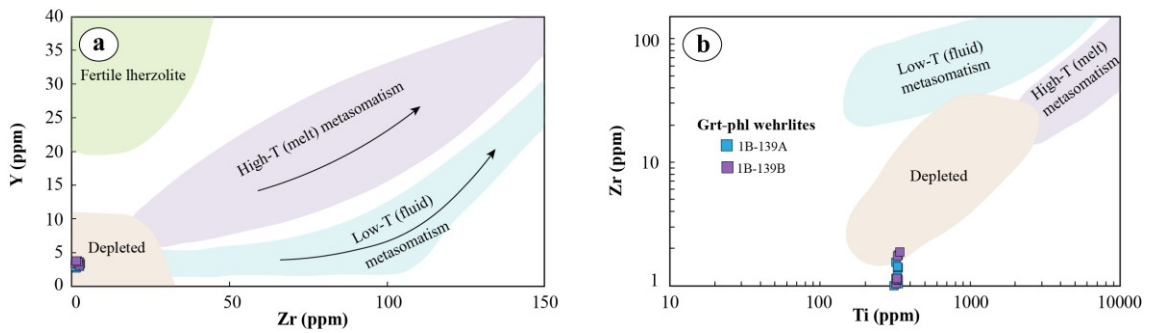


Figure S3. (a) Zr-Y and (b) Zr-Ti patterns of pyrope crystals of the grt-phl wehrellites xenoliths. Fields of depleted and fertile garnet, melt-related and fluid-related metasomatism are after [Griffin and Ryan \(1995\)](#) and [Griffin et al. \(1999b\)](#).

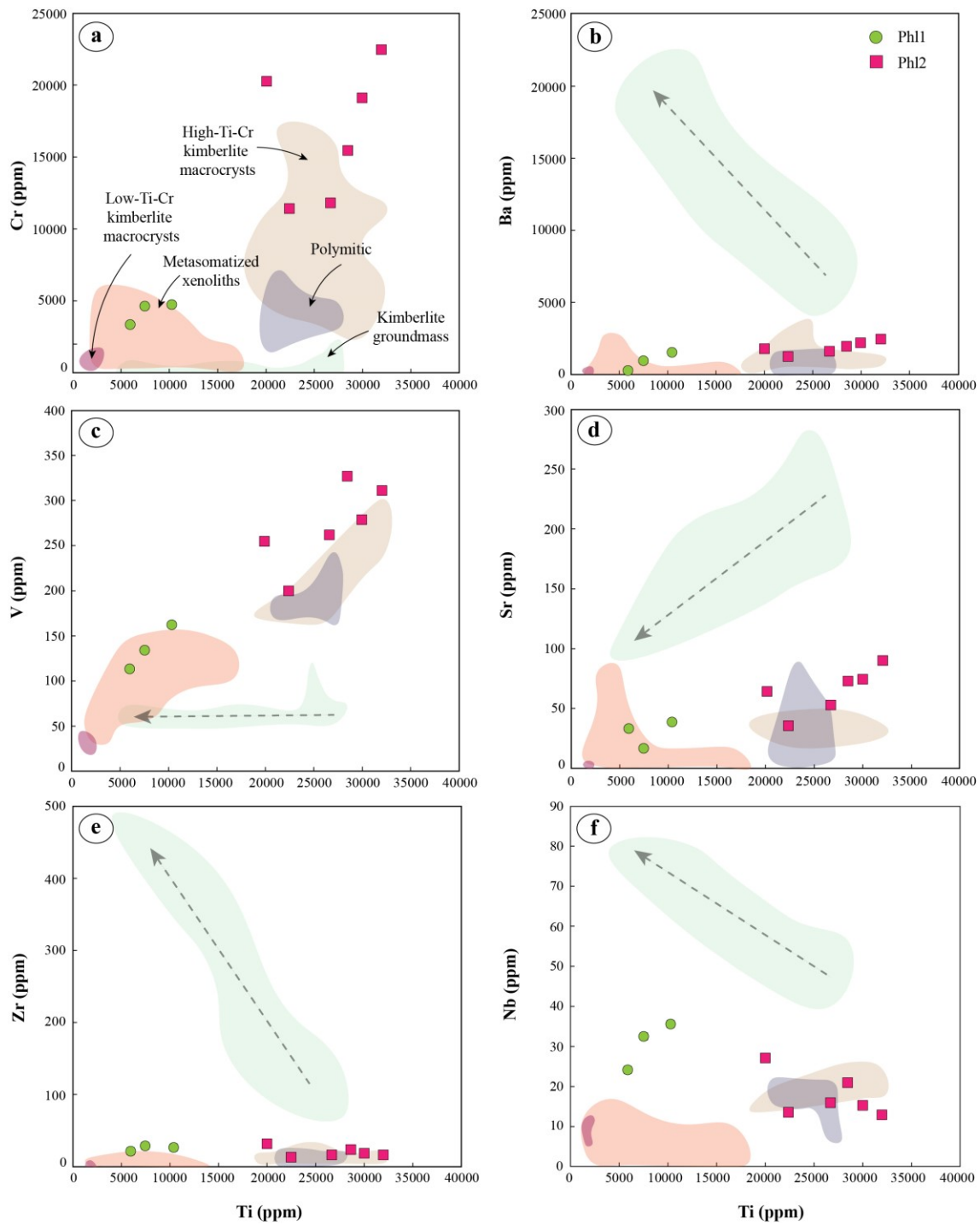


Figure S4. Trace element co-variation diagrams for phlogopite from Catalão xenoliths. (a-f) Phlogopite from metasomatized mantle xenoliths, phlogopite macrocrysts with low-Ti-Cr and high-Ti-Cr compositions, phlogopite from polymict breccias, and phlogopite from kimberlite groundmass are from [Giuliani et al. \(2016\)](#). The arrows show compositional trends towards more evolved compositions for phlogopite of groundmass kimberlite.

Table S1. LA-ICP-MS trace element data of calibration reference materials (NIST612, 355OL, BHVO-2G, and BR-1G).

Limit of detection	Reference Material				Reference material preferred values (PV)			
	NIST612 (run)	355OL (run)	BHVO-2G (run)	BIR-1G (run)	NIST612 (GeoRem 5211)	355OL (Bussweiller et al., 2019)	BHVO-2G (GeoRem 492)	BIR-1G (GeoRem 492)
Li	0.037	42.02 (0.30)	0.97 (0.05)	4.75 (0.06)	3.32 (0.15)	40.20	0.90	4.40
B	0.26	34.99 (0.69)	0.47 (0.14)	3.57 (0.23)	1.30 (0.24)	34.30	—	—
Sc	0.0021	40.98 (0.18)	0.57 (0.05)	33.43 (0.35)	45.40 (0.79)	39.90	0.60	33.00
Ti	0.31	43.98 (0.84)	10.15 (0.89)	17854.29 (282)	6364.29 (54.42)	44.00	9.90	16722.00
V	0.021	39.00 (0.00)	5.33 (0.10)	344.93 (5.66)	356.53 (5.75)	38.80	5.50	308.00
Cr	0.11	35.93 (1.55)	188.00 (2.50)	287.73 (4.76)	395.77 (8.01)	36.40	201.00	293.00
Mn	0.0098	37.97 (0.17)	541.08 (6.34)	1251.29 (15.27)	1299.43 (19.85)	38.70	574.00	1317.00
Co	0.0047	35.00 (0.24)	111.38 (1.60)	45.70 (0.70)	54.74 (0.80)	35.50	116.00	44.00
Ni	0.011	38.84 (0.88)	2713.77 (44.52)	124.18 (2.20)	182.93 (4.06)	38.80	2643.00	116.00
Cu	0.033	36.99 (0.27)	0.44 (0.04)	83.18 (1.78)	80.20 (1.11)	37.80	0.96	127.00
Zn	0.23	38.00 (0.00)	58.25 (1.43)	121.26 (3.46)	86.98 (2.44)	39.10	37.00	102.00
Rb	0.011	31.42 (0.22)	—	9.10 (0.18)	0.20 (0.01)	31.40	—	9.20
Sr	0.0084	78.43 (0.74)	—	407.86 (5.58)	111.11 (1.57)	78.40	—	396.00
Y	0.00061	38.05 (0.47)	—	23.02 (0.38)	13.66 (0.29)	38.30	—	26.00
Zr	0.029	38.01 (0.18)	0.09 (0.01)	158.58 (1.77)	13.18 (0.34)	37.90	0.12	170.00
Nb	0.00075	39.98 (0.25)	0.48 (0.145)	17.82 (0.13)	0.51 (0.02)	38.90	0.39	18.30
Cs	0.00053	42.05 (0.17)	—	0.10 (0.01)	0.01 (0.01)	42.70	—	0.10
Ba	0.048	39.70 (0.56)	—	134.96 (2.78)	6.59 (0.19)	39.30	—	131.00
La	0.00017	35.81 (0.08)	—	15.21 (0.21)	0.59 (0.02)	36.00	—	15.20
Ce	0.00059	38.74 (0.32)	—	37.88 (0.68)	1.93 (0.05)	38.40	—	37.60
Pr	0.00049	37.23 (0.16)	—	5.11 (0.16)	0.37 (0.00)	37.90	—	5.35
Nd	0.0029	35.90 (0.13)	—	24.81 (0.51)	2.46 (0.09)	35.50	—	24.50
Sm	0.0033	38.07 (0.32)	—	6.13 (0.15)	1.11 (0.05)	37.70	—	6.10
Eu	0.00096	35.01 (0.14)	—	2.00 (0.02)	0.50 (0.01)	35.60	—	2.07
Gd	0.0032	36.74 (0.35)	—	5.76 (0.11)	1.70 (0.07)	37.30	—	6.16

Table S1. Continued.

Limit of detection	Reference Material				Reference material preferred values (PV)				
	NIST612 (run)	355OL (run)	BHVO-2G (run)	BIR-1G (run)	NIST612 (GeoRem 5211)	355OL (Bussweiller et al., 2019)	BHVO-2G (GeoRem 492)	BIR-1G (GeoRem 492)	
Tb	0.00047	36.02 (0.20)	–	0.82 (0.01)	0.32 (0.01)	37.60	–	0.92	0.35
Dy	0.002	36.00 (0.30)	–	5.04 (0.03)	2.47 (0.08)	35.50	–	5.28	2.55
Ho	0.00051	38.00 (0.28)	–	0.94 (0.02)	0.53 (0.01)	38.30	–	0.98	0.56
Er	0.0015	38.00 (0.00)	–	2.40 (0.05)	1.58 (0.04)	38.00	–	2.56	1.70
Tm	0.00052	37.967 (0.31)	–	0.31 (0.01)	0.24 (0.01)	36.80	–	0.34	0.24
Yb	0.0025	39.21 (0.32)	–	1.93 (0.06)	1.60 (0.03)	39.20	–	2.01	1.64
Lu	0.00041	36.88 (0.27)	–	0.26 (0.01)	0.23 (0.01)	37.00	–	0.28	0.25
Hf	0.0014	35.01 (0.19)	0.01 (0.00)	4.05 (0.09)	0.53 (0.03)	36.70	–	4.32	0.57
Ta	0.00052	40.00 (0.20)	0.03 (0.01)	1.12 (0.02)	0.03 (0.00)	37.60	–	1.15	0.03
Pb	0.012	38.57 (0.27)	0.02 (0.01)	1.86 (0.05)	3.66 (0.11)	38.57	–	1.70	3.70
Th	0.00038	37.77 (0.24)	–	1.19 (0.02)	0.03 (0.00)	37.79	–	1.22	0.03
U	0.00043	37.42 (0.26)	–	0.44 (0.01)	0.02 (0.00)	37.38	–	0.40	0.02

Table S2. Major elements of each analyzed olivines from the Catalão xenoliths.

Rock type	sp-lherz															
Sample	1A-76A															
Point	39	40	41	42	47	48	57	58	69	70	73	74	87	88	152	153
Info	ol_1_c	ol_1_r	ol_2_c	ol_2_r	ol_3_c	ol_3_r	ol_4_c	ol_4_r	ol_5_c	ol_5_r	ol_6_c	ol_6_r	ol_7_c	ol_7_r	ol_7_c	ol_7_r
SiO₂	40,67	40,76	40,28	40,49	40,26	40,15	40,92	40,41	40,90	41,04	40,22	40,52	40,60	40,28	40,45	40,23
TiO₂	0,00	0,00	0,01	0,02	0,00	0,00	0,00	0,00	0,03	0,11	0,00	0,02	0,05	0,10	0,06	0,00
Al₂O₃	0,00	0,00	0,00	0,00	0,00	0,00	0,00	0,00	0,01	0,00	0,00	0,00	0,00	0,00	0,01	0,00
Cr₂O₃	0,01	0,00	0,05	0,00	0,06	0,03	0,04	0,00	0,00	0,06	0,10	0,03	0,01	0,00	0,05	0,03
FeOt	9,84	9,92	9,71	9,90	9,79	9,77	9,48	9,67	9,59	9,45	9,37	9,63	9,80	9,80	9,41	9,56
MnO	0,21	0,15	0,00	0,11	0,10	0,18	0,16	0,11	0,12	0,25	0,13	0,06	0,10	0,15	0,08	0,14
MgO	49,48	49,59	49,66	49,78	49,41	49,31	49,28	49,03	49,62	49,50	48,93	48,84	48,74	48,91	48,56	48,57
P₂O₅	n.a.	n.a.														
NiO	0,34	0,32	0,31	0,44	0,45	0,40	0,36	0,35	0,39	0,26	0,30	0,38	0,44	0,35	0,38	0,33
CaO	0,00	0,02	0,01	0,00	0,00	0,00	0,00	0,00	0,00	0,03	0,01	0,02	0,05	0,02	0,00	0,02
BaO	0,00	0,00	0,02	0,02	0,00	0,00	0,02	0,00	0,09	0,03	0,13	0,00	0,00	0,02	0,00	0,00
Na₂O	0,00	0,09	0,05	0,00	0,01	0,09	0,03	0,03	0,00	0,02	0,00	0,01	0,03	0,06	0,00	0,05
K₂O	0,00	0,01	0,01	0,00	0,00	0,04	0,03	0,00	0,01	0,00	0,00	0,00	0,02	0,00	0,01	0,03
F	n.a.	n.a.														
Cl	0,00	0,07	0,05	0,00	0,00	0,14	0,02	0,01	0,02	0,00	0,01	0,04	0,11	0,02	0,01	0,01
V	0,01	0,00	0,01	0,01	0,00	0,00	0,04	0,01	0,02	0,03	0,01	0,00	0,00	0,00	0,06	0,04
Total	100,55	100,93	100,17	100,79	100,08	100,12	100,44	99,60	100,79	100,82	99,25	99,58	100,02	99,71	99,07	99,00
Fo	89,77	89,77	90,12	89,86	89,90	89,82	90,11	89,93	90,11	90,09	90,18	89,99	89,76	89,75	90,12	89,93
Fa	10,02	10,08	9,88	10,02	10,00	9,99	9,73	9,96	9,77	9,65	9,69	9,95	10,13	10,09	9,80	9,93
Tp	0,21	0,15	0,00	0,11	0,10	0,19	0,16	0,11	0,12	0,25	0,13	0,06	0,11	0,16	0,09	0,15
Mg#	89,96	89,91	90,12	89,96	89,99	89,99	90,26	90,03	90,22	90,32	90,30	90,04	89,86	89,89	90,19	90,06

Table S2. Continued.

Rock type	sp-lherz	sp-lherz	sp-lherz	sp-lherz	sp-lherz	sp-lherz
Sample	1A-76A	1A-76A	1A-76A	1A-76A	1A-76A	1A-76A
Point	154	155	158	159	160	161
Info	ol_8_c	ol_8_r	ol_9_c	ol_9_r	ol_10_c	ol_10_r
SiO₂	40,01	40,94	40,53	40,74	40,71	40,70
TiO₂	0,00	0,10	0,00	0,05	0,13	0,00
Al₂O₃	0,00	0,00	0,01	0,00	0,01	0,00
Cr₂O₃	0,02	0,04	0,00	0,00	0,01	0,00
FeOt	9,51	9,54	9,92	9,65	10,00	9,79
MnO	0,23	0,06	0,08	0,07	0,17	0,11
MgO	48,66	48,33	48,95	49,40	49,22	48,43
P₂O₅	n.a.	n.a.	n.a.	n.a.	n.a.	n.a.
NiO	0,38	0,28	0,37	0,35	0,43	0,38
CaO	0,04	0,04	0,04	0,00	0,00	0,01
BaO	0,02	0,00	0,01	0,00	0,00	0,08
Na₂O	0,00	0,00	0,03	0,03	0,02	0,07
K₂O	0,03	0,00	0,00	0,00	0,00	0,01
F	n.a.	n.a.	n.a.	n.a.	n.a.	n.a.
Cl	0,00	0,00	0,02	0,01	0,00	0,08
V	0,00	0,01	0,00	0,01	0,04	0,02
Total	98,92	99,33	99,97	100,31	100,83	99,71
Fo	89,90	89,98	89,71	90,05	89,61	89,71
Fa	9,86	9,96	10,20	9,87	10,22	10,18
Tp	0,24	0,06	0,08	0,08	0,18	0,11
Mg#	90,12	90,03	89,79	90,12	89,77	89,81

Table S2. Continued.

Rock type	sp-lherz															
Sample	1A-76B															
Point	124	125	126	127	132	133	152	153	182	183	192	193	204	205	208	209
Info	ol_1_c	ol_1_r	ol_2_c	ol_2_r	ol_3_c	ol_3_r	ol_4_r	ol_4_c	ol_5_r	ol_5_c	ol_6_r	ol_6_c	ol_7_r	ol_7_c	ol_8_r	ol_8_c
SiO₂	39,98	40,04	39,73	39,97	39,96	39,90	39,96	39,39	39,42	39,38	39,52	39,43	39,50	39,41	39,34	39,50
TiO₂	0,06	0,00	0,00	0,04	0,00	0,00	0,09	0,00	0,00	0,02	0,17	0,00	0,00	0,02	0,00	0,00
Al₂O₃	0,00	0,00	0,00	0,00	0,00	0,00	0,00	0,01	0,01	0,00	0,00	0,00	0,00	0,00	0,00	0,00
Cr₂O₃	0,00	0,00	0,00	0,00	0,00	0,00	0,00	0,00	0,00	0,00	0,04	0,00	0,03	0,00	0,01	0,00
FeOt	10,07	9,80	9,91	9,90	9,83	9,88	9,90	9,81	9,56	9,78	9,77	9,96	9,94	9,98	10,15	10,16
MnO	0,14	0,15	0,12	0,26	0,16	0,14	0,17	0,13	0,08	0,14	0,26	0,12	0,08	0,24	0,05	0,17
MgO	49,89	49,47	49,15	49,21	49,49	49,62	49,27	49,47	49,16	49,38	49,27	49,36	49,94	49,78	49,18	49,78
P₂O₅	n.a.	n.a.														
NiO	0,40	0,32	0,42	0,32	0,29	0,37	0,33	0,36	0,38	0,34	0,29	0,31	0,37	0,45	0,43	0,37
CaO	0,01	0,00	0,00	0,00	0,02	0,00	0,02	0,00	0,03	0,03	0,00	0,00	0,00	0,00	0,03	0,00
BaO	0,00	0,10	0,03	0,00	0,05	0,00	0,00	0,04	0,08	0,00	0,00	0,04	0,06	0,01	0,06	0,06
Na₂O	0,00	0,01	0,00	0,03	0,00	0,03	0,04	0,09	0,02	0,10	0,00	0,03	0,00	0,02	0,03	0,03
K₂O	0,02	0,00	0,01	0,00	0,00	0,00	0,03	0,01	0,02	0,01	0,03	0,00	0,03	0,00	0,00	0,03
F	n.a.	n.a.														
Cl	0,00	0,00	0,01	0,02	0,01	0,00	0,09	0,05	0,01	0,11	0,02	0,00	0,01	0,01	0,02	0,00
V	0,03	0,00	0,00	0,05	0,02	0,00	0,04	0,00	0,00	0,00	0,03	0,00	0,00	0,00	0,00	0,06
Total	100,60	99,95	99,38	99,81	99,85	99,94	99,92	99,34	98,76	99,36	99,41	99,27	100,01	99,97	99,29	100,15
Fo	89,69	89,87	89,73	89,61	89,82	89,82	89,71	89,87	90,09	89,87	89,74	89,72	89,88	89,67	89,58	89,57
Fa	10,16	9,98	10,15	10,12	10,01	10,04	10,12	10,00	9,83	9,98	9,99	10,16	10,04	10,09	10,37	10,26
Tp	0,15	0,15	0,12	0,27	0,17	0,14	0,18	0,13	0,09	0,14	0,27	0,12	0,08	0,24	0,05	0,18
Mg#	89,82	90,00	89,84	89,86	89,97	89,95	89,86	89,99	90,16	90,00	89,99	89,83	89,95	89,89	89,62	89,73

Table S2. Continued.

Rock type	sp-lherz															
Sample	1A-76C															
Point	7	8	13	14	21	22	55	56	57	58	59	60	63	64	65	66
Info	ol_1_c	ol_1_r	ol_2_c	ol_2_r	ol_3_c	ol_3_r	ol_4_c	ol_4_r	ol_5_c	ol_5_r	ol_6_c	ol_6_r	ol_7_c	ol_7_r	ol_8_c	ol_8_r
SiO₂	40,85	40,76	40,59	40,61	40,27	40,09	40,27	40,46	40,96	40,38	40,81	40,61	40,59	40,52	40,70	40,97
TiO₂	0,07	0,09	0,05	0,00	0,09	0,00	0,00	0,00	0,00	0,10	0,00	0,00	0,00	0,06	0,09	
Al₂O₃	0,00	0,00	0,00	0,00	0,01	0,00	0,03	0,00	0,00	0,01	0,02	0,00	0,00	0,00	0,00	0,00
Cr₂O₃	0,00	0,02	0,00	0,07	0,00	0,06	0,07	0,00	0,04	0,04	0,00	0,01	0,02	0,11	0,00	0,05
FeOt	10,06	10,10	10,06	10,07	10,23	10,15	10,16	10,07	9,85	9,83	10,04	10,19	10,39	10,17	9,93	10,01
MnO	0,15	0,10	0,13	0,10	0,25	0,26	0,14	0,10	0,14	0,00	0,15	0,10	0,05	0,07	0,13	0,08
MgO	49,22	49,30	49,21	49,37	49,24	49,51	48,43	48,73	49,08	48,94	49,45	49,49	48,95	48,76	48,61	48,84
P₂O₅	n.a.	n.a.														
NiO	0,28	0,39	0,29	0,36	0,47	0,39	0,36	0,28	0,39	0,42	0,30	0,43	0,34	0,33	0,48	0,45
CaO	0,03	0,00	0,00	0,00	0,03	0,00	0,00	0,00	0,01	0,04	0,00	0,02	0,00	0,01	0,00	0,02
BaO	n.a.	n.a.														
Na₂O	0,01	0,00	0,02	0,00	0,00	0,01	0,01	0,00	0,02	0,01	0,00	0,00	0,01	0,00	0,00	0,00
K₂O	0,03	0,00	0,04	0,02	0,00	0,00	0,01	0,03	0,01	0,01	0,02	0,01	0,00	0,01	0,04	0,00
F	n.a.	n.a.														
Cl	0,00	0,00	0,00	0,00	0,00	0,01	0,02	0,00	0,00	0,00	0,00	0,01	0,00	0,00	0,00	0,00
V	0,00	0,00	0,00	0,03	0,01	0,01	0,02	0,00	0,02	0,01	0,00	0,00	0,00	0,00	0,00	0,01
Total	100,72	100,75	100,39	100,61	100,60	100,52	99,50	99,69	100,56	99,80	100,79	100,86	100,43	100,05	99,95	100,52
Fo	89,58	89,60	89,59	89,64	89,33	89,45	89,34	89,51	89,75	89,87	89,63	89,55	89,31	89,45	89,59	89,61
Fa	10,27	10,30	10,28	10,26	10,42	10,29	10,52	10,38	10,11	10,13	10,21	10,34	10,64	10,47	10,27	10,31
Tp	0,15	0,10	0,13	0,11	0,25	0,27	0,14	0,11	0,14	0,00	0,16	0,10	0,05	0,08	0,14	0,09
Mg#	89,71	89,69	89,71	89,73	89,56	89,68	89,47	89,61	89,88	89,87	89,78	89,65	89,36	89,52	89,71	89,69

Table S2. Continued.

Rock type	sp-lherz	sp-lherz	sp-lherz	sp-lherz
Sample	1A-76C	1A-76C	1A-76C	1A-76C
Point	69	70	71	72
Info	ol_9_c	ol_9_r	ol_10_c	ol_10_r
SiO₂	40,51	40,31	40,36	40,26
TiO₂	0,00	0,02	0,00	0,03
Al₂O₃	0,02	0,01	0,00	0,01
Cr₂O₃	0,06	0,00	0,00	0,00
FeOt	10,40	9,97	9,81	9,96
MnO	0,16	0,13	0,09	0,02
MgO	48,44	48,39	48,84	48,33
P₂O₅	n.a.	n.a.	n.a.	n.a.
NiO	0,40	0,38	0,42	0,34
CaO	0,02	0,01	0,00	0,00
BaO	n.a.	n.a.	n.a.	n.a.
Na₂O	0,02	0,00	0,02	0,01
K₂O	0,00	0,00	0,01	0,04
F	n.a.	n.a.	n.a.	n.a.
Cl	0,00	0,00	0,00	0,00
V	0,02	0,00	0,00	0,00
Total	100,11	99,22	99,54	99,00
Fo	89,10	89,51	89,79	89,62
Fa	10,73	10,35	10,12	10,36
Tp	0,17	0,14	0,09	0,03
Mg#	89,25	89,64	89,87	89,64

Table S2. Continued.

Rock type	harz	harz																		
Sample	1A-81	1A-81																		
Point	1	2	3	4	15	16	23	24	45	46	47	48	49	50	57	58	59	60	63	64
Info	ol_1_c	ol_1_r	ol_2_c	ol_2_r	Ol_3_c	ol_3_r	ol_4_c	ol_4_r	ol_5_c	ol_5_r	ol_6_c	ol_6_r	ol_7_c	ol_7_r	ol_8_c	ol_8_r	ol_9_c	ol_9_r	ol_10_c	ol_10_r
SiO₂	40,82	40,55	41,30	41,17	41,35	41,24	41,48	41,31	41,28	41,21	41,37	41,44	41,33	41,10	41,06	40,93	41,09	40,60	40,81	41,12
TiO₂	0,04	0,00	0,06	0,09	0,00	0,00	0,00	0,06	0,08	0,00	0,00	0,08	0,00	0,05	0,02	0,03	0,00	0,03	0,06	0,18
Al₂O₃	0,03	0,00	0,02	0,00	0,00	0,01	0,01	0,00	0,00	0,00	0,00	0,00	0,01	0,00	0,02	0,00	0,00	0,00	0,00	0,02
Cr₂O₃	0,00	0,00	0,00	0,03	0,02	0,00	0,00	0,10	0,01	0,04	0,04	0,04	0,17	0,00	0,00	0,00	0,06	0,06	0,06	0,00
FeOt	7,96	8,09	8,21	8,14	8,10	8,04	8,25	8,24	8,15	8,04	8,25	7,98	8,05	8,07	8,39	8,35	8,30	8,10	8,24	8,18
MnO	0,11	0,23	0,02	0,05	0,12	0,02	0,21	0,09	0,08	0,09	0,00	0,12	0,04	0,04	0,07	0,16	0,17	0,16	0,16	0,08
MgO	50,69	50,55	50,72	50,68	50,15	50,14	50,49	50,38	50,71	50,69	50,54	50,52	50,78	50,89	50,66	50,23	50,19	50,30	50,55	50,83
P₂O₅	0,00	0,00	0,02	0,00	0,00	0,00	0,03	0,00	0,00	0,02	0,00	0,00	0,00	0,00	0,04	0,00	0,00	0,00	0,00	0,02
NiO	0,41	0,30	0,44	0,39	0,37	0,41	0,38	0,38	0,42	0,41	0,36	0,40	0,42	0,48	0,45	0,34	0,37	0,31	0,44	0,34
CaO	0,01	0,02	0,01	0,00	0,00	0,02	0,02	0,00	0,01	0,02	0,00	0,02	0,02	0,00	0,00	0,00	0,00	0,00	0,01	0,00
BaO	n.a.	n.a.																		
Na₂O	0,03	0,02	0,03	0,01	0,06	0,00	0,00	0,01	0,00	0,03	0,00	0,00	0,00	0,01	0,01	0,01	0,03	0,00	0,01	0,04
K₂O	0,02	0,01	0,00	0,00	0,03	0,02	0,00	0,02	0,00	0,01	0,02	0,01	0,02	0,00	0,00	0,01	0,02	0,01	0,01	0,00
F	n.a.	n.a.																		
Cl	0,00	0,01	0,00	0,00	0,00	0,01	0,00	0,01	0,00	0,03	0,01	0,00	0,00	0,02	0,00	0,00	0,00	0,01	0,00	0,00
V	0,00	0,00	0,00	0,03	0,00	0,00	0,02	0,00	0,00	0,06	0,00	0,03	0,00	0,00	0,00	0,05	0,00	0,04	0,05	0,05
Total	100,10	99,78	100,84	100,59	100,19	99,90	100,89	100,59	100,74	100,63	100,58	100,63	100,85	100,64	100,72	100,07	100,27	99,59	100,38	100,86
Fo	91,80	91,54	91,65	91,69	91,58	91,73	91,40	91,51	91,65	91,74	91,61	91,75	91,79	91,80	91,43	91,32	91,35	91,56	91,47	91,65
Fa	8,09	8,22	8,33	8,27	8,30	8,25	8,38	8,39	8,27	8,17	8,39	8,13	8,17	8,17	8,50	8,52	8,48	8,27	8,37	8,28
Tp	0,11	0,23	0,02	0,05	0,12	0,02	0,21	0,10	0,08	0,09	0,00	0,12	0,04	0,04	0,07	0,16	0,17	0,17	0,16	0,08
Mg#	91,90	91,76	91,67	91,73	91,69	91,74	91,60	91,60	91,72	91,82	91,61	91,86	91,83	91,83	91,49	91,46	91,51	91,71	91,62	91,72

Table S2. Continued.

Rock type	sp-lherz													
Sample	1A-81A													
Point	170	177	178	204	205	232	233	234	235	240	241	252	253	254
Info	ol_4_c	ol_5_r	ol_6_c	ol_7_c	ol_7_r	ol_8_c	ol_8_r	ol_9_c	ol_9_r	ol_10_c	ol_10_r	ol_11_c	ol_11_r	ol_12_c
SiO₂	40,82	40,19	40,27	40,51	40,47	40,20	40,29	40,76	40,13	40,65	40,19	40,25	40,68	40,58
TiO₂	0,06	0,00	0,04	0,08	0,12	0,09	0,00	0,00	0,00	0,05	0,00	0,23	0,00	0,06
Al₂O₃	0,00	0,00	0,01	0,00	0,00	0,00	0,02	0,00	0,01	0,00	0,00	0,00	0,00	0,00
Cr₂O₃	0,00	0,02	0,05	0,00	0,01	0,15	0,06	0,00	0,05	0,00	0,02	0,00	0,02	0,00
FeOt	10,02	9,68	9,91	9,82	10,00	9,82	9,65	9,98	9,96	9,98	9,90	9,64	9,50	9,43
MnO	0,14	0,21	0,00	0,12	0,13	0,19	0,10	0,15	0,16	0,07	0,20	0,27	0,17	0,08
MgO	49,34	49,45	49,51	49,21	49,32	49,52	49,34	49,21	48,82	48,99	49,10	48,75	49,00	48,99
P₂O₅	0,00	0,03	0,00	0,00	0,00	0,01	0,00	0,01	0,00	0,06	0,00	0,02	0,00	0,00
NiO	0,35	0,39	0,35	0,36	0,37	0,42	0,34	0,42	0,39	0,38	0,31	0,36	0,40	0,40
CaO	0,02	0,01	0,00	0,00	0,00	0,00	0,00	0,00	0,02	0,01	0,03	0,02	0,00	0,00
BaO	0,00	0,07	0,00	0,00	0,00	0,00	0,05	0,06	0,05	0,01	0,00	0,00	0,00	0,03
Na₂O	0,00	0,03	0,00	0,01	0,03	0,05	0,01	0,03	0,03	0,04	0,00	0,00	0,00	0,01
K₂O	0,01	0,01	0,00	0,01	0,01	0,03	0,02	0,00	0,02	0,01	0,01	0,04	0,00	0,00
F	n.a.													
Cl	0,02	0,01	0,02	0,00	0,03	0,01	0,00	0,00	0,02	0,07	0,00	0,02	0,00	0,01
V	0,00	0,00	0,04	0,04	0,02	0,00	0,00	0,00	0,03	0,01	0,02	0,00	0,00	0,00
Total	100,79	100,10	100,18	100,17	100,51	100,48	99,87	100,63	99,66	100,32	99,77	99,58	99,78	99,59
Fo	89,64	89,91	89,90	89,82	89,66	89,81	90,02	89,64	89,58	89,68	89,65	89,76	90,03	90,18
Fa	10,22	9,88	10,10	10,05	10,20	10,00	9,88	10,21	10,25	10,25	10,14	9,96	9,79	9,74
Tp	0,14	0,22	0,00	0,13	0,14	0,19	0,10	0,15	0,17	0,07	0,20	0,28	0,17	0,08
Mg#	89,77	90,10	89,90	89,93	89,78	89,98	90,11	89,78	89,73	89,74	89,84	90,01	90,19	90,25

Table S2. Continued.

Rock type	sp-lherz														
Sample	1A-81B														
Point	3	4	7	8	9	10	15	16	17	18	19	20	43	44	49
Info	ol_1_c	ol_1_r	ol_2_c	ol_2_r	ol_3_c	ol_3_r	ol_4_c	ol_4_r	ol_5_c	ol_5_r	ol_6_c	ol_6_r	ol_7_c	ol_7_r	ol_8_c
SiO₂	40,13	40,15	40,30	40,18	40,22	40,34	40,31	40,08	40,80	39,97	39,63	40,56	40,32	40,08	39,92
TiO₂	0,03	0,01	0,00	0,00	0,00	0,00	0,01	0,07	0,14	0,00	0,00	0,00	0,03	0,06	0,06
Al₂O₃	0,00	0,01	0,02	0,00	0,00	0,04	0,02	0,01	0,01	0,00	0,03	0,00	0,00	0,00	0,00
Cr₂O₃	0,01	0,00	0,07	0,00	0,00	0,00	0,05	0,09	0,05	0,00	0,06	0,00	0,00	0,00	0,00
FeOt	9,74	9,85	9,51	9,55	9,77	9,72	9,80	9,81	9,80	9,99	9,82	9,59	9,66	9,53	9,96
MnO	0,10	0,10	0,16	0,04	0,15	0,24	0,17	0,07	0,05	0,08	0,16	0,13	0,23	0,13	0,14
MgO	49,02	49,38	49,13	49,42	49,58	49,47	49,76	49,18	49,35	49,56	49,70	49,67	49,97	49,92	49,40
P₂O₅	0,00	0,00	0,00	0,05	0,00	0,01	0,01	0,03	0,02	0,00	0,00	0,00	0,00	0,00	0,00
NiO	0,39	0,37	0,38	0,40	0,35	0,41	0,42	0,32	0,38	0,31	0,35	0,39	0,41	0,34	0,34
CaO	0,01	0,02	0,01	0,02	0,00	0,00	0,01	0,00	0,00	0,00	0,00	0,00	0,01	0,01	0,02
BaO	0,07	0,01	0,00	0,00	0,07	0,06	0,01	0,00	0,00	0,00	0,00	0,05	0,08	0,00	0,07
Na₂O	0,04	0,02	0,02	0,00	0,00	0,04	0,03	0,02	0,02	0,00	0,02	0,00	0,00	0,00	0,00
K₂O	0,01	0,00	0,03	0,01	0,00	0,00	0,00	0,01	0,04	0,03	0,02	0,01	0,02	0,00	0,03
F	n.a.														
Cl	0,00	0,00	0,01	0,00	0,00	0,00	0,02	0,01	0,00	0,01	0,00	0,01	0,01	0,00	0,00
V	0,00	0,00	0,00	0,02	0,00	0,03	0,00	0,00	0,03	0,00	0,02	0,01	0,03	0,02	0,02
Total	99,55	99,91	99,63	99,69	100,14	100,36	100,60	99,68	100,69	99,95	99,81	100,44	100,78	100,09	99,97
Fo	89,88	89,85	90,05	90,17	89,90	89,84	89,89	89,87	89,92	89,77	89,87	90,10	90,00	90,21	89,71
Fa	10,02	10,05	9,78	9,78	9,94	9,91	9,93	10,06	10,02	10,15	9,96	9,76	9,76	9,66	10,15
Tp	0,10	0,10	0,17	0,05	0,16	0,25	0,17	0,07	0,05	0,08	0,16	0,14	0,24	0,13	0,15
Mg#	89,97	89,94	90,20	90,22	90,04	90,07	90,05	89,94	89,97	89,84	90,02	90,22	90,21	90,32	89,84

Table S2. Continued.

Rock type	sp-lherz						
Sample	1A-81B						
Point	50	57	58	61	62	85	86
Info	ol_8_r	ol_9_c	ol_9_r	ol_10_c	ol_10_r	ol_11_c	ol_11_r
SiO₂	40,40	40,59	40,64	40,34	40,52	39,64	39,70
TiO₂	0,00	0,11	0,07	0,02	0,00	0,00	0,00
Al₂O₃	0,00	0,00	0,00	0,00	0,00	0,03	0,00
Cr₂O₃	0,03	0,00	0,05	0,00	0,00	0,04	0,00
FeOt	9,83	9,91	10,07	10,00	10,04	9,97	9,94
MnO	0,15	0,07	0,10	0,13	0,16	0,19	0,25
MgO	49,86	49,63	49,35	49,53	49,31	49,60	49,67
P₂O₅	0,02	0,00	0,02	0,00	0,04	0,01	0,00
NiO	0,36	0,38	0,36	0,46	0,44	0,33	0,36
CaO	0,00	0,01	0,00	0,03	0,00	0,00	0,00
BaO	0,00	0,00	0,07	0,04	0,00	0,02	0,00
Na₂O	0,00	0,00	0,01	0,02	0,01	0,09	0,03
K₂O	0,00	0,00	0,02	0,00	0,01	0,01	0,02
F	n.a.						
Cl	0,00	0,01	0,00	0,02	0,01	0,04	0,01
V	0,00	0,00	0,04	0,04	0,05	0,00	0,00
Total	100,66	100,71	100,78	100,63	100,59	99,95	99,98
Fo	89,89	89,86	89,63	89,70	89,60	89,69	89,67
Fa	9,95	10,07	10,27	10,17	10,23	10,11	10,07
Tp	0,16	0,07	0,10	0,13	0,17	0,19	0,26
Mg#	90,03	89,93	89,72	89,82	89,75	89,87	89,90

Table S2. Continued.

Rock type	sp-lherz															
Sample	1A-81C															
Point	76	106	114	115	116	135	138	139	142	143	164	165	174	175	188	
Info	ol_1_r	ol_4_r	ol_5_c	ol_5_r	ol_6_c	ol_7_r	ol_8_c	ol_8_r	ol_9_c	ol_9_r	ol_10_c	ol_10_r	ol_11_c	ol_11_r	ol_12_c	ol_12_r
SiO₂	40,84	40,24	40,79	40,10	40,42	40,35	40,67	40,71	40,33	40,83	40,55	40,65	40,73	40,86	40,87	40,60
TiO₂	0,00	0,00	0,00	0,04	0,04	0,00	0,00	0,00	0,08	0,00	0,17	0,03	0,04	0,03	0,00	0,04
Al₂O₃	0,00	0,00	0,01	0,03	0,00	0,00	0,00	0,00	0,01	0,00	0,00	0,00	0,00	0,00	0,00	0,00
Cr₂O₃	0,00	0,00	0,03	0,00	0,07	0,00	0,05	0,11	0,05	0,00	0,05	0,05	0,09	0,04	0,02	0,07
FeOt	9,94	9,95	10,03	9,90	10,04	9,74	9,69	9,76	9,74	9,81	9,84	9,97	9,89	9,92	9,90	9,81
MnO	0,14	0,11	0,10	0,12	0,05	0,17	0,07	0,15	0,05	0,22	0,14	0,14	0,03	0,00	0,06	0,17
MgO	49,32	49,24	48,81	48,63	48,69	49,45	48,84	49,04	48,19	48,66	48,94	48,86	48,68	48,88	49,05	48,91
P₂O₅	n.a.	n.a.														
NiO	0,33	0,39	0,35	0,35	0,41	0,31	0,36	0,40	0,38	0,43	0,42	0,35	0,31	0,37	0,41	0,37
CaO	0,03	0,00	0,00	0,01	0,02	0,00	0,01	0,02	0,00	0,00	0,00	0,01	0,02	0,00	0,02	0,04
BaO	n.a.	n.a.														
Na₂O	0,03	0,01	0,04	0,02	0,01	0,02	0,02	0,03	0,02	0,03	0,00	0,01	0,01	0,00	0,02	0,01
K₂O	0,03	0,00	0,01	0,00	0,01	0,00	0,03	0,00	0,00	0,00	0,03	0,01	0,00	0,00	0,03	0,01
F	n.a.	n.a.														
Cl	0,01	0,01	0,02	0,00	0,04	0,00	0,02	0,01	0,00	0,00	0,00	0,00	0,02	0,00	0,00	0,00
V	0,03	0,02	0,00	0,05	0,03	0,01	0,00	0,00	0,00	0,01	0,05	0,01	0,02	0,00	0,00	0,03
Total	100,68	99,96	100,16	99,25	99,83	100,03	99,75	100,24	98,85	99,98	100,19	100,09	99,83	100,09	100,37	100,06
Fo	89,71	89,72	89,57	89,64	89,58	89,89	89,92	89,81	89,77	89,63	89,73	89,60	89,73	89,78	89,77	89,72
Fa	10,14	10,17	10,32	10,24	10,36	9,93	10,01	10,03	10,18	10,14	10,13	10,26	10,23	10,22	10,16	10,10
Tp	0,14	0,11	0,11	0,12	0,05	0,18	0,07	0,15	0,05	0,23	0,15	0,14	0,03	0,00	0,06	0,18
Mg#	89,84	89,82	89,66	89,75	89,63	90,05	89,98	89,95	89,81	89,83	89,86	89,73	89,76	89,78	89,83	89,88

Table S2. Continued.

Rock type	grt-wehr													
Sample	1B-139A													
Point	6	7	20	21	22	23	26	27	28	29	36	37	38	39
Info	ol_4_c	ol_4_r	ol_5_c	ol_5_r	ol_6_c	ol_6_r	ol_7_c	ol_7_r	ol_8_c	ol_8_r	ol_9_c	ol_9_r	ol_10_c	ol_10_r
SiO₂	40,13	40,23	40,44	40,41	40,21	40,41	40,76	40,47	40,51	40,43	40,43	40,07	40,10	40,55
TiO₂	0,00	0,00	0,15	0,12	0,05	0,16	0,05	0,04	0,00	0,16	0,12	0,09	0,14	0,00
Al₂O₃	0,02	0,00	0,02	0,02	0,00	0,01	0,03	0,01	0,01	0,00	0,00	0,02	0,03	0,00
Cr₂O₃	0,05	0,00	0,00	0,00	0,02	0,11	0,04	0,00	0,06	0,01	0,00	0,13	0,00	0,05
FeOt	8,91	8,84	8,51	8,63	8,46	8,53	8,61	8,68	8,87	8,73	8,76	8,67	8,80	8,51
MnO	0,10	0,10	0,11	0,14	0,06	0,07	0,19	0,11	0,04	0,14	0,17	0,06	0,11	0,05
MgO	50,58	50,50	50,33	50,45	50,18	50,15	50,03	50,06	49,94	50,02	49,42	49,62	49,72	49,62
P₂O₅	n.a.													
NiO	0,34	0,45	0,49	0,43	0,35	0,41	0,42	0,33	0,35	0,38	0,35	0,41	0,40	0,36
CaO	0,06	0,03	0,05	0,05	0,06	0,01	0,06	0,04	0,03	0,05	0,08	0,06	0,05	0,06
BaO	n.a.													
Na₂O	0,01	0,04	0,00	0,00	0,04	0,01	0,03	0,00	0,09	0,09	0,00	0,05	0,05	0,03
K₂O	0,01	0,00	0,01	0,01	0,00	0,01	0,00	0,01	0,01	0,02	0,01	0,02	0,01	0,03
F	n.a.													
Cl	0,01	0,00	0,00	0,01	0,00	0,00	0,00	0,03	0,00	0,02	0,01	0,00	0,02	0,00
V	0,04	0,00	0,04	0,05	0,01	0,02	0,00	0,00	0,00	0,02	0,00	0,01	0,00	0,02
Total	100,25	100,18	100,13	100,30	99,46	99,90	100,21	99,77	99,90	100,06	99,35	99,23	99,43	99,29
Fo	90,91	90,97	91,23	91,11	91,30	91,22	91,01	91,03	90,90	90,95	90,79	91,01	90,86	91,17
Fa	8,99	8,93	8,65	8,74	8,64	8,70	8,79	8,86	9,06	8,90	9,03	8,93	9,02	8,78
Tp	0,10	0,10	0,11	0,14	0,07	0,08	0,19	0,12	0,04	0,14	0,18	0,06	0,12	0,05
Mg#	91,00	91,06	91,34	91,24	91,36	91,29	91,19	91,13	90,94	91,08	90,95	91,07	90,97	91,22

Table S2. Continued.

Rock type	grt-wehr											
Sample	1B-139A											
Point	40	41	46	47	56	57	108	109	110	111	112	113
Info	ol_11_c	ol_11_r	ol_12_c	ol_12_r	ol_13_c	ol_13_r	ol_1_c	ol_1_r	ol_2_c	ol_2_r	ol_3_c	ol_3_r
SiO₂	40,23	40,58	40,23	40,35	40,35	40,73	41,11	41,24	41,34	41,23	41,04	41,13
TiO₂	0,03	0,00	0,00	0,09	0,04	0,08	0,07	0,00	0,00	0,00	0,05	0,00
Al₂O₃	0,02	0,01	0,04	0,02	0,00	0,02	0,02	0,02	0,03	0,05	0,05	0,05
Cr₂O₃	0,12	0,00	0,00	0,00	0,15	0,00	0,00	0,01	0,00	0,03	0,14	0,14
FeOt	8,67	8,74	8,50	8,92	8,78	8,88	8,57	8,81	8,67	8,69	8,71	8,74
MnO	0,20	0,00	0,12	0,13	0,15	0,16	0,16	0,17	0,15	0,06	0,07	0,07
MgO	49,63	49,86	49,39	49,47	50,06	49,92	50,10	50,18	49,93	50,06	50,21	50,15
P₂O₅	n.a.	n.a.										
NiO	0,40	0,42	0,28	0,40	0,41	0,31	0,34	0,37	0,51	0,37	0,37	0,36
CaO	0,05	0,04	0,03	0,04	0,05	0,04	0,11	0,04	0,05	0,05	0,05	0,04
BaO	n.a.	n.a.										
Na₂O	0,00	0,05	0,09	0,05	0,03	0,06	0,01	0,03	0,02	0,05	0,02	0,02
K₂O	0,00	0,03	0,20	0,01	0,01	0,00	0,00	0,00	0,02	0,00	0,02	0,00
F	n.a.	n.a.										
Cl	0,01	0,00	0,14	0,01	0,00	0,01	0,00	0,00	0,00	0,01	0,00	0,01
V	0,00	0,00	0,05	0,00	0,03	0,02	0,04	0,00	0,00	0,00	0,02	0,02
Total	99,37	99,72	99,08	99,49	100,04	100,22	100,53	100,86	100,70	100,59	100,75	100,72
Fo	90,88	91,05	91,08	90,69	90,90	90,78	91,09	90,87	90,98	91,07	91,06	91,02
Fa	8,91	8,95	8,79	9,17	8,95	9,06	8,74	8,95	8,87	8,87	8,87	8,90
Tp	0,21	0,00	0,13	0,14	0,15	0,17	0,17	0,17	0,15	0,06	0,07	0,08
Mg#	91,07	91,05	91,19	90,81	91,04	90,93	91,24	91,03	91,12	91,13	91,09	

Table S2. Continued.

Rock type	grt-wehr												
Sample	1B-139B												
Point	41	42	43	44	47	48	49	50	51	52	57	58	66
Info	ol_1_c	ol_1_r	ol_2_c	ol_2_r	ol_3_c	ol_3_r	ol_4_c	ol_4_r	ol_5_c	ol_5_r	ol_6_c	ol_6_r	ol_7_c
SiO₂	41,15	41,08	40,28	40,56	40,80	40,44	40,64	40,98	40,80	40,65	41,04	40,87	41,03
TiO₂	0,01	0,00	0,08	0,12	0,00	0,08	0,09	0,15	0,01	0,05	0,04	0,14	0,02
Al₂O₃	0,00	0,01	0,04	0,00	0,04	0,02	0,00	0,00	0,02	0,01	0,00	0,00	0,00
Cr₂O₃	0,00	0,01	0,04	0,00	0,01	0,00	0,00	0,00	0,00	0,00	0,08	0,00	0,00
FeOt	8,60	8,78	8,46	8,72	8,45	8,60	8,77	8,60	8,81	8,57	8,42	8,69	8,84
MnO	0,16	0,12	0,12	0,11	0,20	0,09	0,14	0,12	0,13	0,16	0,09	0,15	0,02
MgO	50,34	50,42	50,11	50,29	49,54	49,26	49,35	49,61	49,80	49,57	50,02	50,10	50,23
P₂O₅	n.a.												
NiO	0,38	0,36	0,38	0,37	0,32	0,34	0,35	0,38	0,39	0,30	0,39	0,32	0,32
CaO	0,03	0,06	0,06	0,05	0,03	0,04	0,05	0,05	0,06	0,01	0,05	0,05	0,09
BaO	n.a.												
Na₂O	0,01	0,02	0,01	0,03	0,02	0,00	0,02	0,00	0,00	0,03	0,06	0,02	0,04
K₂O	0,02	0,02	0,00	0,02	0,03	0,00	0,02	0,01	0,01	0,01	0,01	0,00	0,00
F	n.a.												
Cl	0,00	0,01	0,01	0,01	0,00	0,01	0,00	0,00	0,00	0,00	0,00	0,03	0,00
V	0,03	0,02	0,02	0,00	0,07	0,05	0,01	0,02	0,04	0,00	0,00	0,04	0,02
Total	100,72	100,90	99,62	100,25	99,50	98,93	99,44	99,90	100,05	99,34	100,20	100,42	100,62
Fo	91,11	90,99	91,23	91,03	91,08	90,99	90,79	91,02	90,85	91,00	91,28	90,98	90,99
Fa	8,73	8,89	8,65	8,86	8,71	8,91	9,06	8,85	9,02	8,83	8,62	8,86	8,99
Tp	0,16	0,12	0,13	0,11	0,21	0,09	0,15	0,13	0,13	0,17	0,09	0,16	0,02
Mg#	91,25	91,10	91,34	91,13	91,27	91,08	90,93	91,14	90,96	91,16	91,37	91,13	91,01

Table S2. Continued.

Rock type	grt-wehr						
Sample	1B-139B						
Point	67	97	98	115	116	134	135
Info	ol_7_r	ol_8_c	ol_8_r	ol_9_c	ol_9_r	ol_10_c	ol_10_r
SiO₂	40,81	40,67	40,94	40,84	40,79	40,82	40,95
TiO₂	0,00	0,00	0,00	0,00	0,00	0,00	0,04
Al₂O₃	0,02	0,03	0,00	0,04	0,03	0,00	0,03
Cr₂O₃	0,09	0,00	0,07	0,05	0,08	0,00	0,01
FeOt	8,67	8,82	9,06	8,95	8,78	8,75	8,52
MnO	0,11	0,11	0,01	0,05	0,11	0,03	0,21
MgO	50,10	49,86	49,65	49,57	49,64	49,38	49,44
P₂O₅	n.a.						
NiO	0,32	0,39	0,37	0,36	0,40	0,31	0,36
CaO	0,03	0,06	0,05	0,08	0,04	0,01	0,03
BaO	n.a.						
Na₂O	0,06	0,00	0,05	0,05	0,01	0,02	0,05
K₂O	0,01	0,00	0,04	0,00	0,00	0,01	0,00
F	n.a.						
Cl	0,00	0,00	0,00	0,00	0,00	0,01	0,00
V	0,00	0,03	0,00	0,00	0,01	0,03	0,03
Total	100,21	99,97	100,25	99,98	99,87	99,37	99,67
Fo	91,04	90,86	90,70	90,76	90,87	90,93	90,98
Fa	8,84	9,02	9,28	9,19	9,02	9,04	8,80
Tp	0,12	0,11	0,01	0,05	0,11	0,03	0,21
Mg#	91,15	90,97	90,71	90,80	90,97	90,96	91,18

Table S3. Major elements of each analyzed orthopyroxenes from the Catalão xenoliths.

Rock type	sp-lherz															
Sample	1A-76A															
Point	5	6	7	8	9	10	15	16	19	20	21	22	23	24	33	34
Info	opx_1_c	opx_1_r	opx_2_c1	opx_2_c2	opx_2_r1	opx_2_r2	opx_3_c	opx_3_r	opx_4_c	opx_4_r	opx_5_c	opx_5_r	opx_6_c	opx_6_r	opx_7_c	opx_7_r
SiO₂	55,46	55,40	55,48	55,60	55,14	55,53	55,28	54,85	55,20	55,08	55,24	55,15	55,57	55,35	55,07	54,95
TiO₂	0,14	0,11	0,00	0,06	0,09	0,00	0,01	0,05	0,06	0,13	0,01	0,10	0,10	0,06	0,18	0,08
Al₂O₃	4,27	3,91	4,85	4,63	4,73	4,25	4,41	4,74	4,75	4,74	4,45	4,56	4,63	4,32	4,81	4,48
Cr₂O₃	0,39	0,38	0,60	0,41	0,58	0,35	0,36	0,49	0,47	0,43	0,32	0,46	0,26	0,24	0,40	0,51
FeOt	6,50	6,55	6,14	6,49	6,24	6,60	6,50	6,50	6,46	6,45	6,70	6,14	6,81	6,53	6,55	6,52
MnO	0,07	0,15	0,12	0,00	0,17	0,10	0,11	0,18	0,10	0,18	0,08	0,14	0,08	0,11	0,00	0,08
MgO	32,85	32,80	32,82	32,73	32,84	33,48	33,35	33,09	33,04	32,91	33,37	33,36	32,84	32,87	33,27	33,47
P₂O₅	0,00	0,00	0,04	0,00	0,01	0,00	0,00	0,01	0,00	0,04	0,04	0,01	0,00	0,10	0,00	0,00
NiO	0,11	0,11	0,08	0,07	0,07	0,04	0,03	0,13	0,06	0,07	0,08	0,07	0,08	0,10	0,08	0,05
CaO	0,19	0,37	0,48	0,18	0,25	0,46	0,44	0,37	0,42	0,32	0,45	0,54	0,40	0,40	0,26	0,26
BaO	0,03	0,00	0,09	0,02	0,00	0,00	0,09	0,00	0,00	0,00	0,06	0,00	0,10	0,00	0,09	0,05
Na₂O	0,02	0,03	0,07	0,04	0,03	0,04	0,08	0,03	0,03	0,05	0,04	0,11	0,06	0,07	0,02	0,03
K₂O	0,01	0,00	0,01	0,00	0,01	0,01	0,02	0,00	0,01	0,00	0,00	0,01	0,01	0,01	0,01	0,10
F	n.a.															
Cl	0,00	0,00	0,04	0,02	0,01	0,00	0,01	0,01	0,01	0,02	0,00	0,00	0,01	0,01	0,02	0,01
V	0,00	0,05	0,00	0,04	0,01	0,02	0,00	0,02	0,00	0,00	0,00	0,01	0,05	0,00	0,00	0,02
Total	100,03	99,84	100,81	100,28	100,17	100,86	100,67	100,45	100,62	100,41	100,82	100,66	100,98	100,16	100,75	100,59
%En	89,67	89,28	89,65	89,68	89,92	89,26	89,39	89,44	89,38	89,53	89,11	89,70	88,89	89,27	89,61	89,71
%Fs	9,95	10,00	9,41	9,97	9,59	9,87	9,77	9,85	9,80	9,85	10,03	9,26	10,34	9,94	9,89	9,80
%Wo	0,37	0,72	0,94	0,35	0,50	0,88	0,84	0,71	0,82	0,62	0,86	1,05	0,77	0,79	0,50	0,50
Mg#	0,90	0,90	0,90	0,90	0,90	0,90	0,90	0,90	0,90	0,90	0,91	0,90	0,90	0,90	0,90	0,90

Table S3. Continued.

Rock type	sp-lherz	sp-lherz	sp-lherz	sp-lherz	sp-lherz	sp-lherz	sp-lherz	sp-lherz						
Sample	1A-76A	1A-76A	1A-76A	1A-76A	1A-76A	1A-76A	1A-76A	1A-76A						
Point	35	36	45	46	53	54	75	76	77	80	81	82	89	90
Info	opx_8_c	opx_8_r	opx_9_c	opx_9_r	opx_10_c	opx_10_r	opx_11_c1	opx_11_c2	opx_11_r1	opx_11_r2	opx_12_c	opx_12_r	opx_13_c	opx_13_r
SiO₂	55,79	55,68	55,49	55,55	55,34	55,08	55,30	55,11	55,18	55,84	55,74	55,86	55,43	55,65
TiO₂	0,06	0,09	0,00	0,00	0,18	0,00	0,04	0,00	0,03	0,10	0,12	0,04	0,12	0,11
Al₂O₃	4,18	4,17	3,90	3,87	4,06	4,34	4,23	4,02	4,00	4,34	4,24	3,98	3,91	3,88
Cr₂O₃	0,23	0,44	0,15	0,12	0,34	0,25	0,50	0,45	0,31	0,31	0,40	0,36	0,21	0,24
FeOt	6,79	6,66	6,75	6,60	6,30	6,71	6,24	6,15	6,35	6,38	6,41	6,50	6,39	6,37
MnO	0,11	0,16	0,15	0,16	0,17	0,21	0,08	0,13	0,18	0,05	0,12	0,21	0,11	0,18
MgO	32,94	33,06	33,60	33,43	33,72	32,79	32,94	32,82	32,83	32,93	32,64	32,73	33,06	32,89
P₂O₅	0,01	0,01	0,00	0,00	0,00	0,02	0,00	0,03	0,01	0,00	0,00	0,00	0,00	0,01
NiO	0,07	0,10	0,05	0,06	0,11	0,09	0,14	0,05	0,06	0,07	0,12	0,05	0,00	0,07
CaO	0,28	0,30	0,27	0,51	0,29	0,45	0,26	0,72	0,20	0,29	0,28	0,24	0,50	0,50
BaO	0,00	0,04	0,00	0,00	0,00	0,00	0,00	0,00	0,00	0,05	0,08	0,04	0,00	0,08
Na₂O	0,02	0,07	0,03	0,06	0,04	0,02	0,02	0,02	0,01	0,02	0,02	0,00	0,10	0,06
K₂O	0,01	0,02	0,03	0,00	0,01	0,04	0,02	0,01	0,01	0,01	0,00	0,00	0,01	0,00
F	n.a.	n.a.	n.a.	n.a.	n.a.	n.a.	n.a.	n.a.						
Cl	0,00	0,01	0,00	0,00	0,00	0,00	0,03	0,01	0,04	0,02	0,02	0,01	0,01	0,01
V	0,06	0,04	0,03	0,03	0,06	0,05	0,00	0,05	0,00	0,00	0,00	0,04	0,00	0,00
Total	100,57	100,86	100,44	100,39	100,62	100,06	99,80	99,57	99,21	100,40	100,19	100,06	99,84	100,03
%En	89,16	89,32	89,42	89,14	90,01	88,92	89,94	89,21	89,87	89,68	89,60	89,55	89,34	89,31
%Fs	10,30	10,10	10,07	9,88	9,44	10,21	9,56	9,38	9,74	9,75	9,86	9,98	9,69	9,71
%Wo	0,54	0,58	0,52	0,98	0,55	0,87	0,51	1,41	0,38	0,57	0,54	0,47	0,97	0,98
Mg#	0,90	0,90	0,90	0,90	0,91	0,90	0,90	0,90	0,90	0,90	0,90	0,90	0,90	0,90

Table S3. Continued.

Rock type	sp-lherz												
Sample	1A-76B												
Point	134	135	140	141	142	143	160	161	172	186	187	200	201
Info	opx_1_c	opx_1_r	opx_2_c	opx_2_r	opx_3_c	opx_3_r	opx_5_r	opx_5_c	opx_7_r	opx_8_r	opx_8_c	opx_10_r	opx_10_c
SiO₂	55,02	55,04	55,60	55,59	55,65	55,40	55,67	55,78	55,02	55,03	55,91	55,04	55,26
TiO₂	0,06	0,00	0,05	0,03	0,21	0,00	0,27	0,22	0,06	0,07	0,19	0,05	0,00
Al₂O₃	3,69	3,50	3,66	3,29	3,76	3,44	3,47	3,57	3,69	3,46	3,64	3,48	3,41
Cr₂O₃	0,31	0,27	0,45	0,30	0,32	0,37	0,15	0,25	0,35	0,23	0,36	0,17	0,15
FeOt	6,64	6,89	6,83	6,76	7,02	6,96	6,62	6,27	6,33	6,80	6,58	6,83	6,61
MnO	0,14	0,15	0,10	0,08	0,15	0,15	0,11	0,23	0,10	0,18	0,10	0,14	0,01
MgO	33,44	33,40	33,29	33,49	33,24	33,40	33,13	33,33	33,70	33,12	33,17	33,19	33,23
P₂O₅	0,00	0,03	0,00	0,02	0,00	0,00	0,01	0,07	0,00	0,08	0,00	0,00	0,03
NiO	0,03	0,08	0,08	0,05	0,00	0,08	0,11	0,13	0,06	0,13	0,12	0,07	0,04
CaO	0,41	0,46	0,50	0,15	0,31	0,31	0,33	0,38	0,58	0,09	0,31	0,30	0,49
BaO	0,01	0,05	0,00	0,00	0,00	0,01	0,05	0,05	0,00	0,12	0,03	0,00	0,02
Na₂O	0,06	0,09	0,08	0,08	0,04	0,06	0,02	0,08	0,11	0,03	0,02	0,04	0,03
K₂O	0,00	0,04	0,03	0,00	0,00	0,00	0,00	0,01	0,00	0,03	0,03	0,00	0,00
F	n.a.												
Cl	0,00	0,00	0,01	0,03	0,02	0,03	0,01	0,00	0,01	0,00	0,00	0,00	0,01
V	0,00	0,06	0,00	0,00	0,00	0,02	0,01	0,02	0,06	0,00	0,00	0,07	0,00
Total	99,80	100,06	100,69	99,88	100,71	100,25	99,96	100,38	100,07	99,37	100,47	99,37	99,29
%En	89,27	88,84	88,82	89,57	88,87	88,99	89,34	89,80	89,46	89,52	89,44	89,13	89,11
%Fs	9,94	10,29	10,23	10,14	10,53	10,41	10,02	9,47	9,43	10,30	9,95	10,29	9,94
%Wo	0,79	0,87	0,96	0,30	0,59	0,60	0,64	0,73	1,10	0,18	0,61	0,57	0,95
Mg#	0,90	0,90	0,90	0,90	0,89	0,90	0,90	0,90	0,90	0,90	0,90	0,90	0,90

Table S3. Continued.

Rock type	sp-lherz															
Sample	1A-76C															
Point	1	2	9	10	15	16	17	18	23	24	27	28	33	34	37	38
Info	opx_1_c	opx_1_r	opx_2_c	opx_2_r	opx_3_c	opx_3_r	opx_4_c	opx_4_r	opx_5_c	opx_5_r	opx_6_c	opx_6_r	opx_7_c	opx_7_r	opx_8_c	opx_8_r
SiO₂	54,40	55,21	55,20	55,24	54,19	54,49	54,98	55,18	54,93	54,97	54,71	55,17	55,05	55,14	55,20	55,03
TiO₂	0,00	0,05	0,10	0,18	0,23	0,00	0,22	0,04	0,00	0,26	0,00	0,02	0,01	0,00	0,04	0,23
Al₂O₃	4,49	4,36	4,42	4,32	4,97	4,51	4,28	4,08	4,22	4,17	4,43	4,19	4,44	4,31	4,66	4,51
Cr₂O₃	0,52	0,46	0,22	0,22	0,34	0,43	0,35	0,23	0,49	0,37	0,40	0,35	0,40	0,17	0,45	0,44
FeOt	6,38	6,50	6,37	6,61	6,15	6,62	6,68	6,88	6,41	6,49	6,58	6,89	6,67	6,76	6,67	6,94
MnO	0,09	0,13	0,11	0,10	0,24	0,16	0,11	0,19	0,20	0,04	0,07	0,12	0,29	0,07	0,24	0,15
MgO	32,25	32,90	32,32	32,80	33,18	33,16	32,95	33,04	32,93	33,01	32,95	32,81	33,10	33,33	33,00	32,94
P₂O₅	0,00	0,00	0,03	0,06	0,00	0,02	0,03	0,00	0,00	0,02	0,00	0,01	0,02	0,06	0,00	0,03
NiO	0,06	0,09	0,09	0,09	0,09	0,11	0,13	0,12	0,14	0,12	0,12	0,05	0,08	0,06	0,11	0,09
CaO	0,93	0,33	0,66	0,12	0,41	0,48	0,30	0,38	0,38	0,39	0,56	0,36	0,27	0,38	0,30	0,25
BaO	n.a.															
Na₂O	0,08	0,03	0,11	0,00	0,21	0,05	0,02	0,04	0,07	0,04	0,05	0,05	0,02	0,04	0,02	0,03
K₂O	0,05	0,01	0,02	0,00	0,00	0,00	0,00	0,02	0,01	0,01	0,00	0,01	0,00	0,00	0,01	0,01
F	n.a.															
Cl	0,01	0,00	0,02	0,00	0,00	0,01	0,00	0,00	0,00	0,00	0,02	0,00	0,02	0,00	0,00	0,00
V	0,01	0,04	0,04	0,00	0,02	0,03	0,08	0,00	0,04	0,03	0,02	0,03	0,03	0,00	0,05	0,05
Total	99,25	100,10	99,70	99,73	100,04	100,06	100,11	100,18	99,82	99,92	99,88	100,07	100,37	100,34	100,75	100,70
%En	88,37	89,45	88,88	89,63	89,87	89,10	89,27	88,88	89,49	89,38	88,96	88,84	89,38	89,12	89,28	88,99
%Fs	9,81	9,91	9,83	10,13	9,34	9,97	10,15	10,38	9,77	9,86	9,97	10,46	10,10	10,14	10,13	10,52
%Wo	1,82	0,64	1,30	0,24	0,79	0,93	0,58	0,73	0,74	0,76	1,08	0,70	0,52	0,73	0,59	0,49
Mg#	0,90	0,90	0,90	0,90	0,91	0,90	0,90	0,90	0,90	0,90	0,90	0,89	0,90	0,90	0,89	0,89

Table S3. Continued.

Rock type	sp-lherz	sp-lherz	sp-lherz	sp-lherz	sp-lherz	sp-lherz
Sample	1A-76C	1A-76C	1A-76C	1A-76C	1A-76C	1A-76C
Point	43	44	45	46	39	40
Info	opx_9_c	opx_9_r	opx_10_c	opx_10_r	opx_9_c	opx_9_r
SiO₂	54,75	54,81	54,34	54,28	55,02	54,92
TiO₂	0,00	0,21	0,13	0,44	0,04	0,00
Al₂O₃	4,74	4,56	4,96	4,62	4,22	4,58
Cr₂O₃	0,37	0,59	0,36	0,35	0,59	0,34
FeOt	6,58	6,71	6,49	6,19	6,77	6,66
MnO	0,10	0,22	0,08	0,04	0,21	0,20
MgO	32,63	32,92	32,61	32,34	33,03	32,94
P₂O₅	0,00	0,00	0,00	0,01	0,02	0,00
NiO	0,06	0,06	0,04	0,04	0,05	0,03
CaO	0,48	0,28	0,21	0,82	0,26	0,28
BaO	n.a.	n.a.	n.a.	n.a.	n.a.	n.a.
Na₂O	0,05	0,05	0,03	0,21	0,00	0,02
K₂O	0,02	0,01	0,01	0,01	0,01	0,00
F	n.a.	n.a.	n.a.	n.a.	n.a.	n.a.
Cl	0,00	0,00	0,00	0,01	0,00	0,00
V	0,02	0,04	0,01	0,08	0,04	0,03
Total	99,81	100,46	99,27	99,44	100,24	99,99
%En	88,99	89,24	89,58	88,83	89,23	89,32
%Fs	10,07	10,21	10,00	9,54	10,26	10,13
%Wo	0,94	0,55	0,42	1,63	0,50	0,55
Mg#	0,90	0,90	0,90	0,90	0,90	0,90

Table S3. Continued.

Rock type	harz	harz															
Sample	1A-81																
Point	5	6	7	8	9	10	11	12	17	18	19	20	22	29	30	35	
Info	opx_1_c	opx_1_r	opx_2_c	opx_2_r	opx_3_c	opx_3_r	opx_4_c	opx_4_r	opx_5_c	opx_5_r	opx_6_c	opx_6_r	opx_7_r	opx_8_c	opx_8_r	opx_9_c	
SiO₂	55,59	55,30	55,72	55,96	55,63	55,37	56,12	55,92	55,41	55,39	56,06	56,09	55,87	55,89	56,16	55,93	
TiO₂	0,05	0,00	0,00	0,00	0,00	0,20	0,04	0,00	0,00	0,17	0,00	0,23	0,12	0,03	0,24	0,07	
Al₂O₃	3,92	3,78	3,74	3,76	3,61	3,49	3,96	3,00	3,83	3,83	3,22	3,13	3,46	3,83	3,09	3,83	
Cr₂O₃	0,76	0,58	0,52	0,72	0,83	0,60	0,77	0,47	0,59	0,51	0,63	0,61	0,48	0,68	0,43	0,64	
FeOt	5,21	5,30	5,15	5,26	5,62	5,66	5,24	5,43	5,38	5,43	5,79	5,49	5,08	5,41	5,54	5,51	
MnO	0,16	0,11	0,16	0,17	0,19	0,19	0,12	0,00	0,11	0,25	0,16	0,16	0,17	0,17	0,20	0,14	
MgO	33,68	34,01	33,95	34,06	34,27	33,57	34,01	33,83	33,62	34,00	34,14	34,09	33,82	34,08	34,26	33,46	
P₂O₅	0,03	0,02	0,00	0,00	0,00	0,00	0,03	0,00	0,05	0,08	0,00	0,04	0,01	0,07	0,01	0,00	
NiO	0,09	0,12	0,09	0,10	0,09	0,09	0,12	0,02	0,08	0,04	0,05	0,11	0,12	0,07	0,01	0,09	
CaO	0,88	0,83	0,84	0,22	0,26	0,35	0,25	0,93	0,65	0,23	0,22	0,58	0,89	0,29	0,19	0,81	
BaO	n.a.																
Na₂O	0,09	0,08	0,17	0,06	0,02	0,04	0,05	0,06	0,11	0,07	0,04	0,02	0,09	0,03	0,01	0,04	
K₂O	0,01	0,01	0,00	0,00	0,00	0,02	0,01	0,00	0,01	0,01	0,02	0,00	0,03	0,01	0,02	0,00	
F	n.a.																
Cl	0,01	0,02	0,00	0,02	0,00	0,00	0,00	0,00	0,00	0,00	0,00	0,00	0,00	0,00	0,00	0,01	
V	0,00	0,02	0,01	0,00	0,01	0,03	0,00	0,01	0,07	0,05	0,00	0,04	0,00	0,00	0,02	0,01	
Total	100,47	100,17	100,36	100,33	100,54	99,61	100,72	99,65	99,91	100,05	100,33	100,60	100,14	100,55	100,19	100,55	
%En	90,46	90,50	90,67	91,65	91,12	90,75	91,61	90,12	90,62	91,38	90,92	90,69	90,64	91,32	91,34	90,12	
%Fs	7,85	7,91	7,72	7,94	8,38	8,58	7,91	8,11	8,13	8,18	8,65	8,20	7,64	8,13	8,29	8,32	
%Wo	1,70	1,59	1,62	0,42	0,49	0,67	0,47	1,77	1,25	0,44	0,43	1,11	1,72	0,55	0,37	1,56	
Mg#	0,92	0,92	0,92	0,92	0,92	0,91	0,92	0,92	0,92	0,91	0,92	0,92	0,92	0,92	0,92	0,92	

Table S3. Continued.

Rock type	harz	harz	harz	harz	harz	harz
Sample	1A-81	1A-81	1A-81	1A-81	1A-81	1A-81
Point	36	41	42	43	44	61
Info	opx_9_r	opx_10_c	opx_10_r	opx_11_c	opx_11_r	opx_12_c
SiO₂	56,02	55,18	55,55	56,11	56,27	56,02
TiO₂	0,03	0,00	0,12	0,01	0,00	0,08
Al₂O₃	3,80	3,89	3,35	3,46	3,36	2,95
Cr₂O₃	0,48	0,60	0,76	0,61	0,43	0,57
FeOt	5,53	5,28	5,39	5,40	5,49	5,58
MnO	0,18	0,01	0,16	0,18	0,17	0,08
MgO	34,59	33,86	33,97	34,28	34,34	33,93
P₂O₅	0,00	0,00	0,00	0,01	0,00	0,00
NiO	0,05	0,10	0,11	0,09	0,11	0,06
CaO	0,20	0,38	0,24	0,53	0,31	0,15
BaO	n.a.	n.a.	n.a.	n.a.	n.a.	n.a.
Na₂O	0,00	0,04	0,03	0,07	0,00	0,00
K₂O	0,00	0,01	0,02	0,01	0,02	0,01
F	n.a.	n.a.	n.a.	n.a.	n.a.	n.a.
Cl	0,00	0,02	0,00	0,00	0,01	0,00
V	0,00	0,02	0,01	0,03	0,04	0,02
Total	100,88	99,39	99,70	100,81	100,54	99,44
%En	91,42	91,28	91,41	90,95	91,22	91,29
%Fs	8,19	7,99	8,13	8,04	8,18	8,43
%Wo	0,38	0,73	0,46	1,01	0,60	0,28
Mg#	0,92	0,92	0,92	0,92	0,92	0,92

Table S3. Continued.

Rock type	sp-lherz															
Sample	1A-81A															
Point	182	183	186	187	188	189	194	195	202	203	244	245	246	247	248	249
Info	opx_1_c	opx_1_r	opx_2_c	opx_2_r	opx_3_c	opx_3_r	opx_4_c	opx_4_r	opx_5_c	opx_5_r	opx_6_c	opx_6_r	opx_7_c	opx_7_r	opx_8_c	opx_8_r
SiO₂	55,69	55,54	55,70	55,65	55,43	55,52	55,34	55,37	55,68	55,51	55,46	55,56	55,40	55,47	55,12	55,12
TiO₂	0,13	0,14	0,00	0,09	0,09	0,10	0,08	0,11	0,00	0,02	0,19	0,08	0,00	0,21	0,15	0,06
Al₂O₃	4,49	4,31	4,33	4,31	4,04	3,96	4,18	3,96	3,92	3,97	3,67	3,85	4,29	4,26	4,38	3,79
Cr₂O₃	0,45	0,23	0,37	0,40	0,27	0,28	0,28	0,16	0,34	0,19	0,43	0,29	0,21	0,30	0,38	0,31
FeOt	6,04	6,25	6,28	6,29	6,70	6,60	6,60	6,91	6,28	6,51	6,72	6,63	6,41	6,41	6,55	6,69
MnO	0,21	0,09	0,12	0,16	0,23	0,22	0,18	0,32	0,19	0,13	0,20	0,01	0,19	0,19	0,05	0,23
MgO	32,96	32,93	33,65	33,23	33,26	33,38	33,61	33,34	33,20	33,47	33,54	33,70	33,39	33,44	33,43	33,16
P₂O₅	0,03	0,03	0,00	0,00	0,05	0,05	0,01	0,00	0,01	0,04	0,03	0,02	0,00	0,00	0,00	0,00
NiO	0,06	0,05	0,06	0,07	0,01	0,07	0,03	0,13	0,00	0,00	0,10	0,06	0,04	0,06	0,11	0,09
CaO	0,54	0,49	0,40	0,48	0,30	0,44	0,41	0,17	0,77	0,62	0,19	0,45	0,62	0,25	0,23	0,28
BaO	0,00	0,12	0,00	0,01	0,05	0,01	0,05	0,04	0,00	0,00	0,00	0,03	0,00	0,00	0,00	0,03
Na₂O	0,11	0,09	0,04	0,05	0,01	0,02	0,05	0,00	0,08	0,05	0,01	0,05	0,13	0,08	0,04	0,00
K₂O	0,03	0,00	0,00	0,03	0,00	0,01	0,01	0,03	0,02	0,01	0,00	0,01	0,02	0,00	0,02	0,04
F	n.a.															
Cl	0,01	0,00	0,02	0,01	0,01	0,02	0,02	0,01	0,02	0,01	0,00	0,00	0,00	0,02	0,03	0,01
V	0,06	0,00	0,01	0,02	0,02	0,01	0,04	0,06	0,00	0,06	0,00	0,01	0,00	0,04	0,00	0,00
Total	100,78	100,27	100,97	100,78	100,48	100,66	100,87	100,62	100,51	100,57	100,54	100,76	100,70	100,72	100,47	99,81
%En	89,72	89,50	89,83	89,56	89,33	89,26	89,37	89,29	89,07	89,09	89,57	89,29	89,20	89,85	89,69	89,35
%Fs	9,22	9,53	9,41	9,50	10,10	9,90	9,84	10,38	9,46	9,72	10,07	9,86	9,61	9,66	9,86	10,11
%Wo	1,06	0,96	0,76	0,93	0,57	0,84	0,79	0,33	1,47	1,19	0,36	0,86	1,19	0,49	0,45	0,54
Mg#	0,91	0,90	0,91	0,90	0,90	0,90	0,90	0,90	0,90	0,90	0,90	0,90	0,90	0,90	0,90	0,90

Table S3. Continued.

Rock type	sp-lherz							
Sample	1A-81A							
Point	263	264	267	268	269	270	277	278
Info	opx_9_c	opx_9_r	opx_10_c	opx_10_r	opx_11_c	opx_11_r	opx_12_c	opx_12_r
SiO₂	55,56	55,45	55,28	55,31	55,21	55,12	55,70	55,63
TiO₂	0,08	0,09	0,10	0,22	0,05	0,00	0,00	0,02
Al₂O₃	4,37	4,29	3,94	4,08	3,84	4,18	4,20	4,18
Cr₂O₃	0,53	0,47	0,38	0,30	0,18	0,17	0,31	0,24
FeOt	6,21	6,30	6,69	6,73	6,53	6,61	6,52	6,47
MnO	0,08	0,20	0,15	0,09	0,16	0,21	0,20	0,18
MgO	33,19	33,28	33,65	33,67	33,85	33,17	33,25	33,23
P₂O₅	0,00	0,07	0,05	0,00	0,05	0,00	0,01	0,00
NiO	0,12	0,14	0,05	0,11	0,08	0,05	0,09	0,07
CaO	0,36	0,32	0,31	0,39	0,20	0,30	0,52	0,55
BaO	0,13	0,00	0,05	0,00	0,09	0,00	0,00	0,00
Na₂O	0,05	0,04	0,05	0,02	0,00	0,03	0,03	0,08
K₂O	0,01	0,03	0,02	0,00	0,01	0,00	0,00	0,00
F	n.a.							
Cl	0,00	0,00	0,00	0,00	0,00	0,00	0,02	0,00
V	0,00	0,04	0,02	0,02	0,00	0,05	0,06	0,00
Total	100,68	100,72	100,74	100,92	100,23	99,89	100,90	100,65
%En	89,86	89,83	89,44	89,25	89,89	89,43	89,19	89,20
%Fs	9,44	9,54	9,97	10,01	9,73	9,99	9,80	9,75
%Wo	0,70	0,63	0,59	0,74	0,38	0,58	1,00	1,05
Mg#	0,90	0,90	0,90	0,90	0,90	0,90	0,90	0,90

Table S3. Continued.

Rock type	sp-lherz															
Sample	1A-81B															
Point	21	22	25	26	27	28	29	30	31	32	37	38	39	40	63	64
Info	opx_1_c	opx_1_r	opx_2_c	opx_2_r	opx_3_c	opx_3_r	opx_4_c	opx_4_r	opx_5_c	opx_5_r	opx_6_c	opx_6_r	opx_7_c	opx_7_r	opx_8_c	opx_8_r
SiO₂	55,04	54,99	55,03	54,77	54,37	54,56	54,73	55,02	55,12	54,60	55,06	54,92	54,67	54,52	55,51	55,63
TiO₂	0,23	0,00	0,16	0,00	0,03	0,07	0,08	0,07	0,10	0,19	0,38	0,00	0,05	0,00	0,10	0,07
Al₂O₃	4,44	4,35	4,20	4,13	4,50	4,52	4,27	4,06	3,90	3,85	3,47	3,53	3,49	3,69	3,74	3,41
Cr₂O₃	0,53	0,40	0,39	0,29	0,29	0,27	0,25	0,21	0,44	0,30	0,49	0,35	0,41	0,41	0,24	0,26
FeOt	6,01	6,33	6,51	6,08	6,80	6,50	6,59	6,76	6,62	6,54	6,55	6,60	6,33	6,51	6,53	6,72
MnO	0,20	0,15	0,13	0,18	0,19	0,18	0,18	0,23	0,03	0,21	0,04	0,19	0,15	0,14	0,10	0,25
MgO	33,27	33,42	33,53	33,38	33,78	33,90	33,26	33,79	33,25	33,54	33,07	33,49	33,49	33,58	33,26	33,46
P₂O₅	0,04	0,04	0,01	0,00	0,00	0,00	0,00	0,00	0,02	0,01	0,00	0,04	0,03	0,00	0,02	0,00
NiO	0,11	0,05	0,09	0,02	0,08	0,11	0,10	0,07	0,03	0,08	0,08	0,04	0,05	0,11	0,05	0,06
CaO	0,48	0,34	0,41	0,42	0,51	0,54	0,30	0,29	0,55	0,39	0,69	0,41	0,64	0,38	0,59	0,25
BaO	0,06	0,00	0,00	0,02	0,00	0,05	0,00	0,00	0,04	0,00	0,00	0,00	0,11	0,00	0,19	0,00
Na₂O	0,22	0,06	0,01	0,12	0,04	0,07	0,04	0,03	0,03	0,04	0,07	0,05	0,01	0,13	0,02	
K₂O	0,00	0,04	0,01	0,00	0,00	0,02	0,01	0,02	0,01	0,00	0,03	0,02	0,02	0,04	0,03	0,00
F	n.a.															
Cl	0,01	0,04	0,00	0,00	0,00	0,01	0,02	0,01	0,00	0,00	0,00	0,00	0,01	0,00	0,00	0,01
V	0,05	0,04	0,04	0,03	0,02	0,00	0,01	0,01	0,01	0,04	0,06	0,05	0,07	0,04	0,05	0,04
Total	100,68	100,24	100,52	99,42	100,61	100,80	99,82	100,56	100,13	99,79	99,96	99,71	99,56	99,42	100,54	100,17
%En	89,95	89,81	89,47	90,00	88,98	89,36	89,48	89,42	89,00	89,47	88,79	89,33	89,30	89,53	89,06	89,45
%Fs	9,11	9,54	9,74	9,19	10,04	9,61	9,94	10,03	9,94	9,79	9,87	9,88	9,47	9,74	9,81	10,07
%Wo	0,93	0,65	0,79	0,81	0,97	1,03	0,58	0,55	1,07	0,74	1,34	0,79	1,23	0,73	1,13	0,48
Mg#	0,91	0,90	0,90	0,91	0,90	0,90	0,90	0,90	0,90	0,90	0,90	0,90	0,90	0,90	0,90	0,90

Table S3. Continued.

Rock type	sp-lherz							
Sample	1A-81B							
Point	67	68	73	74	75	76	81	82
Info	opx_9_c	opx_9_r	opx_10_c	opx_10_r	opx_11_c	opx_11_r	opx_12_c	opx_12_r
SiO₂	54,79	54,90	54,81	55,13	55,40	55,04	55,06	54,52
TiO₂	0,00	0,05	0,09	0,29	0,00	0,00	0,16	0,00
Al₂O₃	3,41	3,58	3,75	3,87	4,02	3,97	3,72	3,90
Cr₂O₃	0,38	0,27	0,49	0,35	0,31	0,31	0,32	0,18
FeOt	6,66	6,36	6,54	6,07	6,56	6,68	6,36	6,64
MnO	0,15	0,14	0,15	0,12	0,08	0,16	0,24	0,12
MgO	33,26	33,49	33,25	33,15	33,43	33,52	33,46	33,91
P₂O₅	0,02	0,00	0,00	0,00	0,00	0,00	0,00	0,00
NiO	0,10	0,12	0,11	0,06	0,12	0,11	0,04	0,06
CaO	0,45	0,80	0,64	0,54	0,34	0,48	0,91	0,36
BaO	0,00	0,00	0,03	0,00	0,00	0,00	0,08	0,00
Na₂O	0,05	0,09	0,06	0,24	0,02	0,02	0,04	0,04
K₂O	0,00	0,01	0,00	0,01	0,00	0,00	0,01	0,02
F	n.a.							
Cl	0,01	0,01	0,01	0,00	0,00	0,01	0,00	0,00
V	0,00	0,03	0,05	0,06	0,03	0,04	0,05	0,05
Total	99,26	99,85	99,96	99,88	100,31	100,33	100,45	99,80
%En	89,12	89,00	88,97	89,74	89,51	89,12	88,79	89,48
%Fs	10,00	9,47	9,81	9,22	9,85	9,96	9,47	9,83
%Wo	0,87	1,53	1,22	1,05	0,65	0,91	1,74	0,69
Mg#	0,90	0,90	0,90	0,91	0,90	0,90	0,90	0,90

Table S3. Continued.

Rock type	sp-lherz															
Sample	1A-81C															
Point	98	99	151	152	153	154	155	162	163	168	169	170	171	176	177	178
Info	opx_2_c	opx_2_r	opx_3_r	opx_4_c	opx_4_r	opx_5_c	opx_5_r	opx_6_c	opx_6_r	opx_7_c	opx_7_r	opx_8_c	opx_8_r	opx_9_c	opx_9_r	opx_10_c
SiO₂	55,07	54,96	55,47	55,57	55,57	55,06	54,99	55,54	55,40	55,43	55,51	55,54	55,27	55,21	55,19	55,33
TiO₂	0,13	0,00	0,14	0,30	0,03	0,12	0,15	0,09	0,00	0,12	0,00	0,00	0,08	0,11	0,20	0,09
Al₂O₃	4,02	3,85	4,06	4,21	4,01	4,21	4,00	3,87	3,81	4,10	3,96	3,82	4,05	4,13	3,90	4,13
Cr₂O₃	0,20	0,33	0,13	0,44	0,20	0,48	0,33	0,30	0,16	0,13	0,17	0,28	0,27	0,24	0,36	0,44
FeOt	6,74	6,76	6,55	6,37	6,87	6,63	6,71	6,70	6,65	6,53	6,60	6,67	6,59	6,13	6,63	6,45
MnO	0,18	0,17	0,03	0,21	0,13	0,15	0,17	0,15	0,18	0,11	0,11	0,15	0,00	0,16	0,19	0,19
MgO	33,21	33,12	32,81	32,26	32,45	32,82	32,61	32,81	32,71	32,97	33,14	32,95	32,64	33,05	33,13	32,84
P₂O₅	n.a.															
NiO	0,06	0,10	0,09	0,03	0,02	0,05	0,08	0,10	0,05	0,08	0,15	0,08	0,07	0,12	0,08	0,07
CaO	0,49	0,31	0,29	0,34	0,11	0,22	0,39	0,46	0,48	0,39	0,30	0,27	0,37	0,23	0,21	0,36
BaO	n.a.															
Na₂O	0,07	0,02	0,05	0,07	0,04	0,02	0,03	0,02	0,10	0,07	0,03	0,04	0,06	0,04	0,01	0,03
K₂O	0,00	0,00	0,01	0,00	0,00	0,01	0,00	0,00	0,01	0,02	0,01	0,00	0,00	0,01	0,02	0,00
F	n.a.															
Cl	0,00	0,00	0,00	0,02	0,01	0,00	0,00	0,01	0,01	0,00	0,00	0,01	0,02	0,00	0,00	0,01
V	0,00	0,04	0,01	0,06	0,00	0,04	0,06	0,04	0,00	0,02	0,01	0,01	0,04	0,02	0,08	0,00
Total	100,17	99,66	99,63	99,89	99,44	99,80	99,52	100,09	99,56	99,98	99,98	99,81	99,45	99,44	99,98	99,93
%En	88,94	89,20	89,42	89,42	89,19	89,43	88,97	88,92	88,93	89,32	89,44	89,34	89,18	90,17	89,54	89,44
%Fs	10,13	10,21	10,01	9,91	10,59	10,13	10,26	10,19	10,15	9,92	9,99	10,14	10,10	9,38	10,05	9,86
%Wo	0,93	0,59	0,58	0,68	0,22	0,44	0,77	0,89	0,93	0,76	0,57	0,52	0,72	0,45	0,41	0,70
Mg#	0,90	0,90	0,90	0,90	0,89	0,90	0,90	0,90	0,90	0,90	0,90	0,90	0,91	0,90	0,90	0,90

Table S3 .Continued.

Rock type	sp-lherz						
Sample	1A-81C						
Point	179	182	183	184	185	144	145
Info	opx_10_r	opx_11_c	opx_11_r	opx_12_c	opx_12_r	opx_13_c	opx_13_r
SiO₂	55,51	55,50	55,19	55,31	55,47	55,31	55,20
TiO₂	0,00	0,00	0,10	0,01	0,00	0,00	0,00
Al₂O₃	4,02	4,28	4,00	3,85	3,92	4,54	4,28
Cr₂O₃	0,29	0,24	0,21	0,16	0,23	0,25	0,30
FeOt	6,49	6,75	6,53	6,77	6,75	6,08	6,46
MnO	0,16	0,15	0,20	0,15	0,27	0,07	0,11
MgO	33,06	32,90	33,05	32,95	32,73	32,96	32,56
P₂O₅	n.a.						
NiO	0,04	0,04	0,07	0,08	0,05	0,03	0,11
CaO	0,20	0,47	0,40	0,39	0,49	0,59	0,46
BaO	n.a.						
Na₂O	0,08	0,05	0,09	0,02	0,07	0,10	0,04
K₂O	0,00	0,01	0,02	0,01	0,00	0,00	0,04
F	n.a.						
Cl	0,01	0,00	0,00	0,02	0,01	0,04	0,01
V	0,04	0,00	0,04	0,00	0,02	0,03	0,05
Total	99,90	100,39	99,89	99,71	100,01	100,00	99,62
%En	89,74	88,86	89,32	88,98	88,77	89,57	89,17
%Fs	9,88	10,23	9,90	10,26	10,27	9,27	9,93
%Wo	0,38	0,90	0,77	0,76	0,96	1,15	0,90
Mg#	0,90	0,90	0,90	0,90	0,90	0,91	0,90

Table S4. Major elements of each analyzed clinopyroxenes from the Catalão xenoliths.

Rock type	sp-lherz															
Sample	1A-76A															
Point	2	3	11	12	13	14	18	25	26	27	28	29	30	31	32	37
Info	cpx_1_r	cpx_2_c	cpx_3_c	cpx_3_r	cpx_4_c	cpx_4_r	cpx_5_r	cpx_6_c	cpx_6_r	cpx_7_c	cpx_7_r	cpx_8_c	cpx_8_r	cpx_9_c	cpx_9_r	cpx_10_c
SiO₂	52,76	53,19	53,52	53,25	53,59	53,44	53,77	53,10	53,57	52,47	52,62	53,36	52,63	52,57	52,69	53,03
TiO₂	0,22	0,35	0,18	0,22	0,19	0,40	0,59	0,47	0,30	0,22	0,58	0,41	0,42	0,30	0,23	0,37
Al₂O₃	6,15	6,06	6,05	6,12	5,68	5,78	6,09	6,23	5,77	6,54	6,54	5,96	6,00	6,82	6,76	6,30
Cr₂O₃	0,87	0,87	0,72	0,73	0,64	0,74	0,87	0,72	0,92	0,97	0,81	0,61	0,70	0,77	0,70	0,72
FeOt	2,09	1,92	1,80	2,04	1,88	2,11	1,75	1,98	2,14	2,02	1,75	1,82	1,92	2,31	2,05	2,09
MnO	0,13	0,02	0,07	0,07	0,00	0,19	0,06	0,15	0,07	0,12	0,00	0,07	0,05	0,03	0,12	0,12
MgO	14,23	14,30	14,27	14,34	14,52	14,48	15,05	14,44	14,99	14,09	14,16	15,17	14,82	14,73	14,64	14,39
P2O5	0,05	0,02	0,00	0,00	0,02	0,00	0,05	0,05	0,01	0,00	0,01	0,00	0,08	0,01	0,01	0,00
NiO	0,00	0,04	0,00	0,00	0,01	0,05	0,06	0,03	0,11	0,04	0,07	0,07	0,00	0,09	0,02	0,07
CaO	20,25	20,43	20,63	20,54	20,87	20,94	20,56	20,03	19,90	20,34	20,50	20,60	20,43	19,87	20,08	20,96
BaO	0,07	0,08	0,03	0,00	0,00	0,00	0,04	0,00	0,00	0,06	0,00	0,02	0,00	0,00	0,03	0,05
Na₂O	1,64	1,69	1,69	1,25	1,31	1,51	1,24	1,57	1,22	1,77	1,81	1,62	1,68	1,80	1,61	1,08
K₂O	0,01	0,03	0,03	0,00	0,03	0,00	0,01	0,02	0,01	0,10	0,00	0,00	0,00	0,04	0,01	0,00
F	n.a.															
Cl	0,01	0,00	0,00	0,01	0,00	0,04	0,02	0,01	0,01	0,01	0,03	0,01	0,01	0,01	0,03	0,02
V	0,02	0,05	0,09	0,04	0,03	0,01	0,02	0,06	0,01	0,02	0,08	0,04	0,03	0,13	0,00	0,02
Total	98,50	99,05	99,07	98,60	98,77	99,66	100,20	98,86	99,03	98,76	98,96	99,73	98,77	99,48	98,96	99,22
%En	47,51	47,57	47,40	47,41	47,49	47,15	48,85	48,22	49,16	47,22	47,40	48,94	48,47	48,61	48,45	46,99
%Fs	3,91	3,58	3,35	3,78	3,45	3,85	3,19	3,71	3,94	3,80	3,29	3,29	3,52	4,28	3,81	3,83
%Wo	48,58	48,84	49,24	48,80	49,06	49,00	47,96	48,07	46,90	48,98	49,31	47,76	48,01	47,12	47,75	49,18
Mg#	0,92	0,93	0,93	0,93	0,93	0,92	0,94	0,93	0,93	0,93	0,94	0,94	0,93	0,92	0,93	0,92

Table S4. Continued.

Rock type	sp-lherz															
Sample	1A-76A															
Point	38	43	44	49	50	51	52	67	68	72	84	85	86	91	92	93
Info	cpx_10_r	cpx_11_c	cpx_11_r	cpx_12_c	cpx_12_r	cpx_13_c	cpx_13_r	cpx_15_c	cpx_15_r	cpx_16_r	cpx_18_r	cpx_19_c	cpx_19_r	cpx_20_c	cpx_20_r	cpx_21_c
SiO₂	53,21	53,94	53,64	53,20	53,45	53,11	53,43	52,53	52,64	52,30	52,54	52,67	52,66	53,06	52,55	52,26
TiO₂	0,39	0,30	0,26	0,52	0,22	0,35	0,72	0,28	0,26	0,38	0,39	0,44	0,31	0,30	0,33	0,42
Al₂O₃	5,85	5,95	6,07	6,13	5,89	5,85	6,27	6,48	6,54	6,39	6,06	5,90	6,54	6,17	5,77	6,95
Cr₂O₃	0,68	0,79	0,59	0,96	0,74	0,52	0,69	0,58	0,57	0,86	0,66	0,79	0,78	0,74	0,69	0,88
FeOt	1,87	2,13	1,83	2,10	2,08	2,04	2,16	2,05	1,92	2,05	1,98	1,92	2,02	2,04	1,83	2,01
MnO	0,04	0,02	0,02	0,04	0,02	0,03	0,02	0,08	0,02	0,09	0,08	0,10	0,13	0,16	0,19	0,16
MgO	14,55	14,90	14,80	14,72	14,34	14,95	15,05	14,11	14,48	14,28	14,55	14,56	14,22	14,10	14,72	14,33
P2O5	0,00	0,00	0,02	0,01	0,04	0,00	0,03	0,06	0,04	0,00	0,06	0,01	0,00	0,05	0,01	0,02
NiO	0,00	0,01	0,07	0,05	0,08	0,02	0,06	0,08	0,03	0,02	0,04	0,00	0,04	0,04	0,03	0,10
CaO	20,94	19,90	20,39	20,48	20,96	20,75	20,98	20,68	20,70	20,77	20,62	20,74	20,44	20,90	20,88	20,15
BaO	0,01	0,00	0,00	0,00	0,04	0,06	0,00	0,00	0,03	0,00	0,07	0,06	0,10	0,08	0,00	0,00
Na₂O	1,11	1,09	1,62	1,13	1,52	1,57	1,44	1,63	1,33	1,40	1,50	1,25	1,70	1,63	1,46	1,26
K₂O	0,02	0,02	0,00	0,03	0,03	0,01	0,02	0,01	0,01	0,02	0,01	0,01	0,02	0,01	0,01	0,00
F	n.a.															
Cl	0,00	0,03	0,02	0,03	0,01	0,00	0,00	0,03	0,00	0,00	0,01	0,01	0,00	0,00	0,00	0,00
V	0,01	0,03	0,12	0,06	0,07	0,03	0,07	0,02	0,01	0,03	0,01	0,10	0,08	0,03	0,05	0,10
Total	98,68	99,13	99,44	99,45	99,48	99,27	100,95	98,63	98,57	98,58	98,58	98,56	99,07	99,32	98,51	98,62
%En	47,48	49,02	48,56	48,08	46,91	48,22	48,02	46,84	47,58	47,04	47,74	47,67	47,33	46,59	47,87	47,87
%Fs	3,42	3,93	3,37	3,85	3,82	3,69	3,87	3,82	3,54	3,79	3,64	3,53	3,77	3,78	3,34	3,77
%Wo	49,10	47,05	48,07	48,07	49,27	48,09	48,11	49,34	48,88	49,17	48,62	48,80	48,89	49,63	48,79	48,37
Mg#	0,93	0,93	0,94	0,93	0,92	0,93	0,93	0,92	0,93	0,93	0,93	0,93	0,92	0,93	0,93	0,93

Table S4. Continued.

Rock type	sp-lherz																
Sample	1A-76B																
Point	122	123	128	129	130	131	136	137	139	144	145	146	147	150	151	180	181
Info	cpx_1_c	cpx_1_r	cpx_2_c	cpx_2_r	cpx_3_c	cpx_3_r	cpx_4_c	cpx_4_r	cpx_5_r	cpx_6_c	cpx_6_r	cpx_7_c	cpx_7_r	cpx_8_c	cpx_8_r	cpx_13_c	cpx_13_r
SiO₂	53,51	53,62	53,09	53,06	53,16	53,39	53,10	53,35	53,52	53,70	53,30	53,37	53,43	53,75	53,92	53,32	53,38
TiO₂	0,55	0,62	0,21	0,37	0,22	0,26	0,46	0,28	0,22	0,38	0,59	0,43	0,23	0,57	0,31	0,30	0,26
Al₂O₃	6,07	5,92	5,49	5,54	5,86	5,39	5,61	5,69	5,94	5,95	5,45	6,09	6,03	5,96	5,86	6,27	6,31
Cr₂O₃	0,89	0,70	0,54	0,81	0,88	0,72	0,77	0,96	0,67	0,80	0,72	0,79	0,79	0,77	0,56	0,76	0,73
FeOt	2,09	2,17	2,86	2,14	2,13	1,95	2,69	2,19	2,08	2,04	1,89	2,12	2,03	1,99	2,60	2,01	1,97
MnO	0,09	0,03	0,02	0,11	0,21	0,01	0,06	0,00	0,09	0,07	0,12	0,11	0,12	0,22	0,17	0,04	0,05
MgO	14,51	14,15	14,97	14,92	14,35	14,64	14,87	14,29	14,46	14,19	14,01	14,11	14,22	14,12	14,70	14,63	14,88
P2O5	0,00	0,00	0,01	0,00	0,03	0,03	0,08	0,00	0,00	0,01	0,04	0,05	0,04	0,01	0,05	0,00	0,02
NiO	0,01	0,04	0,03	0,08	0,03	0,01	0,03	0,04	0,01	0,00	0,04	0,10	0,06	0,07	0,00	0,01	0,05
CaO	20,94	21,02	21,22	21,92	21,69	21,91	21,15	21,26	21,72	21,42	21,72	21,13	21,51	21,09	21,06	21,37	21,24
BaO	0,06	0,00	0,10	0,02	0,00	0,00	0,06	0,00	0,00	0,00	0,00	0,00	0,02	0,08	0,00	0,00	0,00
Na₂O	1,80	1,71	1,62	1,67	1,66	1,51	1,57	1,68	1,65	1,72	1,44	1,84	1,67	1,61	1,41	1,75	1,86
K₂O	0,00	0,00	0,00	0,01	0,02	0,00	0,00	0,00	0,01	0,00	0,03	0,03	0,01	0,01	0,00	0,01	0,01
F	n.a.																
Cl	0,00	0,00	0,00	0,02	0,00	0,00	0,00	0,02	0,01	0,01	0,01	0,02	0,00	0,04	0,00	0,01	0,01
V	0,09	0,04	0,04	0,10	0,03	0,01	0,06	0,06	0,09	0,05	0,08	0,08	0,03	0,04	0,07	0,03	0,00
Total	100,61	100,01	100,18	100,77	100,25	99,83	100,49	99,82	100,49	100,35	99,44	100,26	100,18	100,27	100,80	100,50	100,78
%En	47,22	46,43	47,04	46,81	46,09	46,50	47,10	46,41	46,30	46,17	45,67	46,29	46,14	46,46	46,98	47,02	47,63
%Fs	3,81	4,00	5,05	3,76	3,84	3,48	4,77	3,99	3,73	3,73	3,46	3,90	3,70	3,68	4,67	3,63	3,54
%Wo	48,96	49,57	47,91	49,42	50,07	50,01	48,12	49,60	49,97	50,10	50,87	49,82	50,16	49,86	48,36	49,35	48,83
Mg#	0,93	0,92	0,90	0,93	0,92	0,93	0,91	0,92	0,93	0,93	0,92	0,93	0,91	0,93	0,93	0,93	0,93

Table S4. Continued.

Rock type	sp-lherz							
Sample	1A-76B							
Point	190	198	199	202	206	214	215	218
Info	cpx_15_c	cpx_17_c	cpx_17_r	cpx_18_c	cpx_19_c	cpx_21_c	cpx_21_r	cpx_22_c
SiO₂	53,04	53,46	53,26	53,44	53,73	53,97	54,02	53,14
TiO₂	0,43	0,32	0,14	0,23	0,31	0,11	0,24	0,41
Al₂O₃	6,04	5,82	5,58	5,83	5,91	6,23	6,12	6,00
Cr₂O₃	0,77	0,82	0,69	0,80	0,76	0,91	0,74	0,65
FeOt	2,09	2,07	2,08	1,91	2,52	2,18	2,19	2,25
MnO	0,28	0,02	0,08	0,16	0,09	0,00	0,07	0,05
MgO	14,44	14,95	14,85	14,84	14,55	14,17	14,09	13,90
P2O5	0,00	0,06	0,05	0,02	0,05	0,01	0,00	0,00
NiO	0,00	0,04	0,12	0,01	0,00	0,00	0,04	0,05
CaO	21,32	21,37	21,46	21,70	21,10	21,42	21,33	21,53
BaO	0,01	0,01	0,00	0,09	0,02	0,05	0,00	0,11
Na₂O	1,86	1,82	1,66	1,18	1,55	1,09	1,50	1,57
K₂O	0,00	0,00	0,00	0,00	0,00	0,07	0,00	0,00
F	n.a.							
Cl	0,02	0,01	0,00	0,01	0,01	0,06	0,03	0,13
V	0,08	0,08	0,04	0,06	0,06	0,08	0,05	0,05
Total	100,39	100,83	100,01	100,29	100,67	100,33	100,42	99,83
%En	46,68	47,51	47,24	47,11	46,75	46,02	45,98	45,38
%Fs	3,79	3,68	3,70	3,40	4,54	3,98	4,00	4,11
%Wo	49,53	48,81	49,05	49,50	48,71	50,00	50,02	50,51
Mg#	0,92	0,93	0,93	0,93	0,91	0,92	0,92	0,92

Table S4. Continued.

Rock type	sp-lherz																
Sample	1A-76C																
Point	3	4	5	6	11	12	19	20	25	26	29	31	32	35	36	41	42
Info	cpx_1_c	cpx_1_r	cpx_2_c	cpx_2_r	cpx_3_c	cpx_3_r	cpx_4_c	cpx_4_r	cpx_5_c	cpx_5_r	cpx_6_c	cpx_7_c	cpx_7_r	cpx_8_c	cpx_8_r	cpx_10_c	cpx_10_r
SiO₂	52,41	53,52	52,14	52,21	52,82	52,70	52,68	52,44	52,40	52,30	52,65	52,69	52,86	52,43	52,53	52,65	52,83
TiO₂	0,33	0,41	0,10	0,19	0,37	0,27	0,12	0,55	0,37	0,37	0,35	0,65	0,31	0,38	0,15	0,40	0,37
Al₂O₃	6,07	5,93	6,92	6,80	5,41	6,86	6,92	6,56	6,35	6,17	6,50	6,52	6,53	6,71	6,46	6,49	6,39
Cr₂O₃	0,81	0,70	0,90	0,99	0,66	0,74	0,78	0,82	0,85	0,98	0,93	0,75	0,91	0,94	0,62	0,92	0,87
FeOt	2,27	1,82	1,99	2,03	1,80	2,01	1,94	1,99	2,01	1,82	2,18	1,99	2,11	2,00	1,93	2,03	2,11
MnO	0,07	0,14	0,01	0,07	0,08	0,00	0,17	0,13	0,14	0,09	0,00	0,04	0,04	0,00	0,13	0,14	0,06
MgO	14,84	14,95	15,04	14,88	15,03	14,95	14,31	14,56	14,37	14,66	14,41	14,46	14,88	14,03	14,30	14,54	14,42
P2O5	0,00	0,04	0,00	0,02	0,00	0,00	0,02	0,00	0,00	0,00	0,00	0,00	0,00	0,06	0,03	0,03	0,03
NiO	0,10	0,00	0,04	0,00	0,00	0,00	0,07	0,08	0,05	0,08	0,08	0,00	0,00	0,05	0,02	0,07	0,02
CaO	21,16	21,27	21,40	21,62	21,61	21,21	21,47	21,56	21,87	21,78	21,32	21,69	21,53	21,98	21,89	21,36	21,42
BaO	n.a.																
Na₂O	1,88	1,87	1,68	1,82	1,88	1,91	1,96	1,97	1,97	1,69	1,95	1,95	1,72	1,93	2,01	1,95	1,76
K₂O	0,03	0,02	0,00	0,03	0,00	0,00	0,04	0,03	0,01	0,01	0,02	0,02	0,00	0,04	0,00	0,03	0,04
F	n.a.																
Cl	0,01	0,00	0,00	0,01	0,00	0,01	0,00	0,00	0,00	0,00	0,00	0,00	0,00	0,02	0,00	0,00	0,00
V	0,05	0,00	0,08	0,01	0,04	0,01	0,09	0,09	0,09	0,05	0,03	0,02	0,00	0,01	0,04	0,10	0,03
Total	100,02	100,66	100,27	100,70	99,69	100,66	100,55	100,79	100,49	100,01	100,41	100,76	100,88	100,50	100,14	100,70	100,34
%En	47,38	47,84	47,69	47,16	47,61	47,74	46,42	46,71	46,04	46,78	46,56	46,41	47,19	45,33	45,96	46,85	46,52
%Fs	4,06	3,27	3,54	3,60	3,19	3,59	3,53	3,57	3,60	3,26	3,95	3,58	3,75	3,63	3,47	3,67	3,82
%Wo	48,56	48,90	48,78	49,24	49,20	48,67	50,05	49,72	50,35	49,96	49,49	50,02	49,07	51,04	50,56	49,48	49,66
Mg#	0,92	0,94	0,93	0,93	0,94	0,93	0,93	0,93	0,93	0,92	0,93	0,93	0,93	0,93	0,93	0,92	

Table S4. Continued.

Rock type	sp-lherz	sp-lherz	sp-lherz	sp-lherz	sp-lherz	sp-lherz
Sample	1A-76C	1A-76C	1A-76C	1A-76C	1A-76C	1A-76C
Point	47	48	61	62	67	68
Info	cpx_11_c	cpx_11_r	cpx_12_c	cpx_12_r	cpx_13_c	cpx_13_r
SiO₂	52,61	52,62	53,25	53,28	52,55	52,41
TiO₂	0,40	0,51	0,41	0,43	0,33	0,46
Al₂O₃	6,48	6,22	5,72	5,53	6,53	6,59
Cr₂O₃	0,81	0,83	0,60	0,63	0,74	0,82
FeOt	1,91	2,04	1,80	1,99	2,16	2,24
MnO	0,12	0,08	0,06	0,06	0,03	0,16
MgO	14,74	14,88	14,31	14,48	14,69	14,36
P2O5	0,00	0,00	0,01	0,02	0,00	0,00
NiO	0,00	0,06	0,00	0,09	0,00	0,05
CaO	21,78	21,62	22,24	22,00	21,21	21,33
BaO	n.a.	n.a.	n.a.	n.a.	n.a.	n.a.
Na₂O	1,81	1,90	1,92	1,68	1,69	1,82
K₂O	0,00	0,00	0,01	0,00	0,00	0,02
F	n.a.	n.a.	n.a.	n.a.	n.a.	n.a.
Cl	0,01	0,00	0,00	0,02	0,00	0,00
V	0,06	0,02	0,10	0,05	0,06	0,07
Total	100,71	100,80	100,44	100,25	99,98	100,34
%En	46,85	47,15	45,73	46,11	47,17	46,41
%Fs	3,40	3,63	3,22	3,56	3,88	4,05
%Wo	49,75	49,21	51,05	50,33	48,94	49,54
Mg#	0,93	0,93	0,93	0,93	0,92	0,92

Table S4. Continued.

Rock type	sp-harz										
Sample	1A-81										
Point	13	14	31	32	33	34	37	39	40	54	56
Info	cpx_1_c	cpx_1_r	cpx_2_c	cpx_2_r	cpx_3_c	cpx_3_r	cpx_4_c	cpx_5_c	cpx_5_r	cpx_7_r	cpx_8_r
SiO₂	54,23	54,32	53,96	53,93	53,80	53,73	53,94	53,51	53,23	53,86	53,97
TiO₂	0,01	0,04	0,25	0,27	0,36	0,00	0,28	0,23	0,20	0,21	0,13
Al₂O₃	1,49	1,35	1,44	1,28	1,82	1,62	1,63	1,19	1,33	1,70	1,55
Cr₂O₃	1,24	1,15	1,52	1,87	1,51	1,34	1,38	1,62	1,47	1,40	1,35
FeOt	1,79	1,57	2,13	1,80	1,87	1,75	2,20	2,08	2,00	2,13	1,86
MnO	0,12	0,06	0,08	0,03	0,07	0,05	0,05	0,12	0,09	0,05	0,05
MgO	17,06	16,95	16,69	16,59	16,98	16,76	16,86	17,60	17,58	17,55	17,30
P2O5	0,00	0,00	0,01	0,00	0,03	0,00	0,01	0,03	0,03	0,00	0,00
NiO	0,02	0,00	0,01	0,04	0,13	0,00	0,03	0,01	0,05	0,07	0,02
CaO	21,91	22,08	22,44	22,82	22,80	22,67	22,31	22,28	22,70	21,77	21,91
BaO	n.a.										
Na₂O	1,83	1,76	1,52	1,13	1,01	1,11	1,88	1,77	1,33	1,58	1,65
K₂O	0,00	0,01	0,00	0,01	0,01	0,00	0,03	0,13	0,06	0,08	0,01
F	n.a.										
Cl	0,00	0,00	0,01	0,01	0,01	0,01	0,03	0,05	0,00	0,01	0,01
V	0,05	0,04	0,04	0,02	0,01	0,02	0,07	0,08	0,06	0,05	0,02
Total	99,76	99,33	100,08	99,79	100,40	99,05	100,70	100,71	100,12	100,44	99,81
%En	50,46	50,29	49,07	48,80	49,35	49,25	49,41	50,61	50,21	51,03	50,74
%Fs	2,98	2,62	3,51	2,97	3,04	2,89	3,62	3,36	3,21	3,48	3,07
%Wo	46,57	47,09	47,43	48,23	47,61	47,87	46,97	46,03	46,58	45,49	46,19
Mg#	0,94	0,95	0,93	0,94	0,94	0,94	0,93	0,94	0,94	0,94	0,94

Table S4. Continued.

Rock type	sp-lherz																
Sample	1A-81A																
Point	172	173	174	185	190	191	192	193	196	197	198	201	230	236	237	238	239
Info	cpx_2_c	cpx_2_r	cpx_3_c	cpx_4_r	cpx_5_c	cpx_5_r	cpx_6_c	cpx_6_r	cpx_7_c	cpx_7_r	cpx_8_c	cpx_9_r	cpx_10_c	cpx_11_c	cpx_11_r	cpx_12_c	cpx_12_r
SiO₂	53,36	53,39	53,79	54,03	53,72	53,60	54,28	54,25	53,18	53,39	53,20	53,39	53,92	54,18	54,31	53,55	53,94
TiO₂	0,19	0,18	0,13	0,37	0,28	0,19	0,14	0,36	0,47	0,37	0,45	0,22	0,41	0,14	0,61	0,27	0,25
Al₂O₃	6,00	6,13	6,54	6,03	6,05	5,84	6,59	6,33	6,33	6,83	6,04	6,38	6,29	6,28	5,90	5,74	5,73
Cr₂O₃	0,59	0,54	0,83	0,83	0,84	0,69	0,89	0,56	0,60	0,94	0,74	0,77	0,65	0,82	0,60	0,87	0,49
FeOt	1,96	2,05	2,04	2,05	2,02	1,82	1,90	1,99	2,03	1,98	1,99	1,93	1,94	2,19	1,92	1,94	1,94
MnO	0,00	0,08	0,05	0,12	0,09	0,09	0,05	0,05	0,03	0,08	0,07	0,05	0,02	0,07	0,05	0,12	0,02
MgO	14,89	14,80	14,72	14,34	14,97	14,74	14,40	14,66	14,78	14,09	14,75	14,03	14,40	14,84	14,67	14,62	14,85
P2O5	0,00	0,00	0,00	0,02	0,00	0,05	0,03	0,01	0,00	0,01	0,00	0,00	0,01	0,03	0,05	0,01	0,00
NiO	0,00	0,06	0,07	0,12	0,05	0,03	0,00	0,00	0,03	0,05	0,02	0,00	0,02	0,05	0,03	0,00	0,05
CaO	21,30	21,45	20,73	20,62	20,43	20,64	21,11	21,25	20,43	20,75	20,77	20,39	20,96	20,62	20,75	20,81	20,98
BaO	0,00	0,00	0,00	0,00	0,05	0,01	0,00	0,03	0,06	0,00	0,00	0,00	0,02	0,00	0,00	0,00	0,00
Na₂O	1,58	1,54	1,61	1,27	1,60	1,72	1,43	1,32	1,30	1,73	1,29	1,51	1,67	1,14	1,31	1,45	1,39
K₂O	0,02	0,00	0,02	0,00	0,00	0,00	0,02	0,02	0,01	0,03	0,02	0,03	0,00	0,00	0,02	0,00	0,01
F	n.a.																
Cl	0,00	0,02	0,00	0,00	0,00	0,02	0,02	0,02	0,00	0,03	0,00	0,00	0,05	0,01	0,01	0,00	0,04
V	0,06	0,06	0,04	0,09	0,04	0,05	0,04	0,08	0,08	0,00	0,00	0,05	0,00	0,07	0,06	0,04	0,10
Total	99,94	100,30	100,56	99,87	100,13	99,47	100,88	100,92	99,33	100,26	99,32	98,75	100,34	100,47	100,27	99,42	99,80
%En	47,57	47,20	47,86	47,32	48,64	48,18	47,01	47,21	48,31	46,79	47,90	47,14	47,14	48,05	47,85	47,67	47,88
%Fs	3,52	3,66	3,72	3,80	3,67	3,33	3,48	3,60	3,71	3,68	3,63	3,63	3,56	3,97	3,51	3,55	3,51
%Wo	48,91	49,14	48,43	48,89	47,69	48,49	49,51	49,19	47,97	49,53	48,47	49,23	49,30	47,98	48,64	48,78	48,61
Mg#	0,93	0,93	0,93	0,93	0,93	0,94	0,93	0,93	0,93	0,93	0,93	0,93	0,92	0,93	0,93	0,93	0,93

Table S4. Continued.

Rock type	sp-lherz	sp-lherz	sp-lherz	sp-lherz	sp-lherz	sp-lherz	sp-lherz	sp-lherz	sp-lherz	sp-lherz	sp-lherz	sp-lherz	sp-lherz	sp-lherz
Sample	1A-81A	1A-81A	1A-81A	1A-81A	1A-81A	1A-81A	1A-81A	1A-81A	1A-81A	1A-81A	1A-81A	1A-81A	1A-81A	1A-81A
Point	242	243	250	251	256	257	258	259	265	266	272	273	275	276
Info	cpx_13_c	cpx_13_r	cpx_14_c	cpx_14_r	cpx_15_c	cpx_15_rl	cpx_15_r2	cpx_16_c	cpx_17_c	cpx_17_r	cpx_18_r	cpx_19_c	cpx_20_c	cpx_20_r
SiO₂	53,71	53,56	53,57	54,13	54,19	53,57	53,51	53,67	54,00	54,05	53,77	53,74	54,02	54,28
TiO₂	0,42	0,45	0,18	0,19	0,37	0,63	0,24	0,35	0,26	0,21	0,13	0,22	0,25	0,30
Al₂O₃	6,22	6,06	6,85	6,34	6,14	6,46	6,28	6,62	6,26	6,16	5,96	6,54	6,21	6,15
Cr₂O₃	0,66	0,59	0,89	0,85	0,77	0,71	0,60	0,81	0,81	0,86	0,65	0,74	0,92	0,58
FeOt	1,90	1,81	2,13	2,18	1,98	1,79	2,02	2,03	1,85	2,03	1,73	1,71	1,77	1,69
MnO	0,11	0,24	0,06	0,05	0,12	0,08	0,04	0,04	0,04	0,10	0,09	0,11	0,10	0,03
MgO	14,92	14,59	14,76	14,79	14,66	14,18	14,27	14,03	14,70	14,78	14,97	14,93	14,76	14,61
P2O5	0,03	0,00	0,04	0,03	0,00	0,00	0,01	0,00	0,02	0,00	0,07	0,02	0,05	0,00
NiO	0,00	0,02	0,03	0,06	0,00	0,00	0,01	0,04	0,02	0,03	0,05	0,00	0,02	0,04
CaO	20,62	21,37	20,54	20,68	20,79	21,17	21,02	21,03	20,91	20,81	21,11	20,88	20,95	21,11
BaO	0,12	0,00	0,07	0,00	0,09	0,00	0,00	0,00	0,00	0,00	0,09	0,01	0,00	
Na₂O	1,43	1,48	1,75	1,48	1,47	1,75	1,74	1,70	1,77	1,68	1,60	1,83	1,65	1,65
K₂O	0,04	0,05	0,02	0,01	0,00	0,00	0,00	0,00	0,00	0,02	0,02	0,00	0,01	0,00
F	n.a.	n.a.	n.a.	n.a.	n.a.	n.a.	n.a.	n.a.	n.a.	n.a.	n.a.	n.a.	n.a.	n.a.
Cl	0,01	0,00	0,00	0,00	0,00	0,00	0,02	0,00	0,00	0,00	0,02	0,00	0,00	0,00
V	0,05	0,07	0,02	0,01	0,04	0,05	0,06	0,03	0,01	0,10	0,08	0,03	0,10	0,04
Total	100,21	100,29	100,92	100,81	100,62	100,41	99,82	100,35	100,65	100,84	100,25	100,83	100,82	100,48
%En	48,45	47,13	48,06	47,91	47,73	46,64	46,77	46,33	47,77	47,88	48,12	48,32	47,92	47,54
%Fs	3,45	3,28	3,89	3,97	3,62	3,31	3,71	3,76	3,38	3,69	3,12	3,10	3,22	3,09
%Wo	48,10	49,59	48,04	48,13	48,65	50,05	49,52	49,92	48,85	48,43	48,76	48,58	48,86	49,37
Mg#	0,93	0,93	0,93	0,92	0,93	0,93	0,93	0,92	0,93	0,93	0,94	0,94	0,94	0,94

Table S4. Continued.

Rock type	sp-lherz																
Sample	1A-81B																
Point	1	2	5	11	12	13	14	23	24	33	34	35	36	41	42	47	48
Info	cpx_1_c	cpx_1_r	cpx_2_c	cpx_3_c	cpx_3_r	cpx_4_c	cpx_4_r	cpx_5_c	cpx_5_r	cpx_7_c	cpx_7_r	cpx_8_c	cpx_8_r	cpx_9_c	cpx_9_r	cpx_10_c	cpx_10_r
SiO₂	52,16	52,09	52,83	52,20	52,28	52,82	52,94	52,38	52,69	52,62	52,87	52,70	52,74	52,43	52,52	52,11	52,14
TiO₂	0,38	0,34	0,49	0,30	0,33	0,14	0,37	0,20	0,27	0,17	0,43	0,36	0,36	0,26	0,44	0,32	0,27
Al₂O₃	5,82	5,95	5,83	6,01	6,00	6,04	5,97	6,03	5,98	6,07	5,96	6,38	6,23	6,80	6,55	6,44	6,18
Cr₂O₃	0,66	0,69	0,78	0,66	0,76	0,58	0,57	0,82	0,74	0,70	0,60	0,83	0,77	0,82	0,96	0,89	0,93
FeOt	1,98	1,94	2,04	1,76	1,95	1,93	1,80	2,03	2,11	1,87	1,86	1,79	1,88	2,20	2,06	1,98	1,78
MnO	0,14	0,09	0,03	0,05	0,11	0,13	0,14	0,14	0,00	0,00	0,04	0,02	0,10	0,08	0,12	0,08	0,16
MgO	14,36	14,56	14,80	14,53	14,98	15,01	14,93	14,76	15,15	14,45	14,67	14,38	14,24	14,42	14,23	14,24	14,38
P2O5	0,00	0,00	0,00	0,02	0,03	0,06	0,04	0,02	0,02	0,11	0,02	0,00	0,07	0,00	0,00	0,00	0,00
NiO	0,01	0,06	0,07	0,04	0,00	0,03	0,03	0,04	0,00	0,00	0,10	0,06	0,09	0,05	0,05	0,06	0,03
CaO	21,34	21,20	21,46	21,16	21,44	21,06	21,34	21,39	21,62	21,67	21,73	21,47	21,73	21,34	21,23	21,40	21,92
BaO	0,00	0,00	0,00	0,00	0,00	0,04	0,11	0,04	0,00	0,00	0,08	0,00	0,06	0,00	0,00	0,00	0,15
Na₂O	1,58	1,69	1,65	1,88	1,69	1,81	1,82	1,50	1,64	1,78	1,83	1,71	1,88	1,63	1,77	1,33	1,78
K₂O	0,00	0,01	0,09	0,01	0,02	0,04	0,00	0,01	0,00	0,02	0,02	0,02	0,00	0,00	0,00	0,00	0,02
F	n.a.																
Cl	0,00	0,00	0,04	0,00	0,00	0,01	0,00	0,02	0,01	0,02	0,01	0,02	0,00	0,01	0,00	0,00	0,02
V	0,08	0,07	0,10	0,02	0,08	0,05	0,08	0,00	0,06	0,01	0,05	0,02	0,02	0,03	0,04	0,03	0,08
Total	98,51	98,69	100,20	98,63	99,66	99,71	100,14	99,34	100,29	99,48	100,29	99,74	100,20	100,06	99,97	98,89	99,83
%En	46,61	47,15	47,20	47,30	47,58	48,07	47,74	47,20	47,53	46,49	46,83	46,67	46,06	46,54	46,44	46,35	46,19
%Fs	3,61	3,52	3,65	3,21	3,47	3,46	3,22	3,64	3,71	3,37	3,33	3,26	3,41	3,98	3,76	3,61	3,21
%Wo	49,78	49,32	49,16	49,49	48,95	48,47	49,04	49,16	48,76	50,13	49,84	50,07	50,53	49,48	49,80	50,05	50,60
Mg#	0,93	0,93	0,93	0,94	0,93	0,93	0,94	0,93	0,93	0,93	0,93	0,93	0,92	0,93	0,93	0,93	0,93

Table S4. Continued.

Rock type	sp-lherz														
Sample	1A-81B														
Point	51	52	53	54	55	56	59	60	65	66	69	70	71	72	77
Info	cpx_11_c	cpx_11_r	cpx_12_c	cpx_12_r	cpx_13_c	cpx_13_r	cpx_14_c	cpx_14_r	cpx_15_c	cpx_15_r	cpx_16_c	cpx_16_r	cpx_17_c	cpx_17_r	cpx_18_c
SiO₂	52,34	52,83	52,69	52,50	52,75	52,97	52,01	52,09	52,91	52,97	52,84	52,52	52,79	52,41	52,11
TiO₂	0,29	0,20	0,39	0,20	0,46	0,30	0,37	0,44	0,14	0,50	0,30	0,41	0,40	0,43	0,33
Al₂O₃	6,09	5,96	6,47	6,39	6,14	6,26	6,37	6,18	5,95	5,87	6,45	6,27	6,09	6,14	6,87
Cr₂O₃	0,74	0,55	0,92	0,86	0,85	0,94	0,84	0,89	0,68	0,68	0,78	0,68	0,72	0,75	0,93
FeOt	2,13	1,98	1,90	2,03	2,12	2,19	2,05	2,12	1,94	1,87	1,90	1,70	2,01	1,88	1,86
MnO	0,14	0,00	0,03	0,10	0,10	0,12	0,12	0,05	0,00	0,14	0,05	0,00	0,12	0,09	0,05
MgO	14,31	14,62	14,47	14,83	14,55	14,63	14,64	14,75	14,78	14,92	14,23	14,61	14,67	14,15	14,67
P2O5	0,00	0,00	0,00	0,00	0,08	0,00	0,00	0,07	0,00	0,00	0,01	0,00	0,00	0,00	0,06
NiO	0,09	0,02	0,05	0,02	0,17	0,07	0,00	0,06	0,02	0,05	0,01	0,08	0,00	0,02	0,05
CaO	21,40	21,26	21,52	21,08	21,36	21,61	21,79	21,29	21,57	21,84	21,43	21,71	21,78	21,56	21,29
BaO	0,01	0,00	0,00	0,01	0,02	0,07	0,09	0,01	0,03	0,00	0,00	0,00	0,00	0,06	0,00
Na₂O	1,70	1,71	1,79	1,87	1,74	1,60	1,71	1,75	1,87	1,76	1,75	1,78	1,45	1,85	1,88
K₂O	0,01	0,01	0,01	0,01	0,03	0,00	0,00	0,00	0,02	0,03	0,02	0,03	0,00	0,00	0,02
F	n.a.														
Cl	0,00	0,00	0,02	0,02	0,01	0,00	0,00	0,00	0,01	0,00	0,13	0,01	0,02	0,03	0,00
V	0,09	0,02	0,03	0,08	0,06	0,08	0,07	0,08	0,01	0,09	0,09	0,04	0,05	0,01	0,02
Total	99,34	99,16	100,27	99,99	100,43	100,83	100,07	99,76	99,92	100,73	99,97	99,83	100,09	99,39	100,14
%En	46,35	47,15	46,67	47,66	46,80	46,60	46,54	47,22	47,12	47,13	46,35	46,88	46,65	46,10	47,31
%Fs	3,87	3,57	3,43	3,65	3,82	3,92	3,66	3,81	3,47	3,31	3,47	3,06	3,59	3,43	3,36
%Wo	49,78	49,28	49,89	48,69	49,37	49,48	49,80	48,97	49,41	49,57	50,18	50,06	49,76	50,47	49,33
Mg#	0,92	0,93	0,93	0,93	0,92	0,92	0,93	0,93	0,93	0,93	0,93	0,94	0,93	0,93	0,93

Table S4. Continued.

Rock type	sp-lherz	sp-lherz	sp-lherz
Sample	1A-81B	1A-81B	1A-81B
Point	78	79	80
Info	cpx_18_r	cpx_19_c	cpx_19_r
SiO₂	52,16	52,07	52,11
TiO₂	0,27	0,18	0,25
Al₂O₃	6,78	6,24	6,17
Cr₂O₃	0,87	0,76	0,92
FeOt	2,11	2,16	2,03
MnO	0,19	0,01	0,07
MgO	14,59	14,72	14,49
P2O5	0,00	0,00	0,01
NiO	0,06	0,05	0,09
CaO	21,17	21,63	21,12
BaO	0,07	0,03	0,00
Na₂O	1,57	1,61	1,49
K₂O	0,02	0,01	0,03
F	n.a.	n.a.	n.a.
Cl	0,00	0,00	0,00
V	0,02	0,05	0,05
Total	99,89	99,52	98,85
%En	47,08	46,77	47,03
%Fs	3,81	3,84	3,70
%Wo	49,10	49,38	49,27
Mg#	0,93	0,92	0,93

Table S4. Continued.

Rock type	sp-lherz																
Sample	1A-81C																
Point	77	78	79	80	83	102	104	105	108	109	110	111	112	118	119	136	137
Info	cpx_1_c	cpx_1_r	cpx_2_c	cpx_2_r	cpx_4_c	cpx_5_c	cpx_6_c	cpx_6_r	cpx_7_c	cpx_7_r	cpx_8_c	cpx_8_r	cpx_9_c	cpx_10_c	cpx_10_r	cpx_11_c	cpx_11_r
SiO₂	52,37	52,37	52,29	52,38	53,11	52,68	52,40	52,41	52,42	52,94	52,05	52,09	52,61	52,06	52,19	52,20	52,44
TiO₂	0,20	0,36	0,39	0,36	0,31	0,22	0,38	0,37	0,30	0,37	0,37	0,40	0,28	0,38	0,45	0,32	0,40
Al₂O₃	6,20	6,18	6,32	5,97	5,45	5,41	6,52	6,33	6,08	5,93	6,61	6,02	6,17	6,54	6,62	6,57	6,56
Cr₂O₃	0,99	0,52	0,71	0,65	0,67	0,82	0,91	0,89	0,98	0,70	0,84	0,92	0,84	0,92	0,86	0,77	0,86
FeOt	2,19	2,36	2,13	2,09	1,95	1,90	2,09	2,04	2,72	2,62	2,03	1,85	2,27	2,05	2,06	2,30	1,96
MnO	0,02	0,05	0,00	0,12	0,09	0,16	0,04	0,05	0,16	0,05	0,22	0,06	0,15	0,07	0,10	0,04	0,06
MgO	14,49	14,53	14,77	14,61	14,99	14,68	13,91	13,90	14,85	14,95	14,06	14,47	14,53	14,13	14,73	14,54	14,34
P2O5	n.a.																
NiO	0,00	0,07	0,03	0,06	0,08	0,00	0,07	0,00	0,00	0,00	0,03	0,01	0,10	0,10	0,03	0,01	0,04
CaO	21,59	21,27	21,64	21,75	21,73	22,16	21,18	21,26	21,23	21,09	22,04	22,10	21,26	21,73	21,44	21,83	21,33
BaO	n.a.																
Na₂O	1,98	1,44	1,85	1,80	1,90	1,79	1,92	1,99	1,75	1,69	1,94	1,95	1,52	2,05	1,71	1,68	1,97
K₂O	0,00	0,00	0,03	0,00	0,00	0,00	0,00	0,00	0,03	0,04	0,00	0,00	0,00	0,02	0,04	0,00	0,00
F	n.a.																
Cl	0,01	0,00	0,01	0,00	0,00	0,00	0,02	0,01	0,01	0,01	0,00	0,00	0,00	0,00	0,00	0,00	0,00
V	0,07	0,09	0,06	0,09	0,00	0,07	0,03	0,05	0,07	0,05	0,05	0,04	0,08	0,05	0,04	0,09	0,10
Total	100,11	99,22	100,23	99,87	100,27	99,90	99,44	99,29	100,56	100,45	100,24	99,92	99,80	100,06	100,23	100,37	100,04
%En	46,40	46,66	46,87	46,51	47,30	46,36	45,90	45,84	46,95	47,34	45,31	46,10	46,74	45,73	47,07	46,13	46,60
%Fs	3,94	4,25	3,80	3,73	3,44	3,37	3,87	3,77	4,83	4,65	3,66	3,31	4,10	3,72	3,69	4,09	3,57
%Wo	49,66	49,09	49,33	49,76	49,26	50,27	50,23	50,40	48,22	48,01	51,03	50,59	49,16	50,55	49,24	49,78	49,82
Mg#	0,92	0,92	0,93	0,93	0,93	0,93	0,92	0,92	0,91	0,91	0,93	0,93	0,92	0,93	0,92	0,93	0,93

Table S4. Continued.

Rock type	sp-lherz	sp-lherz	sp-lherz	sp-lherz	sp-lherz	sp-lherz
Sample	1A-81C	1A-81C	1A-81C	1A-81C	1A-81C	1A-81C
Point	140	141	180	181	186	187
Info	cpx_12_c	cpx_12_r	cpx_13_c	cpx_13_r	cpx_14_c	cpx_14_r
SiO₂	52,74	53,01	53,25	53,56	52,84	52,23
TiO₂	0,46	0,31	0,25	0,30	0,20	0,39
Al₂O₃	6,69	5,79	6,04	5,86	5,91	6,05
Cr₂O₃	0,82	0,71	0,66	0,59	0,52	0,99
FeOt	2,01	1,98	1,97	2,02	2,38	2,31
MnO	0,08	0,00	0,14	0,12	0,07	0,02
MgO	14,16	14,56	14,42	14,59	14,98	14,86
P2O5	n.a.	n.a.	n.a.	n.a.	n.a.	n.a.
NiO	0,09	0,04	0,00	0,00	0,04	0,02
CaO	21,59	21,96	21,48	21,69	21,08	21,46
BaO	n.a.	n.a.	n.a.	n.a.	n.a.	n.a.
Na₂O	1,92	1,74	2,00	1,72	1,69	1,77
K₂O	0,00	0,01	0,01	0,02	0,01	0,01
F	n.a.	n.a.	n.a.	n.a.	n.a.	n.a.
Cl	0,01	0,00	0,01	0,01	0,00	0,03
V	0,01	0,07	0,06	0,03	0,05	0,05
Total	100,58	100,17	100,30	100,50	99,76	100,20
%En	45,97	46,29	46,57	46,60	47,61	47,07
%Fs	3,67	3,53	3,58	3,62	4,24	4,11
%Wo	50,36	50,18	49,85	49,78	48,16	48,83
Mg#	0,93	0,93	0,93	0,93	0,92	0,92

Table S4. Continued.

Rock type	grt-wehr														
Sample	1B-139A														
Point	4	5	24	25	30	31	32	33	34	35	48	49	58	59	61
Info	cpx_1_c	cpx_1_r	cpx_2_c	cpx_2_r	cpx_3_c	cpx_3_r	cpx_4_c	cpx_4_r	cpx_5_c	cpx_5_r	cpx_6_c	cpx_6_r	cpx_7_c	cpx_7_r	cpx_8_r
SiO₂	54,66	54,93	54,58	54,68	54,00	53,74	53,98	53,94	53,89	53,97	53,89	54,11	54,67	54,30	54,73
TiO₂	0,03	0,09	0,21	0,27	0,14	0,25	0,37	0,33	0,23	0,09	0,00	0,12	0,13	0,27	0,18
Al₂O₃	1,09	1,05	1,21	1,19	1,47	1,28	1,14	1,10	1,32	1,25	1,34	1,39	1,21	1,21	1,22
Cr₂O₃	1,54	1,78	1,86	1,57	1,74	1,73	1,74	1,38	1,86	1,57	1,49	1,74	1,73	1,38	2,13
FeOt	2,42	2,39	2,62	2,56	2,97	2,81	2,69	2,65	3,01	2,89	2,78	2,89	2,81	2,68	2,69
MnO	0,11	0,22	0,03	0,00	0,20	0,06	0,07	0,20	0,12	0,04	0,14	0,06	0,14	0,09	0,05
MgO	17,46	17,62	18,16	17,75	17,53	17,74	17,66	17,87	17,97	17,85	17,60	17,81	17,94	17,82	17,36
P2O5	n.a.														
NiO	0,05	0,08	0,07	0,15	0,06	0,01	0,11	0,04	0,04	0,10	0,03	0,13	0,04	0,14	0,09
CaO	20,88	20,85	20,25	20,62	19,62	19,43	20,44	20,26	19,22	19,73	19,70	19,21	19,16	19,73	20,07
BaO	n.a.														
Na₂O	1,33	1,24	1,37	1,28	1,51	1,55	1,40	1,33	1,45	1,46	1,44	1,40	1,46	1,42	1,44
K₂O	0,07	0,08	0,08	0,13	0,12	0,07	0,08	0,07	0,14	0,08	0,11	0,15	0,11	0,13	0,09
F	n.a.														
Cl	0,00	0,00	0,00	0,02	0,02	0,01	0,00	0,01	0,01	0,01	0,01	0,00	0,00	0,04	0,02
V	0,02	0,06	0,07	0,05	0,02	0,06	0,02	0,09	0,06	0,02	0,00	0,04	0,05	0,07	0,03
Total	99,65	100,37	100,49	100,28	99,41	98,73	99,70	99,26	99,30	99,06	98,53	99,03	99,46	99,29	100,08
%En	51,61	51,91	53,12	52,21	52,65	53,31	52,15	52,68	53,69	53,04	52,82	53,59	53,90	53,20	52,15
%Fs	4,02	3,94	4,30	4,21	5,01	4,73	4,46	4,39	5,04	4,81	4,69	4,87	4,74	4,48	4,53
%Wo	44,37	44,15	42,58	43,58	42,34	41,95	43,38	42,93	41,27	42,14	42,49	41,53	41,37	42,32	43,31
Mg#	0,93	0,93	0,93	0,93	0,91	0,92	0,92	0,92	0,91	0,92	0,92	0,92	0,92	0,92	0,92

Table S4. Continued.

Rock type	grt-wehr	grt-wehr	grt-wehr	grt-wehr	grt-wehr
Sample	1B-139A	1B-139A	1B-139A	1B-139A	1B-139A
Point	62	64	65	66	67
Info	cpx_9_c	cpx_10_c	cpx_10_r	cpx_11_c	cpx_11_r
SiO₂	54,61	54,72	54,30	54,38	54,27
TiO₂	0,21	0,05	0,00	0,10	0,06
Al₂O₃	1,24	1,04	1,08	1,02	1,11
Cr₂O₃	1,59	1,57	1,57	1,60	1,74
FeOt	2,71	2,59	2,46	2,43	2,68
MnO	0,10	0,06	0,01	0,09	0,05
MgO	17,68	17,81	17,39	17,39	17,68
P2O5	n.a.	n.a.	n.a.	n.a.	n.a.
NiO	0,03	0,05	0,01	0,07	0,03
CaO	19,90	20,29	20,93	20,67	20,43
BaO	n.a.	n.a.	n.a.	n.a.	n.a.
Na₂O	1,48	1,24	1,19	1,33	1,24
K₂O	0,15	0,07	0,05	0,08	0,13
F	n.a.	n.a.	n.a.	n.a.	n.a.
Cl	0,00	0,00	0,00	0,00	0,02
V	0,05	0,09	0,04	0,02	0,08
Total	99,72	99,58	99,04	99,16	99,51
%En	52,77	52,62	51,43	51,74	52,20
%Fs	4,54	4,30	4,09	4,05	4,44
%Wo	42,69	43,08	44,48	44,20	43,36
Mg#	0,92	0,92	0,93	0,93	0,92

Table S4. Continued.

Rock type	grt-wehr															
Sample	1B-139B															
Point	45	46	53	54	55	56	59	60	61	62	88	89	117	118	128	
Info	cpx_1_c	cpx_1_r	cpx_2_c	cpx_2_r	cpx_3_c	cpx_3_r	cpx_4_c	cpx_4_r	cpx_5_c	cpx_5_r	cpx_6_c	cpx_6_r	cpx_7_c	cpx_7_r	cpx_8_c	
SiO₂	54,76	54,64	55,04	55,13	54,69	54,60	54,80	54,59	54,63	54,64	54,27	54,68	55,01	54,89	55,02	
TiO₂	0,19	0,00	0,15	0,19	0,18	0,25	0,08	0,08	0,33	0,29	0,21	0,22	0,00	0,19	0,30	
Al₂O₃	1,37	1,43	1,17	1,33	1,08	1,03	1,06	1,10	1,48	1,36	1,15	1,10	1,42	1,35	1,17	
Cr₂O₃	1,62	1,66	1,43	1,72	1,85	1,39	1,70	1,55	1,52	1,88	1,58	1,51	1,70	1,81	1,57	
FeOt	2,79	2,80	2,63	2,76	3,00	2,66	2,60	2,72	2,73	2,66	2,60	2,50	2,88	2,86	2,55	
MnO	0,13	0,19	0,05	0,03	0,07	0,08	0,11	0,08	0,12	0,15	0,02	0,02	0,17	0,02	0,07	
MgO	17,83	17,62	17,35	17,72	17,60	17,72	17,96	17,53	18,07	17,83	17,21	17,57	18,04	17,93	17,28	
P2O5	n.a.															
NiO	0,06	0,03	0,03	0,07	0,03	0,03	0,02	0,05	0,05	0,10	0,07	0,07	0,07	0,06	0,06	
CaO	19,86	19,75	20,81	20,09	20,16	20,70	20,38	20,15	20,02	20,29	20,53	20,64	19,90	20,12	20,56	
BaO	n.a.															
Na₂O	1,35	1,60	1,27	1,41	1,74	1,63	1,29	1,24	1,54	1,48	1,19	1,24	1,44	1,53	1,30	
K₂O	0,11	0,10	0,08	0,14	0,08	0,00	0,11	0,09	0,28	0,03	0,11	0,09	0,13	0,12	0,07	
F	n.a.															
Cl	0,00	0,00	0,00	0,00	0,01	0,00	0,01	0,02	0,00	0,00	0,00	0,00	0,00	0,00	0,01	
V	0,07	0,03	0,06	0,10	0,06	0,02	0,07	0,00	0,05	0,04	0,01	0,11	0,06	0,00	0,03	
Total	100,15	99,84	100,09	100,67	100,53	100,10	100,19	99,20	100,82	100,74	98,94	99,74	100,80	100,87	99,99	
%En	52,97	52,79	51,36	52,58	52,11	51,99	52,72	52,28	53,16	52,59	51,48	51,98	53,13	52,76	51,60	
%Fs	4,65	4,71	4,37	4,59	4,98	4,38	4,28	4,55	4,51	4,41	4,37	4,15	4,76	4,72	4,27	
%Wo	42,38	42,50	44,27	42,83	42,91	43,63	43,00	43,18	42,32	43,00	44,14	43,87	42,11	42,53	44,12	
Mg#	0,92	0,92	0,92	0,92	0,91	0,92	0,92	0,92	0,92	0,92	0,93	0,92	0,92	0,92	0,92	

Table S4. Continued.

Rock type	grt-wehr	grt-wehr	grt-wehr	grt-wehr	grt-wehr	grt-wehr
Sample	1B-139B	1B-139B	1B-139B	1B-139B	1B-139B	1B-139B
Point	129	130	131	132	133	14
Info	cpx_8_r	cpx_9_c	cpx_9_r	cpx_10_c	cpx_10_r	cpx_11_c
SiO₂	54,89	54,40	54,92	54,51	54,37	54,51
TiO₂	0,16	0,20	0,00	0,32	0,28	0,15
Al₂O₃	1,20	1,18	1,22	1,23	1,20	1,42
Cr₂O₃	1,61	2,08	2,18	1,62	1,99	1,74
FeOt	2,67	2,44	2,68	2,75	2,71	3,01
MnO	0,07	0,02	0,08	0,04	0,19	0,17
MgO	17,56	17,26	17,50	18,08	18,05	17,97
P2O5	n.a.	n.a.	n.a.	n.a.	n.a.	n.a.
NiO	0,13	0,05	0,11	0,07	0,08	0,05
CaO	20,15	20,65	20,15	20,19	20,31	20,47
BaO	n.a.	n.a.	n.a.	n.a.	n.a.	n.a.
Na₂O	1,30	1,45	1,53	1,30	1,04	1,12
K₂O	0,10	0,07	0,08	0,15	0,00	0,02
F	n.a.	n.a.	n.a.	n.a.	n.a.	n.a.
Cl	0,00	0,00	0,00	0,00	0,00	0,00
V	0,04	0,06	0,02	0,03	0,05	0,07
Total	99,88	99,86	100,46	100,28	100,26	100,69
%En	52,36	51,57	52,26	52,97	52,84	52,29
%Fs	4,47	4,09	4,49	4,51	4,45	4,92
%Wo	43,17	44,34	43,25	42,51	42,71	42,79
Mg#	0,92	0,93	0,92	0,92	0,92	0,91

Table S5. Major elements of each analyzed spinel from the Catalão xenoliths.

Rock type	sp-lherz									
Sample	1A-76A									
Point	59	60	61	62	63	64	65	66	146	151
Info	sp_1_c	sp_1_r	sp_2_c	sp_2_r	sp_3_c	sp_3_r	sp_4_c	sp_4_r	sp_6_c	sp_8_r
SiO₂	0,00	0,00	0,00	0,00	0,00	0,00	0,00	0,00	0,00	0,00
TiO₂	0,14	0,00	0,13	0,00	0,03	0,02	0,00	0,08	0,09	0,00
Al₂O₃	57,55	57,78	57,77	57,75	57,62	57,77	57,71	57,73	57,20	57,93
Cr₂O₃	9,04	9,57	9,60	9,53	9,22	8,98	8,96	9,26	9,29	9,61
FeOt	12,60	12,23	12,08	12,07	12,62	12,46	11,84	12,07	12,13	11,99
MnO	0,24	0,24	0,07	0,20	0,03	0,14	0,17	0,00	0,16	0,21
MgO	19,42	19,35	19,38	19,08	19,23	19,14	19,48	19,53	19,81	19,62
P₂O₅	0,03	0,01	0,02	0,03	0,01	0,00	0,07	0,06	0,04	0,00
NiO	0,26	0,36	0,41	0,27	0,31	0,39	0,31	0,32	0,32	0,33
CaO	0,00	0,00	0,02	0,00	0,00	0,00	0,01	0,00	0,00	0,02
BaO	0,00	0,13	0,03	0,00	0,01	0,05	0,00	0,00	0,12	0,04
Na₂O	0,00	0,01	0,00	0,00	0,00	0,01	0,01	0,02	0,00	0,04
K₂O	0,00	0,00	0,00	0,00	0,00	0,01	0,00	0,01	0,01	0,00
F	n.a									
Cl	0,03	0,00	0,01	0,00	0,00	0,00	0,02	0,00	0,00	0,00
V	0,06	0,05	0,07	0,12	0,09	0,06	0,10	0,08	0,05	0,08
Total	99,38	99,73	99,58	99,05	99,16	99,03	98,68	99,16	99,21	99,86
Cr#	9,53	10,00	10,03	9,97	9,69	9,44	9,44	9,72	9,82	10,01
Mg#	73,31	73,82	74,10	73,81	73,09	73,25	74,57	74,25	74,44	74,47
Fet#	26,69	26,18	25,90	26,19	26,91	26,75	25,43	25,75	25,56	25,53
Fe³⁺	0,04	0,03	0,02	0,02	0,03	0,03	0,03	0,04	0,03	
Fe²⁺	0,23	0,24	0,24	0,25	0,24	0,24	0,23	0,23	0,22	0,23

Table S5. Continued.

Rock type	sp-lherz															
Sample	1A-76B															
Point	148	149	166	167	168	169	174	175	176	177	178	179	188	189	222	
Info	sp_1_c	sp_1_r	sp_2_c	sp_2_r	sp_3_c	sp_3_r	sp_4_c	sp_4_r	sp_5_c	sp_5_r	sp_6_c	sp_6_r	sp_7_c	sp_7_r	sp_8_c	sp_8_r
SiO₂	0,00	0,00	0,00	0,00	0,00	0,00	0,00	0,00	0,00	0,00	0,00	0,00	0,00	0,00	0,00	0,00
TiO₂	0,04	0,09	0,05	0,01	0,00	0,00	0,00	0,00	0,00	0,00	0,09	0,04	0,09	0,06	0,14	0,00
Al₂O₃	57,58	57,79	57,64	57,69	56,95	57,08	57,00	57,08	57,56	57,53	57,12	57,53	57,66	56,92	57,56	57,65
Cr₂O₃	9,24	9,25	9,36	9,20	8,96	9,04	9,42	9,28	9,48	9,56	9,16	9,26	9,23	8,81	9,23	9,30
FeOt	12,19	12,23	12,70	12,83	12,86	12,97	12,29	12,54	12,76	12,81	13,05	12,97	12,29	12,68	12,21	12,28
MnO	0,12	0,16	0,17	0,07	0,07	0,27	0,09	0,14	0,06	0,16	0,04	0,03	0,24	0,05	0,09	0,04
MgO	19,35	19,41	19,69	19,62	19,90	19,41	19,49	19,16	19,85	19,63	19,82	19,85	19,34	19,57	19,10	19,89
P₂O₅	0,01	0,00	0,01	0,04	0,02	0,00	0,00	0,00	0,03	0,00	0,00	0,00	0,00	0,00	0,03	0,03
NiO	0,25	0,34	0,31	0,34	0,31	0,35	0,32	0,29	0,34	0,34	0,30	0,33	0,35	0,31	0,36	0,37
CaO	0,00	0,02	0,04	0,00	0,02	0,01	0,04	0,00	0,02	0,01	0,00	0,00	0,03	0,01	0,04	0,00
BaO	0,12	0,10	0,09	0,00	0,08	0,01	0,00	0,02	0,00	0,00	0,01	0,00	0,00	0,05	0,00	0,00
Na₂O	0,01	0,03	0,06	0,07	0,00	0,01	0,03	0,01	0,00	0,00	0,00	0,04	0,00	0,00	0,01	0,00
K₂O	0,02	0,00	0,01	0,00	0,00	0,01	0,00	0,04	0,02	0,01	0,00	0,00	0,00	0,00	0,00	0,00
F	n.a	n.a														
Cl	0,00	0,03	0,00	0,06	0,00	0,00	0,01	0,03	0,02	0,00	0,00	0,00	0,02	0,01	0,02	0,00
V	0,06	0,05	0,04	0,08	0,14	0,04	0,11	0,05	0,09	0,02	0,05	0,09	0,06	0,07	0,04	0,09
Total	98,98	99,50	100,16	99,99	99,31	99,19	98,79	98,63	100,21	100,06	99,64	100,15	99,32	98,55	98,83	99,65
Cr#	9,71	9,70	9,82	9,67	9,55	9,61	9,98	9,83	9,95	10,03	9,72	9,75	9,70	9,40	9,71	9,77
Mg#	73,89	73,88	73,42	73,16	73,39	72,74	73,86	73,14	73,50	73,20	73,02	73,18	73,72	73,35	73,59	74,28
Fet#	26,11	26,12	26,58	26,84	26,61	27,26	26,14	26,86	26,50	26,80	26,98	26,82	26,28	26,65	26,41	25,72
Fe³⁺	0,03	0,04	0,05	0,06	0,06	0,04	0,04	0,05	0,05	0,05	0,06	0,06	0,03	0,05	0,03	0,05
Fe²⁺	0,24	0,23	0,22	0,22	0,22	0,23	0,22	0,23	0,22	0,23	0,23	0,22	0,23	0,24	0,22	

Table S5. Continued.

Rock type	sp-lherz														
Sample	1A-76C														
Point	49	50	51	52	53	54	73	74	75	76	77	78	79	80	81
Info	sp_1_c	sp_2_c	sp_3_c	sp_4_c	sp_5_c	sp_6_c	sp_7_c	sp_7_r	sp_8_c	sp_8_r	sp_9_c	sp_10_c	sp_11_c	sp_12_c	sp_13_c
SiO₂	0,00	0,00	0,00	0,00	0,00	0,00	0,01	0,00	0,00	0,00	0,00	0,00	0,00	0,00	0,00
TiO₂	0,00	0,06	0,00	0,00	0,00	0,09	0,15	0,12	0,00	0,00	0,11	0,12	0,06	0,00	0,08
Al₂O₃	57,31	57,23	57,24	57,11	57,18	57,00	57,81	57,72	57,96	57,55	57,61	57,77	57,23	57,01	57,74
Cr₂O₃	9,99	10,03	10,18	10,17	10,09	10,23	9,97	10,19	9,58	9,84	9,32	9,67	9,78	10,14	10,21
FeOt	13,56	13,48	13,61	13,57	12,70	12,67	12,35	12,80	13,35	13,45	13,32	12,37	12,53	13,12	12,95
MnO	0,17	0,17	0,11	0,23	0,20	0,19	0,18	0,14	0,17	0,22	0,05	0,08	0,00	0,13	0,27
MgO	18,80	18,78	18,61	18,87	18,81	18,91	19,17	19,11	19,01	18,44	18,62	18,95	18,78	18,61	18,64
P₂O₅	0,00	0,00	0,05	0,00	0,01	0,00	0,03	0,01	0,00	0,06	0,00	0,00	0,00	0,00	0,00
NiO	0,34	0,32	0,35	0,36	0,34	0,26	0,36	0,39	0,50	0,40	0,30	0,38	0,31	0,28	0,42
CaO	0,00	0,02	0,00	0,00	0,01	0,00	0,02	0,00	0,02	0,02	0,00	0,00	0,00	0,02	0,00
BaO	n.a														
Na₂O	0,03	0,00	0,00	0,00	0,02	0,01	0,00	0,03	0,00	0,00	0,00	0,00	0,00	0,00	0,04
K₂O	0,02	0,00	0,03	0,02	0,00	0,00	0,00	0,00	0,01	0,00	0,02	0,01	0,01	0,02	0,01
F	n.a														
Cl	0,00	0,00	0,00	0,00	0,00	0,00	0,02	0,00	0,00	0,00	0,00	0,00	0,01	0,00	0,01
V	0,05	0,09	0,08	0,10	0,11	0,10	0,07	0,06	0,03	0,05	0,12	0,07	0,08	0,11	0,04
Total	100,27	100,16	100,26	100,41	99,45	99,44	100,11	100,56	100,62	100,02	99,47	99,42	98,79	99,44	100,42
Cr#	10,47	10,52	10,66	10,67	10,58	10,74	10,37	10,59	9,98	10,29	9,79	10,09	10,29	10,66	10,60
Mg#	71,20	71,29	70,91	71,25	72,53	72,68	73,46	72,69	71,73	70,96	71,36	73,20	72,77	71,65	71,96
Fet#	28,80	28,71	29,09	28,75	27,47	27,32	26,54	27,31	28,27	29,04	28,64	26,80	27,23	28,35	28,04
Fe³⁺	0,04	0,03	0,03	0,04	0,03	0,02	0,02	0,03	0,04	0,03	0,02	0,02	0,03	0,02	
Fe²⁺	0,26	0,26	0,27	0,25	0,25	0,25	0,25	0,25	0,25	0,27	0,27	0,25	0,26	0,26	0,26

Table S5. Continued.

Rock type	sp-harz									
Sample	1A-81									
Point	25	26	27	28	65	66	67	68	69	70
Info	sp_1_c	sp_1_r	sp_2_c	sp_2_r	sp_3_c	sp_3_r	sp_4_c	sp_4_r	sp_5_c	sp_5_r
SiO₂	0,00	0,01	0,04	0,00	0,02	0,00	0,00	0,00	0,00	0,02
TiO₂	0,14	0,05	0,03	0,13	0,06	0,11	0,13	0,24	0,07	0,06
Al₂O₃	40,52	40,57	40,97	40,89	40,90	40,69	40,30	40,90	41,29	41,29
Cr₂O₃	24,85	24,69	24,96	24,74	23,76	23,71	24,34	23,16	23,47	23,82
FeOt	16,37	16,61	16,40	16,46	17,45	17,82	17,71	17,85	17,56	17,33
MnO	0,09	0,22	0,17	0,18	0,17	0,17	0,18	0,20	0,23	0,20
MgO	16,65	16,64	17,04	16,96	16,59	16,16	16,82	16,50	17,00	16,87
P₂O₅	0,01	0,04	0,02	0,00	0,00	0,00	0,00	0,01	0,04	0,05
NiO	0,21	0,19	0,20	0,13	0,21	0,23	0,26	0,23	0,23	0,23
CaO	0,00	0,01	0,03	0,00	0,00	0,00	0,01	0,03	0,01	0,04
BaO	n.a									
Na₂O	0,05	0,01	0,00	0,00	0,03	0,00	0,05	0,00	0,02	0,00
K₂O	0,00	0,00	0,01	0,00	0,00	0,00	0,03	0,00	0,02	0,03
F	n.a									
Cl	0,00	0,00	0,00	0,00	0,00	0,00	0,00	0,00	0,01	0,00
V	0,12	0,11	0,09	0,14	0,13	0,17	0,07	0,16	0,09	0,05
Total	99,01	99,14	99,97	99,63	99,33	99,07	99,91	99,28	100,05	99,97
Cr#	29,15	28,99	29,01	28,87	28,04	28,10	28,83	27,53	27,60	27,90
Mg#	64,46	64,11	64,95	64,75	62,88	61,79	62,86	62,23	63,32	63,44
Fet#	35,54	35,89	35,05	35,25	37,12	38,21	37,14	37,77	36,68	36,56
Fe³⁺	0,09	0,10	0,10	0,10	0,11	0,11	0,13	0,12	0,13	0,12
Fe²⁺	0,29	0,29	0,28	0,29	0,30	0,31	0,28	0,30	0,28	0,29

Table S5. Continued.

Rock type	sp-lherz																
Sample	1A-81A																
Point	180	181	206	207	208	209	210	211	212	213	214	215	216	217	218	219	220
Info	sp_1_c	sp_1_r	sp_2_rl	sp_2_c1	sp_2_c2	sp_2_r2	sp_3_r1	sp_3_c1	sp_3_c2	sp_3_r2	sp_4_c	sp_4_r	sp_5_c	sp_5_r	sp_6_c	sp_6_r	sp_7_r1
SiO₂	0,00	0,00	0,00	0,00	0,00	0,00	0,00	0,00	0,00	0,00	0,00	0,00	0,00	0,00	0,00	0,00	0,00
TiO₂	0,12	0,02	0,07	0,00	0,00	0,10	0,00	0,08	0,01	0,01	0,00	0,01	0,03	0,00	0,07	0,00	0,00
Al₂O₃	58,31	58,40	58,16	57,31	57,47	58,00	58,05	57,72	57,82	58,18	57,84	57,75	57,97	57,97	57,54	58,00	57,83
Cr₂O₃	9,21	9,31	9,47	9,51	9,57	9,47	9,22	9,39	9,33	9,28	9,74	9,75	9,55	9,47	9,40	9,29	9,67
FeOt	12,11	11,93	11,86	11,94	11,77	11,68	11,60	11,65	11,61	11,72	11,73	11,76	11,95	11,87	12,02	11,72	11,72
MnO	0,09	0,12	0,24	0,18	0,07	0,21	0,10	0,11	0,15	0,02	0,13	0,07	0,01	0,10	0,15	0,05	0,08
MgO	19,29	19,52	18,75	19,19	19,17	19,37	19,33	19,21	19,22	19,46	19,41	19,31	18,92	19,03	19,13	19,30	19,12
P₂O₅	0,00	0,01	0,00	0,00	0,02	0,01	0,00	0,00	0,01	0,01	0,07	0,00	0,06	0,00	0,00	0,01	0,00
NiO	0,30	0,33	0,37	0,40	0,42	0,44	0,30	0,37	0,39	0,39	0,36	0,33	0,34	0,34	0,46	0,27	
CaO	0,01	0,00	0,00	0,00	0,00	0,00	0,01	0,01	0,00	0,01	0,00	0,00	0,02	0,01	0,01	0,01	0,00
BaO	0,03	0,05	0,06	0,00	0,00	0,00	0,00	0,00	0,05	0,00	0,00	0,01	0,02	0,02	0,01	0,05	0,04
Na₂O	0,01	0,00	0,01	0,00	0,06	0,01	0,01	0,02	0,05	0,00	0,00	0,00	0,00	0,00	0,00	0,00	0,00
K₂O	0,00	0,00	0,04	0,00	0,00	0,00	0,02	0,00	0,00	0,00	0,00	0,00	0,01	0,01	0,00	0,01	0,00
F	n.a																
Cl	0,00	0,00	0,00	0,00	0,02	0,00	0,00	0,03	0,00	0,00	0,00	0,01	0,00	0,01	0,00	0,00	0,00
V	0,07	0,08	0,07	0,09	0,09	0,07	0,07	0,08	0,01	0,04	0,12	0,05	0,05	0,06	0,06	0,09	0,07
Total	99,55	99,76	99,11	98,65	98,64	99,35	98,71	98,66	98,64	99,12	99,39	99,05	98,94	98,89	98,73	98,99	98,79
Cr#	9,58	9,66	9,85	10,02	10,05	9,87	9,63	9,84	9,77	9,66	10,15	10,17	9,95	9,88	9,87	9,70	10,09
Mg#	73,96	74,46	73,81	74,13	74,38	74,73	74,81	74,62	74,69	74,76	74,68	74,53	73,84	74,09	73,95	74,59	74,42
Fet#	26,04	25,54	26,19	25,87	25,62	25,27	25,19	25,38	25,31	25,24	25,32	25,47	26,16	25,91	26,05	25,41	25,58
Fe³⁺	0,02	0,02	0,01	0,03	0,03	0,02	0,02	0,02	0,02	0,02	0,02	0,01	0,01	0,02	0,02	0,01	
Fe²⁺	0,24	0,24	0,25	0,24	0,23	0,24	0,23	0,23	0,23	0,24	0,24	0,25	0,25	0,24	0,24	0,25	

Table S5. Continued.

Rock type	sp-lherz								
Sample	1A-81A								
Point	221	222	223	224	225	226	227	228	229
Info	sp_7_c1	sp_7_c2	sp_7_r2	sp_8_c	sp_8_r	sp_9_c	sp_9_r	sp_10_c	sp_10_r
SiO₂	0,00	0,00	0,00	0,00	0,00	0,00	0,00	0,00	0,00
TiO₂	0,02	0,01	0,04	0,02	0,00	0,05	0,06	0,00	0,00
Al₂O₃	57,66	57,61	58,25	58,18	58,28	57,79	58,19	57,93	57,91
Cr₂O₃	9,58	9,51	9,28	9,45	9,30	9,80	9,59	9,41	9,93
FeOt	11,60	12,06	12,27	11,78	11,74	12,17	12,16	12,27	12,20
MnO	0,25	0,03	0,12	0,23	0,13	0,02	0,06	0,10	0,11
MgO	19,06	18,99	18,96	18,99	19,26	19,19	19,28	19,35	18,95
P₂O₅	0,00	0,01	0,04	0,03	0,00	0,02	0,02	0,00	0,02
NiO	0,39	0,25	0,29	0,40	0,38	0,31	0,30	0,35	0,26
CaO	0,03	0,01	0,00	0,00	0,00	0,04	0,00	0,00	0,02
BaO	0,14	0,05	0,00	0,00	0,00	0,12	0,00	0,00	0,02
Na₂O	0,02	0,00	0,00	0,01	0,00	0,01	0,04	0,00	0,01
K₂O	0,00	0,01	0,00	0,00	0,01	0,01	0,01	0,00	0,00
F	n.a								
Cl	0,00	0,02	0,02	0,02	0,02	0,01	0,02	0,01	0,03
V	0,04	0,04	0,05	0,00	0,10	0,09	0,05	0,06	0,10
Total	98,80	98,59	99,31	99,11	99,22	99,61	99,78	99,48	99,55
Cr#	10,03	9,97	9,65	9,82	9,67	10,21	9,96	9,82	10,32
Mg#	74,54	73,73	73,36	74,19	74,52	73,76	73,86	73,76	73,47
Fet#	25,46	26,27	26,64	25,81	25,48	26,24	26,14	26,24	26,53
Fe³⁺	0,02	0,02	0,02	0,01	0,02	0,02	0,02	0,03	0,02
Fe²⁺	0,24	0,25	0,25	0,24	0,24	0,24	0,24	0,24	0,25

Table S5. Continued.

Rock type	sp-lherz																	
Sample	1A-81B																	
Point	45	46	83	87	88	89	90	92	93	94	95	96	97	98	99	100	101	102
Info	sp_1_c	sp_1_r	sp_2_c	sp_3_c	sp_3_r	sp_4_c	sp_4_r	sp_5_c	sp_6_c	sp_6_r	sp_7_c	sp_7_r	sp_8_c	sp_8_r	sp_9_c	sp_9_r	sp_10_c	sp_10_r
SiO₂	0,00	0,01	0,00	0,00	0,00	0,00	0,00	0,00	0,00	0,00	0,00	0,00	0,00	0,00	0,00	0,00	0,00	0,00
TiO₂	0,05	0,04	0,00	0,00	0,00	0,00	0,02	0,00	0,00	0,00	0,00	0,06	0,07	0,00	0,00	0,06	0,02	0,00
Al₂O₃	58,09	58,37	57,98	57,78	58,47	58,29	58,32	58,62	58,34	58,52	58,60	58,71	58,13	58,58	58,39	58,32	58,04	57,91
Cr₂O₃	9,11	8,94	8,97	8,80	8,75	9,20	9,65	9,27	9,43	9,47	8,87	8,83	9,00	9,10	9,32	9,44	9,28	9,39
FeOt	11,97	11,78	11,79	12,22	12,30	12,10	11,90	11,98	11,96	11,82	11,97	11,74	12,05	11,98	12,15	12,33	12,24	12,40
MnO	0,19	0,03	0,24	0,26	0,10	0,17	0,04	0,04	0,10	0,09	0,07	0,03	0,08	0,12	0,14	0,12	0,06	0,17
MgO	19,12	19,23	19,14	19,07	18,94	19,17	19,10	18,99	19,50	19,63	18,89	18,90	19,19	19,25	19,20	19,39	18,89	18,81
P₂O₅	0,01	0,04	0,00	0,00	0,04	0,02	0,00	0,05	0,05	0,03	0,00	0,02	0,00	0,00	0,00	0,05	0,00	0,02
NiO	0,29	0,46	0,31	0,27	0,26	0,42	0,29	0,34	0,32	0,40	0,27	0,37	0,37	0,35	0,30	0,31	0,26	0,30
CaO	0,00	0,03	0,00	0,00	0,04	0,03	0,00	0,00	0,02	0,02	0,01	0,00	0,00	0,00	0,03	0,00	0,02	0,00
BaO	0,03	0,03	0,06	0,10	0,00	0,00	0,00	0,06	0,01	0,01	0,00	0,07	0,06	0,00	0,02	0,00	0,00	0,00
Na₂O	0,00	0,03	0,02	0,00	0,05	0,01	0,00	0,01	0,00	0,03	0,02	0,01	0,00	0,00	0,02	0,04	0,00	0,00
K₂O	0,00	0,00	0,00	0,00	0,02	0,00	0,01	0,00	0,00	0,04	0,02	0,01	0,02	0,02	0,00	0,02	0,01	0,06
F	n.a																	
Cl	0,01	0,00	0,00	0,02	0,00	0,00	0,01	0,01	0,00	0,00	0,00	0,02	0,01	0,00	0,00	0,00	0,00	0,01
V	0,13	0,08	0,02	0,03	0,10	0,06	0,07	0,02	0,11	0,04	0,01	0,07	0,07	0,01	0,06	0,14	0,05	0,12
Total	99,00	99,07	98,52	98,54	99,08	99,46	99,42	99,38	99,85	100,09	98,75	98,84	99,05	99,41	99,62	100,22	98,88	99,17
Cr#	9,52	9,32	9,40	9,27	9,12	9,57	9,99	9,59	9,78	9,79	9,22	9,17	9,41	9,44	9,67	9,80	9,69	9,81
Mg#	74,01	74,42	74,32	73,56	73,29	73,86	74,10	73,85	74,40	74,76	73,78	74,15	73,95	74,13	73,81	73,70	73,33	73,01
Fet#	25,99	25,58	25,68	26,44	26,71	26,14	25,90	26,15	25,60	25,24	26,22	25,85	26,05	25,87	26,19	26,30	26,67	26,99
Fe³⁺	0,02	0,02	0,02	0,03	0,02	0,02	0,01	0,01	0,02	0,03	0,01	0,01	0,02	0,02	0,03	0,01	0,02	
Fe²⁺	0,24	0,24	0,24	0,24	0,25	0,24	0,25	0,25	0,24	0,23	0,25	0,25	0,24	0,24	0,24	0,25	0,25	

Table S5. Continued.

Rock type	sp-lherz	sp-lherz
Sample	1A-81B	1A-81B
Point	103	104
Info	sp_11_c	sp_11_r
SiO₂	0,00	0,01
TiO₂	0,00	0,02
Al₂O₃	58,27	58,36
Cr₂O₃	9,64	9,01
FeOt	12,36	12,02
MnO	0,00	0,04
MgO	18,98	19,14
P₂O₅	0,00	0,02
NiO	0,35	0,28
CaO	0,00	0,04
BaO	0,11	0,00
Na₂O	0,01	0,02
K₂O	0,00	0,00
F	n.a	n.a
Cl	0,02	0,02
V	0,04	0,06
Total	99,79	99,03
Cr#	9,99	9,39
Mg#	73,23	73,96
Fet#	26,77	26,04
Fe³⁺	0,02	0,02
Fe²⁺	0,25	0,24

Table S5. Continued.

Rock type	sp-lherz													
Sample	1A-81C													
Point	96	146	148	149	156	157	158	159	160	161	166	167	172	
Info	sp_1_c	sp_3_c	sp_4_c	sp_4_r	sp_5_c	sp_5_r	sp_6_c	sp_6_r	sp_7_c	sp_7_r	sp_8_c	sp_8_r	sp_9_c	sp_9_r
SiO₂	0,00	0,00	0,00	0,00	0,00	0,00	0,00	0,00	0,00	0,00	0,00	0,00	0,00	0,00
TiO₂	0,01	0,00	0,16	0,09	0,00	0,00	0,03	0,03	0,20	0,10	0,00	0,14	0,11	0,01
Al₂O₃	57,93	57,82	57,94	58,07	57,89	57,76	57,74	57,56	57,63	57,95	58,36	58,58	58,31	58,17
Cr₂O₃	10,01	9,95	9,22	9,69	9,32	9,42	9,60	9,42	9,44	9,66	9,93	9,58	9,94	9,91
FeOt	12,21	12,41	12,25	12,09	12,23	12,15	12,12	12,30	12,17	12,41	12,04	12,12	12,08	12,08
MnO	0,22	0,14	0,03	0,15	0,15	0,07	0,14	0,11	0,15	0,08	0,08	0,13	0,12	0,11
MgO	19,19	19,13	19,09	19,06	19,41	19,22	19,22	19,07	19,13	19,26	18,92	18,99	19,14	19,47
P₂O₅	n.a	n.a												
NiO	0,32	0,33	0,36	0,31	0,39	0,34	0,43	0,37	0,36	0,28	0,43	0,33	0,34	0,38
CaO	0,00	0,00	0,01	0,02	0,00	0,00	0,00	0,01	0,00	0,00	0,02	0,00	0,00	0,01
BaO	n.a	n.a												
Na₂O	0,00	0,00	0,01	0,03	0,00	0,00	0,00	0,00	0,00	0,03	0,01	0,03	0,00	0,00
K₂O	0,01	0,00	0,00	0,01	0,00	0,00	0,01	0,00	0,00	0,00	0,00	0,01	0,01	0,01
F	n.a	n.a												
Cl	0,01	0,00	0,00	0,01	0,00	0,00	0,00	0,01	0,01	0,00	0,01	0,01	0,02	0,00
V	0,08	0,08	0,07	0,06	0,09	0,02	0,06	0,04	0,09	0,10	0,04	0,05	0,11	0,09
Total	99,97	99,86	99,14	99,59	99,49	98,98	99,35	98,91	99,18	99,87	99,84	99,95	100,16	100,25
Cr#	10,39	10,35	9,65	10,07	9,75	9,86	10,04	9,89	9,90	10,06	10,25	9,89	10,26	10,26
Mg#	73,69	73,32	73,54	73,76	73,87	73,82	73,87	73,44	73,70	73,44	73,68	73,62	73,85	74,18
Fet#	26,31	26,68	26,46	26,24	26,13	26,18	26,13	26,56	26,30	26,56	26,32	26,38	26,15	25,82
Fe³⁺	0,02	0,02	0,02	0,02	0,03	0,02	0,02	0,03	0,02	0,02	0,01	0,01	0,02	
Fe²⁺	0,24	0,25	0,25	0,25	0,24	0,24	0,24	0,24	0,25	0,25	0,26	0,25	0,24	

Table S5. Continued.

Rock type	grt-wehr	grt-wehr	grt-wehr	grt-wehr	grt-wehr	grt-wehr
Sample	1B-139B	1B-139B	1B-139B	1B-139B	1B-139B	1B-139B
Point	80	81	82	83	86	87
Info*	sp_1_c	sp_1_r	sp_2_c	sp_2_r	sp_5_c	sp_5_r
SiO₂	0,13	0,15	0,12	0,19	0,11	0,14
TiO₂	5,04	5,09	5,08	4,90	4,84	4,79
Al₂O₃	10,53	10,61	10,82	10,74	10,32	10,28
Cr₂O₃	44,74	44,29	44,03	44,35	44,93	44,79
FeOt	26,07	26,15	26,23	26,06	25,89	25,85
MnO	0,38	0,41	0,38	0,37	0,36	0,34
MgO	12,19	12,23	12,19	12,18	12,50	12,05
P₂O₅	n.a	n.a	n.a	n.a	n.a	n.a
NiO	0,18	0,18	0,08	0,06	0,19	0,23
CaO	0,00	0,03	0,01	0,00	0,00	0,00
BaO	n.a	n.a	n.a	n.a	n.a	n.a
Na₂O	0,00	0,00	0,00	0,03	0,01	0,04
K₂O	0,00	0,00	0,01	0,01	0,00	0,00
F	n.a	n.a	n.a	n.a	n.a	n.a
Cl	0,02	0,01	0,01	0,02	0,02	0,01
V	0,27	0,29	0,24	0,21	0,21	0,22
Total	99,55	99,43	99,19	99,11	99,38	98,74
Cr#	74,02	73,68	73,18	73,49	74,50	74,50
Mg#	45,47	45,47	45,31	45,44	46,25	45,38
Fet#	54,53	54,53	54,69	54,56	53,75	54,62
Fe³⁺	0,19	0,19	0,19	0,19	0,21	0,20
Fe²⁺	0,52	0,52	0,52	0,52	0,50	0,51

* Spinel around garnet.

Table S6. Major elements of each analyzed garnet from the Catalão xenoliths.

Rock type	grt-wehr														
Sample	1B-139A														
Point	8	9	10	11	42	43	50	82	83	85	89	90	92	96	97
Info	grt_4_c1	grt_4_c2	grt_4_r1	grt_4_r2	grt_5_c	grt_5_r	grt_6_c	grt_1_c1	grt_1_c2	grt_1_r2	grt_2_c1	grt_2_c2	grt_2_r2	grt_3_c1	grt_3_c2
SiO₂	41,64	41,16	41,27	41,89	41,87	41,73	41,63	41,75	41,48	41,41	41,27	41,40	41,72	41,67	41,81
TiO₂	0,00	0,24	0,07	0,09	0,21	0,00	0,33	0,03	0,09	0,00	0,00	0,14	0,00	0,03	0,11
Al₂O₃	19,43	19,63	19,26	19,19	18,91	18,88	19,32	19,45	19,68	19,07	19,48	19,51	19,53	19,51	19,50
Cr₂O₃	5,05	4,97	5,62	5,54	5,08	5,14	5,32	5,25	5,16	5,78	5,26	5,47	5,28	5,56	5,82
FeOt	8,35	8,49	8,61	8,24	8,74	8,88	8,54	8,43	8,15	8,37	8,36	8,31	8,45	8,34	8,31
MnO	0,45	0,51	0,51	0,58	0,45	0,57	0,30	0,47	0,56	0,59	0,31	0,55	0,60	0,36	0,32
MgO	19,16	19,50	19,39	19,28	19,61	19,58	19,30	19,25	19,54	19,19	18,87	18,96	19,11	19,09	18,85
NiO	0,00	0,00	0,00	0,03	0,02	0,00	0,02	0,08	0,00	0,00	0,00	0,01	0,01	0,01	0,01
CaO	5,28	5,23	5,27	5,38	5,37	5,46	5,27	5,13	5,23	5,42	5,30	5,31	5,27	5,38	5,31
Na₂O	0,00	0,02	0,00	0,04	0,04	0,09	0,05	0,05	0,04	0,03	0,00	0,02	0,03	0,02	0,02
K₂O	0,02	0,03	0,00	0,01	0,17	0,14	0,29	0,02	0,02	0,03	0,00	0,01	0,02	0,01	0,00
Cl	0,02	0,00	0,00	0,03	0,02	0,02	0,00	0,00	0,00	0,01	0,00	0,00	0,01	0,01	0,02
V	0,02	0,08	0,08	0,06	0,05	0,04	0,08	0,08	0,03	0,09	0,06	0,04	0,07	0,04	0,05
Total	99,41	99,85	100,09	100,35	100,53	100,52	100,44	99,98	99,98	99,97	98,91	99,73	100,08	100,03	100,12
Py %	68,68	68,87	68,51	68,62	68,50	67,96	68,81	68,91	69,32	68,24	68,51	68,31	68,29	68,55	68,53
Al %	16,80	16,84	17,07	16,45	17,13	17,29	17,08	16,93	16,22	16,71	17,02	16,79	16,95	16,81	16,94
Sp %	0,92	1,02	1,03	1,17	0,89	1,12	0,60	0,95	1,13	1,19	0,64	1,13	1,21	0,73	0,66
Gr %	13,60	13,27	13,39	13,77	13,48	13,63	13,52	13,20	13,34	13,86	13,83	13,76	13,55	13,90	13,87
Mg#	80,35	80,36	80,06	80,66	80,00	79,72	80,11	80,28	81,04	80,33	80,10	80,27	80,12	80,31	80,18

Table S6. Continued.

Rock type	grt-wehr	grt-wehr
Sample	1B-139A	1B-139A
Point	98	99
Info	grt_3_r1	grt_3_r2
SiO₂	41,78	41,43
TiO₂	0,09	0,00
Al₂O₃	19,28	19,41
Cr₂O₃	5,76	5,15
FeOt	8,32	8,44
MnO	0,47	0,44
MgO	18,78	18,98
NiO	0,04	0,00
CaO	5,30	5,08
Na₂O	0,01	0,05
K₂O	0,01	0,00
Cl	0,00	0,00
V	0,06	0,05
Total	99,89	99,03
Py %	68,23	68,73
Al %	16,97	17,14
Sp %	0,96	0,90
Gr %	13,84	13,22
Mg#	80,08	80,04

Table S6. Continued.

Rock type	grt-wehr														
Sample	1B-139B														
Point	1	2	3	4	27	28	68	69	70	71	102	103	105	106	107
Info	grt_1_c	grt_1_r	grt_1_c1	grt_1_r1	grt_2_c	grt_2_r	grt_3_a	grt_3_b	grt_3_c	grt_3_d	grt_3_c1	grt_3_c2	grt_3_r1	grt_3_r2	grt_3_r3
SiO₂	41,58	41,13	41,23	41,24	41,69	41,28	41,59	41,55	41,65	41,48	41,48	41,47	41,09	41,45	41,64
TiO₂	0,00	0,01	0,00	0,02	0,14	0,00	0,29	0,00	0,04	0,02	0,00	0,06	0,13	0,00	0,01
Al₂O₃	19,54	19,79	19,76	19,69	19,43	19,43	19,09	18,91	18,91	19,19	19,71	19,13	18,81	19,28	18,72
Cr₂O₃	4,99	5,13	4,99	4,88	5,24	5,31	5,45	5,54	5,49	5,50	5,39	5,47	5,49	5,15	5,35
FeOt	8,48	8,32	8,26	8,42	8,59	8,38	8,34	8,29	8,39	8,44	8,37	8,11	8,45	8,28	8,28
MnO	0,47	0,35	0,46	0,40	0,56	0,55	0,37	0,35	0,22	0,37	0,39	0,32	0,30	0,44	0,44
MgO	19,28	19,33	19,12	18,96	19,19	19,24	18,95	19,08	18,68	18,87	18,95	18,88	19,07	19,04	18,73
NiO	0,00	0,00	0,05	0,01	0,00	0,00	0,00	0,00	0,00	0,00	0,02	0,06	0,00	0,00	0,00
CaO	5,56	5,29	5,25	5,24	5,27	5,34	5,43	5,29	5,48	5,20	5,30	5,39	5,41	5,37	5,31
Na₂O	0,04	0,02	0,02	0,01	0,03	0,00	0,00	0,06	0,01	0,05	0,20	0,01	0,04	0,02	0,02
K₂O	0,04	0,02	0,00	0,00	0,00	0,00	0,01	0,02	0,00	0,03	0,05	0,02	0,00	0,00	0,00
Cl	0,00	0,02	0,01	0,01	0,00	0,01	0,01	0,00	0,00	0,00	0,00	0,00	0,00	0,00	0,00
V	0,04	0,07	0,05	0,03	0,05	0,09	0,08	0,09	0,07	0,04	0,08	0,07	0,02	0,04	0,06
Total	99,98	99,46	99,18	98,91	100,15	99,61	99,62	99,11	98,93	99,15	99,75	98,98	98,78	99,05	98,56
Py %	68,13	69,02	68,80	68,49	68,26	68,48	68,31	68,79	68,06	68,47	68,45	68,70	68,41	68,50	68,26
Al %	16,81	16,67	16,69	17,08	17,14	16,75	16,31	16,78	17,15	17,19	16,97	16,55	17,01	16,71	16,93
Sp %	0,95	0,71	0,93	0,82	1,13	1,11	0,75	0,71	0,45	0,77	0,81	0,66	0,61	0,89	0,91
Gr %	14,11	13,59	13,58	13,62	13,48	13,66	14,07	13,71	14,34	131,57	13,77	14,09	13,96	13,90	13,90
Mg#	80,21	80,54	80,48	80,04	79,93	80,35	80,19	80,39	79,87	79,93	80,14	80,58	80,08	80,39	80,13

Table S7. Major elements of each analyzed phlogopite from the Catalão xenoliths.

Rock type	grt-wehr														
Sample	1B-139A														
Point	70	86	87	88	93	94	95	102	103	105	106	107	12	13	14
Info	phl_43_c	phl_1_c	phl_2_c	phl_3_c	phl_4_c	phl_5_c	phl_6_c	phl_7_c	phl_8_c	phl_10_c	phl_11_c	phl_12_c	phl_13_c	phl_14_c	phl_15_c
Phl type	Phl1	Phl2													
SiO₂	39,60	38,77	38,74	39,09	39,18	38,73	38,60	39,22	38,64	38,83	39,39	39,55	38,81	38,84	39,32
TiO₂	0,87	3,19	3,33	3,15	3,37	3,19	3,20	3,93	3,69	3,62	3,81	3,86	3,73	3,52	3,31
Al₂O₃	14,48	14,35	14,45	14,24	14,46	14,78	14,63	14,11	14,56	14,64	14,55	14,33	13,39	13,74	13,66
Cr₂O₃	0,59	2,56	2,74	2,74	2,63	2,56	2,42	2,39	2,42	2,16	2,23	2,30	2,09	2,06	2,02
FeOt	4,07	4,87	4,91	4,15	4,54	4,79	4,55	4,31	4,36	4,50	4,52	4,46	4,42	4,23	4,23
MnO	0,00	0,06	0,00	0,05	0,07	0,05	0,04	0,00	0,00	0,00	0,05	0,04	0,12	0,04	0,08
MgO	23,46	21,84	21,22	21,63	21,25	21,42	21,18	22,09	22,19	22,00	22,01	22,17	21,88	21,87	21,80
P₂O₅	0,04	n.a.													
NiO	0,15	0,14	0,09	0,09	0,12	0,00	0,05	0,14	0,15	0,11	0,05	0,11	0,18	0,14	0,11
CaO	0,00	0,01	0,02	0,02	0,00	0,07	0,02	0,02	0,07	0,00	0,02	0,03	0,00	0,01	0,01
BaO	0,12	n.a.													
Na₂O	0,17	0,10	0,23	0,18	0,14	0,19	0,17	0,24	0,18	0,17	0,20	0,17	0,21	0,27	0,11
K₂O	10,31	10,33	10,25	9,92	9,71	10,24	10,01	10,23	9,65	10,42	10,39	10,37	10,38	10,50	10,57
F	0,63	0,92	0,29	0,26	0,35	0,27	0,29	0,38	0,87	0,36	0,50	0,31	0,34	0,37	0,66
Cl	0,02	0,04	0,03	0,03	0,02	0,00	0,01	0,01	0,01	0,03	0,01	0,03	0,03	0,02	0,01
V	0,00	0,11	0,07	0,17	0,10	0,17	0,11	0,08	0,17	0,14	0,08	0,08	0,04	0,02	0,15
Total	94,51	97,30	96,36	95,69	95,93	96,45	95,26	97,17	96,96	96,99	97,80	97,80	95,61	95,62	96,02

Table S7. Continued.

Rock type	grt-wehr														
Sample	1B-139A	1A-139A	1A-139A												
Point	15	16	17	18	19	44	45	52	53	54	55	1	2	3	4
Info	phl_16_c	pjh_17_c	pjh_18_c	pjh_19_c	pjh_20_c	pjh_21_c	pjh_21_r	pjh_22_c	pjh_22_r	pjh_23_c	pjh_23_r	pjh_24_c	pjh_24_r	pjh_25_c	pjh_25_r
Phl type	Phl2														
SiO₂	38,61	39,61	39,42	39,16	39,22	39,23	39,11	39,87	39,47	39,87	39,64	38,54	39,41	39,11	38,95
TiO₂	3,21	3,32	3,88	3,59	3,75	3,85	3,53	3,41	3,31	3,30	3,20	4,63	4,36	4,30	4,33
Al₂O₃	13,94	13,38	13,78	13,33	13,61	13,52	13,38	13,41	13,37	13,43	13,38	14,24	14,07	13,96	13,55
Cr₂O₃	2,98	2,90	2,48	2,04	2,53	2,11	2,66	2,54	2,06	2,78	2,73	2,17	2,18	2,37	2,49
FeOt	4,18	4,19	4,14	4,43	4,26	3,91	3,87	3,85	3,65	3,70	3,82	5,51	5,18	4,89	5,17
MnO	0,00	0,03	0,00	0,10	0,14	0,04	0,05	0,02	0,00	0,04	0,06	0,00	0,00	0,00	0,00
MgO	21,78	22,08	22,09	22,28	22,23	22,61	22,64	22,80	22,73	22,55	22,57	19,50	20,36	20,53	20,36
P₂O₅	n.a.	0,01	0,00	0,00	0,00										
NiO	0,08	0,15	0,14	0,14	0,23	0,19	0,22	0,13	0,24	0,12	0,35	0,07	0,08	0,10	0,08
CaO	0,00	0,00	0,00	0,00	0,00	0,01	0,00	0,03	0,00	0,02	0,03	0,02	0,04	0,01	0,02
BaO	n.a.	0,00	0,00	0,00	0,00										
Na₂O	0,16	0,27	0,13	0,13	0,18	0,15	0,09	0,17	0,13	0,19	0,16	0,16	0,27	0,16	0,14
K₂O	10,48	10,46	10,79	10,37	10,43	10,23	10,51	10,27	10,35	10,16	10,18	9,69	9,05	9,88	10,03
F	0,61	0,60	0,40	0,50	0,45	0,47	0,59	0,50	0,61	0,77	0,72	0,42	0,30	0,23	0,45
Cl	0,00	0,01	0,02	0,02	0,03	0,01	0,02	0,02	0,02	0,05	0,04	0,01	0,02	0,02	0,01
V	0,07	0,08	0,07	0,01	0,08	0,10	0,11	0,08	0,05	0,02	0,14	0,05	0,03	0,10	0,02
Total	96,10	97,08	97,34	96,11	97,13	96,41	96,78	97,10	95,98	96,99	97,03	95,01	95,33	95,66	95,60

Table S7. Continued.

Rock type	grt-wehr	grt-wehr	grt-wehr	grt-wehr	grt-wehr	grt-wehr	grt-wehr	grt-wehr	grt-wehr	grt-wehr	grt-wehr	grt-wehr	grt-wehr	grt-wehr
Sample	1A-139A	1A-139A	1A-139A	1A-139A	1A-139A	1A-139A	1A-139A	1A-139A	1A-139A	1A-139A	1A-139A	1A-139A	1A-139A	1A-139A
Point	5	8	12	13	14	15	16	17	18	19	20	21	23	25
Info	p _{hl_26_c}	p _{hl_27_c}	p _{hl_28_c}	p _{hl_29_r}	p _{hl_29_r}	p _{hl_30_c1}	p _{hl_30_c2}	p _{hl_30_c3}	p _{hl_30_c4}	p _{hl_30_c5}	p _{hl_30_c6}	p _{hl_30_c7}	p _{hl_31_r}	p _{hl_32_r}
Phl type	Phl2	Phl2	Phl2	Phl2	Phl2	Phl2	Phl2	Phl2	Phl2	Phl2	Phl2	Phl2	Phl2	Phl2
SiO₂	39,48	39,43	39,10	38,76	38,49	39,04	39,29	39,34	38,94	38,80	38,67	39,10	38,97	39,60
TiO₂	4,88	4,28	4,36	4,39	3,97	3,28	4,27	3,74	4,28	4,37	4,05	4,20	4,16	4,24
Al₂O₃	13,40	12,97	13,95	13,78	14,14	15,12	13,55	13,19	13,25	13,52	14,58	14,61	14,01	13,35
Cr₂O₃	1,85	2,32	2,30	2,97	2,59	3,02	2,68	2,45	3,01	2,71	2,79	1,93	2,73	2,64
FeOt	5,24	5,08	4,95	4,65	5,16	4,81	4,73	4,66	4,51	4,67	4,65	5,39	4,51	4,79
MnO	0,00	0,00	0,00	0,00	0,00	0,00	0,00	0,00	0,00	0,00	0,00	0,00	0,00	0,00
MgO	20,67	20,99	20,13	19,39	20,91	19,32	20,18	21,62	20,95	20,87	20,36	19,75	20,37	20,05
P₂O₅	0,04	0,00	0,01	0,01	0,02	0,05	0,02	0,00	0,00	0,03	0,00	0,01	0,01	0,00
NiO	0,10	0,10	0,13	0,15	0,07	0,04	0,12	0,08	0,15	0,07	0,07	0,08	0,08	0,18
CaO	0,04	0,02	0,02	0,02	0,15	0,07	0,05	0,04	0,00	0,03	0,03	0,01	0,02	0,00
BaO	0,00	0,00	0,00	0,00	0,00	0,00	0,00	0,00	0,00	0,00	0,00	0,00	0,00	0,00
Na₂O	0,10	0,12	0,06	0,16	0,22	0,41	0,18	0,19	0,16	0,19	0,24	0,18	0,18	0,10
K₂O	9,79	9,73	10,17	10,12	9,77	10,17	10,00	9,40	10,33	10,33	10,18	10,19	10,30	10,44
F	0,56	0,55	0,50	1,05	0,50	0,71	0,45	0,53	0,51	0,42	0,27	0,39	0,40	0,42
Cl	0,01	0,01	0,01	0,05	0,01	0,02	0,02	0,02	0,02	0,01	0,02	0,02	0,02	0,02
V	0,08	0,03	0,02	0,02	0,08	0,08	0,06	0,04	0,06	0,02	0,05	0,08	0,07	0,03
Total	96,22	95,61	95,71	95,52	96,07	96,13	95,59	95,28	96,17	96,03	95,96	95,92	95,82	95,85

Table S7. Continued.

Rock type	grt-wehr	grt-wehr	grt-wehr	grt-wehr	grt-wehr	grt-wehr	grt-wehr	grt-wehr	grt-wehr	grt-wehr	grt-wehr	grt-wehr	grt-wehr	grt-wehr	grt-wehr
Sample	1A-139A	1A-139A	1A-139A	1A-139A	1A-139A	1A-139A	1A-139A	1A-139A	1A-139A	1A-139A	1A-139A	1A-139A	1A-139A	1A-139A	1A-139A
Point	26	27	28	29	30	31	32	33	35	37	39	40	42	43	44
Info	phl_32_c1	phl_32_c2	phl_32_c3	phl_32_r	phl_33_r	phl_33_c1	phl_33_c2	phl_33_r	phl_34_c	phl_34_r	phl_35_c1	phl_35_c2	phl_35_r	phl_36_c1	phl_36_c2
Phl type	Phl2	Phl2	Phl2	Phl2	Phl2	Phl2	Phl2	Phl2	Phl2	Phl2	Phl2	Phl2	Phl2	Phl2	Phl2
SiO₂	39,09	39,19	38,98	38,64	39,67	39,70	39,25	39,18	39,60	38,79	39,38	39,55	38,92	39,03	38,62
TiO₂	4,31	4,48	4,38	4,54	3,93	3,95	3,77	3,85	3,79	3,69	3,08	3,73	3,63	3,81	3,58
Al₂O₃	13,63	13,33	13,69	14,47	13,56	13,40	13,54	14,34	14,20	14,06	14,00	14,32	14,96	14,15	14,38
Cr₂O₃	2,31	2,07	2,98	2,45	1,87	1,86	2,02	2,04	1,95	2,75	1,98	2,50	3,06	2,82	3,21
FeOt	4,83	4,96	4,70	4,81	4,34	4,17	4,14	4,33	4,21	4,30	3,88	4,15	4,03	4,23	4,03
MnO	0,00	0,00	0,00	0,00	0,00	0,00	0,00	0,00	0,00	0,00	0,00	0,00	0,00	0,00	0,00
MgO	20,78	20,87	20,72	20,45	20,83	21,38	21,72	21,33	21,26	21,47	21,44	20,52	20,15	20,39	20,70
P₂O₅	0,00	0,04	0,01	0,03	0,00	0,02	0,03	0,01	0,02	0,00	0,00	0,02	0,00	0,01	0,05
NiO	0,08	0,09	0,06	0,08	0,13	0,11	0,16	0,14	0,18	0,14	0,18	0,15	0,14	0,09	0,13
CaO	0,00	0,00	0,01	0,02	0,01	0,00	0,01	0,05	0,02	0,01	0,01	0,00	0,02	0,04	0,04
BaO	0,00	0,00	0,00	0,00	0,00	0,00	0,00	0,00	0,00	0,00	0,00	0,00	0,00	0,00	0,00
Na₂O	0,14	0,11	0,14	0,12	0,14	0,21	0,17	0,20	0,17	0,14	0,23	0,26	0,18	0,18	0,16
K₂O	10,22	10,30	10,26	10,31	10,36	10,29	10,31	9,73	9,87	9,99	9,87	9,80	10,09	10,18	10,21
F	0,38	0,31	0,40	0,50	0,52	0,58	0,54	0,58	0,61	0,54	0,57	0,37	0,36	0,52	0,49
Cl	0,01	0,02	0,01	0,02	0,02	0,02	0,02	0,04	0,02	0,01	0,02	0,02	0,01	0,01	0,02
V	0,05	0,06	0,07	0,03	0,01	0,08	0,05	0,07	0,10	0,05	0,02	0,01	0,01	0,02	0,03
Total	95,85	95,83	96,41	96,45	95,39	95,77	95,71	95,87	96,00	95,94	94,64	95,40	95,56	95,47	95,65

Table S7. Continued.

Rock type	grt-wehr	grt-wehr	grt-wehr	grt-wehr	grt-wehr	grt-wehr	grt-wehr	grt-wehr	grt-wehr	grt-wehr	grt-wehr	grt-wehr	grt-wehr	grt-wehr
Sample	1A-139A	1A-139A	1A-139A	1A-139A	1A-139A	1A-139A	1A-139A	1A-139A	1A-139A	1A-139A	1A-139A	1A-139A	1A-139A	1A-139A
Point	45	46	47	48	49	50	51	52	53	54	55	56	57	58
Info	phl_36_c3	phl_37_r	phl_38_r	phl_38_c1	phl_38_c2	phl_38_c3	phl_38_r	phl_39_r	phl_39_c	phl_39_r	phl_40_r	phl_40_c1	phl_40_c2	phl_40_r
Phl type	Phl2	Phl2	Phl2	Phl2	Phl2	Phl2	Phl2	Phl2	Phl2	Phl2	Phl2	Phl2	Phl2	Phl2
SiO₂	39,48	39,40	39,16	39,47	39,45	39,47	39,05	38,76	38,54	38,94	39,53	39,10	39,43	39,76
TiO₂	3,80	2,88	2,87	2,61	2,83	2,82	2,71	2,80	2,84	2,59	2,85	2,78	2,85	2,80
Al₂O₃	14,20	14,07	14,71	13,95	14,02	14,09	13,86	14,47	14,57	14,69	14,42	13,84	13,95	14,11
Cr₂O₃	1,88	2,74	2,13	2,05	3,26	3,07	2,96	3,43	3,43	4,09	3,61	3,05	2,86	2,90
FeOt	4,26	4,12	3,89	3,74	3,99	4,12	4,13	3,99	4,12	4,27	4,18	3,99	3,91	4,01
MnO	0,00	0,00	0,00	0,00	0,00	0,00	0,00	0,00	0,00	0,00	0,00	0,00	0,00	0,00
MgO	21,21	21,41	21,73	23,02	21,68	21,76	22,35	21,69	21,62	20,33	21,04	21,06	21,71	21,12
P₂O₅	0,03	0,02	0,00	0,00	0,02	0,02	0,04	0,00	0,02	0,00	0,02	0,03	0,00	0,01
NiO	0,11	0,04	0,17	0,21	0,10	0,10	0,16	0,09	0,09	0,07	0,09	0,12	0,10	0,09
CaO	0,02	0,03	0,00	0,01	0,02	0,05	0,02	0,02	0,00	0,01	0,02	0,02	0,03	0,02
BaO	0,00	0,00	0,00	0,00	0,00	0,00	0,00	0,00	0,00	0,00	0,00	0,00	0,00	0,00
Na₂O	0,11	0,14	0,13	0,13	0,21	0,21	0,18	0,20	0,20	0,17	0,20	0,19	0,15	0,18
K₂O	10,24	9,88	10,09	10,28	9,69	9,95	10,18	10,38	10,43	10,37	10,06	10,54	10,19	10,03
F	0,61	0,63	0,46	0,52	0,50	0,43	0,51	0,58	0,50	0,46	0,57	0,55	0,54	0,59
Cl	0,02	0,02	0,02	0,02	0,02	0,02	0,01	0,01	0,02	0,01	0,02	0,04	0,02	0,02
V	0,00	0,04	0,01	0,02	0,03	0,07	0,07	0,01	0,03	0,05	0,04	0,04	0,01	0,06
Total	95,97	95,43	95,38	96,02	95,80	96,18	96,23	96,43	96,39	96,04	96,67	95,34	95,73	95,68

Table S7. Continued.

Rock type	grt-wehr	grt-wehr	grt-wehr	grt-wehr	grt-wehr	grt-wehr	grt-wehr	grt-wehr	grt-wehr	grt-wehr
Sample	1A-139A	1A-139A	1A-139A	1A-139A	1A-139A	1A-139A	1A-139A	1A-139A	1A-139A	1A-139A
Point	59	60	61	62	63	67	77	79	80	81
Info	phl_41_r	phl_41_c1	phl_41_c2	phl_41_c3	phl_41_r	phl_42_r	phl_44_c	phl_45_c1	phl_45_c2	phl_45_c3
Phl type	Phl2	Phl2	Phl2	Phl2	Phl2	Phl2	Phl2	Phl2	Phl2	Phl2
SiO₂	39,04	39,47	39,34	39,81	39,71	39,13	39,91	38,35	38,93	39,39
TiO₂	2,89	2,82	2,88	2,85	2,91	2,71	2,77	4,51	4,06	3,67
Al₂O₃	14,53	14,25	14,30	14,13	14,08	14,62	13,80	14,42	14,55	14,56
Cr₂O₃	3,20	3,07	3,32	3,31	3,02	2,56	2,69	2,29	3,03	2,85
FeOt	4,02	4,26	4,05	4,02	4,06	3,51	4,42	4,97	4,35	4,38
MnO	0,00	0,00	0,00	0,00	0,00	0,00	0,00	0,00	0,00	0,00
MgO	21,21	20,71	20,87	21,02	21,13	21,99	20,80	20,81	20,24	20,55
P₂O₅	0,01	0,00	0,00	0,00	0,04	0,00	0,00	0,00	0,02	0,03
NiO	0,12	0,14	0,12	0,09	0,13	0,11	0,16	0,08	0,08	0,13
CaO	0,02	0,03	0,01	0,01	0,01	0,00	0,03	0,01	0,00	0,05
BaO	0,00	0,00	0,00	0,00	0,00	0,00	0,00	0,00	0,00	0,00
Na₂O	0,18	0,24	0,17	0,16	0,18	0,10	0,20	0,29	0,20	0,17
K₂O	10,44	10,26	10,45	10,37	10,31	10,57	9,89	9,72	9,99	9,73
F	0,65	0,54	0,38	0,47	0,59	0,78	0,59	0,41	0,51	0,43
Cl	0,01	0,03	0,01	0,02	0,01	0,02	0,02	0,01	0,01	0,02
V	0,03	0,03	0,06	0,03	0,04	0,03	0,01	0,07	0,01	0,05
Total	96,34	95,84	95,96	96,28	96,21	96,13	95,29	95,96	95,99	96,00
										96,22

Table S7. Continued.

Rock type	grt-wehr														
Sample	1B-139B														
Point	19	21	23	24	32	33	34	35	37	38	39	40	6	7	8
Info	pht 7 c	pht 1 c	pht 1 r	pht 8 c	pht 9 c	pht 10 c	pht 11 c	pht 12 c	pht 13 c	pht 14 c	pht 15 c	pht 15 r	pht 6 c	pht 7 c	pht 16 r
Phl type	Phl1														
SiO₂	42,00	41,36	41,19	41,76	41,65	41,91	41,85	41,24	41,82	41,99	41,04	41,60	41,68	41,78	41,12
TiO₂	1,32	1,13	1,22	1,10	1,24	1,20	1,25	1,04	0,95	1,28	1,08	1,21	0,88	1,01	1,08
Al₂O₃	12,38	12,62	12,07	12,24	12,41	12,27	12,21	12,01	12,11	12,25	13,13	13,55	13,02	12,54	13,77
Cr₂O₃	0,77	0,64	0,55	0,45	0,88	0,68	0,72	0,66	0,78	0,78	0,97	0,98	0,66	0,67	0,65
FeOt	3,77	3,92	3,86	3,75	3,66	3,67	3,63	3,61	3,58	3,57	3,65	3,87	3,30	3,17	3,34
MnO	0,00	0,03	0,03	0,07	0,04	0,00	0,06	0,00	0,02	0,02	0,05	0,02	0,00	0,00	0,00
MgO	24,48	24,41	24,52	24,50	24,60	24,85	24,88	24,92	24,84	25,12	25,93	25,84	24,42	25,01	24,02
P₂O₅	n.a.	0,01	0,02	0,03											
NiO	0,21	0,21	0,17	0,12	0,19	0,21	0,17	0,15	0,19	0,18	0,21	0,13	0,14	0,16	0,19
CaO	0,00	0,06	0,02	0,05	0,09	0,02	0,01	0,01	0,00	0,04	0,01	0,00	0,03	0,07	0,11
BaO	n.a.	0,00	0,00	0,00											
Na₂O	0,16	0,19	0,13	0,11	0,12	0,17	0,11	0,16	0,21	0,19	0,17	0,20	0,20	0,33	0,33
K₂O	10,54	10,29	10,38	10,46	10,09	10,61	10,52	9,73	9,96	10,01	10,47	10,35	10,37	10,61	10,03
F	0,60	0,80	0,65	0,73	0,74	0,69	0,79	0,94	0,82	0,86	0,59	0,54	0,72	0,57	0,71
Cl	0,03	0,01	0,03	0,01	0,03	0,02	0,03	0,04	0,03	0,03	0,03	0,02	0,03	0,03	0,03
V	0,00	0,02	0,01	0,04	0,03	0,01	0,03	0,02	0,02	0,00	0,09	0,09	0,01	0,00	0,06
Total	96,27	95,69	94,82	95,37	95,78	96,30	96,24	94,53	95,31	96,32	97,42	98,39	95,46	95,94	95,48

Table S7. Continued.

Rock type	grt-wehr														
Sample	1B-139B	1B-139B	1B-139B	1B-139B	1B-139B	1A-139B									
Point	14	15	16	19	20	9	10	11	12	13	16	17	18	76	77
Info	phl_18_r	phl_18_c	phl_18_c	phl_19_c	phl_19_c	phl_1_c	phl_2_c	phl_2_r	phl_3_c	phl_3_r	phl_4_c	phl_4_r	phl_6_c	phl_16_c	phl_16_r
Phl type	Phl1	Phl1	Phl1	Phl1	Phl1	Phl2									
SiO₂	41,23	41,45	41,26	40,82	41,58	39,91	39,96	39,76	39,50	39,44	38,93	38,96	39,13	39,74	39,86
TiO₂	1,14	1,05	1,17	1,14	0,99	3,98	3,43	3,41	3,46	3,53	4,06	3,55	3,58	4,05	4,00
Al₂O₃	13,07	12,78	12,99	13,88	12,02	13,16	13,12	13,30	13,74	13,12	13,14	13,40	13,05	13,81	13,28
Cr₂O₃	0,72	0,66	0,69	0,70	0,72	2,59	2,22	2,23	2,62	2,94	2,59	2,68	2,59	3,03	2,98
FeOt	3,68	3,54	3,36	3,36	3,41	4,15	4,09	4,06	4,06	4,62	4,80	4,55	4,72	4,27	4,55
MnO	0,01	0,00	0,00	0,02	0,00	0,12	0,02	0,07	0,02	0,02	0,00	0,03	0,00	0,00	0,08
MgO	24,15	24,33	24,41	24,06	24,87	20,12	20,35	20,98	21,02	20,73	20,53	20,63	20,40	20,40	20,70
P₂O₅	0,03	0,00	0,00	0,00	0,00	n.a.									
NiO	0,21	0,18	0,22	0,24	0,20	0,14	0,13	0,11	0,09	0,10	0,13	0,05	0,23	0,07	0,10
CaO	0,02	0,03	0,01	0,01	0,05	0,02	0,00	0,03	0,04	0,00	0,02	0,02	0,05	0,00	0,02
BaO	0,00	0,00	0,00	0,25	0,00	n.a.									
Na₂O	0,26	0,20	0,16	0,23	0,22	0,08	0,10	0,14	0,24	0,22	0,22	0,05	0,13	0,27	0,12
K₂O	10,61	10,60	10,66	10,55	10,60	10,37	10,25	10,22	10,46	10,22	10,11	10,17	10,28	10,06	9,96
F	0,72	0,79	0,85	0,86	0,73	0,46	0,59	0,28	0,37	0,27	0,60	0,55	0,55	0,28	0,31
Cl	0,02	0,02	0,03	0,03	0,03	0,01	0,01	0,03	0,03	0,02	0,02	0,02	0,03	0,03	0,01
V	0,01	0,02	0,02	0,05	0,03	0,07	0,09	0,06	0,06	0,09	0,07	0,11	0,04	0,15	0,08
Total	95,87	95,66	95,81	96,20	95,43	95,16	94,33	94,67	95,70	95,31	95,22	94,76	94,79	96,16	96,02

Table S7. Continued.

Rock type	grt-wehr														
Sample	1A-139B														
Point	78	79	84	108	109	110	111	112	113	114	24	25	26	27	28
Info	phl_17_c	phl_17_c	phl_18_c	phl_28_c	phl_29_c	phl_29_r	phl_30_c	phl_30_r	phl_31_c	phl_31_r	phl_24_c	phl_25_c	phl_26_r	phl_27_r	phl_28_r
Phl type	Phl2														
SiO₂	39,08	39,55	39,73	39,34	39,44	39,00	39,50	39,50	39,71	39,34	39,79	38,45	39,29	42,50	39,72
TiO₂	4,53	4,51	4,46	3,69	3,62	3,76	3,68	3,62	3,66	3,73	3,70	3,09	2,97	2,58	2,86
Al₂O₃	13,76	13,70	13,32	13,97	13,71	13,62	13,45	13,76	13,69	13,70	13,06	14,55	13,78	13,79	13,60
Cr₂O₃	2,86	2,59	2,55	2,97	3,07	3,38	2,37	2,58	2,59	2,49	1,95	2,69	2,92	2,58	3,13
FeOt	4,42	4,50	4,28	4,53	4,29	4,36	4,13	4,40	4,32	4,19	4,25	4,12	4,18	3,62	3,99
MnO	0,02	0,03	0,14	0,00	0,01	0,02	0,00	0,00	0,09	0,03	0,00	0,00	0,00	0,00	0,00
MgO	20,30	20,23	20,15	20,10	20,42	20,49	20,61	20,35	20,85	20,27	21,55	21,33	21,17	19,54	21,25
P₂O₅	n.a.	0,01	0,02	0,01	0,00	0,02									
NiO	0,10	0,13	0,15	0,04	0,13	0,09	0,14	0,07	0,20	0,13	0,12	0,09	0,10	0,11	0,12
CaO	0,00	0,04	0,01	0,00	0,03	0,06	0,00	0,02	0,00	0,00	0,02	0,01	0,04	0,02	0,04
BaO	n.a.	0,00	0,00	0,00	0,00	0,00									
Na₂O	0,14	0,14	0,15	0,23	0,08	0,18	0,09	0,18	0,19	0,23	0,27	0,22	0,14	0,26	0,23
K₂O	10,21	10,19	10,25	9,92	10,19	9,98	10,22	10,07	9,99	10,17	10,38	10,45	10,42	9,75	10,44
F	0,32	0,25	0,29	0,47	0,39	0,41	0,53	0,40	0,43	0,62	0,51	0,50	0,48	0,61	0,44
Cl	0,01	0,03	0,01	0,01	0,02	0,01	0,02	0,02	0,02	0,03	0,01	0,01	0,02	0,01	0,03
V	0,12	0,10	0,13	0,12	0,10	0,04	0,11	0,07	0,13	0,11	0,00	0,07	0,01	0,02	0,02
Total	95,86	95,97	95,61	95,37	95,49	95,38	94,84	95,04	95,84	95,05	95,61	95,58	95,53	95,40	95,88

Table S7. Continued.

Rock type	grt-wehr									
Sample	1A-139B									
Point	29	32	33	34	35	36	37	38	39	40
Info	phl_29_c	phl_32_r	phl_33_c	phl_34_c	phl_35_c	phl_36_r	phl_37_r	phl_38_r	phl_39_r	phl_40_r
Phl type	Phl2									
SiO₂	40,29	39,39	40,38	40,22	39,42	39,22	38,60	39,33	39,14	38,62
TiO₂	3,01	2,93	2,89	2,94	2,93	4,33	4,40	4,38	4,68	4,33
Al₂O₃	13,10	13,23	13,16	13,07	13,98	13,27	13,54	13,40	13,34	14,36
Cr₂O₃	2,43	3,27	2,80	2,53	2,18	2,78	2,70	2,71	2,13	3,65
FeOt	3,96	4,19	3,85	3,94	3,94	4,89	4,98	5,20	5,29	5,11
MnO	0,00	0,00	0,00	0,00	0,00	0,00	0,00	0,00	0,00	0,00
MgO	21,65	21,80	21,23	21,51	21,86	20,37	19,87	19,46	20,17	18,92
P₂O₅	0,00	0,00	0,02	0,00	0,01	0,02	0,00	0,00	0,03	0,03
NiO	0,13	0,14	0,13	0,14	0,14	0,17	0,08	0,14	0,12	0,09
CaO	0,00	0,03	0,04	0,02	0,04	0,03	0,03	0,05	0,03	0,06
BaO	0,00	0,00	0,00	0,00	0,00	0,00	0,00	0,00	0,00	0,00
Na₂O	0,17	0,20	0,23	0,20	0,25	0,22	0,18	0,27	0,11	0,17
K₂O	10,39	10,37	10,50	10,40	10,40	10,41	10,40	10,29	10,34	10,21
F	0,55	0,38	0,46	0,54	0,62	0,41	0,35	0,30	0,38	0,39
Cl	0,03	0,01	0,02	0,02	0,02	0,01	0,01	0,02	0,01	0,02
V	0,03	0,01	0,03	0,03	0,06	0,03	0,04	0,07	0,06	0,04
Total	95,73	95,94	95,73	95,56	95,84	96,16	95,17	95,63	95,84	96,00
										95,69

Table S8. Trace elements of each analyzed olivine from the Catalão xenoliths

Rock type	sp-lherz						
Sample	1A-76A	1A-76A	1A-76A	1A-76A	1A-76A	1A-76A	1A-76B
Spot	Ol1	Ol2	Ol3	Ol4	Ol5	Ol6	Ol1
Li	1,59	1,484	1,536	1,76	1,66	1,71	1,73
B	0,32	0,4	0,51	0,45	0,46	0,3	0,36
Sc	0,862	0,946	0,936	0,99	0,977	1,02	0,88
Ca	13	24	10	18	25	29	23
Ti	4,22	3,46	4,27	4,95	4,19	11,9	21
V	0,231	0,177	0,22	0,218	0,24	0,226	0,209
Cr	1,96	2,22	1,94	1,58	1,04	2,6	3,05
Co	135,6	131,4	135,5	139	137,1	137,5	144
Ni	2840	2910	2890	3000	2950	2930	3040
Cu					0,075	0,045	
Zn	28,5	25,6	27,1	28,8	30,1	35,5	29,7
Rb							
Sr					0,0215		
Y							
Zr							
Nb	0,0018						
Cs							
Ba						0,0088	
La				0,000	0,002	0,001	
Ce	0,001	0,001			0,004		
Pr						0,001	
Nd							
Sm							
Eu		0,001					
Gd		0,003					
Tb							
Dy		0,006					
Ho							
Er							
Tm							
Yb				0,004	0,004		0,006
Lu		0,001	0,001		0,001	0,001	0,002
Hf							
Ta	0,001						
Pb	0,009	0,007			0,049	0,020	
Th							
U							

Table S8. Continued.

Rock type	sp-lherz						
Sample	1A-76B	1A-76B	1A-76B	1A-76B	1A-76B	1A-76C	1A-76C
Spot	Ol2	Ol3	Ol4	Ol5	Ol6	Ol1	Ol2
Li	1,83	1,77	1,61	1,58	1,68	1,789	1,597
B	0,42		0,33	0,35	0,39	0,48	0,353
Sc	0,97	0,95	1,107	1,16	1,09	0,902	0,92
Ca	17	14	31	38	34	11	20
Ti	5,09	3,22	4,31	5,31	2,99	4,62	5,67
V	0,202	0,231	0,275	0,253	0,252	0,151	0,168
Cr	2,27	1,6	2,55	1,8	1,59	1,41	2,21
Co	138	136	145	139	143	126,5	124,6
Ni	2980	2940	3050	2890	3050	3060	2940
Cu							
Zn	27,3	28,2	30,8	31,1	31,7	25,8	24,6
Rb							
Sr							0,0142
Y				0,0022	0,0022	0,0028	0,0019
Zr							
Nb						0,014	0,0073
Cs							
Ba							0,0112
La	0,005	0,000				0,007	0,006
Ce	0,008					0,011	0,008
Pr	0,001						
Nd							
Sm							
Eu							
Gd							0,005
Tb							
Dy		0,004					
Ho							
Er							
Tm		0,001					
Yb	0,005	0,003	0,007	0,004			
Lu		0,001		0,001	0,001		0,001
Hf							
Ta							
Pb		0,010	0,008			0,074	0,022
Th						0,001	0,001
U						0,001	0,001

Table S8. Continued.

Rock type	sp-lherz	sp-lherz	sp-lherz	sp-lherz	harz	harz	harz
Sample	1A-76C	1A-76C	1A-76C	1A-76C	1A-81	1A-81	1A-81
Spot	Ol3	Ol4	Ol5	Ol6	Ol1	Ol2	Ol3
Li	1,877	1,62	1,594	1,48	1,386	1,401	1,203
B	0,49	0,45	0,44	0,34	0,67	0,76	0,6
Sc	0,959	1,102	1,101	1,08	1,432	1,356	1,454
Ca	12	35	27	30,9	31	25	45
Ti		4,56	4,78	4,42	18,7	29,6	15,49
V	0,372	0,244	0,293	0,217	0,689	0,776	0,653
Cr		2,17	3,2	2,21	5,5	7,7	6,8
Co	133,4	135,6	137,1	133	131,2	132,9	122,5
Ni	3020	2920	3000	2960	2940	3030	2871
Cu	0,044				0,088	0,087	
Zn	27,6	26,6	27,9	27	44	46,1	45
Rb							
Sr					0,034	0,025	0,020
Y	0,0035	0,0048					
Zr							
Nb					0,328	0,188	0,214
Cs							
Ba					0,006	0,009	
La	0,003	0,000		0,001	0,027	0,017	0,019
Ce	0,006	0,001		0,002	0,022	0,015	0,014
Pr					0,002		
Nd							
Sm							
Eu							
Gd							
Tb							
Dy	0,003					0,007	
Ho					0,001		
Er					0,003		
Tm	0,001				0,001		
Yb	0,005	0,003				0,003	
Lu	0,001	0,001		0,000	0,001	0,001	
Hf							0,003
Ta					0,001		
Pb			0,012	0,012	0,023		
Th					0,019	0,011	0,007
U	0,001				0,016	0,005	0,010

Table S8. Continued.

Rock type	harz	harz	sp-lherz	sp-lherz	sp-lherz	sp-lherz	sp-lherz
Sample	1A-81	1A-81	1A-81A	1A-81A	1A-81A	1A-81A	1A-81A
Spot	Ol4	Ol5	Ol1	Ol2	Ol3	Ol4	Ol5
Li	1,322	1,31	1,952	1,661	1,63	1,757	1,561
B	0,54	0,5	0,46	0,4	0,6	0,51	0,31
Sc	1,317	1,251	0,921	0,943	1,03	1,066	0,887
Ca	45	33	18	17	23	9	12,8
Ti	45,7		4,08	3,92	3,62	3,91	4,69
V	0,925	0,751	0,29	0,303	0,262	0,322	0,286
Cr	9,4	8,4	2,8	2,5	2,67	3,3	2,83
Co	129,4	127,8	136,1	130,9	135	135,2	130,7
Ni	3040	2840	2940	2878	2963	2980	2854
Cu	0,063	0,053		0,065			
Zn	46,4	41,8	29,2	27,6	27,6	27,3	28,4
Rb							
Sr	0,025	0,048					
Y	0,0038						
Zr							
Nb	0,120	0,102				0,0018	
Cs							
Ba					0,0092	0,008	
La	0,018	0,007					
Ce	0,011	0,005		0,001		0,001	
Pr							
Nd							
Sm							
Eu							
Gd				0,005			
Tb							
Dy					0,005		
Ho	0,001						
Er							
Tm							
Yb					0,005		
Lu	0,000				0,001		
Hf						0,004	
Ta							
Pb	0,047	0,025					
Th	0,015	0,004					
U	0,010	0,004					

Table S8. Continued.

Rock type	sp-lherz						
Sample	1A-81B	1A-81B	1A-81B	1A-81B	1A-81B	1A-81C	1A-81C
Spot	Ol1	Ol2	Ol3	Ol4	Ol5	Ol3	Ol4
Li	1,735	1,73	1,846	1,87	1,79	1,69	1,623
B	0,57			0,53	0,42	0,31	0,45
Sc	0,88	0,854	0,847	0,818	1,099	1,09	1,07
Ca	12		12	5	29	29	25,6
Ti	9	40,5	3,82	2,89	4,36	15,7	3,96
V	0,266	0,31	0,249	0,266	0,286	0,233	0,232
Cr	1,5	2,5		3,1	0,4	2,2	1,4
Co	134,2	134,4	134,1	132	131	137,4	134,2
Ni	3050	2990	2990	2930	2870	2997	3020
Cu			0,051	0,059			
Zn	27,1	30	29,1	29,5	28,8	28,7	27,8
Rb							
Sr							
Y				0,0045	0,0063		
Zr							
Nb				0,0015			
Cs							
Ba							
La				0,000			
Ce							
Pr							
Nd							
Sm							
Eu							
Gd							
Tb							
Dy							
Ho							
Er							
Tm			0,001		0,002		
Yb					0,003		
Lu	0,004						
Hf							
Ta						0,001	
Pb							
Th							
U							

Table S8. Continued.

Rock type	sp-lherz	grt-wehr	grt-wehr	grt-wehr	grt-wehr	grt-wehr	grt-wehr
Sample	1A-81C	1B-139A	1B-139A	1B-139A	1B-139A	1B-139A	1B-139A
Spot	Ol5	Ol1	Ol2	Ol3	Ol4	Ol5	Ol6
Li	1,692	1,947	1,937	1,9	1,819	1,9	1,913
B	0,43	0,66	0,35	0,39	0,33	0,68	0,6
Sc	1,106	1,301	1,28	1,292	1,31	1,26	1,33
Ca	2	323	330	342	329	292	325
Ti	2,86	105,1	100,6	84,7	69,1	104,8	104,3
V	0,3	7,06	6,85	7,14	6,81	7,07	6,99
Cr	2	255,2	244,4	217,9	213,8	195,7	214
Co	136,7	133,1	127,9	133,2	129,9	134,2	130,5
Ni	2900	2940	2851	2910	2840	2880	2884
Cu		2,47	2,46	2,31	2,35	2,49	2,51
Zn	29,1	76,6	75	76,8	74,2	77,7	77,4
Rb					0,0183		
Sr	0,0138						
Y		0,0072	0,0072	0,0053	0,0064	0,0085	0,0064
Zr		1,160	1,150	1,099	1,059	1,129	1,082
Nb		0,301	0,314	0,322	0,312	0,294	0,284
Cs							
Ba			0,049	0,021			
La				0,004		0,001	
Ce				0,010		0,002	0,001
Pr							
Nd							
Sm							
Eu							
Gd							
Tb							
Dy						0,004	
Ho		0,001					
Er				0,002			
Tm							
Yb							
Lu	0,002						
Hf		0,025	0,031	0,023	0,023	0,025	0,019
Ta		0,022	0,017	0,022	0,017	0,023	0,019
Pb							
Th							
U							

Table S8. Continued.

Rock type	grt-wehr	grt-wehr	grt-wehr	grt-wehr	grt-wehr
Sample	1B-139B	1B-139B	1B-139B	1B-139B	1B-139B
Spot	Ol1	Ol2	Ol3	Ol4	Ol5
Li	2,05	1,92	2,19	1,99	1,988
B	0,78	0,47	0,39	0,46	0,75
Sc	1,29	1,291	1,266	1,346	1,343
Ca	292	335	339	324	320
Ti	113	108,9	102,2	110	106,4
V	7,17	7,09	7,11	7,25	7,36
Cr	251	237,9	228,3	241,6	242,4
Co	133,4	129,6	131,4	133	131,1
Ni	2850	2820	2900	2940	2896
Cu	2,66	2,38	2,65	2,54	2,48
Zn	75,6	74	75,8	77,6	76,3
Rb					
Sr	0,027	0,019			0,03
Y	0,0039	0,006		0,0058	0,0064
Zr	1,190	1,154	1,131	1,199	1,111
Nb	0,312	0,320	0,414	0,327	0,320
Cs					
Ba					
La	0,002	0,002			0,002
Ce	0,004	0,006			
Pr		0,001			0,001
Nd					0,006
Sm					
Eu					
Gd					
Tb					
Dy					
Ho					
Er					
Tm	0,001				
Yb			0,005	0,008	
Lu					
Hf	0,028	0,034	0,028	0,023	0,033
Ta	0,017	0,021	0,018	0,016	0,021
Pb		0,000			
Th					
U					

Table S9. Trace elements of each analyzed orthopyroxene from the Catalão xenoliths.

Rock type	sp-lherz						
Sample	1A-76A	1A-76A	1A-76A	1A-76A	1A-76A	1A-76A	1A-76B
Spot	Opx1	Opx2	Opx3	Opx4	Opx5	Opx6	Opx1
Li	1,450	0,841	0,923	1,225	0,795	1,460	1,047
B	0,605	0,54	0,62	0,58	0,47	0,66	0,52
Sc	17,29	16,87	16,45	20,51	17,18	17,37	18,39
Ti	499,9	501	460	599	523	506	526
V	100,6	96,9	97,3	112,4	101,6	95,4	101,9
Cr	2058	2056	2517	3200	2850	2118	2752
Co	46,6	47,9	50,5	53,8	53,4	48,3	53,9
Ni	529	552	615	665	654	564	660
Cu	0,092	0,103	0,122	0,15	0,096	0,1	0,138
Zn	24,9	27,7	34,2	36,7	32,9	30,8	34,1
Rb			0,018		0,0125		
Sr	0,055	0,102	0,039	0,215	0,064	0,063	0,089
Y	0,621	0,661	0,433	1,123	0,68	0,63	0,885
Zr	0,213	0,211	0,25	0,478	0,242	0,242	0,358
Nb	0,0111	0,0087	0,0133	0,0188	0,0138	0,0114	
Cs							
Ba		0,027			0,035		
La			0,00081		0,00029		
Ce	0,00074	0,0009			0,0011	0,0039	
Pr					0,00095		
Nd	0,0047	0,0073			0,0045	0,0035	
Sm	0,0065				0,0051	0,011	
Eu	0,0027			0,0091		0,0032	
Gd	0,028	0,027	0,0156	0,056	0,025		
Tb	0,0079	0,0072	0,0026	0,0134	0,0044	0,0075	
Dy	0,08	0,085	0,045	0,125	0,066	0,063	0,134
Ho	0,0202	0,0252	0,0156	0,0381	0,0247	0,0252	0,032
Er	0,092	0,1	0,07	0,172	0,107	0,105	0,142
Tm	0,0221	0,0216	0,0201	0,0316	0,0198	0,0217	0,0294
Yb	0,24	0,233	0,173	0,313	0,218	0,19	0,215
Lu	0,035	0,043	0,0347	0,0477	0,0403	0,0397	0,0483
Hf	0,03	0,01	0,0077	0,0216	0,023	0,0216	
Ta					0,0018		
Pb	0,0107		0,041	0,032	0,043	0,0124	
Th			0,0005				
U							

Table S9. Continued.

Rock type	sp-lherz						
Sample	1A-76B	1A-76B	1A-76B	1A-76B	1A-76B	1A-76C	1A-76C
Spot	Opx2	Opx3	Opx4	Opx5	Opx6	Opx1	Opx2
Li	1,193	0,906	2,17	2,1	0,81	0,985	0,985
B	0,33	0,39	0,48	0,39	0,44	0,34	0,5
Sc	19,1	16,28	16,1	16,3	20,18	17,62	18,78
Ti	573	487	473	473	586	504	529
V	107,5	94,7	94,8	99,5	109,5	106,5	107,5
Cr	2864	2360	1984	2045	2820	2931	2912
Co	53,3	51,7	49,4	48,9	55,1	54,5	54,3
Ni	657	613	568	548	674	675	662
Cu	0,212	0,056	0,085	0,146	0,088	0,087	0,097
Zn	32	30,5	26,7	24,5	32,9	32,7	32,7
Rb							
Sr	0,092		0,0265	0,058	0,145	0,045	0,088
Y	0,896	0,449	0,569	0,492	1,096	0,546	0,767
Zr	0,295	0,18	0,194	0,181	0,423	0,244	0,287
Nb		0,0093	0,008	0,0085		0,0129	0,0105
Cs							
Ba		0,0104		0,074		0,042	
La				0,00131		0,00122	
Ce				0,0015		0,0016	
Pr							0,00063
Nd		0,0058					0,0096
Sm		0,004			0,022		
Eu		0,0024		0,004	0,0087	0,0029	0,0067
Gd		0,0053		0,019	0,056		0,032
Tb		0,003		0,0054	0,0116	0,0045	0,0078
Dy	0,124	0,053	0,046	0,073	0,136	0,049	0,092
Ho	0,0333	0,0166	0,0177	0,0192	0,0354	0,0146	0,0263
Er	0,144	0,095	0,091	0,077	0,157	0,101	0,138
Tm	0,0297	0,0183	0,0248	0,016	0,0311	0,0168	0,0297
Yb	0,275	0,221	0,24	0,192	0,289	0,222	0,256
Lu	0,046	0,0384	0,0398	0,036	0,0581	0,0417	0,0435
Hf		0,0149	0,0154	0,0133	0,037	0,0189	0,029
Ta							
Pb	0,05			0,031			
Th							
U							

Table S9. Continued.

Rock type	sp-lherz	sp-lherz	sp-lherz	sp-lherz	harz	harz	harz
Sample	1A-76C	1A-76C	1A-76C	1A-76C	1A-81	1A-81	1A-81
Spot	Opx3	Opx4	Opx5	Opx6	Opx1	Opx2	Opx3
Li	0,511	0,613	0,647	1,02	1,858	1,861	2,39
B	0,57	0,58	0,57	0,56	0,83	0,78	0,78
Sc	17,3	19,4	18,92	19,06	21,07	19,87	24,21
Ti	507	569	561	571	533	457	619
V	98,1	108,3	107,2	109,3	104	97,4	112,1
Cr	2440	2744	2684	2698	4660	4144	5130
Co	51,3	52,9	53,8	52,2	47,5	47,5	51,7
Ni	641	640	652	632	595	592	641
Cu		0,15	0,137	0,257	0,137	0,35	0,214
Zn	24,7	30,1	31,1	28,8	32,2	34,3	41,8
Rb				0,357		0,258	0,022
Sr		0,082	0,074	0,234	3,09	3,04	5,52
Y	0,619	0,82	0,81	0,718	0,543	0,395	0,818
Zr	0,205	0,366	0,288	0,32	1,08	0,622	1,5
Nb			0,0115	0,0105	0,21	0,231	0,036
Cs				0,051		0,0182	
Ba			0,034	0,397	0,91	1,21	1,8
La			0,0036	0,0145	0,339	0,267	0,359
Ce				0,0174	0,535	0,318	0,367
Pr					0,058	0,0212	0,026
Nd					0,013	0,095	0,093
Sm			0,006	0,011	0,024	0,0106	0,027
Eu			0,0062	0,0051	0,0122	0,0096	0,0109
Gd			0,037		0,022	0,027	0,065
Tb			0,0062	0,0074	0,012	0,0051	0,0116
Dy	0,069	0,102	0,082	0,074	0,067	0,059	0,118
Ho	0,0255	0,0348	0,0307	0,0235	0,0231	0,0136	0,0305
Er	0,09	0,115	0,112	0,127	0,089	0,058	0,122
Tm	0,0253	0,0276	0,0278	0,0288	0,0193	0,0113	0,0182
Yb	0,21	0,261	0,216	0,212	0,169	0,127	0,209
Lu	0,0494	0,0486	0,0459	0,0408	0,0244	0,0208	0,0251
Hf			0,0168	0,0182	0,05	0,0303	0,065
Ta							
Pb		0,15	0,049	0,05	0,164	0,184	0,24
Th					0,059	0,0671	0,0484
U					0,0588	0,0371	0,042

Table S9. Continued.

Rock type	harz	harz	sp-lherz	sp-lherz	sp-lherz	sp-lherz	sp-lherz
Sample	1A-81	1A-81	1A-81A	1A-81A	1A-81A	1A-81A	1A-81A
Spot	Opx4	Opx5	Opx1	Opx2	Opx3	Opx4	Opx5
Li	2,07	1,32	1,914	1,85	1,95	1,596	0,928
B	1,95	0,52	0,43	1,15	1,2	1,25	0,54
Sc	21,21	20,03	14,58	14,84	15,55	16,58	19,27
Ti	523	520	371	367,9	426	429	507
V	105	94,1	96,2	98,7	104,9	105,3	117
Cr	4620	4000	1758	1916	2149	2214	2679
Co	47,4	47,5	45,2	42,5	46,8	48,2	52,8
Ni	584	574	532	555	545	591	655
Cu	1,6	0,115	0,058	0,237	0,334	0,219	0,149
Zn	35,3	38,3	23,24	23,37	24,5	24,7	31,1
Rb	3,29	0,026		0,823	0,476	0,072	
Sr	12	6,3		0,192	0,356	0,192	0,055
Y	0,511	0,363	0,33	0,308	0,529	0,528	0,877
Zr	1,01	0,979	0,139	0,152	0,147	0,196	0,297
Nb	0,357	0,111	0,0103	0,0118	0,0126		0,0086
Cs	0,538			0,132	0,086	0,014	
Ba	19,3	0,78		0,042	0,076	0,041	0,059
La	0,393	0,523		0,0019	0,0012	0,00103	0,00102
Ce	0,52	0,44		0,0062	0,0041	0,0042	
Pr	0,039	0,0299					0,0013
Nd	0,165	0,084					0,011
Sm	0,025		0,0042				
Eu	0,0086	0,0082				0,0022	0,0117
Gd				0,0065			0,028
Tb	0,0076	0,0065	0,0031		0,0072	0,0059	0,0087
Dy	0,072	0,05	0,049	0,024	0,055	0,074	0,083
Ho	0,0181	0,0152	0,0094	0,0086	0,0217	0,0218	0,0291
Er	0,075	0,056	0,057	0,051	0,089	0,087	0,13
Tm	0,0138	0,0114	0,0126	0,0137	0,0196	0,0209	0,0265
Yb	0,105	0,094	0,153	0,141	0,179	0,198	0,249
Lu	0,0198	0,0234	0,0323	0,0271	0,0341	0,0333	0,0493
Hf	0,037	0,032		0,0061	0,0162	0,0143	0,0322
Ta							
Pb	0,387	1,4		0,07	0,061	0,032	0,064
Th	0,0896	0,129			0,0008		
U	0,066	0,106					

Table S9. Continued.

Rock type	sp-lherz						
Sample	1A-81B	1A-81B	1A-81B	1A-81B	1A-81B	1A-81C	1A-81C
Spot	Opx1	Opx2	Opx3	Opx4	Opx5	Opx1	Opx2
Li	1,295	0,728	1,349	1,245	1,585	1,448	0,903
B	0,45	0,55	0,63	0,56	0,6	0,569	0,364
Sc	17,18	19,05	19,42	19	17,96	15,59	16,66
Ti	436	474	489	494	444	414	438
V	102,6	111,5	112,8	115,7	106,1	98,9	98,9
Cr	2134	2472	2636	2466	2161	2096	2099
Co	48,8	51,4	51,4	50,2	47,1	47,5	48,7
Ni	583	631	642	612	563	576	604
Cu	0,08		0,099	0,086	0,088	0,05	0,047
Zn	39	30,1	29,7	26,3	25,7	25,5	27,9
Rb							
Sr	0,0134	0,0229	0,059	0,059	0,0255		0,0186
Y	0,589	0,76	0,855	0,781	0,669	0,401	0,59
Zr	0,193	0,265	0,321	0,282	0,178	0,144	0,147
Nb	0,0095	0,0068		0,0104	0,0138	0,0037	0,0048
Cs							
Ba					0,015		
La	0,0005	0,00032					
Ce	0,0025					0,0012	
Pr			0,0007				
Nd		0,0068					
Sm					0,0046		0,01
Eu		0,0063	0,0021	0,0064			
Gd				0,03			
Tb	0,0022	0,0065	0,0116	0,0121	0,0062	0,0021	0,0062
Dy	0,054	0,113	0,098	0,078	0,086	0,036	0,054
Ho	0,0181	0,0267	0,0388	0,0322	0,0275	0,0171	0,0176
Er	0,079	0,105	0,129	0,132	0,108	0,065	0,0911
Tm	0,023	0,0265	0,0281	0,0295	0,021	0,012	0,0221
Yb	0,195	0,234	0,247	0,23	0,235	0,155	0,207
Lu	0,0379	0,042	0,0411	0,0441	0,0418	0,0295	0,0358
Hf	0,0141	0,011	0,021	0,024	0,0131	0,0147	0,0135
Ta							
Pb							
Th							
U							

Table S9. Continued.

Rock type	sp-lherz	sp-lherz	sp-lherz
Sample	1A-81C	1A-81C	1A-81C
Spot	Opx3	Opx4	Opx5
Li	1,566	1,32	1,211
B	0,46	0,46	1,45
Sc	21,43	19,35	17,8
Ti	504	463	431,8
V	121,3	111,9	106
Cr	2224	1940	1804
Co	46,8	46	44,4
Ni	543	517	493
Cu	0,083		
Zn	26,5	27	22,1
Rb		0,054	1,91
Sr		0,056	0,312
Y	0,618	0,545	0,469
Zr	0,216	0,174	0,154
Nb	0,0066	0,0058	0,044
Cs		0,009	0,214
Ba			0,248
La	0,011		
Ce			
Pr			
Nd			
Sm			
Eu	0,0034	0,0029	
Gd			
Tb	0,0088	0,0054	
Dy	0,056	0,064	0,049
Ho	0,0223	0,0138	
Er	0,102	0,092	0,075
Tm	0,0228	0,0172	
Yb	0,216	0,183	0,157
Lu	0,0427	0,0356	0,036
Hf	0,017	0,0126	
Ta			
Pb			
Th			
U			

Table S10. Trace elements of each analyzed clinopyroxene from the Catalão xenoliths.

Rock type	sp-lherz						
Sample	1A-76A	1A-76A	1A-76A	1A-76A	1A-76A	1A-76A	1A-76B
Spot	Cpx1	Cpx2	Cpx3	Cpx4	Cpx5	Cpx6	Cpx1
Li	1,509	1,77	1,021	1,086	1,069	1,35	1,187
B	0,35	0,37	0,6	0,64	0,53	0,54	0,38
Sc	64,6	66,2	86,2	74,3	71,8	74,7	75,8
Ti	2054	2072	2451	2302	2131	2292	2219
V	249,8	261,2	281	269,2	262,3	270,1	274,6
Cr	5650	6110	4770	5420	5110	5150	5150
Co	16,84	18,32	14,15	15,26	17,54	15,55	19,06
Ni	272,5	292,9	249,8	268,5	274	253	273
Cu	1,75	1,83	1,607	1,85	1,701	1,67	1,72
Zn	11	15,8	9,57	12,2	12,1	9,44	11,52
Rb	0,0144	0,016	0,642	0,075	0,426	0,0167	0,0182
Sr	8,03	8,29	25,5	8,69	8,3	8,05	8,18
Y	16,34	16,72	17,15	17,1	15,7	16,85	16,23
Zr	5,53	5,62	6,5	6,1	5,71	6,18	5,93
Nb	0,0222	0,0233	0,057	0,166	0,045	0,0215	0,0225
Cs		0,059			0,0426		
Ba	0,09	0,082		2,47	0,162	0,091	0,209
La	0,0036	0,0021	0,0525	0,224	0,0046	0,0042	0,0036
Ce	0,146	0,143	0,168	0,51	0,149	0,145	0,149
Pr	0,087	0,106	0,0829	0,116	0,077	0,081	0,0831
Nd	1,1	1,073	1,043	1,174	1,06	1,053	1,026
Sm	0,87	0,81	0,85	0,905	0,838	0,882	0,826
Eu	0,396	0,414	0,355	0,384	0,371	0,395	0,381
Gd	1,56	1,64	1,57	1,65	1,63	1,65	1,62
Tb	0,325	0,342	0,315	0,339	0,34	0,334	0,337
Dy	2,72	2,73	2,81	2,93	2,7	2,84	2,59
Ho	0,621	0,634	0,664	0,67	0,646	0,662	0,636
Er	2,026	2,03	2,042	2,08	1,97	2,15	1,93
Tm	0,295	0,317	0,319	0,315	0,29	0,317	0,305
Yb	1,89	2,13	2,23	2,2	2,07	2,18	2,02
Lu	0,296	0,288	0,323	0,305	0,28	0,328	0,293
Hf	0,322	0,305	0,382	0,401	0,353	0,376	0,414
Ta						0,00081	
Pb	0,0134	0,027	0,014	0,177	0,046	0,026	
Th		0,00069	0,0159	0,035	0,0197		
U		0,00121	0,0095	0,0014			

Table S10. Continued.

Rock type	sp-lherz						
Sample	1A-76B	1A-76B	1A-76B	1A-76B	1A-76B	1A-76C	1A-76C
Spot	Cpx2	Cpx3	Cpx4	Cpx5	Cpx6	Cpx1	Cpx2
Li	1,061	1,097	1,073	1,109	1,196	1,633	1,225
B	0,6	0,32		0,32	0,37	0,4	0,46
Sc	72,2	66,2	69,4	72,6	71,1	71,7	75,1
Ti	2268	2039	2143	2147	2330	2172	2221
V	273,2	254,2	265,7	268,3	265,7	265	267,6
Cr	5550	5770	5510	5180	5460	5360	5280
Co	17,96	22,7	16,48	16,9	16,3	18,04	17,23
Ni	285	320	277	274	269	285,1	279
Cu	1,87	1,74	1,71	1,8	1,65	1,76	1,75
Zn	10,63	16,7	8,81	9,85	9,5	10,06	8,46
Rb	0,242		0,233	0,019		0,124	0,22
Sr	8,44	7,68	8,23	8,2	8,02	7,95	8,41
Y	16,73	15,25	15,59	15,5	16,2	16,14	16,77
Zr	5,83	5,54	5,57	5,46	5,97	6,07	6,09
Nb	0,035	0,0299	0,0279	0,0204	0,0263	0,0223	0,0251
Cs	0,0595		0,0111			0,0123	0,0286
Ba	0,269	0,106	0,196	0,097	0,078	0,159	0,217
La	0,0056	0,0046	0,0059	0,0045	0,0044	0,003	0,004
Ce	0,156	0,138	0,147	0,146	0,156	0,139	0,16
Pr	0,081	0,079	0,0822	0,082	0,089	0,084	0,0823
Nd	1,125	1,075	1,04	1,08	1,15	0,98	1,08
Sm	0,84	0,87	0,87	0,81	0,936	0,83	0,868
Eu	0,399	0,349	0,349	0,386	0,405	0,385	0,377
Gd	1,6	1,52	1,6	1,62	1,74	1,652	1,55
Tb	0,311	0,301	0,322	0,313	0,34	0,322	0,33
Dy	2,63	2,54	2,6	2,51	2,71	2,56	2,68
Ho	0,606	0,587	0,627	0,614	0,641	0,627	0,621
Er	1,97	1,85	1,92	1,91	1,95	1,876	1,96
Tm	0,305	0,29	0,288	0,294	0,332	0,297	0,312
Yb	2,06	1,88	1,94	2	2,09	1,893	2,07
Lu	0,294	0,251	0,278	0,272	0,29	0,281	0,304
Hf	0,378	0,31	0,364	0,331	0,334	0,406	0,381
Ta							
Pb	0,032	0,022	0,0089			0,021	
Th	0,00152		0,00094			0,00067	
U	0,002					0,00095	

Table S10. Continued.

Rock type	sp-lherz	sp-lherz	sp-lherz	sp-lherz	harz	harz	harz
Sample	1A-76C	1A-76C	1A-76C	1A-76C	1A-81	1A-81	1A-81
Spot	Cpx3	Cpx4	Cpx5	Cpx6	Cpx1	Cpx2	Cpx3
Li	2,453	1,227	1,332	1,296	0,873	0,858	1,17
B	0,47	0,38	0,39	0,37	1,84	1,4	4,08
Sc	77,4	75,8	78	71,5	81,6	83,7	76
Ti	2441	2428	2508	2447	1421	1281	1170
V	269,1	275,4	280,2	270,1	258,6	232,9	210,4
Cr	5510	5770	5680	6040	9440	8470	9470
Co	20,3	16,38	16,83	15,88	20,3	34,7	19,57
Ni	298	283	281	274,4	318		339
Cu	1,74	1,75	1,73	1,84	2,18		1,86
Zn	21,7	9,5	9,55	8,1	19,7	13,7	24,08
Rb	0,0213				0,992	1,3	5,9
Sr	7,93	8,03	7,91	8,25	209	307	215
Y	17,26	17,8	18,19	18,27	9,8	8,92	7,41
Zr	6,52	6,32	6,45	6,32	15,73	14,61	14,5
Nb	0,0189	0,0172	0,0246	0,0284	2,81	3,01	3,84
Cs		0,0013			0,0288	0,086	0,306
Ba	0,136	0,081	0,115	0,082	40,6	73,1	
La	0,0033	0,0038	0,0024	0,004	9,83	10,88	10,04
Ce	0,148	0,15	0,138	0,157	15,44	16,51	16,21
Pr	0,083	0,069	0,0806	0,0889	1,206	1,299	1,285
Nd	1,07	1,127	1,18	1,15	4,76	4,99	4,77
Sm	0,97	0,763	0,86	1	1,32	1,35	1,217
Eu	0,402	0,418	0,42	0,437	0,522	0,496	0,415
Gd	1,76	1,6	1,71	1,9	1,83	1,75	1,45
Tb	0,354	0,344	0,362	0,352	0,311	0,291	0,254
Dy	2,75	2,9	2,97	3,11	2,15	1,96	1,61
Ho	0,662	0,677	0,684	0,724	0,415	0,34	0,329
Er	2,13	2,13	2,2	2,25	1,03	0,992	0,844
Tm	0,327	0,341	0,35	0,344	0,147	0,135	0,117
Yb	2,24	2,24	2,3	2,43	0,93	0,802	0,81
Lu	0,304	0,32	0,325	0,346	0,121	0,114	0,104
Hf	0,396	0,343	0,41	0,395	0,749	0,662	0,759
Ta		0,0009			0,0158	0,0236	0,0187
Pb	0,026	0,0176	0,0236	0,056	2,93	3,41	3,26
Th					0,682	0,36	1,057
U					0,252	0,145	0,347

Table S10. Continued.

Rock type	harz	harz	sp-lherz	sp-lherz	sp-lherz	sp-lherz	sp-lherz
Sample	1A-81	1A-81	1A-81A	1A-81A	1A-81A	1A-81A	1A-81A
Spot	Cpx4	Cpx5	Cpx1	Cpx2	Cpx3	Cpx4	Cpx5
Li	0,809	1,085	2,152	2,91	3,97	2,821	2,278
B	1,63	2,07	0,47	0,54	0,51	0,65	0,46
Sc	76	83,2	63,8	66,7	64	72,6	70,8
Ti	1434	1426	1818	1914	1864	2025	1909
V	244,8	247,2	264,3	268,4	264,3	277,8	282,7
Cr	8980	9110	6190	6190	6190	5640	5480
Co	23,17	23,02	14,74	18,35	15,91	16,14	17,2
Ni	422	408	259,2	312	280,2	276,7	288
Cu	1,66	1,63	1,94	1,87	1,94	1,71	1,6
Zn	24,4	25,4	10,59	13,06	10,16	9,24	9,95
Rb	4,05	6,4					
Sr	325	291	6,42	6,33	6,38	6,26	6,37
Y	8,68	8,67	18	18,19	18,3	18,09	17,23
Zr	12,59	13,7	4,97	5,47	5,03	5,47	5,02
Nb	4,05	4,49			0,0246	0,028	0,028
Cs	0,322	0,59					
Ba	52,3	64,7		0,081	0,015		0,048
La	13,7	11,88				0,00206	0,0041
Ce	19,6	17,76	0,107	0,116	0,102	0,118	0,117
Pr	1,42	1,309	0,063	0,0609	0,062	0,0583	0,064
Nd	4,75	4,81	0,835	0,852	0,86	0,816	0,92
Sm	1,14	1,097	0,789	0,749	0,756	0,83	0,81
Eu	0,441	0,446	0,381	0,434	0,412	0,39	0,369
Gd	1,566	1,67	1,66	1,82	1,86	1,81	1,75
Tb	0,271	0,273	0,345	0,387	0,377	0,371	0,362
Dy	1,88	1,84	3	3,08	3,08	2,94	2,91
Ho	0,361	0,362	0,671	0,689	0,677	0,702	0,661
Er	0,979	0,95	2,02	2,05	2,122	1,99	1,95
Tm	0,124	0,144	0,326	0,315	0,314	0,311	0,316
Yb	0,935	0,979	2,07	2,19	2,13	2,2	2,02
Lu	0,114	0,147	0,293	0,3	0,314	0,314	0,299
Hf	0,584	0,623	0,278	0,286	0,288	0,294	0,317
Ta	0,0197	0,0248	0,099				
Pb	3,81	3,69					
Th	0,812	0,847					
U	0,27	0,281					

Table S10. Continued.

Rock type	sp-lherz						
Sample	1A-81A	1A-81B	1A-81B	1A-81B	1A-81B	1A-81B	1A-81C
Spot	Cpx6	Cpx1	Cpx2	Cpx3	Cpx4	Cpx5	Cpx1
Li	2,54	1,909	2,08	2,88	1,69	1,635	2,93
B	0,65	0,75	1,24	2,9	0,57	0,91	
Sc	68,8	78,5	74,6	76,6	79,6	87,6	72,2
Ti	1930	1869	1909	2015	1969	2155	2004
V	271,6	286,9	274,9	294,7	282,8	296,2	279,4
Cr	5650	4910	5170	5290	4860	4820	5880
Co	16,46	16,57	15,6	16,97	16,3	14,65	16,33
Ni	265,9	262,5	258	266	260	243,4	276
Cu	2,13	1,661	1,79	2,1	1,68	1,66	1,74
Zn	10,35	9,58	9,85	11,5	9,19	8,36	10,5
Rb	0,0262	0,0167	1,09	8,1	0,531	0,91	
Sr	6,44	6,18	6,9	59,2	7,48	22,1	6,27
Y	18,16	16,82	17,74	17,61	18,25	17,74	17,73
Zr	5,47	5	5,22	16,1	5,46	6,72	5,39
Nb	0,0267	0,0176	0,05	1,35	0,063	0,323	
Cs			0,23	0,609	0,0359	0,154	
Ba	0,138		0,463	51,6	1,19	6,8	
La	0,0071		0,0036	1,37	0,057	1,75	
Ce	0,104	0,092	0,105	1,96	0,191	2,9	0,1045
Pr	0,072	0,0668	0,058	0,226	0,069	0,318	0,059
Nd	0,864	0,74	0,782	1,44	0,846	1,54	0,77
Sm	0,79	0,71	0,77	0,78	0,75	0,838	0,76
Eu	0,401	0,365	0,383	0,415	0,42	0,396	0,404
Gd	1,82	1,615	1,74	1,72	1,82	1,72	1,75
Tb	0,37	0,351	0,355	0,372	0,367	0,364	0,349
Dy	2,92	2,77	2,92	2,86	2,96	3,08	3,04
Ho	0,706	0,658	0,697	0,689	0,672	0,659	0,651
Er	2,12	1,94	2,1	2,14	2,17	2,15	2,19
Tm	0,314	0,302	0,317	0,334	0,327	0,319	0,314
Yb	2,19	1,92	2,19	2,24	2,32	2,15	2,13
Lu	0,314	0,295	0,3	0,298	0,309	0,315	0,295
Hf	0,302	0,321	0,344	0,619	0,316	0,387	0,278
Ta	0,148					0,0109	
Pb			0,061	0,146	0,038	0,058	
Th			0,0021	0,416		0,21	
U			0,0012	0,139		0,0332	

Table S10. Continued.

Rock type	sp-lherz	sp-lherz	sp-lherz	sp-lherz	grt-wehr	grt-wehr	grt-wehr
Sample	1A-81C	1A-81C	1A-81C	1A-81C	1B-139A	1B-139A	1B-139A
Spot	Cpx2	Cpx3	Cpx4	Cpx5	Cpx1	Cpx2	Cpx3
Li	2,65	1,81	3,08	3,21	0,609	0,542	1,124
B				0,6	0,73	0,47	1,34
Sc	74,3	79,6	73,2	70,4	15,23	15,12	14,83
Ti	2162	1905	2091	2004	425	533	749
V	279,6	290,5	283	280,5	281,1	274,7	272,8
Cr	5860	4855	5770	5910	9380	9250	9030
Co	15,58	17,08	17,17	17,02	20,28	20,46	21,96
Ni	275,1	268,3	299	283,5	374	378	406
Cu	1,775	1,65	1,71	1,616	2,14	2,06	2,21
Zn	9,15	9,82	11,82	10,8	16,64	16,49	17,09
Rb		0,0213		0,09	0,97	0,033	7,48
Sr	6,34	6,37	6,22	6,47	187,4	215,3	209
Y	18,47	16,91	18,59	17,87	2,613	2,63	2,167
Zr	5,69	5,04	5,51	5,26	36,8	36,7	43,6
Nb	0,0243	0,0133	0,0286	0,0145	0,755	0,594	1,42
Cs		0,0049		0,0065	0,018		0,499
Ba	0,059	0,04		0,26	2,55	2,14	3,13
La		0,0031	0,00062	0,0028	14,62	15,48	9,38
Ce	0,113	0,1024	0,095	0,103	42,5	44	29,3
Pr	0,053	0,0504	0,06	0,06	5,95	6,36	4,5
Nd	0,767	0,655	0,772	0,831	24	25,58	19,45
Sm	0,88	0,733	0,783	0,828	3,56	3,95	3,07
Eu	0,412	0,335	0,416	0,4	0,884	0,937	0,744
Gd	1,76	1,57	1,79	1,78	2,01	2,03	1,61
Tb	0,373	0,343	0,369	0,384	0,188	0,2	0,1741
Dy	3,05	2,89	3,02	2,8	0,782	0,885	0,734
Ho	0,713	0,626	0,705	0,695	0,106	0,117	0,0988
Er	2,21	2,01	2,23	2,111	0,225	0,209	0,164
Tm	0,34	0,31	0,306	0,285	0,0223	0,022	0,015
Yb	2,18	1,84	2,18	2,12	0,089	0,099	0,099
Lu	0,326	0,293	0,312	0,283	0,0113	0,012	0,0119
Hf	0,335	0,324	0,291	0,3	0,765	0,924	1,465
Ta					0,0379	0,0241	0,068
Pb					0,989	1,027	0,798
Th					0,0295	0,0227	0,063
U					0,0025		0,0235

Table S10. Continued.

Rock type	grt-wehr						
Sample	1B-139A	1B-139A	1B-139B	1B-139B	1B-139B	1B-139B	1B-139B
Spot	Cpx4	Cpx5	Cpx1	Cpx2	Cpx3	Cpx4	Cpx5
Li	0,581	0,851	1,201	0,789	0,752	0,634	0,785
B	0,45	1,43	1,51	0,52	0,95	1,022	1,43
Sc	18,28	18	19,89	15,85	17,46	17,48	17,02
Ti	659	1196	1398	864	754	763	945
V	273,2	265,2	249,4	264,9	272,6	276,3	275,2
Cr	9500	9290	9260	9230	9710	9520	9650
Co	22,14	21,82	23,89	22,22	22	22,27	22,8
Ni	408	391,7	427	416	411	413	433
Cu	2,18	2,45	2,49	2,334	2,36	2,35	2,62
Zn	17,89	18,02	17,56	17,96	17,34	17,21	18,3
Rb	0,119	4,7	7,64	1,065	1,06	0,557	5,28
Sr	394	381	378	246,6	351	289	531
Y	3,106	3,63	3,17	2,26	3,03	2,97	2,96
Zr	46,6	56,9	72,5	48,3	44,6	46	53,9
Nb	0,969	6,1	6,81	0,918	1,066	1,68	6,03
Cs		0,106	0,189	0,0294	0,0564	0,028	0,138
Ba	3,8	85	330	1,51	3	15,4	
La	13,51	18	9,18	6,85	14,4	13,34	15,07
Ce	43,3	52,4	30,49	25,33	45	42,1	45,1
Pr	6,98	7,81	4,43	3,83	6,27	5,92	6,03
Nd	30,5	32,7	21	17,73	28,3	26,5	26,49
Sm	5	5,01	3,8	3,14	4,64	4,61	4,18
Eu	1,202	1,239	1,017	0,808	1,181	1,143	1,072
Gd	2,56	2,8	2,19	1,77	2,55	2,51	2,32
Tb	0,262	0,275	0,23	0,194	0,246	0,245	0,218
Dy	1,025	1,15	1,124	0,807	1,093	1,029	1,051
Ho	0,131	0,157	0,138	0,0996	0,129	0,142	0,128
Er	0,272	0,307	0,287	0,185	0,242	0,259	0,249
Tm	0,032	0,0346	0,0275	0,019	0,0221	0,0276	0,0247
Yb	0,108	0,164	0,116	0,085	0,144	0,133	0,113
Lu	0,0142	0,015	0,0126	0,0116	0,0085	0,011	0,0134
Hf	1,602	1,54	3,65	2,14	1,483	1,644	1,68
Ta	0,055	0,388	0,331	0,0406	0,0497	0,103	0,356
Pb	0,94	1,082	0,647	0,569	1,074	1,026	1,054
Th	0,0337	0,222	0,228	0,0319	0,0295	0,0692	0,245
U	0,0047	0,058	0,0398	0,0058	0,0061	0,0113	0,0487

Table S11. Trace elements of each analyzed garnet from the Catalão xenoliths.

Rock type	grt-wehr						
Sample	1B-139A						
Spot	Grt1	Grt2	Grt3	Grt4	Grt5	Grt6	Grt7
Li	0,118	0,105	0,105			0,073	0,111
B		0,6	0,62	0,52	0,64		
Sc	140,4	138,8	139,1	138,1	138	137,7	138,5
Ti	339,5	327,5	334	333,6	331,5	341,6	330,4
V	342,3	328,5	342,8	339,2	332,7	341,5	336
Cr	34600	33180	35500	33020	33180	34460	33220
Co	43,1	44,2	43,7	43,7	44,7	43,9	44,5
Ni	32,7	33,8	33,1	32,9	33,2	33,63	34,3
Cu	0,181	0,142	0,144	0,206	0,179	0,162	0,224
Zn	17,2	17,7	17,9	18,6	18,7	17,72	18,3
Rb					0,035		
Sr			0,073	0,068		0,057	0,086
Y	3,05	3,29	3,16	2,97	3,09	2,97	2,94
Zr	1,354	1,145	1,77	1,56	0,986	1,395	1,059
Nb	0,261	0,17	0,264	0,187	0,155	0,23	0,182
Cs							
Ba							
La	0,013			0,0134	0,0053	0,0136	
Ce	0,085	0,045	0,11	0,099	0,047	0,0838	0,048
Pr	0,0344		0,0399	0,0374	0,0175	0,0262	0,0213
Nd	0,196	0,146	0,284	0,263	0,184	0,219	0,192
Sm	0,083		0,138	0,117	0,063	0,091	0,074
Eu	0,0325			0,036	0,0417	0,0272	0,029
Gd	0,14	0,121	0,18	0,164	0,102	0,114	0,116
Tb	0,0322		0,0418	0,0317	0,0319	0,0308	0,0336
Dy	0,3	0,383	0,362	0,348	0,349	0,316	0,41
Ho	0,121	0,119	0,108	0,108	0,118	0,104	0,117
Er	0,436	0,483	0,456	0,448	0,482	0,482	0,482
Tm	0,093	0,095	0,089	0,081	0,094	0,101	0,088
Yb	0,866	0,922	0,85	0,812	0,847	0,843	0,87
Lu	0,158	0,179	0,151	0,147	0,128	0,142	0,152
Hf	0,0254			0,036	0,034	0,033	0,035
Ta					0,0049	0,0075	
Pb					0,029		0,024
Th	0,0035				0,0054	0,0088	0,006
U	0,0109			0,0064	0,0059	0,0066	0,0068

Table S11. Continued.

Rock type	grt-wehr						
Sample	1B-139A	1B-139B	1B-139B	1B-139B	1B-139B	1B-139B	1B-139B
Spot	Grt8	Grt1	Grt2	Grt3	Grt4	Grt5	Grt6
Li	0,088	0,121	0,121	0,069	0,094		
B	0,69		0,69		0,71	0,54	0,63
Sc	134,7	139,9	141,1	141,4	139,6	139,8	139,9
Ti	321,5	327,5	333,2	329,5	340,9	342,6	355,8
V	326,7	338,3	343,8	337,2	335,1	343,5	357,1
Cr	31440	32570	33350	32710	32730	33100	36830
Co	44,1	43,97	44,11	44,8	44,46	44,8	43,5
Ni	32,8	32,22	33,1	46,3	33,79	34,1	33,11
Cu	0,129	0,104	0,195	0,21	0,181	0,134	0,148
Zn	18,04	17,69	17,69	18,7	17,42	17,73	17,6
Rb						0,058	0,044
Sr			0,029	0,058			0,085
Y	3,118	3,372	3,118	3,19	3,13	3,25	3,08
Zr	1,009	0,841	1,105	1,75	1,037	1,115	1,85
Nb	0,158	0,143	0,163	0,281	0,16	0,154	0,319
Cs							
Ba							
La			0,0042	0,0129			0,016
Ce	0,044		0,048	0,094	0,05	0,0468	0,128
Pr	0,0188	0,0117	0,0157	0,0275			0,033
Nd	0,189	0,115	0,167	0,191	0,19	0,192	0,329
Sm	0,073	0,071	0,062	0,066			0,099
Eu	0,015	0,0217	0,0282	0,033			0,046
Gd	0,095	0,159	0,126	0,106	0,131	0,154	0,185
Tb	0,0342	0,0284	0,0332	0,0296	0,0364	0,0357	0,0321
Dy	0,363	0,373	0,314	0,334	0,371	0,363	0,408
Ho	0,103	0,134	0,105	0,115	0,119	0,1258	0,104
Er	0,482	0,595	0,448	0,49	0,477	0,505	0,407
Tm	0,095	0,104	0,094	0,088	0,097	0,094	0,103
Yb	0,816	0,964	0,87	0,912	0,801	0,917	0,83
Lu	0,166	0,163	0,16	0,148	0,149	0,154	0,148
Hf	0,0181	0,025	0,032	0,039			0,047
Ta							
Pb							
Th	0,007	0,0049	0,008	0,0079			0,0075
U	0,0053	0,0076	0,0053	0,0088			0,0141

Table S12. Trace elements for each analyzed phlogopites from the Catalão xenoliths.

Rock type	grt-wehr						
Sample	1B-139A	1B-139A	1B-139A	1B-139A	1B-139B	1B-139B	1B-139B
Phl type	Ph2	Ph2	Ph2	Ph2	Ph1	Ph1	Ph1
Spot	Phl1	Phl3	Phl4	Phl5	Ph1	Phl2	Phl3
Li	10,97	5,91	6,62	4,77	1,45	1,406	1,81
B	0,78	1,77	1,83	2,31	3,6	1,19	18,8
Sc	7,3	6,89	4,13	10,64	2,21	2,14	2,03
Ti	29940	28500	26650	19970	10340	7480	5900
V	278,5	327	262,3	255,1	161,9	134,2	114
Cr	19120	15480	11820	20250	4720	4600	3310
Co	63,9	63,5	62,5	59,1	58	59,5	41,6
Ni	1060	1279	1394	1018	1710	1736	1160
Cu	0,346	0,343	0,86	1,08	5,7	2,36	9,1
Zn	41,3	41,2	39,9	37,2	34,7	37,8	36,4
Rb	547	531	640	439	553	573	530
Sr	74,6	72,5	52,1	64	38	17,3	33,8
Y	0,057	0,61	0,091	0,119	0,186	0,127	0,38
Zr	17,9	24,3	15,13	30,3	26	29,6	22,3
Nb	15,31	20,86	15,76	26,97	35,6	32,58	24,1
Cs	3,49	3,79	3,55	3,93	4,59	4,09	5,03
Ba	2114	1988	1633	1782	1600	940	170
La	0,0258	0,323	0,0523	0,071	0,72	0,548	0,75
Ce	0,0152	0,7	0,063	0,104	1,56	1,358	1,59
Pr	0,0038	0,08	0,0131	0,0117	0,142	0,154	0,101
Nd		0,295	0,024	0,042	0,58	0,707	0,54
Sm		0,041			0,066	0,098	0,056
Eu	0,0114	0,0292	0,0071	0,0108	0,025	0,0341	0,015
Gd		0,039			0,042	0,058	
Tb		0,0068	0,0017		0,0055	0,0039	0,0061
Dy		0,063	0,015		0,02	0,02	0,058
Ho		0,0187	0,0018	0,0022	0,0047	0,0044	0,018
Er		0,06	0,0086	0,0126	0,0202	0,011	0,048
Tm		0,01	0,0046		0,0016	0,0015	0,0099
Yb	0,005	0,076	0,043	0,0118	0,024		0,064
Lu	0,00059	0,0141	0,0072	0,0038	0,0049	0,0015	0,0192
Hf	0,659	0,798	0,553	1,05	0,704	0,917	0,6
Ta	1,35	1,823	1,308	2,453	2,51	2,725	1,56
Pb	0,188	0,185	0,168	0,173	0,36	0,074	1,29
Th	0,0027	0,196	1,97	0,129	1,91	0,044	0,43
U	0,0036	0,0295	0,0336	0,0324	0,08	0,0068	0,263

Table S12. Continued.

Rock type	grt-wehr	grt-wehr
Sample	1B-139B	1B-139B
Phl type	Ph2	Ph2
Spot	Phl5	Phl6
Li	1,313	
B	0,96	
Sc	8,51	2,93
Ti	31990	22440
V	310,6	199,8
Cr	22430	11410
Co	68,6	61,3
Ni	1076	1460
Cu	0,35	0,406
Zn	41,9	36,6
Rb	537	650
Sr	89,6	36,1
Y	0,201	0,0325
Zr	14,35	13,18
Nb	13,11	13,61
Cs	3,41	2,93
Ba	2426	1227
La	0,0476	0,0144
Ce	0,039	0,0087
Pr	0,0072	0,0018
Nd		
Sm		
Eu	0,0093	0,0098
Gd		0,0063
Tb		
Dy	0,0093	
Ho	0,0039	
Er	0,023	
Tm	0,0084	
Yb	0,097	
Lu	0,0146	
Hf	0,531	0,454
Ta	0,979	1,158
Pb	0,199	0,088
Th	0,1	
U	0,0095	0,0012